Novel Aspects of the Reactions of Hydrogenases with Small Molecule Inhibitors



A thesis submitted to the Board of the Faculty of Physical Sciences, for the degree of Doctor of Philosophy, University of Oxford

Annemarie F. Wait
Merton College
Trinity Term 2011

Abstract

Novel Aspects of the Reactions of Hydrogenases with Small Molecule Inhibitors

Annemarie F. Wait, Merton College
A Thesis Submitted for the degree of DPhil, Trinity Term 2011

Hydrogenases catalyse the reversible oxidation and production of H_2. They have been the subject of intense interest in recent years since these enzymes, or catalysts inspired by them, may greatly enhance our exploitation of H_2 as an energy carrier in a future 'green' H_2-based economy. However, a major challenge to the future use of these catalysts is their reactions with small molecule inhibitors, such as O_2 or CO.

This thesis presents studies using Protein Film Electrochemistry, in which an enzyme is adsorbed onto an electrode to give an electroactive film. Although most hydrogenases are inhibited or irreversibly damaged by even trace O_2, certain O_2-tolerant hydrogenases are unusual in that they are able to sustain H_2 oxidation activity in the presence of O_2. Results outlined in this thesis suggest that the O_2 tolerance of the membrane-bound [NiFe]-hydrogenase from *Ralstonia eutropha* relies upon O_2 attack generating exclusively the 'Ready' inactive state (formed by complete, four-electron reduction of O_2), which subsequently reactivates both rapidly and at high potential. The results contributed to a new explanation for how hydrogenases in certain microbes survive O_2. Electrochemical studies performed on a variant enzyme suggest that a modified proximal FeS cluster plays a role in conferring this O_2 tolerance. Studies of an enzymatic H_2/O_2 fuel cell employing the O_2-tolerant [NiFe]-hydrogenase Hyd1 from *Escherichia coli* as the anodic catalyst highlight the subtle influence of the reactions of the hydrogenase with O_2 on the power characteristics of the fuel cell under various operating conditions.

This research also identifies straight-chain aldehydes as unprecedented inhibitors of H_2 production by the [FeFe]-hydrogenases. However, some of these results cannot currently be made freely available as they are to be published at a later date in academic journals.

Acknowledgements

Firstly I would like to thank Prof. Fraser Armstrong for giving me the opportunity to work in his group, and for providing so much help and support throughout my projects. Thank you also to Prof. Bärbel Freidrich, Dr. Oliver Lenz and co-workers for their collaboration and for having me to stay and work in Berlin, and thanks to all our other collaborators, including the groups of Prof. Juan Fontecilla-Camps, Dr. Thomas Happe, and Dr. Kylie Vincent.

In the Armstrong group, special thanks go to Dr. James Cracknell and Dr. Alison Parkin for their endless support throughout my DPhil. I also thank my Part II students, Gregory Morley and David Jennings for all their hard work and effort. A big thank you goes to Dr. Victor Climent for helping electrochemistry make sense and to Holly Reeve for teaching Microsoft Word to behave. Thank you to all my proof readers – Dr. Victor Climent, Dr. James Cracknell, Dr. Sadagopan Krishnan, Dr. Michael Lukey, Dr. Alison Parkin, Carina Foster, Suzannah Hexter, Holly Reeve, Sally Sheard and Thomas Woolerton. A huge thank you to all the other members of the Armstrong group, past and present, who have provided so much help to me and have, most importantly, made my time in the group incredibly enjoyable. I could not have performed any of the experiments in this thesis without the help of the support staff in the Chemistry department, in particular Ashleigh, Terri, Nenad, Paul, Andy, Charlie, Les, Tom, Keith, Trish and Pam. I also thank Merton College and the EPSRC for the financial support they have provided.

Finally a massive thank you to Tom, for managing to put up with me both in and outside of lab and to my family, especially my parents, who have provided so much love and support, without which producing this thesis would not have been possible.

Collaborations

Various protein samples studied in this thesis were generously provided by collaborators, as outlined below:

Hydrogenase	**Collaborator**
Ralstonia eutropha H16	B. Friedrich, O. Lenz and co-workers
Ralstonia eutropha C19G/C120G	B. Friedrich, O. Lenz and co-workers
Escherichia coli Hyd2	S. Hexter, Armstrong Group
Chlamydomonas reinhardtii HydA1	T. Happe and co-workers
Clostridium acetobutylicum HydA	T. Happe and co-workers
Desulfovibrio desulfuricans HydAB	J. Fontecilla-Camps and co-workers

In Chapter 3, the data presented in Figure 3.5 were obtained by Dr. K. Vincent and co-workers and the growth curves displayed in Figure 3.22 were recorded by Mr. T. Goris, who also produced the protein variants. In Chapter 4, the fuel cell diagram generated using computer-aided design (Figure 4.4A) was produced by Mr. A. Green and the data on the pH dependence of the activity of bilirubin oxidase displayed in Figure 4.7B were obtained by Dr. L. dos Santos. In Chapter 6, the data in Figures 6.13C and D, and the CO inhibition data presented in Figure 6.19 were provided by Miss C. Foster. The calculations performed using density functional theory outlined in Section 6.4 and Appendix A11 were performed by Mr. T. Krämer.

Some of the experiments in Sections 4.3, 4.4.3, and 4.5.2.2 were performed by Mr. G. Morley under my supervision. The results in Figures 5.16B and 5.17B and some of those outlined in Sections 6.2.3, 6.2.4 and 6.3.3 were obtained by Mr. D. Jennings under my supervision, and the NMR experiments in Section 6.5 were performed with his help.

Publications

Goris, T.; Wait, A. F.; Saggu, M.; Fritsch, J.; Heidary, N.; Stein, M.; Zebger, I.; Lendzian, F.; Armstrong, F. A.; Friedrich, B.; Lenz, O., A Unique Iron-Sulfur Cluster is Crucial for Oxygen Tolerance of a [NiFe]-Hydrogenase. *Nature Chemical Biology* **2011**, 7, (5), 310-318.

Wait, A. F.; Brandmayr, C.; Stripp, S. T.; Cavazza, C.; Fontecilla-Camps, J. C.; Happe, T.; Armstrong, F. A., Formaldehyde - A Rapid and Reversible Inhibitor of Hydrogen Production by [FeFe]-Hydrogenases. *Journal of the American Chemical Society* **2011**, 133, (5), 1282-1285.

Wait, A. F.; Parkin, A.; Morley, G. M.; dos Santos, L.; Armstrong, F. A., Characteristics of Enzyme-Based Hydrogen Fuel Cells Using an Oxygen-Tolerant Hydrogenase as the Anodic Catalyst. *Journal of Physical Chemistry C* **2010**, 114, (27), 12003-12009.

Cracknell, J. A.; Wait, A. F.; Lenz, O.; Friedrich, B.; Armstrong, F. A., A Kinetic and Thermodynamic Understanding of O_2 Tolerance in [NiFe]-Hydrogenases. *Proceedings of the National Academy of Sciences* **2009**, 106, (49), 20681-20686.

Armstrong, F. A.; Belsey, N. A.; Cracknell, J. A.; Goldet, G.; Parkin, A.; Reisner, E.; Vincent, K. A.; Wait, A. F., Applications of Dynamic Electrochemical Methods to Elucidate Mechanisms of Hydrogen Oxidation and Production by Enzymes and Establish Directions for Future Technology. *Chemical Society Reviews* **2009**, 38, 36-51.

Goldet, G.; Wait, A. F.; Cracknell, J. A.; Vincent, K. A.; Ludwig, M.; Lenz, O.; Friedrich, B.; Armstrong, F. A., Hydrogen Production under Aerobic Conditions by Membrane-Bound Hydrogenases from Ralstonia Species. *Journal of the American Chemical Society* **2008**, 130, (33), 11106-11113.

Symbols and Abbreviations

Å	Angstrom
A	Ampere
A	surface area of an electrode
Aa	*Aquifex aeolicus*
*Aa*Hase1	membrane-bound hydrogenase from *Aquifex aeolicus*
ABTS	2,2'-azinobis(3-ethylbenzothiazoline-6-sulfonic acid)
ADP	adenosine diphosphate
A_p	pre-exponential factor (Arrhenius)
ATP	adenosine triphosphate
Av	*Allochromatium vinosum*
C	capacitance
C	cysteine
Ca	*Clostridium acetobutylicum*
Cr	*Chlamydomonas reinhardtii*
Cys	cysteine
D	aspartic acid
D	diffusion coefficient
Da	Dalton
Dd	*Desulfovibrio desulfuricans*
Df	*Desulfovibrio fructosovorans*
DFT	Density Functional Theory
Dg	*Desulfovibrio gigas*
E	electrode potential
e^-	electron
E_a	activation energy
Ec	*Escherichia coli*
*Ec*Hyd1	*Escherichia coli* Hydrogenase 1
*Ec*Hyd2	*Escherichia coli* Hydrogenase 2
E_{eq}	equilibrium (zero current) potential
$E_{1/2}$	reduction potential under conditions of interest
ENDOR	Electron Nuclear Double Resonance
EPR	Electron Paramagnetic Resonance
E_{switch}	switch potential
EXAFS	Extended X-ray Absorption Fine Structure
$E^{\ominus}$	standard reduction potential
F	Faraday's contant = 96,485 C mol^{-1}
Fe_d	distal iron
Fe_p	proximal iron
FTIR	Fourier Tranform Infra-Red
G	glycine
g	gram
Glu	glutamic acid
H	enthalpy
H	hydrogenase or histidine (as appropriate in text)
h	Planck's constant = 6.626×10^{-34} J s

Hmd hydrogenase	H_2-forming methylenetetrahydromethanopterin dehydrogenase
hr	hour
Hyd	hydrogenase
HYSCORE	Hyperfine Sublevel Correlation spectroscopy
i	current
j	flux
K	Kelvin
k	kilo
k	rate constant
$K^{\neq}$	equilibrium constant for formation of activated complex
k_B	the Boltzmann constant = 1.38×10^{-23} J K^{-1}
$K_I^{O2,app}$	O_2 tolerance factor
K_M	Michaelis constant
L	litre
Lys	lysine
m	milli or metre (as appropriate in text)
M	mol dm^{-3} or methionine (as appropriate in text)
MBH	membrane-bound hydrogenase
min	minute
mol	mole
*Mv*BO	*Myrothecium verrucaria* bilirubin oxidase
n	nano
n	number of electrons
NAD^+/NADH	nicotinamide adenine dinucleotide (oxidised/reduced)
NADPH	nicotinamide adenine dinucleotide phosphate
NMR	Nuclear Magnetic Resonance
OCV	open circuit voltage
PEM	proton exchange membrane
PFE	Protein Film Electrochemistry
PGE	pyrolytic graphite edge-plane
ppm	parts per million
Q	charge or reaction quotient (as stated in text)
Q	quinone
QH_2	quinol
R	the gas constant = 8.314 J K^{-1} mol^{-1}
RDE	rotating disk electrode
Re	*Ralstonia eutropha* H16
RH	regulatory hydrogenase
rpm	revolutions per minute
S	entropy
s	second
SCE	saturated calomel electrode
SH	soluble hydrogenase
SHE	standard hydrogen electrode
T	temperature
TST	Transition State Theory
v	kinematic viscosity, scan rate or reaction rate (as stated in text)
V	volt

vs.	*versus*
W	watt
WT	wild-type
w/v	weight by volume
XANES	X-ray Absorption Near Edge Spectroscopy
XAS	X-ray Absorption Spectroscopy
α	transfer coefficient
Γ	electroactive coverage
$\Delta G^{\neq}$	free energy of activation
η	overpotential
κ	transition coefficient
Ω	ohm
$\emptyset$	electric potential
^{o}C	degree Celsius

Table of Contents

Abstract i
Acknowledgements iii
Collaborations v
Publications vii
Symbols and Abbreviations ix
Chapter 1 Introduction 1
1.1 Hydrogen as an Energy Solution 2
1.2 Hydrogen in Biology 5
1.3 Techniques for Studying Hydrogenases 8
1.4 The [NiFe]-Hydrogenases 10
1.4.1 The Overall Protein Structure 10
1.4.2 The [NiFe]-Active Site 12
1.4.3 Active and Inactive States of [NiFe]-Hydrogenases 13
1.4.4 Proposed Catalytic Cycle of a [NiFe]-Hydrogenase 15
1.4.5 Gas and Proton Transport 17
1.5 The [FeFe]-Hydrogenases 18
1.5.1 The Overall Three Dimensional Structure 18
1.5.2 The H-Cluster of [FeFe]-Hydrogenases 19
1.5.3 Redox States of [FeFe]-Hydrogenases 20
1.5.4 The Catalytic Cycle of [FeFe]-Hydrogenases 23
1.5.5 Gas and Proton Transport 24
1.6 Inhibition of Hydrogenases by Small Molecules 26
1.6.1 Hydrogen 26
1.6.2 Oxygen 26
1.6.3 Carbon Monoxide and Cyanide 27
1.6.4 Sulfide 28
1.6.5 Other Small Molecules 29
1.7 Technological Applications 30
1.8 Outline of this Thesis 32
Chapter 2 Electrochemical Theory 35
2.1 Introduction to Protein Film Electrochemistry 36
2.2 The Three-Electrode System 38
2.3 Cyclic Voltammetry 39

2.3.1 An Introduction to Cyclic Voltammetry 39
2.3.2 Non-Faradaic Current 40
2.3.3 Faradaic Current 41
2.3.4 Interfacial Electron Transfer 43
2.3.5 Mass Transport 47
2.3.6 Catalytic Voltammetry 49
2.4 Chronoamperometry 52
Chapter 3 Investigations into the Origins of the O_2 Tolerance of a [NiFe]-Hydrogenase 55
Abstract 56
3.1 Introduction 57
3.1.1 An Introduction to *Ralstonia eutropha* 57
3.1.2 The Hydrogenases Present in *Ralstonia eutropha* 57
3.1.3 The Structure of the MBH from *Ralstonia eutropha* 58
3.1.4 An Introduction to the Modified Proximal Cluster 60
3.1.5 The O_2 Tolerance of *Re*MBH^{WT} 62
3.1.6 Summary of the Inactive States Formed 64
3.1.7 Introduction to the Electrochemistry of *Re*MBH^{WT} 66
3.1.7.1 Catalytic Bias 66
3.1.7.2 Anaerobic Inactivation 69
3.1.7.3 The Effect of Varying the H_2 Concentration 70
3.2 Probing the Recovery of Inactive States 72
3.2.1 Rates of Recovery from Anaerobic Inactivation 72
3.2.2 Rates of Recovery from Aerobic Inactivation 74
3.2.3 The Potential of Reactivation 78
3.2.4 Implications of Reactivation Behaviour for O_2 Tolerance 79
3.3 Role of Modified Proximal Cluster in O_2 Tolerance 81
3.3.1 Electrochemical Characterisation of *Re*MBH$^{C19G/C120G}$ 82
3.3.1.1 Catalytic Bias 82
3.3.1.2 Potential of Anaerobic Inactivation 83
3.3.1.3 Comparison of the $K_M(H_2)$ for *Re*MBH^{WT} and *Re*MBH$^{C19G/C120G}$ 84
3.3.1.4 Rates of Anaerobic Inactivation and Reactivation 88
3.3.1.5 The Effect of Short-term Exposure to O_2 90
3.3.1.6 The Effect of Long-term Exposure to O_2 91
3.3.1.7 The Extent of Inhibition by CO 93
3.4 Discussion 98

Chapter 4 Characteristics of an Enzymatic H_2/O_2 Fuel Cell Using an O_2-Tolerant Hydrogenase as the Anode Catalyst 103
Abstract 104
4.1 Introduction 105
4.1.1 An Introduction to Enzymatic Fuel Cells 105
4.1.2 Enzyme Biocatalysts for H_2/O_2 Fuel Cells 107
4.1.3 Characteristics of an Ideal Fuel Cell 109
4.2 Experimental Design 111
4.2.1 The Fuel Cell 111
4.2.2 The Anodic Biocatalyst 112
4.2.3 The Cathodic Biocatalyst 113
4.3 Electrochemical Characterisation of the Catalysts 115
4.3.1 Enzyme Activity under Varying Substrate Concentrations 115
4.3.2 The Effect of pH on Catalytic Activity 117
4.3.3 Temperature Dependence of Enzyme Activity 119
4.3.4 Cell Voltage Available from *Ec*Hyd1/*Mv*BO Electrodes 120
4.4 *Ec*Hyd1/*Mv*BO Membrane Fuel Cell 121
4.4.1 An Introduction to Proton Exchange Membranes 121
4.4.2 Characteristics of an *Ec*Hyd1/*Mv*BO PEM Fuel Cell 122
4.4.3 O_2 Crossover into the Anode Compartment 124
4.5 Membraneless *Ec*Hyd1/*Mv*BO Fuel Cells 126
4.5.1 An Introduction to Membraneless Fuel Cells 126
4.5.2 Hydrogen-rich *Ec*Hyd1/*Mv*BO Membraneless Fuel Cell 127
4.5.2.1 Characteristics of a Hydrogen-rich Membraneless Fuel Cell 127
4.5.2.2 The Effect of Adding a Second *Mv*BO Electrode 130
4.5.2.3 The Effect of CO on Fuel Cell Performance 132
4.5.3 Hydrogen-poor *Ec*Hyd1/*Mv*BO Membraneless Fuel Cell 134
4.5.3.1 Introduction to Low H_2 Fuel Cells 134
4.5.3.2 Characteristics of a Hydrogen-Poor Membraneless Fuel Cell 134
4.5.3.3 Recovery of Fuel Cell Performance using a Second Anode 137
4.6 Discussion 140
Chapter 5 Aldehydes as Reversible Inhibitors of H_2 Production by [FeFe]-Hydrogenases 147
Abstract 148
5.1 Introduction 149
5.1.1 Introduction to the [FeFe]-Hydrogenases 149

5.1.1.1 The Hydrogenases Studied 149
5.1.1.2 Bidirectional Catalysis 151
5.1.1.3 Anaerobic Inactivation to Form the H_{ox}^{inact} State 153
5.1.1.4 Sensitivity of [FeFe]-Hydrogenases Towards CO and O_2 155
5.1.2 Formaldehyde as an Inhibitor 156
5.1.2.1 Common Reactions of Formaldehyde 156
5.1.2.2 Previous Studies of Aldehyde Inhibition of Hydrogenases 158
5.1.2.3 Target Sites for Formaldehyde in [FeFe]-Hydrogenases 159
5.2 Detection of Inhibition using an Assay 160
5.3 Studies using Protein Film Electrochemistry 162
5.3.1 Experimental Design 162
5.3.2 Inhibition of H_2 Production 162
5.3.3 Inhibition of H_2 Oxidation 166
5.3.4 The Effect of the Direction of Catalysis on Inhibition 168
5.4 Formaldehyde Protection Against CO 168
5.5 Inhibition by Other Aldehydes 170
5.6 Discussion 170
Chapter 6 The Reactions of [FeFe]-Hydrogenases with Aldehydes as a Probe for the Mechanism of H_2 Production 173
Abstract 174
6.1 Introduction 175
6.1.1 The Aims of the Studies Outlined in this Chapter 175
6.1.2 Summary of the Redox States of [FeFe]-Hydrogenases 175
6.1.3 Proposed Mechanisms for [FeFe]-Hydrogenases 177
6.2 Detailed Studies of Aldehyde Inhibition 177
6.3 Potential Dependence of Formaldehyde Inhibition 177
6.4 Studies using Density Functional Theory (DFT) 178
6.5 Attempts to Ascertain if Alcohol is Produced 178
6.6 Discussion 178
Chapter 7 Materials and Methods 179
7.1 Working Electrodes 180
7.2 Electrochemical Cell 181
7.3 Gas Control 183
7.4 Electrochemical Apparatus 183
7.5 Buffer Solutions 183
7.6 Enzyme Preparation 184

7.6.1 *Ralstonia* Hydrogenases (*Re*MBH^{WT} and *Re*MBH$^{C19G/C120G}$) 184
7.6.2 *Escherichia coli* Hydrogenases (*Ec*Hyd1 and *Ec*Hyd2) 184
7.6.3 Bilirubin oxidase from *Myrothecium verrucaria* (*Mv*BO) 184
7.6.4 The [FeFe]-Hydrogenase *Dd*HydAB 185
7.6.5 The [FeFe]-Hydrogenases *Ca*HydA and *Cr*HydA1 185
7.7 Preparation of Hydrogenase Films 185
7.8 Activation of *Ec*Hyd1 and *Ec*Hyd2 186
7.9 Modification of Electrodes for *Mv*BO 186
7.10 Proton Exchange Membrane 188
7.11 Fuel Cell Measurements 189
7.12 Solution Assay 189
7.13 Buffer Exchange 190
7.14 Aldehydes 191
References 193
Appendices I
A1 Derivation of the Nernst Equation II
A2 Normalising Data to Account for Film Loss IV
A3 Derivation of Equation 3.1 V
A4 Derivation of Equations 3.2 and 3.4 VII
A5 Sequence Alignment for [NiFe]-Hydrogenases IX
A5.1 Small Subunit Alignment IX
A5.2 Large Subunit Alignment X
A6 Reversibility of Formaldehyde Inhibition XII
A7 Straight *vs.* Branched-chain Aldehydes XIII
A8 Determination of K_I XIV
A9 The Arrhenius Equation XVII
A10 The Eyring Equation XVIII
A11 Calculated Structures of States XX
A12 Long-term NMR Experiment XXI
A13 The Effect of Methanol on *Dd*HydAB XXII

Chapter 1 Introduction

1.1 Hydrogen as an Energy Solution

The 2010 Energy Outlook report by the U.S. Department of Energy predicts that world energy consumption is set to increase by 49% between 2007 and 2035.[1] However, currently around 80% of global energy demand is met by the consumption of fossil fuels,[2,3] which are non-renewable, and their combustion results in the release of gases including CO_2, which is now widely accepted to be a major contributor to climate change.[4] It is therefore necessary to reduce the use of these fossil fuels and move towards alternative renewable and 'clean' fuels; the UK is currently committed to reducing its greenhouse gas emissions by at least 80% by 2050, relative to 1990 levels.[5] This goal may be achieved in part through carbon capture and storage and by reduction of the overall energy demand by improved energy efficiency.[6]

In recent years, there has been considerable interest in the idea of creating a green 'hydrogen economy' to overcome the depletion of fossil fuels.[7-10] Despite the strong chemical bond in H_2 ($\Delta H_{\text{dissociation}} = 435.88$ kJ mol^{-1} at 25 ºC)[11], hydrogen atoms form even stronger bonds to oxygen. Therefore, H_2 and O_2 react cleanly and exothermically to produce water as the only by-product, making H_2 an attractive fuel. Acting as an energy carrier, H_2 could be used to store energy generated from renewable resources, such as wind, solar or tidal energy. The chemically-stored energy could then be released as required, for example through electricity generation using a hydrogen fuel cell.

Although fuel cells are generally considered a modern technology, Grove and Schoebein first demonstrated nearly two centuries ago a device in which electricity can be produced from H_2 and O_2 using Pt as the catalyst.[12,13] Fuel cells provide a clean and thermodynamically efficient means of converting chemical energy into electricity[14] and

allow H_2 to become an alternative fuel to petrol or diesel in transportation. A car incorporating a H_2/O_2 fuel cell was recently released by Honda; H_2 gas is stored under pressure in a tank before flowing to the fuel cell where it combines with O_2 from the atmosphere to generate electricity that is used to power the motor.[15] However, the widespread introduction of these H_2-powered cars would require a delivery infrastructure for H_2 refuelling. In fact, in order for H_2 to become a useful energy carrier, several major challenges must be overcome, including the development of methods for mass (renewable) production and safe and efficient storage of H_2.[10,16]

Despite being the most abundant element in the Universe, constituting 88.6% of all atoms,[11] hydrogen is not naturally available in its elemental form on Earth.[8] Instead, it usually exists in chemical compounds with other elements, and production of H_2 from these hydrogen-containing compounds requires considerable energy.[8,10] Molecular hydrogen is currently produced largely by steam reformation of non-renewable fossil fuels[9,10] and therefore, if H_2 is to become a widely used energy carrier, alternative methods for its production are required.

The reverse process of a fuel cell, the electrolysis of water to produce H_2 and O_2, was first demonstrated by Faraday in 1820.[17] Conventional electrolysis uses two electrodes (based on Ni, Pt or Pd) to generate O_2 at the anode and high purity H_2 at the cathode.[18] The electricity used to drive the electrolysis is usually derived from the combustion of fossil fuels, and therefore the process is both economically and environmentally costly. However, if the electricity can be provided by renewable resources, then the technique becomes cost-effective and provides a possible means of generating H_2 in a future green economy. It should be noted, nevertheless, that if low temperature electrolysis using Pt or

Pd in neutral pH were adopted on a mass scale, then the poor availability and high cost of the noble metal catalysts may become limiting; therefore electrolysis using the more abundant metal nickel for the electrodes may be preferable, although this would require alkaline conditions and elevated temperatures.[18,19]

Sunlight is a particularly attractive energy resource, since the amount of solar power reaching the Earth's surface exceeds the total human demand by a factor of ~1,500.[20] Photovoltaic cells are used to generate electricity from the energy provided by sunlight, and this electricity could then be used to drive the electrolysis of water to release H_2.[18] However, the most efficient photovoltaic cells contain monocrystalline silicon which is produced via a complicated and expensive process; dye-sensitised solar cells, although less expensive to produce, suffer low efficiencies to date.[18,21,22]

A more attractive target for H_2 production is 'artificial photosynthesis', which is inspired by biology, and is currently the focus of intensive research.[18,23-25] In an artificial photosynthetic system, fuel is generated by a reduction process that utilises photochemically excited electrons.[26] In an ideal case, sunlight would be used to photocatalytically split water to generate H_2 and O_2; the oxidation of O^{2-} to $\frac{1}{2}O_2$ replenishes the electrons used in the reduction of protons to form H_2 (the fuel).[23] The rate limiting factor in these water-splitting reactions is generally the activity of the H_2 and O_2 production catalysts, and their lack of specificity. Biological catalysts (enzymes) are in general highly active and specific for their substrate, and therefore may provide valuable insight for the development of new synthetic catalysts. As will be discussed in the following sections, nature has evolved highly efficient catalysts for H_2-cycling, known as hydrogenases, and these will be the focus of the work in this thesis.

1.2 Hydrogen in Biology

Utilising H_2 as a fuel is not without precedent; in nature, H_2 acts as an important energy source for many bacteria.[9] The level of H_2 in the Earth's lower atmosphere today is only around 0.5 parts per million by volume,[11] which is too low for H_2 to be taken up by microbes.[27] However, there are a number of biological processes by which H_2 can be produced. Photosynthetic bacteria, cyanobacteria and green algae such as *Chlamydomonas reinhardtii* produce H_2 photobiologically, using solar energy to convert water, reduced sulfur compounds or organic compounds into H_2.[28] Additionally, nitrogen-fixing microorganisms, such as *Rhizobium leguminosarum*, generate H_2 in a side-reaction during nitrogen fixation in the root nodules of plants.[9] Hydrogen may also be formed as a product of fermentation by bacteria such as *Clostridium acetobutylicum*; H_2 is evolved in order to remove the reducing equivalents (e^-) produced during the fermentation of sugars.[29]

Although H_2 is generated by many organisms, it does not accumulate because it is such a valuable energy carrier that as soon as it is released by one organism, it is used by another.[9] The cycling of H_2 in a submerged wetland soil environment is illustrated in Figure 1.1.[9,19,30] Oxidation of H_2 can be coupled to the reduction of a range of molecules, including O_2, nitrate and sulfate. Since O_2 is the strongest of these oxidising agents, it is the preferred choice for organisms. However, under anaerobic conditions the electrons produced from H_2 oxidation are used to reduce alternative compounds. For each type of microorganism in Figure 1.1, a representative reduction process that is coupled to H_2 oxidation is given.

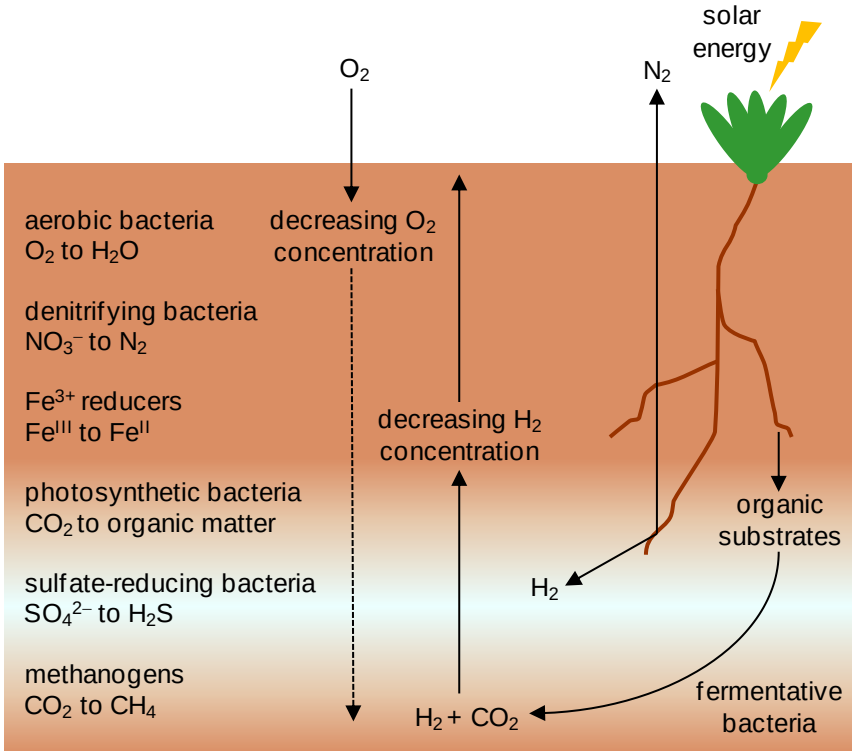


Figure 1.1. A schematic representation of the production and uptake of H_2 in a wetland soil environment. For each type of H_2-uptake organism, a representative reduction process that is coupled to the oxidation of H_2 is given. Figure adapted from references 9,30 and 19.

In the wetland soil environment depicted in Figure 1.1, O_2 and H_2 gradients exist; the level of O_2 decreases as the depth increases, while the level of H_2 increases with increasing depth.[30] The depletion of H_2 observed towards the surface can be explained as follows. The H_2 produced deep beneath the surface by anaerobic fermentation and N_2 fixation is mostly consumed by microorganisms such as methanogens (which couple the oxidation of H_2 to the reduction of CO_2 and acetate to form methane) that live deep within the soil.[9,27] This leaves a smaller quantity of H_2 available for diffusion towards the surface of the soil. Conrad *et al.*[30] discovered that for a bacterium the 'threshold' for H_2 (defined as the concentration below which H_2 cannot be consumed) decreases as the redox potential of the reduction reaction to which H_2 oxidation is coupled increases. Therefore, the H_2 thresholds of the bacterial species are expected to decrease with decreasing soil

depth, as the coupled reduction processes become more favourable (the reduction potential for the conversion of CO_2 to CH_4 is just -100 mV, compared to +800 mV for O_2 to water, both at pH 7).[19] Thus, sulfate-reducing bacteria, such as *Desulfovibrio desulfuricans*, which couple H_2 oxidation to the reduction of sulfate to sulfide, have a higher affinity (lower threshold) for H_2 than the methanogens. Further towards the surface, Fe^{3+}-reducers and denitrifying bacteria exhibit even lower thresholds for H_2, since the depleting level of H_2 means a higher affinity for this reducing agent is required in order to survive. The bacteria with the highest affinity for H_2 are found at the surface, where the H_2 concentration is lowest. A further challenge for these bacteria arises due to the fact that the top 1 to 5 mm of soil is oxic and therefore these bacteria must also survive in the presence of O_2.[30] These aerobic bacteria include Knallgas bacteria, such as *Ralstonia eutropha*, which couple H_2 oxidation to the reduction of O_2. These bacteria are of interest in technological applications, due to their unusual tolerance towards O_2 and their ability to function under low levels of H_2.

The interconversion of protons and H_2 (Equation 1.1) in biological processes is catalysed by hydrogenases.

$$2H^+ + 2e^- \rightleftharpoons H_2 \qquad [1.1]$$

These enzymes are abundant in the microbial world and the minimum fragment common to all hydrogenases is [Fe(CO)(CN)(RS)].[31] Different types of hydrogenases, which share no similarity in their genetic sequences, have arisen as a result of convergent evolution.[32] The three classes of hydrogenase are named according to the structure of their active sites; [NiFe]- and [FeFe]-hydrogenases contain bimetallic catalytic sites, and [Fe]-hydrogenases possess a mononuclear metal centre. The [NiFe]-hydrogenases are typically

involved in the oxidation of H_2, whereas [FeFe]-hydrogenases are more frequently associated with the reduction of protons.[33] These two classes will be discussed in detail in Sections 1.4 and 1.5. The [Fe]-hydrogenases, on the other hand, do not catalyse the direct oxidation of H_2 or reduction of protons. These FeS cluster-free hydrogenases are found in some methanogens and are H_2-forming methylenetetrahydromethanopterin dehydrogenases (Hmd hydrogenases) that couple production of H_2 to the oxidation (dehydrogenation) of N^5,N^{10}-methylene-5,6,7,8-tetrahydromethanopterin, or oxidation of H_2 to the reverse reaction.[34]

1.3 Techniques for Studying Hydrogenases

The characterisation of hydrogenases has involved a combination of different techniques. A common method for studying the activity of enzymes is to perform solution assays, which follow either the consumption of substrate or generation of product over time, using methods such as spectrophotometry and amperometry. This enables a specific activity of a hydrogenase sample to be calculated, and also allows the effects of inhibitors on the activity of the enzyme to be monitored. However, as will be discussed in Chapter 5, this technique is not suitable for studying the reversibility of inhibition by non-volatile small molecules and spectroscopic techniques are required to obtain structural infomation.

Precise structural information may be obtained from X-ray crystallography experiments, and crystal structures have now been solved for a number of hydrogenases in various states.[35-41] However, protons cannot be detected by crystallography and therefore limitations arise in determining the intermediates of catalysis for a H_2-cycling enzyme using this technique. Fourier Transform Infra-Red (FTIR) spectroscopy monitors the bond

stretching frequencies of the CO and CN^- ligands present in hydrogenases (which will be discussed in Sections 1.4.2 and 1.5.2), alterations in which are related to changes in charge density on the metal ions.[42] All paramagnetic and diamagnetic states can be studied using FTIR spectroscopy and this technique provided the first evidence for the identity of the CO and CN^- diatomic ligands in the active site.[43,44] Mössbauer spectroscopy is particularly useful for studying proteins such as hydrogenases that contain Fe (^{57}Fe). This technique provides information on the electronic structure of an Fe atom, its local environment and any changes that result from transitions to a different state.[45] Hydrogenases contain FeS clusters, as will be discussed in Sections 1.4.1 and 1.5.1, and alongside Electron Paramagnetic Resonance (EPR), Mössbauer spectroscopy has enabled the characterisation of the different redox states of these FeS clusters. The technique of EPR can also be used to detect paramagnetic states of the active sites, and can provide a wide variety of information including the oxidation state of a metal, its spin state, the type of ligands and the exchange coupling interactions with other metal centres. Electron Nuclear Double Resonance (ENDOR) is useful in the detection and characterisation of paramagnetic states of [NiFe]-hydrogenases, since measurements of the hyperfine coupling of the unpaired electron on Ni to magnetic ligand nuclei give detailed information about the electronic structure and geometrical arrangement.[46]

Information regarding the coordination number and geometry around the metal centres can be obtained by X-ray Absorption Spectroscopy (XAS) and X-ray Absorption Near Edge Spectroscopy (XANES).[47] Ligand changes cause smaller shifts in edge energies than those caused by metal-centred redox processes, and therefore XAS can be used to monitor changes in metal oxidation states, provided that no large changes in ligand environment occur. Extended X-ray Absorption Fine Structure (EXAFS) can be used to

determine the number and type of ligands surrounding the metal[45] and to calculate metal-ligand distances,[48] since the frequency of oscillations is directly related to the distance between the absorbing and back-scattering atoms involved.

Finally, Protein Film Electrochemistry (PFE) is a technique that measures the response of enzyme activity (measured as catalytic current) to changes in the potential experienced by the protein. Since the enzyme is immobilised onto an electrode surface, the same enzyme sample can be transferred between different solutions, allowing the removal of volatile and non-volatile inhibitors. The work outlined in this thesis was performed using PFE, and this technique is described in detail in Chapter 2.

1.4 The [NiFe]-Hydrogenases

1.4.1 The Overall Protein Structure

As will be discussed in Section 1.6.2, a major challenge for the future use of [NiFe]-hydrogenases in technological applications is that many are unable to sustain H_2 oxidation activity in the presence of O_2. Until very recently, crystal structures for only these 'standard' O_2-sensitive [NiFe]-hydrogenases, including those from *Desulfovibrio gigas* (*Dg*),[35,36] *Desulfovibrio fructosovorans* (*Df*)[49] and *Allochromatium vinosum* (*Av*)[38] had been obtained. However, the crystal structure has now been solved for an O_2-tolerant [NiFe]-hydrogenase, the membrane-bound hydrogenase (MBH) from *Ralstonia eutropha* H16 (*Re*, discussed in Chapter 3).[41]

The [NiFe]-hydrogenases include respiratory, H_2-sensing and NAD^+-reducing enzymes. The work in this thesis was performed on respiratory [NiFe]-hydrogenases, and therefore this discussion focuses on this type of hydrogenase. The respiratory [NiFe]-hydrogenases

are heterodimeric proteins, with a large subunit containing the catalytic site and a small subunit containing a chain of FeS clusters. The two subunits interact strongly with one another through hydrophobic interactions.[38] The active site is buried deep within the protein, and is 'wired' to the surface via the chain of FeS clusters. This FeS relay contains three clusters; in the case of the O_2-sensitive or 'standard' [NiFe]-hydrogenases, the proximal cluster, located closest to the active site is a [4Fe4S]-cluster, the medial cluster is a [3Fe4S]-species and the distal cluster, furthest from the active site, is a second [4Fe4S]-cluster. A representation of the crystal structure of the 'standard' O_2-sensitive [NiFe]-hydrogenase from *Df* is shown in Figure 1.2, and the approximate distances between the FeS clusters are given.

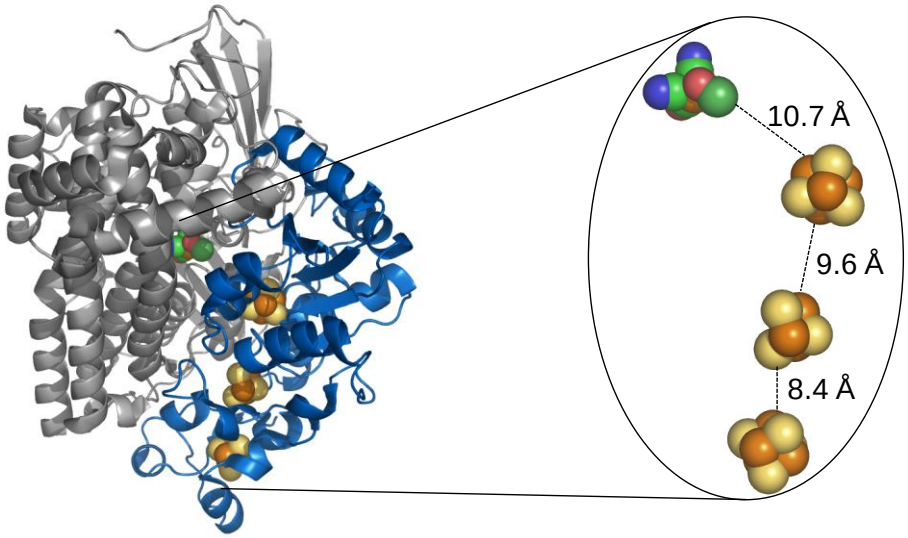


Figure 1.2. The structure of the [NiFe]-hydrogenase from *Desulfovibrio fructosovorans* (Protein Data Bank code 1YRQ) and an enlargement of the active site and FeS clusters with the distances between them shown (nearest atom to nearest atom, measured using PyMOL).

Importantly, the distances between the FeS clusters in [NiFe]-hydrogenases are small enough (< 14 Å) that the rate of electron tunnelling is sufficiently fast so as not to limit the rate of catalysis.[50] The exact nature of the FeS clusters present in the O_2-tolerant *Re*MBH will be discussed in Chapter 3. The crystal structures of the [NiFe]-hydrogenases

also reveal the presence of a Mg^{2+} cation close to the C-terminus, and a possible role for this metal ion will be discussed in Section 1.4.5.[38,51]

1.4.2 The [NiFe]-Active Site

The active site of a [NiFe]-hydrogenase consists of one Ni and one Fe atom (Figure 1.3).[19] The Ni atom is coordinated by four cysteine ligands, two of which are bridging to the Fe atom, which is itself further coordinated to three biologically unusual diatomic ligands, one CO and two CN^-.[44,52]

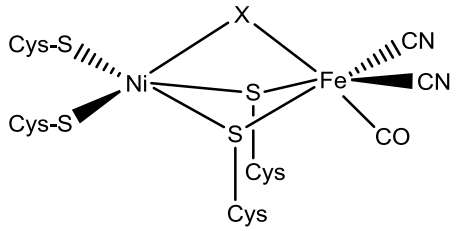


Figure 1.3. A representation of the active site of a [NiFe]-hydrogenase. The identity of the bridging X atom has been suggested to be a hydride in the active form of the enzyme, and an oxygenic or sulfur-based species in inactive states (see text).

In coordination chemistry, the '18-electron rule' is often used to predict the stability of organometallic compounds; thermodynamically stable transition metal compounds are expected to have a total of 18 metal valence electrons (including those supplied by the ligands).[53,54] Assuming the Fe atom to be in the +2 oxidation state, then in the absence of the ligand represented as X in Figure 1.3 this metal would have only 16 valence electrons. This Fe atom is therefore susceptible to attack and usually has this additional ligand. In the active form of the enzyme, it has been suggested that X may represent a hydride bridge (although this is too small to identify crystallographically); in the inactive form, this site may be occupied by an oxygen-based[36,55,56] or sulfur-based[51] ligand.

A sub-class of the [NiFe]-hydrogenases is comprised of hydrogenases in which one of the cysteine ligands to the Ni atom of the active site is replaced by a selenocysteine. Crystal structures have been obtained for two of these so-called [NiFeSe]-hydrogenases, from *Desulfomicrobium baculatum*[57] and *Desulfovibrio vulgaris* Hildenborough.[58] These hydrogenases contain three [4Fe4S]-clusters; the medial [3Fe4S]-cluster present in the [NiFe]-hydrogenases is replaced by a [4Fe4S]-cluster in the [NiFeSe]-hydrogenases.[57] In addition, whereas a Mg^{2+} cation has been identified in the [NiFe]-hydrogenases,[38,51] this ion is believed to be a transition metal (possibly Fe^{2+}) in the [NiFeSe]-hydrogenases.[57]

1.4.3 Active and Inactive States of [NiFe]-Hydrogenases

The [NiFe]-hydrogenases are able to cycle through a range of different redox states, which are believed to involve changes in the formal oxidation state of the Ni atom. Figure 1.4 outlines the different states identified for a 'standard' O_2-sensitive [NiFe]-hydrogenase and the interconversions between them.[59,60] Also included in the diagram are the routes of inactivation caused by common inhibitors, and these will be discussed in Section 1.6.[19]

The oxidation state of the Ni atom varies in the different redox states of the [NiFe]-hydrogenases,[45] while the Fe remains in the low spin Fe(II) state,[61] favoured by the strong field CO and CN^- ligands.[44] States that are EPR-active (paramagnetic, containing Ni(III) or Ni(I)) are indicated by an asterisk in Figure 1.4. Characterisation of the diamagnetic, EPR-silent (Ni(II)) states has been achieved using FTIR spectroscopy, which monitors shifts in the CO and CN vibrations.[44,62] Three active states of the enzyme have been identified: Ni-SI_a, Ni-C and Ni-R (indicated by the red box in Figure 1.4). A proton-coupled one electron reduction of Ni-SI_a forms the Ni-C state, which is believed to

contain Ni(III) and a bridging hydride (X = H^-).[63] This state is sensitive to light and upon illumination the active site loses the hydride to form the Ni-L state, which contains Ni(I) and is stable only at low temperature.[64] The Ni-C state can also react with CO, and the CO-bound state converts to Ni-L when exposed to light.[65] Reduction of the Ni-C state generates the Ni-R state, which is thought to contain Ni(II) with the bridging hydride still present. However, this state exists as a mixture of two or more isoelectronic forms that differ in their degree of protonation of either the coordinating cysteines or of the bound substrate.[65]

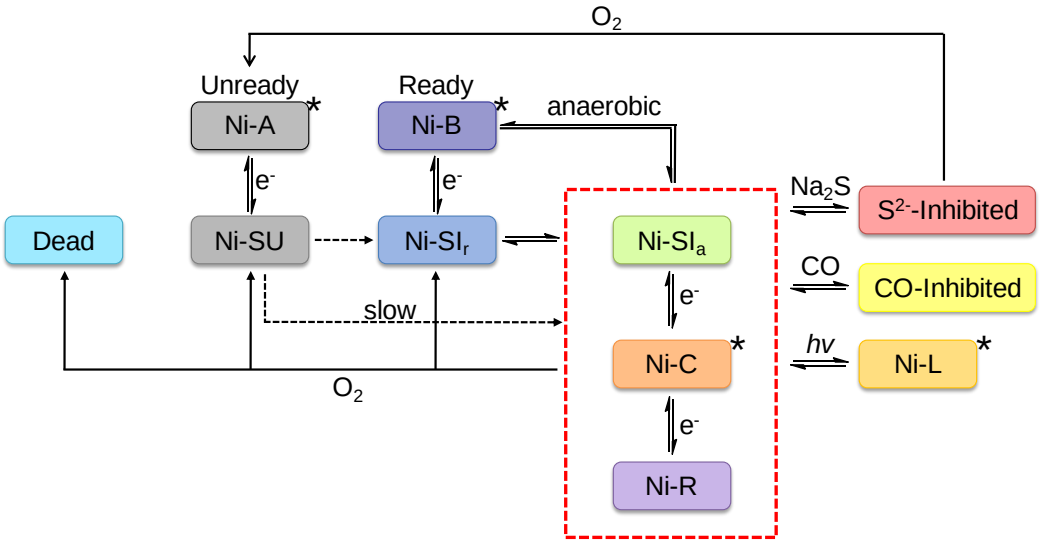


Figure 1.4. A schematic representation of the different redox states of a 'standard' [NiFe]-hydrogenase, and its reactions with various inhibitors to generate inactive states. The states within the red box are active states believed to be involved in the catalytic cycle and those states with an asterisk are paramagnetic and therefore EPR-active. Figure adapted from references 19, 59 and 60.

In the presence of O_2, standard [NiFe]-hydrogenases form the catalytically inactive states Ni-A (Unready) and Ni-B (Ready).[66] The Ni-B state can also be generated anaerobically at high potential and is thought to contain a bridging hydroxyl ligand in the active site.[43,67] There is evidence to suggest that the Ni-A state contains a peroxide bridging ligand, although there have also been suggestions that this state contains oxygenated sulfur

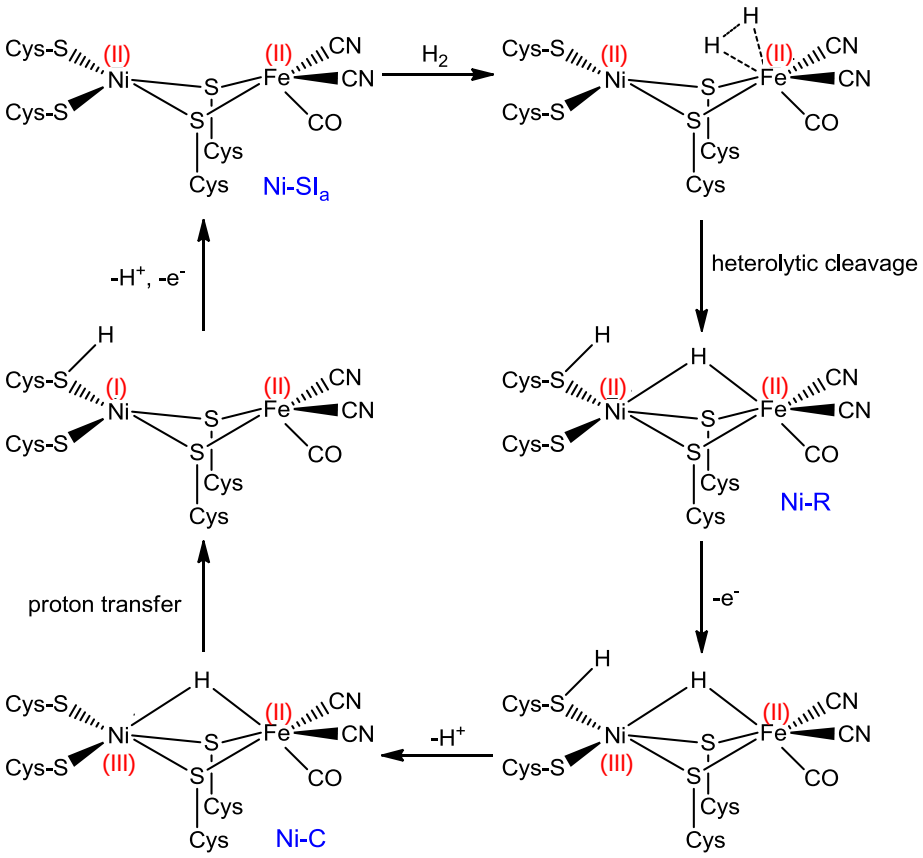
species.[60] The Ni-A and Ni-B states differ in their rates of reductive reactivation; the Ni-B state recovers rapidly, whereas reactivation of the Ni-A state is slow.[66] One electron reduction of the Ni-A and Ni-B states generates the Ni-SU and Ni-SI_r states respectively.[65] The Ni-SI_r state exists in two forms that are isoelectronic and interconverted by a proton; the $(Ni\text{-}SIr)_I$ state contains Ni(II) and Fe(II) coordinated by a hydroxide ligand, whereas the $(Ni\text{-}SI_r)_{II}$ state has a loosely coordinating water ligand.[65] Loss of the water (or hydroxide) ligand regenerates the active, Ni-SI_a state of the enzyme.[68] The reactions of [NiFe]-hydrogenases with O_2 will be discussed in more detail in Section 1.6.1 and Chapter 3.

1.4.4 Proposed Catalytic Cycle of a [NiFe]-Hydrogenase

The catalytic cycle of [NiFe]-hydrogenases is believed to involve the three states Ni-SI_a, Ni-C and Ni-R.[45,69] The most oxidised of these states, Ni-SI_a, does not contain the ligand X that is included in the illustration of the active site shown in Figure 1.3, and therefore this state is believed to bind H_2 during H_2 oxidation. To date, it is uncertain whether H_2 binds to the Ni or Fe atom.[70] The Ni(II) is only 4-coordinate and therefore may bind a H_2 molecule, which then undergoes heterolytic splitting to give H^+ and H^-.[65] Experimental evidence that suggests H_2 binds to the Ni rather than the Fe atom includes the observations that the inhibitor CO binds to Ni[39] and that the gas channel (discussed in the following section) ends closest to the Ni.[71] However, the Fe atom is less than 3 Å from the Ni atom, and therefore the location of the gas channel does not completely rule out binding to the Fe.[72] The spin state of the Ni(II) in the Ni-SI_a state is unknown, and recent studies using Density Functional Theory suggest that the mechanism may be explained by a two-state model in which H_2 can bind to both the Ni and Fe atoms.[70,73] The binding of H_2 to the Fe is favoured if the Ni(II) is high spin, and Keith *et al.* proposed that at high H_2

concentrations catalysis may be slowed by the binding of two H_2 molecules, one to each metal.[70] The authors also suggest that [NiFe]-hydrogenases may have more than one reaction pathway available, and therefore that catalysis may occur via different mechanisms depending on the conditions. Calculations using Density Functional Theory performed by Pardo *et al.* suggest that two different reaction pathways exist; one for H_2 oxidation and one for H_2 production.[72]

Although there is debate over which metal first binds the H_2 molecule, it is generally accepted that the next step involves heterolytic cleavage of the H_2 molecule to generate a hydride that bridges the Ni and Fe metal centres.[63] The cleavage of H_2 is assisted by a base, which may be a terminal or bridging cysteine ligand or a water molecule bound to the Fe.[63,74,75] One possible mechanism, proposed by Siegbahn *et al.* and proceeding via H_2 binding to the Fe, is shown in Scheme 1.1. In this proposed mechanism, the proton released from the heterolytic splitting of the H_2 molecule is transferred to one of the terminal cysteine residues on the Ni atom. This results in the Ni-R state with Ni(II) and a bridging hydride. The cysteine residue is deprotonated via the proton transfer pathway (discussed in the following section) and loss of an electron via the FeS relay generates the Ni(III)-containing Ni-C state. Regeneration of the Ni-SI_a state proceeds via loss of the hydride ligand as a proton (again transferred via the terminal cysteine) and oxidation of Ni(I) to Ni(II).



Scheme 1.1. One possible catalytic mechanism for [NiFe]-hydrogenases proceeding via H_2 binding to the Fe atom.[63] The Ni-SI_a, Ni-R and Ni-C states are labelled in blue. It should be noted that as drawn there will be an overall charge on the active site.

1.4.5 Gas and Proton Transport

Although the gaseous substrate (H_2) of hydrogenases is small, [NiFe]-hydrogenases contain gas tunnels that allow transport of this molecule through the enzyme to the active site.[60] Evidence for the presence of gas tunnels within these enzymes was obtained by exposing crystals of the [NiFe]-hydrogenase from *Df* to high-pressure Xe gas; ten Xe atoms were trapped inside the hydrophobic gas channels.[76] The locations of these Xe atoms were used as the starting points for molecular dynamics simulations of transport of Xe and H_2 through the protein. Although the bulky Xe atoms cannot reach the active site, the simulations suggest that H_2 can[71] and the H_2 molecules travelling along the gas tunnels reach the active site closer to the Ni atom than the Fe.[71,76]

Protons are both the product of H_2 oxidation and the substrate for H_2 production by [NiFe]-hydrogenases and therefore transport of this species between the active site and the protein surface is essential for catalysis. Several proton transfer pathways have been proposed for [NiFe]-hydrogenases; the pathway is relatively well-defined close to the active site, but further towards the protein surface the number of acidic and basic residues (including apartate, glutamate and histidine) and water molecules increases to such an extent that many proton pathways are available.[60,69] As mentioned in Section 1.4.1, crystal structures of the [NiFe]-hydrogenases reveal the presence of a Mg^{2+} cation close to the C-terminus of the large subunit.[38,51] Modelling studies based on *Df* and *Dg* [NiFe]-hydrogenases suggest that the network of hydrogen bonds between the active site and the Mg^{2+} may be involved in a proton transport pathway through the enzyme, as may water molecules coordinating the Mg^{2+} ion.[38,69,77,78]

1.5 The [FeFe]-Hydrogenases

1.5.1 The Overall Three Dimensional Structure

Only two [FeFe]-hydrogenases have been crystallised to date; the periplasmic HydAB from *Desulfovibrio desulfuricans* (*Dd*HydAB)[37] and hydrogenase-1 from *Clostridium pasteurianum* (*Cp*I).[40] The number of FeS clusters present within the protein varies between different [FeFe]-hydrogenases but the active site, known as the 'H-cluster' and discussed in more detail in the following section, is highly conserved.[60,79] The [FeFe]-hydrogenases can contain up to four subunits, although most are monomeric.[60] The structure of *Dd*HydAB, which is the only [FeFe]-hydrogenase studied in this work for which a structure is available, is shown in Figure 1.5. This hydrogenase has two subunits; the larger subunit contains the H-cluster and a ferredoxin-like domain containing two

[4Fe4S]-clusters, whereas the smaller subunit forms a 'belt' around the large subunit.[37,60] As discussed for the [NiFe]-hydrogenases, rapid electron transfer requires the distance between the centres in the electron transport relay to be < 14 Å.[50] The distances between the H-cluster and the additional FeS clusters indicated in Figure 1.5 are therefore sufficiently small to allow these redox centres to be involved in electron transport.[45,60]

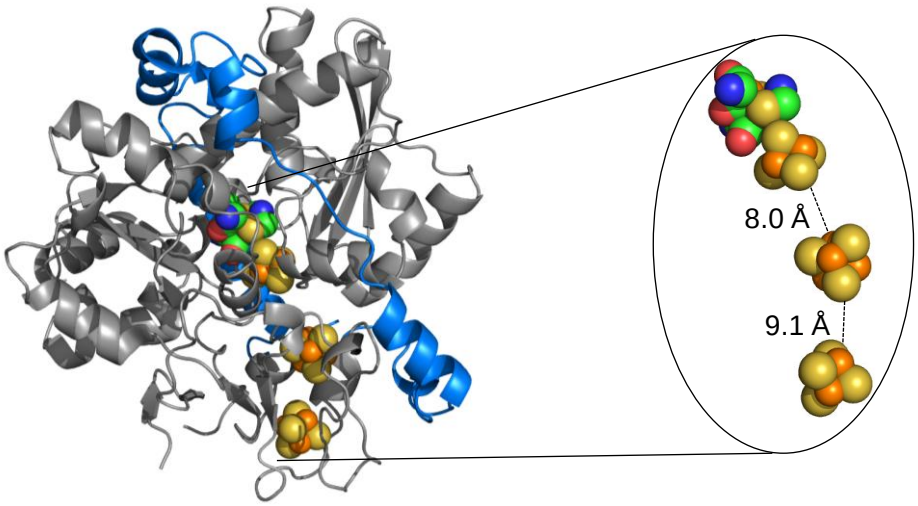


Figure 1.5. The structure of the [FeFe]-hydrogenase HydAB from *Desulfovibrio desulfuricans* (Protein Data Bank code 1HFE) and an enlargement of the active site and FeS clusters with the distances between them shown (nearest atom to nearest atom, measured using PyMOL).

The modelled structures of the other [FeFe]-hydrogenases studied in this work, *Clostridium acetobutylicum* HydA (*Ca*HydA) and *Chlamydomonas reinhardtii* HydA1 (*Cr*HydA1), are discussed in more detail in Chapter 5. Interestingly, the algal [FeFe]-hydrogenase *Cr*HydA1 contains only the H-cluster with no additional FeS clusters.[80,81]

1.5.2 The H-Cluster of [FeFe]-Hydrogenases

The active site of an [FeFe]-hydrogenase is a complex structure known as the 'H-cluster', as shown in Figure 1.6. The H-cluster contains a 2Fe moiety, in which each Fe is bound to at least one CO and CN^- ligand,[82,83] and a [4Fe4S]-cluster, which is attached to one of

the Fe atoms via a bridging cysteine.[45,60] This Fe atom is designated the proximal Fe, Fe_p, whereas the Fe atom further from the [4Fe4S]-cluster is known as the distal Fe, Fe_d.[83] The two Fe atoms are bridged by the two sulfur atoms of a non-protein 1,3-dithiolate ligand, which contains a bridgehead atom represented by X in Figure 1.6. Despite considerable debate about the identity (C, O or N) of the atom X,[40,84,85] the bridging dithiolate ligand has now been definitively assigned, using HYSCORE, as a di(thiomethyl)-amine (*i.e.* the bridgehead atom is the N atom of the secondary amine group, R_2NH).[86]

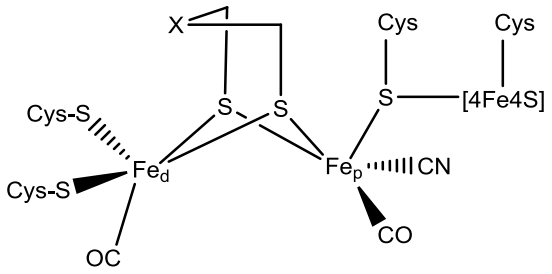


Figure 1.6. A representation of the active site (H-cluster) of an [FeFe]-hydrogenase. The bridgehead atom (X) of the dithiolate ligand bridging between the proximal (Fe_p) and distal (Fe_d) Fe atoms has been assigned as an N atom.

1.5.3 Redox States of [FeFe]-Hydrogenases

As described for the [NiFe]-hydrogenases in Section 1.4.3, the [FeFe]-hydrogenases are also able to cycle through different redox states. Figure 1.7 summarises the various redox states (differentiated by the metal-centred oxidation levels of the H-cluster) accessible to the H-cluster of an [FeFe]-hydrogenase.[19,45,87] Also included are the reactions of these hydrogenases with common small molecule inhibitors, which will be discussed in more detail in Section 1.6.

The diamagnetic H_{ox}^{inact} state is an inactive form of the enzyme that is obtained during the aerobic purification of some [FeFe]-hydrogenases, such as *Dd*HydAB.[45,88-90] In this 'over-oxidised' state, the two Fe atoms are most likely both low spin Fe(II) (due to the strong

field ligands CO and CN^-) and the FeS cluster moiety is in the $[4Fe4S]^{2+}$ state.[45,90-92] There is a bridging CO ligand and the vacant coordination site on the Fe_d atom is filled by H_2O or HO^-.[85,92,93] This inactive state can undergo a reversible one electron reduction to form a transient state, designated H_{trans}, in which the additional electron is believed to reside on the FeS cluster, $[4Fe4S]^{1+}$.[90,94] This state is EPR-active (as indicated by the asterisk in Figure 1.7) and the oxygenic species is assumed still to be bound to the Fe_d, although no crystal structure has been obtained for this state.[45] The H-cluster can then undergo an irreversible conformational change that favours transfer of the electron from the FeS cluster to the 2Fe moiety, to give a $[4Fe4S]^{2+}$ cluster and an $Fe_d(II)Fe_p(I)$ mixed valence state.[90,95] This state is known as H_{ox} and does not contain an oxygenic ligand bound at Fe_d. It has been suggested that the transition from H_{trans} to H_{ox} may involve two electrons, which could reduce a sulfenic acid group (Cys-SOH to Cys-SH) or a disulfide bond involving one or two of the thiol groups attached to the H-cluster.[93]

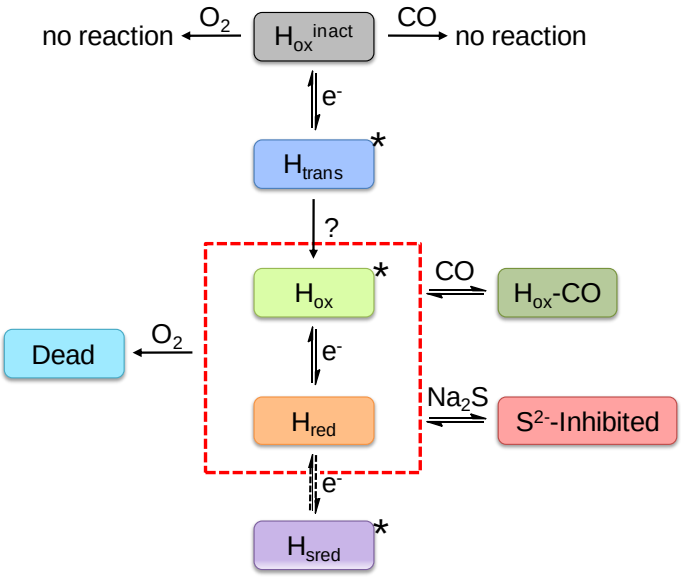


Figure 1.7. A schematic representation of the different redox states of an [FeFe]-hydrogenase, and its reactions with various inhibitors to generate inactive states. The states within the red box are active states believed to be involved in the catalytic cycle and those states with an asterisk are paramagnetic and therefore EPR-active. Figure adapted from reference 19.

A further one electron reduction of H_{ox} generates the EPR-silent H_{red} state, in which both Fe atoms are Fe(I).[45] For *Dd*HydAB, it has been shown that the bridging CO ligand moves to a terminal position on Fe_d in this state, although this is not the case for *Cr*HydA1.[85,87] It was reported by van Dijk *et al.* that oxidation back to H_{ox}^{inact} can only be achieved by a two electron oxidant in the presence of iron and EDTA.[96] However, PFE studies show that, for *Dd*HydAB and *Cr*HydA1, H_{ox}^{inact} can easily be generated by exposing the enzyme to an oxidising potential (discussed in Chapter 5).[97,98]

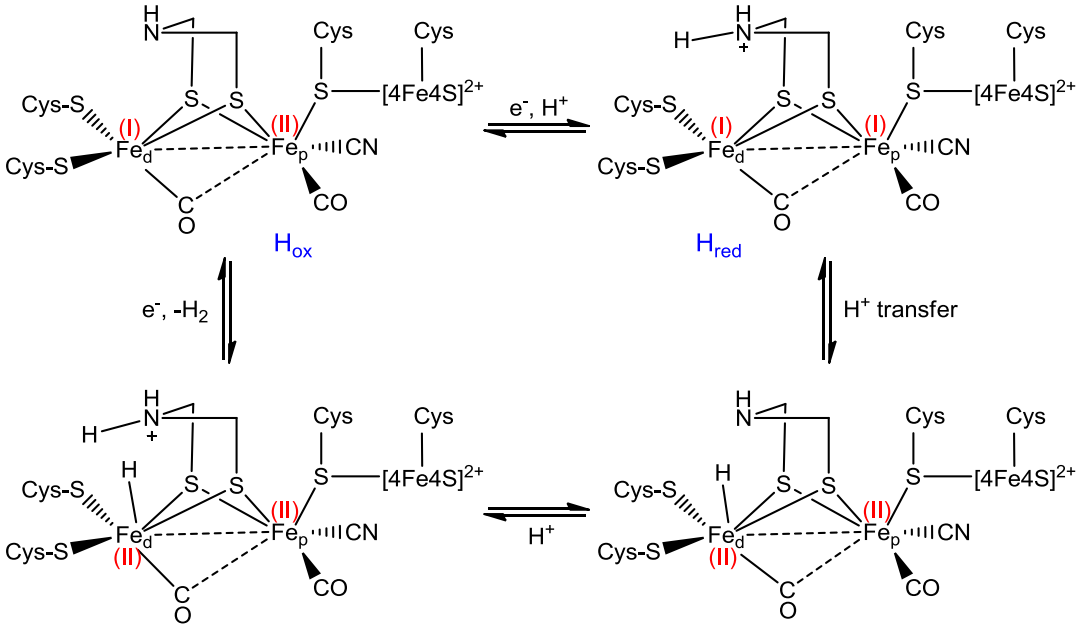
Upon further reduction, a 'super-reduced' state of the enzyme (H_{sred}) can be obtained. In this state, the additional electron is believed to reside on the FeS cluster at the active site to generate a $[4Fe4S]^{1+}$ cluster, with both Fe atoms in the 2Fe moiety in the Fe(I) state.[87,99] This species should therefore be EPR-active, although it has not been observed using this technique to date.

Studies by Roseboom *et al.* performed on *Dd*HydAB determined the midpoint potential of the H_{red}/H_{sred} couple to be ~-540 mV *vs.* the normal hydrogen electrode (NHE), measured at pH 8. The reduction was observed to be largely irreversible.[93] This was consistent with an earlier study which showed that the H_2 production activity of *Cp*I decreases significantly at very low potential (below -425 mV, pH 7).[100] However, studies using protein film electrochemistry have not observed a decrease in activity at very low potential[98,101] and investigations on *Cr*HydA1 using fourier transform infra-red (FTIR) spectroscopy have suggested that the H_{sred} state forms reversibly and that this state is relatively stable, unlike H_{ox} and H_{red}, which decay over time.[87] These studies also concluded that in the H_{sred} state the CO ligand resides in a terminal position on the Fe_d atom.[87] The midpoint potential obtained for the H_{red}/H_{sred} transition for *Cr*HydA1

(-460 mV *vs.* NHE, pH 8) is higher than that determined for *Dd*HydAB, despite the fact that the H_{ox}/H_{red} transition occurs at a similar potential (-400 mV *vs.* NHE).[87,93] The H-cluster itself is highly conserved between these two [FeFe]-hydrogenases, whereas the overall protein structure varies; *Cr*HydA1 lacks the FeS cluster electron transfer relay. The greater variation in the H_{red}/H_{sred} midpoint potential is therefore to be expected if the additional electrons reside on the FeS cluster, since the protein environment surrounding the [4Fe4S] cluster varies to a greater extent than that close to the 2Fe moiety.[87]

1.5.4 The Catalytic Cycle of [FeFe]-Hydrogenases

Most catalytic cycles proposed to date involve only two states of the [FeFe]-hydrogenases, H_{ox} and H_{red},[45,69,93,94] and one such mechanism is illustrated in Scheme 1.2.[45,69,102]



Scheme 1.2. A possible mechanism for H_2-cycling by an [FeFe]-hydrogenase, involving the H_{ox} and H_{red} states.[45,69,102] The H atom bound to the Fe_d(II) is assumed to be a hydride ligand.

In this mechanism, H_2 production (clockwise cycle in Scheme 1.2) proceeds via addition of a proton to the bridgehead N atom in the H_{red} state. The proton transfers to the distal Fe

atom (to form an Fe_d(II)-hydride) and the proximal Fe also formally becomes Fe_p(II).[91,92,103] The bridgehead N atom can then pick up a second proton that combines with the hydride on Fe_d to release H_2 and, with concomitant addition of an electron, regenerate the H_{ox} state.

However, this mechanism is not yet fully understood. As for the [NiFe]-hydrogenases, there is a possibility that H_2 oxidation and H_2 production may not follow the same pathway.[45] In addition, the mechanism outlined in Scheme 1.2 does not provide a role for the [4Fe4S]-cluster located within the H-cluster and recent studies (including those outlined in this thesis) suggest that a super-reduced state of the enzyme, two electrons below the H_{ox} state, may also play a role in the catalytic cycle.[87,104,105] Other possible mechanisms for H_2 production by [FeFe]-hydrogenases are discussed in detail in Chapter 6.

1.5.5 Gas and Proton Transport

The catalytic cycle outlined in the previous section assumes that H_2 binds to the Fe_d atom of the H-cluster. Evidence that this atom is the site of H_2 binding includes the observation that the crystal structures of *Dd*HydAB and *Cp*I both reveal the presence of a static hydrophobic gas channel that connects the Fe_d atom to the protein surface.[37,79] Experiments similar to those outlined in Section 1.4.5 have been performed in an attempt to trap Xe atoms inside this gas channel.[60] However, in the case of *Dd*HydAB [FeFe]-hydrogenase only one site is well-occupied by Xe; this site represents a large cavity that is connected to the distal Fe atom by a narrow tunnel. Computational studies based on *Cp*I have suggested that a dynamic gas channel may also exist, which meets the static tunnel at the large cavity.[106] Recent studies involving mutagenesis of certain residues along the

proposed static gas channel and central cavity found that alteration of these amino acids does not affect the kinetic properties of the enzyme.[107] This suggests that H_2 may in fact travel through transient dynamic channels or even along a conserved hydrophilic channel, although more research will be required to clarify the route for gas transport through [FeFe]-hydrogenases.[107]

It has been proposed that the bridgehead N atom present in the H-cluster may play a role in proton transfer in [FeFe]-hydrogenases.[85] This secondary amine can accept or release a proton (as shown in Scheme 1.2) and is sufficiently close to a conserved cysteine (Cys) residue (Cys178 in *Dd*HydAB or Cys299 in *Cp*I) to allow proton transfer between the bridgehead N atom and the S atom of the cysteine.[85] Recent computational studies have shown that a proton can be readily transferred from the cysteine residue to the di(thiomethyl)-amine bridging ligand provided that the 2Fe moiety is in a reduced $Fe_d(I)Fe_p(I)$ or 'super-reduced' H-$Fe_d(II)Fe_p(I)$ state.[105] This also supports the proposal that during catalysis a proton binds to Fe_d, as in the mechanism given in Scheme 1.2. A proton pathway has been identified from Cys178 or Cys299 to the protein surface in crystal structures of *Dd*HydAB and *Cp*I respectively.[40,85] Computational studies suggest that proton transfer occurs via a concerted mechanism, from glutamic acid (Glu) residue Glu159 to Glu156 via serine (Ser) residue Ser198, and then from Glu156 to Cys178 via a water molecule (*Dd*HydAB numbering).[105] A similar pathway is also proposed for *Cp*I.[105] An alternative proton pathway identified from the structure of *Dd*HydAB commences at the CN^- ligand bound to Fe_d and proceeds via the conserved residues lysine (Lys) 237 and Glu240. However, residue Glu245, which is involved in this proton transfer chain, is a non-conserved residue and this pathway also requires protonation of a CN^- ligand.[60]

1.6 Inhibition of Hydrogenases by Small Molecules

1.6.1 Hydrogen

Although H_2 is the substrate for H_2 oxidation by hydrogenases, this molecule can also act as a product inhibitor of H_2 production (H^+ reduction). The extent of product inhibition by H_2 depends on the type of hydrogenase;[31] [NiFe]-hydrogenases, normally associated with H_2 oxidation, suffer from significant product inhibition (their inhibition constants lie in the micromolar region),[108,109] whereas the [FeFe]-hydrogenases, more commonly regarded as H_2-producers, exhibit weaker product inhibition (their inhibition constants are in the millimolar range).[101] There have also been suggestions that H_2 may act as a substrate inhibitor of H_2 oxidation by [NiFe]-hydrogenases; two molecules of H_2 may bind, one to each metal atom of the active site, to slow the rate of catalysis[70] or excess H_2 molecules may block cavities involved in the gas transport channel.[110]

1.6.2 Oxygen

As mentioned in previous sections, hydrogenases are inhibited by O_2, which may limit the potential for their future use in biotechnological applications. The [FeFe]-hydrogenases are particularly sensitive to this inhibitor; the active states of these enzymes undergo irreversible damage by O_2, to form the 'dead' state as indicated in Figure 1.7. It has been proposed that the O_2 molecule initially binds to the 2Fe moiety of the H-cluster (most likely in the H_{ox} state), before causing irreversible damage to the [4Fe4S]-cluster via transfer of a reactive oxygen species or long-range oxidation.[111] However, the inactive H_{ox}^{inact} state of these enzymes does not react with O_2 and therefore acts as a 'resting' state that provides protection from this inhibitor. Therefore, certain [FeFe]-hydrogenases, such as *Dd*HydAB, can be purified aerobically in the H_{ox}^{inact} state.[19,89,112]

In contrast to the [FeFe]-hydrogenases, [NiFe]-hydrogenases undergo largely reversible inhibiton by O_2. As discussed in Section 1.4.3, the 'standard' O_2-sensitive [NiFe]-hydrogenases react with O_2 to form a combination of two inactive states; the Ni-B (Ready) state and the Ni-A (Unready) state.[66] The structure and characteristics of these states were introduced in Section 1.4.3 and will be discussed in more detail in Chapter 3. Also included in Figure 1.4 is a 'dead' state of the enzyme formed under aerobic conditions; reports suggest that even the [NiFe]-hydrogenases suffer a degree of irreversible activity loss during exposure to O_2.[66] This permanent damage may be due to oxidation of S atoms of cysteine residues close to the active site[19] or damage to FeS clusters.[66]

Importantly, certain [NiFe]-hydrogenases exhibit tolerance towards O_2; these enzymes are able to sustain catalytic activity under aerobic conditions.[113] To date, several O_2-tolerant [NiFe]-hydrogenases have been identified, including membrane-bound hydrogenases from *Ralstonia eutropha*,[97,114] *Ralstonia metallidurans*,[113] *Escherichia coli*[115] and *Aquifex aeolicus*.[59] The origins of this unusual O_2 tolerance is explored using the membrane-bound [NiFe]-hydrogenase from *Ralstonia eutropha* H16 (*Re*MBH) in Chapter 3.

1.6.3 Carbon Monoxide and Cyanide

The diatomic CO and CN^- ligands present in hydrogenases are highly unusual, since both molecules are commonly regarded as toxic. Carbon monoxide is a competitive inhibitor of the O_2-sensitive [NiFe]-hydrogenases and binds to the Ni atom of the enzyme to form a CO-inhibited state (Figure 1.4).[39,109,114,116] However, as will be discussed in more detail in Chapter 3, the O_2-tolerant [NiFe]-hydrogenases exhibit only weak CO inhibition.[114,115,117] The [FeFe]-hydrogenases are highly sensitive to CO; carbon monoxide reversibly inhibits

H_2 oxidation by these enzymes, but CO inhibition of H_2 production is largely irreversible.[101] As will be discussed in more detail in Chapters 5 and 6, CO is believed to target the H_{ox} state of the [FeFe]-hydrogenases, as demonstrated in Figure 1.7.[95,118,119]

The inhibition of hydrogenases by CN^- is less well understood. Studies on the [NiFe]-hydrogenase from *Azotobacter vinelandii* found that cyanide inhibition occurs to a greater extent when the hydrogenase is exposed to CN^- in the presence of air rather than H_2.[120,121] This led to the suggestion that only the oxidised form of the hydrogenase can bind exogenous CN^-.[121] Later work provided more evidence to support this proposal, by showing that the oxidised form of the hydrogenase is irreversibly inhibited by CN^- whereas reduced states are insensitive to this inhibitor.[122] However, recent preliminary electrochemical studies on purified [NiFe]-hydrogenases suggest that CN^- may, in fact, act as a reversible inhibitor of these enzymes.[123]

1.6.4 Sulfide

The crystal structure of the [NiFe]-hydrogenase from *Desulfovibrio vulgaris* Miyazaki F revealed the presence of a non-protein sulfur-species bridging the Ni and Fe atoms in the active site.[124] Exposure of the as-isolated hydrogenase to H_2 under reducing conditions resulted in the release of H_2S,[125] leading to the suggestion that exogenous sulfide may act as a reversible inhibitor of these enzymes. Electrochemical studies confirmed that sulfide is a reversible inhibitor of O_2-sensitive [NiFe]-hydrogenases, particularly when it exists as a neutral H_2S molecule.[126] However, although the [NiFe]-hydrogenases from the sulfate-reducing *Df* and *Dg* are inhibited by sulfide, the product of inhibition is only stable at high potentials that are unlikely to be reached *in vivo*.[31,126] The electrochemical data support the crystallographic evidence that sulfide binds in a bridging position as S^{2-} or

HS^- (analogous to the bridging HO^- in the Ni-B (Ready) state)[126] and pre-treatment of an O_2-sensitive [NiFe]-hydrogenase with sulfide prior to exposure to O_2 favours formation of only the Ni-A state (rather than the mixture of Ni-A and Ni-B states obtained in the absence of sulfide).[31,127] Importantly, the O_2-tolerant [NiFe]-hydrogenase *Re*MBH does not react with sulfide,[31,128] which may prove useful in biotechnological applications since commercially-produced H_2 often contains traces of H_2S.[129]

The [FeFe]-hydrogenase *Dd*HydAB also reacts with sulfide but this enzyme only reactivates at very low potentials.[128] Furthermore, the sulfide-inhibited state does not react with O_2 and sulfide therefore protects this [FeFe]-hydrogenase from O_2 damage.

1.6.5 Other Small Molecules

In 1954, Krasna *et al.* reported nitric oxide, NO, as an inhibitor of hydrogenases.[130] Later work discovered that this small molecule inhibits H_2 oxidation of the soluble hydrogenase from *Ralstonia eutropha* H16 in a partially reversible process.[131] Studies on this enzyme, along with others performed on the membrane-bound [NiFe]-hydrogenase from *Azotobacter vinelandii* showed that inhibition of the as-isolated enzyme under non-turnover conditions is irreversible.[131,132] It was proposed that NO does not bind at the active site, but instead may target the FeS clusters of the hydrogenase.[131,132] Recent electrochemical studies on the membrane-bound [NiFe]-hydrogenases from *Ralstonia eutropha* H16 and *Allochromatium vinosum* support the hypothesis that NO does not bind at the active site; inhibition does not depend on the H_2 concentration, thus suggesting that NO does not compete with H_2 for binding.[128]

Acetylene, HC≡CH, is a known reversible inhibitor of O_2-sensitive [NiFe]-hydrogenases.[133-135] In contrast to NO, which does not compete with H_2 for binding, the

presence of H_2 or CO protects the hydrogenase from inhibition by acetylene, suggesting that this small molecule binds at the NiFe active site.[128,135] As-isolated aerobically purified enzymes do not react with acetylene, but following reduction to an active state the [NiFe]-hydrogenase becomes susceptible to attack.[136] However, electrochemical studies have shown that two O_2-tolerant [NiFe]-hydrogenases (the membrane-bound hydrogenase from *Ralstonia eutropha* H16 and *Escherichia coli* Hydrogenase 1) are not inhibited by acetylene.[128] In addition, the [FeFe]-hydrogenases are insensitive to inhibition by acetylene,[128,137] which may be consistent with this small molecule binding at the Ni atom of the NiFe active site.[137]

Inhibition of hydrogenases by a further class of small molecules, the aldehydes (RCHO), is explored in the work presented in Chapters 5 and 6 of this thesis.

1.7 Technological Applications

Hydrogenases, or synthetic catalysts inspired by these enzymes, may find use in various (bio)technological applications. In order for H_2 to become a viable energy carrier, it must be producible on a large scale from renewable energy sources and without the use of expensive precious metal catalysts. In biology, H_2 production can be achieved via dark fermentation processes (ideally using waste materials as the substrate) or photobiological H_2 production, which generates H_2 using energy from sunlight.[138,139] The latter occurs naturally in purple photosynthetic bacteria, green algae and cyanobacteria, although studies have shown that efficient H_2 evolution by cyanobacteria requires genetic engineering to create mutants that are unable to re-oxidise the H_2 that is produced.[138,140,141] An artificial complex capable of light-driven H_2 production was created by the successful fusion of the MBH from *Re* to the cyanobacterial

Photosystem I.[142] Other systems capable of photobiological H_2 production have involved photoelectrochemical cells with hydrogenase-modified cathodes,[143-145] or the adsorption of hydrogenase onto semiconducting particles with[146] or without[147-149] the co-adsorption of a ruthenium dye.

It has also been proposed that hydrogenases, or their synthetic analogues, may replace Pt as the H_2 oxidation catalyst in H_2/O_2 fuel cells. However, despite the demonstration that an O_2-tolerant hydrogenase can be used as the anodic catalyst in a fuel cell capable of generating electricity from a mixture of just 3% H_2 in still air,[113] there have been very few other demonstrations of fuel cells containing hydrogenases. A summary of the hydrogenase fuel cell studies performed to date is given in Chapter 4.

Other more niche applications of hydrogenases include implantable devices and biosensors.[150,151] For instance, a successful H_2 biosensor was produced by immobilising a hydrogenase between clay and poly(butylviologen) on a glass carbon electrode.[152] Another possible application involves the electronic coupling of pairs of complementary redox enzymes via their attachment to a conducting particle in order to generate a heterogeneous catalyst that couples a specific oxidation reaction to a reduction process.[153] In one example, co-adsorption of hydrogenase and carbon monoxide dehydrogenase onto graphite platelets generated a catalyst capable of catalysing the water gas shift reaction, which converts CO and water into CO_2 and H_2, and is used to remove CO (which poisons Pt)[154] from industrially produced H_2.[155] Hydrogenases may also prove useful in the otherwise costly regeneration of NADPH (nicotinamide adenine dinucleotide phosphate), using H_2 as the substrate and producing protons as the only by-product.[139,156]

For many technological applications, such as fuel cell catalysis or immobilisation onto semiconductors for photo-H_2 production, it is desirable to reduce the 'footprint' of the hydrogenase on the surface by removing the protein backbone. As a consequence, much research has been performed on producing synthetic catalysts that mimic the active sites of hydrogenases.[157,158] However, producing bimetallic functional mimics has proved challenging; structural mimics of the [NiFe]- and [FeFe]-hydrogenases generally exhibit only slow catalytic activity that requires significant overpotentials, and these synthetic compounds often have low turnover numbers and are susceptible to rapid decomposition.[158-160] One possible cause for the poor performance of synthetic analogues is that the catalytic centres of these relatively small compounds lack the protein environment provided by hydrogenases. One very recent example of a bioinspired H_2 production electrocatalyst contains a single nickel atom and utilises a pendant amine base, similar to the bridgehead N atom present in [FeFe]-hydrogenases, to facilitate proton transfer.[161,162] This catalyst exhibits a very high turnover frequency for H_2 production (above 100,000 s^{-1}), although the overpotential required is greater than for hydrogenases.[162] Such advances in the synthesis of hydrogenase-inspired catalysis opens the possibility that, as the understanding of the structure and mechanism of hydrogenases improves, more efficient biomimetic H_2-cycling catalysts may be developed in the future.

1.8 Outline of this Thesis

The work outlined in this thesis investigates the inhibition of hydrogenases by small molecules using Protein Film Electrochemistry (described in detail in Chapter 2). The first half of the thesis focuses on H_2 oxidation by [NiFe]-hydrogenases; specifically, the O_2-tolerant membrane-bound hydrogenases from *Ralstonia eutropha* H16 (*Re*MBH,

Chapter 3) and *Escherichia coli* (*Ec*Hyd1, Chapter 4). Chapter 3 presents studies into the origins of the O_2 tolerance exhibited by *Re*MBH, with a focus on reactivation kinetics and the role of a modified proximal FeS cluster. Chapter 4 explores the influence of the reactions of even an O_2-tolerant hydrogenase with O_2 on the power characteristics of an enzymatic fuel cell utilising *Ec*Hyd1 as the anodic catalyst.

The second half of the thesis concentrates on H_2 production by [FeFe]-hydrogenases. Chapters 5 and 6 present detailed studies of aldehyde inhibition of these hydrogenases, however some of these results cannot currently be made freely available as they are to be published at a later date in academic journals. Experimental materials and methods are provided in Chapter 7.

Chapter 2 Electrochemical Theory

2.1 Introduction to Protein Film Electrochemistry

Protein Film Electrochemistry (PFE) is a technique in which a small sample of redox enzyme is immobilised onto an electrode surface as a mono/submonolayer film.[163] The protein is 'wired' to the electrode, allowing fast electron transfer, and the electrode acts as the source or sink for electrons. Throughout this thesis, the enzyme molecules are adsorbed onto the surface of pyrolytic graphite edge-plane electrodes, as described in detail in Chapter 7. A cartoon representation of a hydrogenase molecule, immobilised onto an electrode and in contact with a solution containing H_2 and protons, is shown in Figure 2.1.

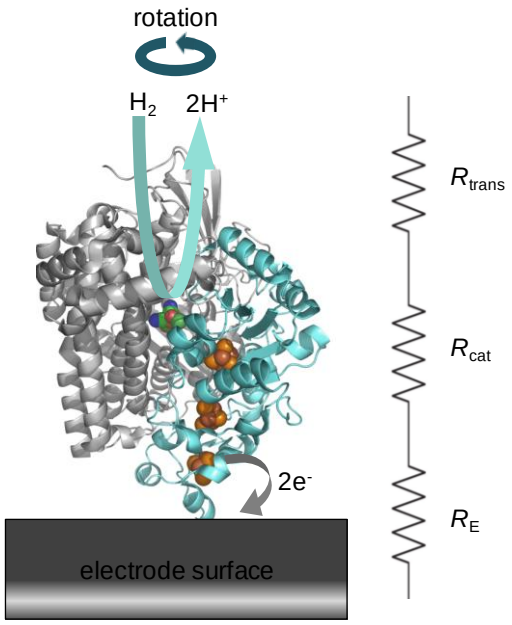


Figure 2.1. A schematic representation of a hydrogenase molecule adsorbed onto a rotating disk electrode. Catalytic electron flow through the enzyme can be regarded as passing through a series of resistors[164]: R_E, corresponding to interfacial electron transfer; R_{cat}, representing electron transfer through the enzyme itself and R_{trans}, which reflects the rate at which substrate moves to the electrode surface.

During PFE experiments, the potential experienced by the enzyme is precisely controlled, and can be varied rapidly. The rate of catalysis (turnover) is proportional to

the measured current. Since the enzyme molecules are confined to the electrode surface, complications involving their diffusion to the electrode are removed.[163] This electrochemical technique enables large numbers of experiments to be performed on very small samples of protein (typically less than a picomole of enzyme is adsorbed onto the electrode surface)[19] and therefore is particularly useful for the study of hydrogenases, for which preparation is time-consuming and yields are often low.[9] One enzyme film may be transferred between solutions of varying composition or pH. Both cyclic voltammetry (potential sweep) and chronoamperometry (potential step) experiments can be performed and the electrode can be rotated in order to provide a continuous supply of substrate to (and removal of product from) the electrode surface.

Catalytic electron flow through the enzyme is linked in series to the rate of transport of substrate to the enzyme, and to the rate of interfacial (electrode-enzyme) electron exchange.[19] Each step can be regarded as a resistor,[164] as indicated in Figure 2.1, and the total resistance, R_{tot}, is given by the sum of the three resistances, R_E, R_{cat}, and R_{trans} (Equation 2.1):

$$R_{tot} = R_E + R_{cat} + R_{trans} \qquad [2.1]$$

In order to study the inherent properties of the enzyme, corresponding to R_{cat}, it is necessary to minimise R_E and R_{trans}.[165] The resistance R_E corresponds to interfacial electron exchange between the electrode and the protein and is affected by both the extent to which the redox centres are buried and the strength of electrical contact between the enzyme and the electrode surface. Electron transfer is efficient only if the enzyme molecules are correctly orientated on the electrode; electron transfer is only rapid over distances < 14 Å[50] and therefore an enzymatic electron transfer site must be

within this distance of the electrode surface for the process to be fast. The term R_{trans} in Equation 2.1 is dependent on the rate at which substrate moves towards the electrode surface (and the rate of product diffusion away from it). This mass transport can be controlled by rotating the electrode at high speeds, as discussed in detail in Section 2.3.5.

2.2 The Three-Electrode System

For non-microelectrode studies, the voltage, E, applied between the working and reference electrode, (assuming that a finite current, i, flows between them), is given by the following equation:

$$E = (\emptyset_w - \emptyset_s^w) + iR_s + (\emptyset_s^{ref} - \emptyset_{ref}) \quad [2.2]$$

where R_s is the solution resistance, $\emptyset_w$ and $\emptyset_{ref}$ are the electric potentials of the working and reference electrodes, and $\emptyset_s^w$ and $\emptyset_s^{ref}$ represent the electric potential of the solution close to the working and reference electrodes respectively. Protein Film Electrochemistry experiments involve the measurement of current as a function of changes in the potential difference at the working electrode and solution interface, $(\emptyset_w - \emptyset_s^w)$. The potentiostat fixes the potential between the working electrode and a reference electrode, such as a saturated calomel electrode, for which $(\emptyset_s^{ref} - \emptyset_{ref})$ has a precisely known value. The reference electrode provides a constant value for $(\emptyset_s^{ref} - \emptyset_{ref})$, and therefore changes in the applied potential are reflected as changes in $(\emptyset_w - \emptyset_s^w)$ (*i.e.* at the working electrode and solution interface).

However, for a two-electrode system, significant current may be drawn through the reference electrode, leading to significant changes in the potential difference between

the reference electrode and the solution, ($Ø_s^{ref}$-$Ø_{ref}$), and an additional factor, iR_s. This term reflects the electrical resistance of the bulk solution between the working electrode and the reference electrode, which opposes the flow of current between these two electrodes. In order for the applied potential to reflect only ($Ø_w$-$Ø_s^w$), experiments are therefore performed using a three-electrode system, as shown in Figure 2.2.

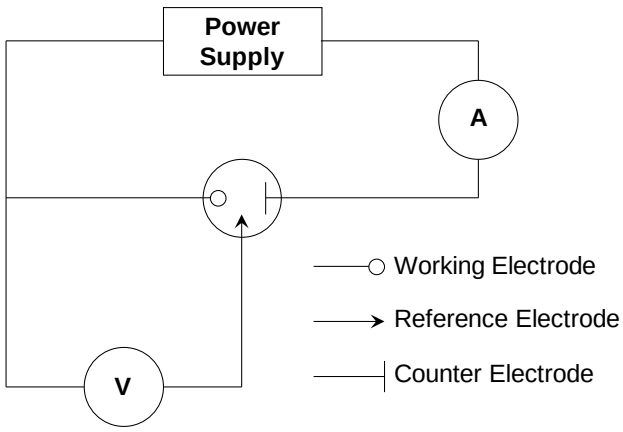


Figure 2.2. A diagram showing the three-electrode system, adapted from reference 166.

The potential of the working electrode, relative to that of the reference electrode, is monitored using a device with a high internal resistance, so that the current drawn through the reference electrode remains negligible, and its potential remains constant. Current instead flows between the working electrode and the third electrode, known as the counter electrode, which is poised by the potentiostat at the potential required to balance the current induced to flow through the working electrode.[167] In the work outlined in this thesis, a Pt wire was used as the counter electrode.

2.3 Cyclic Voltammetry

2.3.1 An Introduction to Cyclic Voltammetry

In cyclic voltammetry, the potential of the working electrode ($Ø_w$-$Ø_s^w$) is swept back and forth between two potentials, E_1 and E_2, at a chosen scan rate.[165] This produces a

triangular potential cycle with respect to time, as shown in Figure 2.3A for a scan rate of 10 mV s^{-1}. Using this technique, current is measured as a function of the applied potential (Figure 2.3B). The period during which the applied potential increases can be referred to as the oxidative scan; a decreasing applied potential corresponds to the reductive scan, as illustrated by the arrows in Figures 2.3A and B.

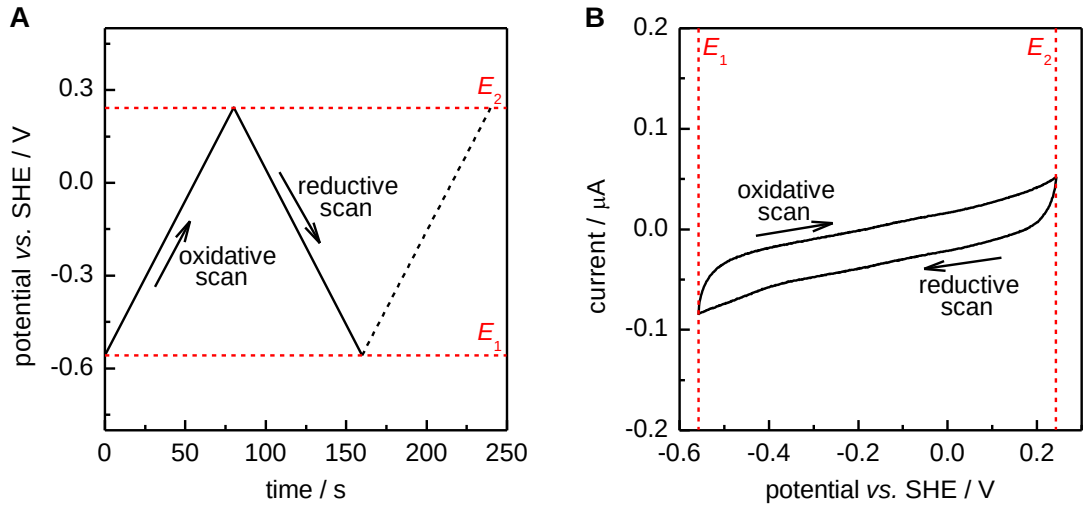


Figure 2.3. (A) Shows the variation in applied potential (between E_1 and E_2) with time and (B) displays the non-Faradaic current produced by a blank, unmodified pyrolytic graphite edge-plane rotating disk electrode, as a function of potential over the same range.

2.3.2 Non-Faradaic Current

The current recorded during a cyclic voltammogram can simplistically be viewed as comprising two components: Faradaic and non-Faradaic current. The non-Faradaic current, which gives rise to the cyclic voltammogram of a blank, unmodified electrode as shown in Figure 2.3B, occurs as a result of the electrode surface and solution interface charging like a capacitor as the applied potential is varied. Charge cannot cross the electrode-solution interface for a blank electrode with no electroactive species, and therefore charge accumulates at the electrode surface and in solution. For a given applied potential, the charge at the electrode surface, q_m, is equal in magnitude

but opposite in sign to that of the solution, q_s, as favourable electrostatic interactions occur between the electrode and electrolytes in solution (*i.e.* $q_m = -q_s$).[165,166] The charge in the solution arises primarily due to an excess of either cations or anions (depending on the charge of the electrode) close to the electrode surface, resulting in an electrical double layer and a potential difference across the two layers of charge. As the applied potential is varied, the charges at the electrode-solution interface rearrange, resulting in current flow between the working and counter electrode. The electrode-solution interface therefore behaves like a capacitor. The charge on a capacitor, q, is given by the product of the potential across the capacitor, E, and the capacitance, C:

$$q = EC \qquad [2.3]$$

The charging current, i, is given by the change in charge with respect to time:

$$i = \frac{\mathrm{d}q}{\mathrm{d}t} = C\frac{\mathrm{d}E}{\mathrm{d}t} = Cv \qquad [2.4]$$

The change in potential with time is equivalent to the scan rate, v, in a cyclic voltammetry experiment. Therefore, it is clear that the size of the charging (or capacitive) current increases with scan rate.[166] It should also be noted that complex chemistry occurring at the surface of pyrolytic graphite edge-plane electrodes may appear as effective capacitance.

2.3.3 Faradaic Current

Faradaic current is a consequence of the reduction or oxidation of redox active species, leading to electron transfer at the electrode surface. During cyclic voltammetry experiments, the currents arising from these redox processes are superimposed on the

non-Faradaic currents caused by the blank, unmodified electrode (Figure 2.3B), which can therefore be regarded as a background current.

Under equilibrium conditions, there is no net flow of electrons and the ratio of the concentrations of reduced to oxidised species adsorbed on the electrode surface is given by the Nernst equation (Equation 2.5, derived in Appendix A1)[168,169]:

$$E_{eq} = E^{o} - \frac{RT}{nF} \ln Q \qquad [2.5]$$

where E_{eq} is the equilibrium potential, E^{o} is the standard reduction potential for the redox couple, R is the gas constant, T is temperature in Kelvin, n is the number of electrons involved in the process, F is Faraday's constant and Q is the reaction quotient, corresponding to the ratio of reduced to oxidised species.

However, in dynamic electrochemistry experiments, a potential is applied which induces a current to flow. For a redox enzyme adsorbed onto an electrode in a PFE experiment, this current provides a measure of the catalytic activity of the enzyme. However, it is important to recognise that the inherent activity of the catalytic centre is not the only factor that contributes to the overall activity of the enzyme-modified electrode; the rate of electron transfer to and from the electrode and mass transport of substrate to the enzyme also affect the magnitude of the measured current (as illustrated by the inclusion of resistors R_E and R_{trans} respectively in Figure 2.1).[19] These contributions to the observed current are discussed in the following sections.

2.3.4 Interfacial Electron Transfer

The Butler-Volmer equation describes the potential dependence of the rate of electron transfer in a redox reaction. This equation can be derived by considering the following simple, general reaction[165]:

$$O + ne^- \underset{k_{ox}}{\overset{k_{red}}{\rightleftharpoons}} R$$

where O and R represent two chemical species adsorbed onto an electrode surface, that are interconverted by the transfer of n electrons (e^-). The rate constants k_{red} and k_{ox} correspond, respectively, to the first-order rate constants for the reduction and oxidation processes.

The electrical current recorded for a process is a measure of the rate at which electric charge flows. This depends on the surface area of the electrode, A, the charge being transported (represented by the charge per mole of electrons, given by Faraday's constant, F), and the flux of electrons, j, which can be regarded as the number of electrons reaching the electrode surface per second. Therefore, the currents arising from the reduction (i_{red}) and oxidation (i_{ox}) processes are given by Equations 2.6 and 2.7 respectively:

$$i_{red} = FAj_{red} \quad [2.6]$$

$$i_{ox} = FAj_{ox} \quad [2.7]$$

The fluxes for the reduction and oxidation process are given by Equations 2.8 and 2.9:

$$j_{red} = nk_{red}\Gamma_O \quad [2.8]$$

$$j_{ox} = nk_{ox}\Gamma_R \quad [2.9]$$

where n is the number of electrons, and Γ_O and Γ_R are the electroactive coverages of oxidised or reduced species per unit area. The net current (i) flowing for the overall reaction is given by $i = i_{ox} - i_{red}$. Substituting the expressions for j_{red} and j_{ox} into those for i_{red} and i_{ox} therefore yields:

$$i = nFA(k_{ox}\Gamma_R - k_{red}\Gamma_O) \qquad [2.10]$$

Transition State Theory[170] (TST) assumes that the reagents form an activated complex (transition state) before proceeding to generate the products.[171] The activated complex is assumed to be in equilibrium with the reagents before forming the products, and the equilibrium constant for formation of the activated complex is denoted $K^{\ddagger}$. Using $\Delta G^{\ddagger} = -RT\ln K^{\ddagger}$, TST predicts the rate of a reaction to be given by Equation 2.11:

$$k = A_p \exp\left(\frac{-\Delta G^{\ddagger}}{RT}\right) \qquad [2.11]$$

where A_p is a constant pre-exponential factor and $\Delta G^{\ddagger}$ is the free energy of activation.

As discussed in the previous section, at equilibrium (corresponding to the equilibrium potential, E_{eq}), no current flows. Therefore, in order to drive the electrode reaction and induce current flow, a potential that is different from E_{eq} must be applied. The overpotential, η, is defined as the difference between the applied potential, E, and E_{eq} (*i.e.* $\eta = E - E_{eq}$).

The rate of a reduction (k_{red}) or oxidation (k_{ox}) process depends on the potential applied and also on the transition coefficient, α, which describes the sensitivity of the transition state to changes in potential. The value of α lies in the range 0 to 1; a value close to 0 implies that the transition state closely resembles the reactants, whereas values close to

1 represent a transition state similar to the products. The value of α is usually ~0.5, corresponding to a transition state with intermediate characteristics.[165] Incorporating these dependencies into the rate equation given by Equation 2.11 yields Equations 2.12 and 2.13 as the expressions for k_{red} and k_{ox} respectively:

$$k_{red} = A_p \exp\left(\frac{-\Delta G^{\ddagger}_{red}}{RT}\right) \exp\left(\frac{-\alpha n F(E-E_{1/2})}{RT}\right) \quad [2.12]$$

$$k_{ox} = A_p \exp\left(\frac{-\Delta G^{\ddagger}_{ox}}{RT}\right) \exp\left(\frac{(1-\alpha) n F(E-E_{1/2})}{RT}\right) \quad [2.13]$$

In these equations, $E_{1/2}$ is defined as the reduction potential of the redox couple under the conditions of interest. These equations can be simplified to Equations 2.14 and 2.15 by defining $k_{o,red}$ and $k_{o,ox}$ as the first exponential terms of the expressions for k_{red} and k_{ox} respectively:

$$k_{red} = k_{o,red} \exp\left(\frac{-\alpha n F(E-E_{1/2})}{RT}\right) \quad [2.14]$$

$$k_{ox} = k_{o,ox} \exp\left(\frac{(1-\alpha) n F(E-E_{1/2})}{RT}\right) \quad [2.15]$$

Since $k_{o,red} = k_{o,ox} = k_o$ under standard equilibrium conditions, and $k_{o,red}$ and $k_{o,ox}$ are independent of the potential, substitution of Equations 2.14 and 2.15 into Equation 2.10 yields Equation 2.16:

$$i = nFAk_o \Gamma_R \exp\left(\frac{(1-\alpha) n F(E-E_{1/2})}{RT}\right) - nFAk_o \Gamma_O \exp\left(\frac{-\alpha n F(E-E_{1/2})}{RT}\right) \quad [2.16]$$

At equilibrium, $i = 0$ and therefore:

$$nFAk_o\Gamma_R\exp\left(\frac{(1-\alpha)nF(E_{eq}-E_{1/2})}{RT}\right)=nFAk_o\Gamma_O\exp\left(\frac{-\alpha nF(E_{eq}-E_{1/2})}{RT}\right)=i_o \quad [2.17]$$

where i_o is the exchange current, which represents the balanced Faradaic oxidation and reduction currents contributing to the net zero current. By dividing the two expressions for i_o by the exponential terms containing $(E_{eq}-E_{1/2})$, expressions for the products $nFAk_o\Gamma_R$ and $nFAk_o\Gamma_O$ can be obtained and substituted into Equation 2.16 to yield the Butler-Volmer equation (Equation 2.18), which describes the variation in current as a function of the overpotential, η:[166]

$$i = i_o\exp\left(\frac{(1-\alpha)nF\eta}{RT}\right)-i_o\exp\left(\frac{-\alpha nF\eta}{RT}\right) \quad [2.18]$$

A large value of the exchange current, i_o, corresponds to a reversible electrode process; only a small overpotential is required to induce current flow and the observed current is due to both the reductive and oxidative processes except at very large overpotentials. In contrast, a small i_o results in an irreversible process; such a large overpotential is required to induce current flow that when one exponential term (for example corresponding to k_{red}) is significant, the other (k_{ox}) tends to zero. The value of α can be determined for such an irreversible process using Tafel Analysis, which involves plotting ln(i) against potential.[165]

An alternative method for determining the rate of electron transfer uses Marcus Theory. This model predicts that electron transfer will be fast if the oxidised and reduced species are similar in terms of geometry and solvation.[165] According to the Franck-Condon principle, nuclei can be assumed to be stationary over the time frame of electron transfer.[168] Additionally, the reduced product must be formed with an energy

equal to that of the sum of the energies of the electron and the oxidised species. Therefore, the oxidised species must be energetically excited to the transition state prior to electron transfer. The energy required to form this transition state increases as the difference in molecular geometry and solvation between the oxidised and reduced species increases. This model is equivalent to the Butler-Volmer equation when the maximum applied overpotential is much smaller than the reorganisation energy, which is defined as the energy required to reorganise the system geometry prior to the electron transfer.[172]

2.3.5 Mass Transport

In order for the catalytic current to reflect the processes occurring at the enzyme, it is necessary to ensure that the catalytic reaction is not controlled by diffusion of the reactants. This can be achieved by the use of a microelectrode, for which diffusion is radial rather than linear.[173] However, the experiments described in this thesis use hydrodynamic rotating disk electrodes (RDEs) to control both substrate transport to the electrode surface and dispersion of the product away from it by inducing forced convection. Rotation of an RDE results in the laminar flow pattern illustrated in Figure 2.4.[165,167] The electrode behaves like a pump; it pulls the solution upwards towards the electrode surface, before spinning it and releasing it outwards in a radial direction.[167] Both diffusion and convection of the substrate must be considered, although effects due to migration can be neglected assuming that sufficient supporting electrolyte is present, such as 0.1 M NaCl.[165]

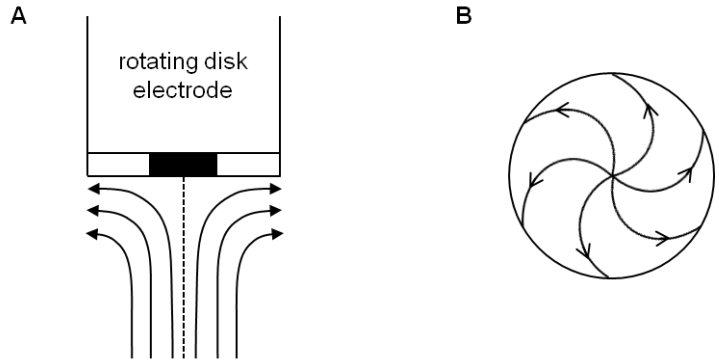


Figure 2.4. Schematic diagrams of the laminar flow at a rotating disk electrode viewed (A) from the side and (B) from below.[166,167]

The Levich equation[165] (Equation 2.19) describes the variation in the mass transport limited current (i_{lim}) as a function of the rotation rate.

$$i_{lim} = 0.62nFA[S]_{bulk}D^{2/3}v^{-1/6}\omega^{1/2} \qquad [2.19]$$

In this equation, n is the number of electrons involved in the process, F is Faraday's constant, A is the electrode area, $[S]_{bulk}$ is the concentration of the substrate in the bulk solution, D is the diffusion coefficient of the substrate, v is the kinematic viscosity of the solvent and ω is the electrode rotation rate.

It is clear from Equation 2.19 that i_{lim} has a linear dependence on the square root of the rotation rate ($\omega^{1/2}$). The limiting current is also related to the ratio of the surface to bulk concentrations of substrate ($[S]_{sur}$ and $[S]_{bulk}$ respectively) by Equation 2.20.[166]

$$\frac{[S]_{sur}}{[S]_{bulk}} = 1 - \frac{i}{i_{lim}} \qquad [2.20]$$

According to this expression, if the observed current, i, is much smaller than i_{lim}, then the surface concentration of substrate is approximately equal to that of the bulk concentration. As i approaches i_{lim}, on the other hand, the concentration at the surface

depletes to almost zero, leading to a large concentration gradient and a correspondingly rapid rate of mass transport.[166]

When the rotation rate is sufficiently high, transport of the substrate to the enzyme is no longer rate limiting, and thus the observed current becomes independent of rotation rate. The relationship between the observed limiting current and the rotation rate is then described by the Koutecky-Levich equation (Equation 2.21).[19]

$$\frac{1}{i_{\max,\omega}} = \frac{1}{i_{\max,\omega=\infty}} + \frac{1}{0.62\, nFA[\mathrm{S}]_{\mathrm{bulk}} D^{2/3} \nu^{-1/6} \omega^{1/2}} \qquad [2.21]$$

The term $i_{\max,\omega}$ is the observed limiting current at rotation rate ω, and $i_{\max,\omega=\infty}$ corresponds to the maximum limiting current obtained at an infinite rotation rate. The value of $i_{\max,\omega=\infty}$ can be determined from the *y*-intercept of a plot of $1/i_{\max,\omega}$ against $1/\omega^{1/2}$. Alternatively, its value can be estimated from the limiting current at a rotation rate above which no further increase in limiting current is observed.[19] In work presented throughout this thesis, electrode rotation rates ≥ 2500 rpm were used, to ensure that in each case $i_{\max,\omega} \approx i_{\max,\omega=\infty}$, and thus that the observed currents reflect the inherent properties of the enzyme rather than mass transport limitation. The limiting current for enzymatic processes is referred to simply as $i_{\max}$ in the remainder of this chapter.

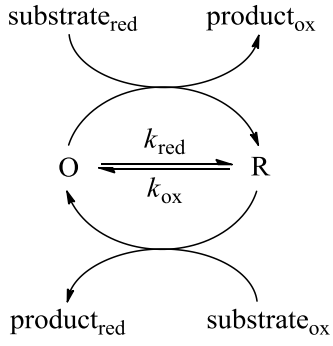
2.3.6 Catalytic Voltammetry

Faradaic currents due to the inherent properties of the adsorbed enzyme molecules can result from either non-turnover or catalytic processes.[173] In the absence of catalysis, non-turnover signals may be observed due to reversible electron transfer between the electrode surface and redox centres present in the immobilised enzyme molecules.

Measurement of these signals may be achieved by performing cyclic voltammograms in the absence of substrate, by use of an inhibitor or by altering the potential at a sufficiently rapid rate so as to outrun catalysis.[164] For each redox centre present in the enzyme, the oxidative and reductive peaks in the cyclic voltammogram are centred at the reduction potential of the site. The area under these peaks can be used to calculate the electroactive coverage of enzyme molecules on the electrode surface; for a one-electron redox process, the area of each peak is proportional to $AvΓ$, where A is the electrode area, v is the scan rate and $Γ$ is the electroactive coverage.[164]

However, although non-turnover signals are relatively easy to measure for small redox proteins that give high electroactive coverages (for example, ferredoxins),[174] such signals can be difficult to measure for larger enzymes that contain multiple redox sites and give low electroactive coverage. Rare examples of hydrogenases for which non-turnover signals have been detected are the [NiFe]-hydrogenase from *Allochromatium vinosum*[175] and the [NiFeSe]-hydrogenase from *Desulfomicrobium baculatum*.[176]

The work outlined in this thesis focuses on catalytic cyclic voltammetry; in the presence of substrate, electron transfer is coupled to a catalytic process (as illustrated in Scheme 2.1) and therefore the electrons are no longer confined to the enzyme film.[163]



Scheme 2.1. Schematic representation of the coupling of oxidation or reduction of the immobilised enzyme to the reduction or oxidation of substrate.

The catalytic current of an ideal electroactive enzyme is expected to show a sigmoidal potential dependence, as shown in Figure 2.5 for an oxidation process. The potential of catalysis, E_{cat}, corresponding to the point of maximum change in current with respect to potential, reflects the potential of the redox site up to which electron transfer is not rate-determining. This site is the 'control centre' of the enzyme, and is often the active site.[19]

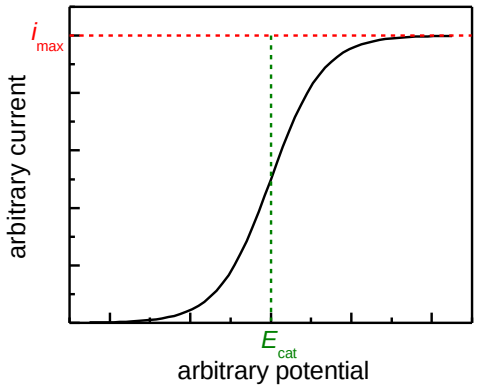


Figure 2.5. The sigmoidal current *vs.* potential trace corresponding to oxidation of a substrate by a redox enzyme adsorbed onto a rotating disk electrode.

The rate of catalysis is initially determined by the rate of electron transfer to generate the oxidised state of the enzyme that can then oxidise the substrate. Therefore, the current increases with driving force, which corresponds to an increase in the difference between the applied and equilibrium potentials (the overpotential, η). However, at very high overpotential, the current reaches a plateau, corresponding to i_{max} in Figure 2.5. At this point, the observed rate of catalysis is no longer limited by the rate of electron transfer; instead, potential-independent steps limit the rate of reaction. Under conditions where rotation is sufficiently rapid that mass transport is not limiting, this maximum current reflects the maximum turnover frequency of the enzyme, k_{cat}^{max}:

$$i_{max} = nFA\Gamma k_{cat}^{max} \qquad [2.22]$$

However, the turnover frequency can only be calculated if the electroactive coverage can be determined through the detection of non-turnover signals.

Cyclic voltammograms recorded for films of immobilised enzymes often do not reach the plateau shown in Figure 2.5, even in the absence of factors such as inactivation. One explanation for this is that a variety of orientations of the enzyme molecules on the electrode surface can give rise to dispersion in the rate of interfacial electron transfer between the electrode surface and the enzyme.[177] Protein molecules orientated with a redox centre close to the electrode surface may experience rapid and efficient electron transfer, whereas others may undergo much less efficient transfer. This can result in a residual slope in the current *vs.* potential plot, even at high overpotentials, as the rate of electron transfer is still rate-determining for some molecules.

2.4 Chronoamperometry

An alternative method for studying the catalytic activity of an electroactive enzyme is chronoamperometry. In this technique, the current obtained at a constant applied potential is monitored as a function of time,[166] and therefore this method is more useful than cyclic voltammetry for determining the rates of reactions, since in voltammetry the potential and time domains are convoluted. In chronoamperometry, the potential can be stepped between different values to induce changes in the catalytic activity (current). An example chronoamperometry experiment for an enzyme with a catalytic bias towards oxidising its substrate is illustrated in Figure 2.6; Figure 2.6A shows a plot of the applied potential *vs.* time and Figure 2.6B demonstrates the resulting catalytic current as a function of time. At low potential, little current is observed (green line). However, a step to a higher potential drives the oxidation process, as observed by

a positive current (blue line). The slow decrease in current over time is an effect termed 'film loss' and may be due to enzyme molecules dissociating from or re-orientating on the electrode surface, or denaturation of the enzyme on the electrode surface. Chronoamperometry data can be normalised to remove the effects of film loss, as described in Appendix A2. The red arrow in Figure 2.6B indicates addition of an inhibitor, leading to a decrease in catalytic oxidation current.

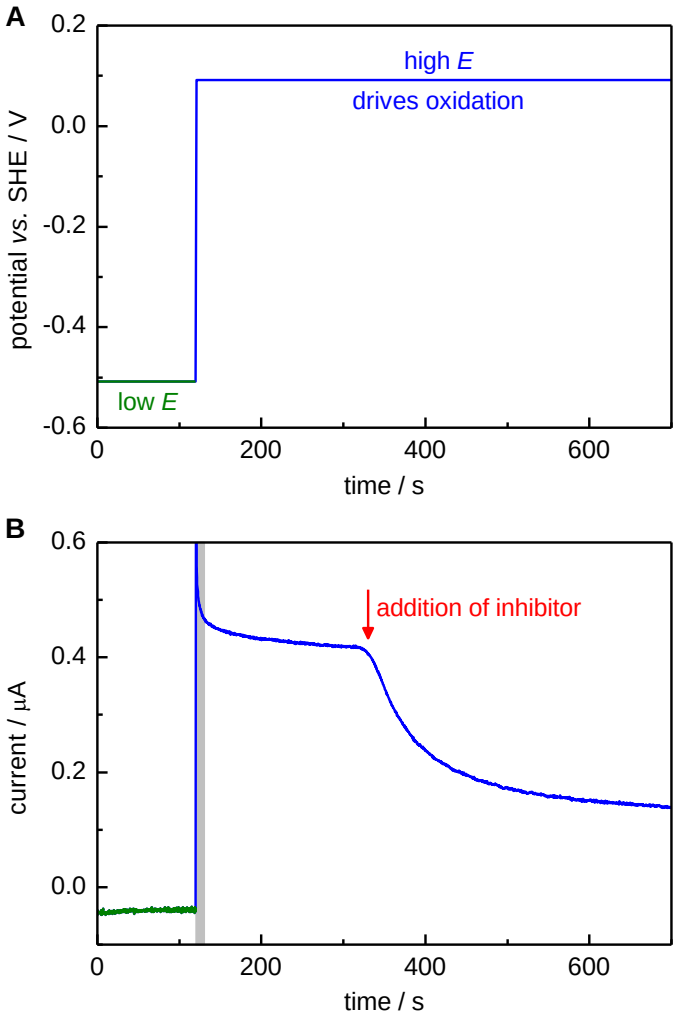


Figure 2.6. A shematic representation of a typical chronoamperometry experiment. (A) Shows the applied potential as a function of time. (B) Represents the corresponding changes in catalytic current; at low potential (green line), no oxidation occurs, whereas at a higher potential (blue line) catalytic oxidation is induced, leading to a positive current. The red arrow represents addition of an inhibitor of the enzyme, leading to a decrease in enzymatic oxidation current. The grey box highlights the charging current of the pyrolytic graphite edge-plane rotating disk electrode.

In chronoamperometry experiments, the current consists of both Faradaic and non-Faradic components, as described for cyclic voltammetry. The grey box in Figure 2.6B highlights the charging current caused by the non-Faradaic response of the pyrolytic graphite working electrode to the potential step, which is superimposed on the enzymatic Faradaic currents. The non-Faradaic current decays exponentially with time and is significant for approximately the first 10 s following a potential step.[178] Therefore, in experiments monitoring the rate of change in enzyme activity following a potential step, the data collected over the first 10 s should be neglected. This limits the processes that can be studied using this technique, since accurate rates cannot be calculated for very rapid reactions that are complete within the 'dead time' during which the charging current is significant. Additionally, in order for currents recorded in chronoamperometry to reflect the rates of catalytic processes, it must be ensured that electron transfer and mass transport are not limiting.

Chapter 3 Investigations into the Origins of the O_2 Tolerance of a [NiFe]-Hydrogenase

Abstract

This chapter investigates the reactions of the membrane-bound [NiFe]-hydrogenase from *Ralstonia eutropha* H16 (*Re*MBH^{WT}) with O_2. This enzyme is an example of a hydrogenase that is able to catalyse H_2 oxidation in the presence of O_2, a property that is required if hydrogenases are to be used successfully in technological applications.

The inherent properties of *Re*MBH^{WT} were studied using Protein Film Electrochemistry (PFE) and experiments were designed to probe electrocatalytic activity, CO tolerance and recovery from inactive states. In collaboration with Dr. James Cracknell, a model was designed to explain the kinetic and thermodynamic origins of the O_2 tolerance displayed by this enzyme. It was concluded that the key requirements for O_2 tolerance are that the [NiFe]-hydrogenase must form only the Ready (Ni-B) inactive state, and that this should recover rapidly and at relatively high potential.

To further test this model, mutations were made in the small subunit of *Re*MBH by Tobias Goris. Two cysteine residues close to the proximal FeS cluster (which are highly conserved in O_2-tolerant [NiFe]-hydrogenases) were exchanged to glycines (conserved in O_2-sensitive [NiFe]-hydrogenases) to create a variant protein, *Re*MBH$^{C19G/C120G}$. The PFE experiments described in this chapter suggest that without the additional cysteine residues this variant cannot sustain H_2 oxidation activity in the presence of O_2 because electron transfer to the active site is not sufficiently reliable or fast. It is thus proposed that a modified proximal cluster confers O_2 tolerance in *Re*MBH^{WT}.

This chapter is reproduced in part from: Goldet, G.; Wait, A. F., *et al.*, *J. Am. Chem. Soc.* **2008**, 130, (33), 11106-11113 (http://pubs.acs.org/doi/abs/10.1021/ja8027668), Cracknell, J. A.; Wait, A. F., *et al.*, *Proc. Natl Acad. Sci.* **2009**, 106, (49), 20681-20686 and Goris, T.; Wait, A. F., *et al.*, *Nat. Chem. Biol.* **2011**, 7, (5), 310-318.

3.1 Introduction

3.1.1 An Introduction to *Ralstonia eutropha*

Ralstonia eutropha H16 (*Re*) is a Knallgas bacterium that lives in the aerobic region close to the surface of wetland soils. This environment contains low levels of H_2, as described in Chapter 1.[179] Due to the limited and fluxional availability of H_2, Knallgas bacteria have a high affinity for H_2, and their threshold for H_2 uptake (as defined in Chapter 1) has been reported as ~1 ppm (around 1 nM dissolved H_2).[30] The β-proteobacterium *Re* is able to grow chemolithotrophically on mixtures of H_2, O_2 and CO_2, using H_2 as an energy source and CO_2 as a carbon source. The CO_2 is used to produce hydrocarbons via the Calvin-Benson-Bassham cycle.[180,181] The electrons produced from H_2 oxidation are ultimately transferred to O_2, which acts as the terminal electron acceptor.[182] This coupling of H_2 oxidation to O_2 reduction resembles a H_2/O_2 fuel cell (see Chapter 4) and suggests that the hydrogenases present in *Re* should be capable of maintaining catalytic activity in the presence of O_2, a property defined as 'O_2 tolerance'.[97,181]

3.1.2 The Hydrogenases Present in *Ralstonia eutropha*

Three types of [NiFe]-hydrogenase are produced by *Re*: a soluble hydrogenase (SH), regulatory hydrogenase (RH) and membrane-bound hydrogenase (MBH).[179] All three have been shown to exhibit O_2 tolerance.[33,114,179,183-185] The SH is located in the cytoplasm and is a six subunit complex that contains both a hydrogenase and diaphorase moiety. This enzyme couples H_2 oxidation to the reduction of NAD^+ to NADH.[179,186] The RH is responsible for regulating gene expression by sending signals via a histidine kinase, in order to control the synthesis of the SH and MBH depending on the availability of H_2.[182,187] The MBH, on which this chapter focuses, is located on the periplasmic side of

the membrane and couples H_2 oxidation to the respiratory chain via its *in vivo* partner, cytochrome *b*, and a pool of electron-carrier quinols present in the membrane.[188-190] Figure 3.1 demonstrates this process in a cartoon format. A proton gradient is generated as protons are taken up from the cytoplasmic side of the membrane and released on the periplasmic side. This gradient acts as an energy store, and can be used to generate adenosine triphosphate (ATP) from adenosine diphosphate (ADP) via controlled diffusion of the protons through the transmembrane enzyme ATP synthase.[191]

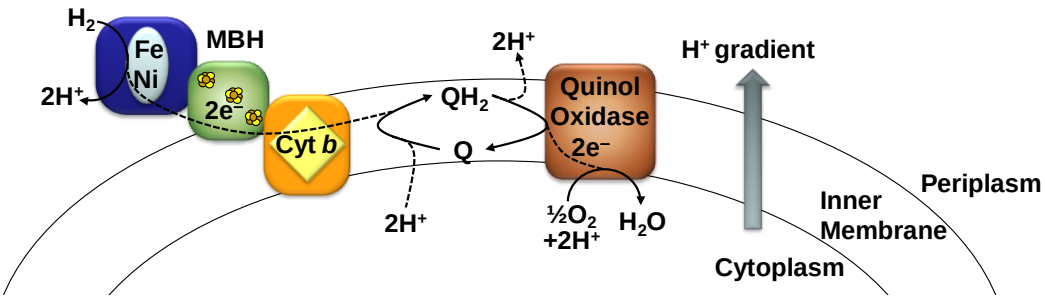


Figure 3.1. A cartoon representation of the coupling of H_2 oxidation by *Re*MBH^{WT} to O_2 reduction via cytochrome *b* and the quinol pool (adapted from references 179,190). Quinones (Q, reduced to quinols, QH_2) are used to transfer electrons from cytochrome *b* to a quinol oxidase, where O_2 is ultimately reduced to H_2O.

3.1.3 The Structure of the MBH from *Ralstonia eutropha*

The X-ray crystal structure of the MBH from *Re* (*Re*MBH^{WT}, where WT denotes the wild-type enzyme) has very recently been solved[41] and is illustrated in Figure 3.2. The overall protein structure is similar to those of the O_2-sensitive [NiFe]-hydrogenases from *Desulfovibrio fructosovorans* (*Df*),[49] *Desulfovibrio gigas* (*Dg*)[35] and *Allochromatium vinosum* (*Av*).[38]

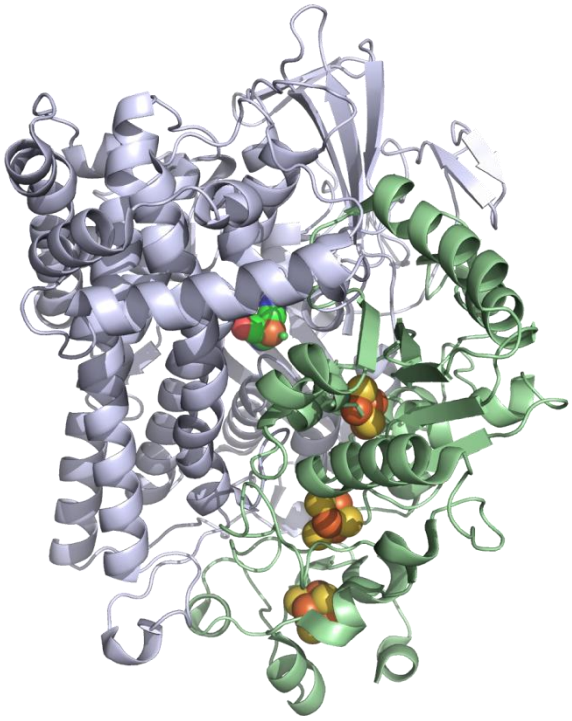


Figure 3.2. A representation of the structure of *Re*MBH^{WT}, produced using PyMOL.[41] The large subunit is shown in grey and the small subunit in green. The active site and FeS clusters are represented by spheres, with each atom coloured according to its element.

The structure of *Re*MBH^{WT} consists of a large subunit (HoxG, 67.1 kDa) containing the active site and a small subunit (HoxK, 34.6 kDa) containing the FeS cluster relay.[181,189,192] *In vivo*, *Re*MBH^{WT} is attached to the membrane via a specific anchor peptide located at the C-terminal of the small subunit.[188] The active site of *Re*MBH^{WT} is similar to that of O_2-sensitive 'standard' [NiFe]-hydrogenases, as indicated by the crystal structure[41] and spectroscopic evidence.[47,114] The FeS relay is a linear arrangement composed of three FeS clusters: the proximal cluster, closest to the active site, the medial cluster, and the distal cluster, located furthest from the active site and close to the protein surface.[41] The exact nature of the individual FeS clusters will be discussed in more detail in the following section.

3.1.4 An Introduction to the Modified Proximal Cluster

Recent EPR studies performed on *Re*MBH^{WT} revealed the presence of a paramagnetic signal at high redox potential (+290 mV) that is not observed for O_2-sensitive [NiFe]-hydrogenases.[193] Work on another O_2-tolerant membrane-bound [NiFe]-hydrogenase, from *Aquifex aeolicus* (*Aa*Hase1), showed that this centre magnetically couples to both the medial [3Fe4S]-cluster of the small subunit and the NiFe active site of the large subunit.[41] This coupling suggests that the paramagnetic centre lies in between the active site and the medial cluster, thus implying a structural and/or redox modification at or close to the proximal cluster. Similar additional paramagnetic centres, observed as 'wings' in the high potential EPR spectra, have also been observed for the O_2-tolerant MBH *Escherichia coli* Hydrogenase 1 (*Ec*Hyd1).[115]

Figure 3.3 shows a sequence alignment of the small, FeS cluster-containing subunits of various [NiFe]-hydrogenases. The four cysteine residues highlighted in yellow (corresponding to Cys17, Cys20, Cys115 and Cys149 according to the numbering in *Re*MBH) are conserved amongst all the [NiFe]-hydrogenases included in the alignment, regardless of their degree of sensitivity towards O_2. Crystal structures show that these four cysteines are located around the proximal FeS cluster, which has previously been identified as a [4Fe4S]-cluster in the O_2-sensitive [NiFe]-hydrogenases.[35,38,49,194] The sequence alignment also reveals the presence of two additional cysteine residues (Cys19 and Cys120 in *Re*MBH) that are conserved in the O_2-tolerant membrane-bound [NiFe]-hydrogenases (*Re*MBH, *Ec*Hyd1 and *Aa*Hase1) but are instead present as glycine residues in the O_2-sensitive hydrogenases.

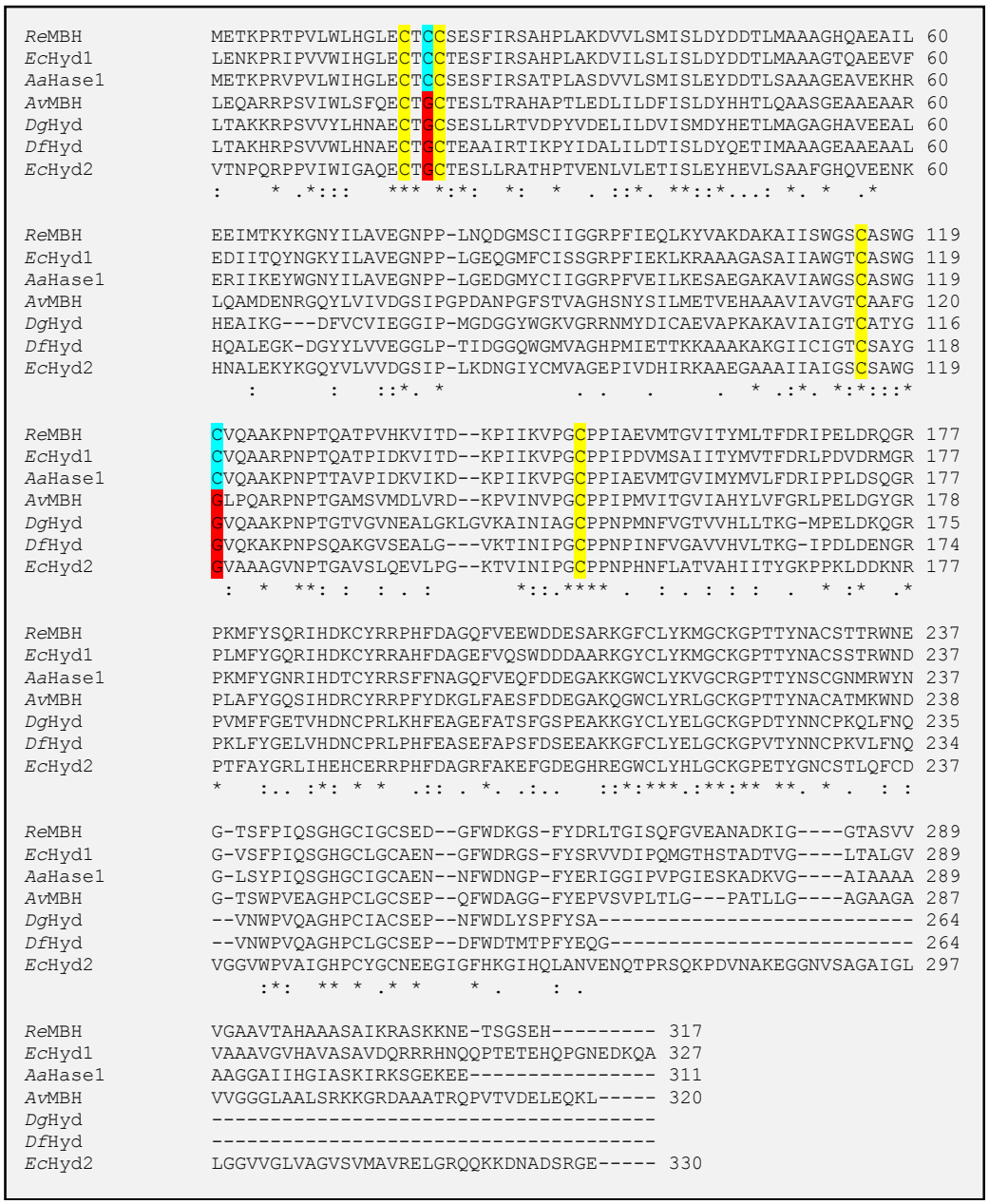


Figure 3.3. Multiple sequence alignment of the small subunits of various [NiFe]-hydrogenases, generated using the program ClustalW2. The following enzymes are included: *Re*MBH, *Ec*Hyd1, *Aa*Hase1, *Av*MBH, *Desulfovibrio gigas* periplasmic [NiFe]-hydrogenase (*Dg*Hyd), *Desulfovibrio fructosovorans* periplasmic [NiFe]-hydrogenase (*Df*Hyd) and *Escherichia coli* Hydrogenase 2 (*Ec*Hyd2). Indicated on the alignment are identical residues (*), conserved substitutions (:) and semi-conserved substitutions (.). The conserved cysteine residues highlighted in yellow surround the proximal FeS cluster and two additional cysteines, conserved only in O_2-tolerant hydrogenases, are highlighted in blue, with the corresponding glycines, found in O_2-sensitive hydrogenases, highlighted in red. In each case, the Tat-signal sequence has been removed.

Figure 3.4 compares the proximal cluster region of the recently solved crystal structure of *Re*MBH^{WT} with that of the O_2-sensitive *Desulfovibrio gigas* periplasmic [NiFe]-hydrogenase (*Dg*Hyd).[41,194]

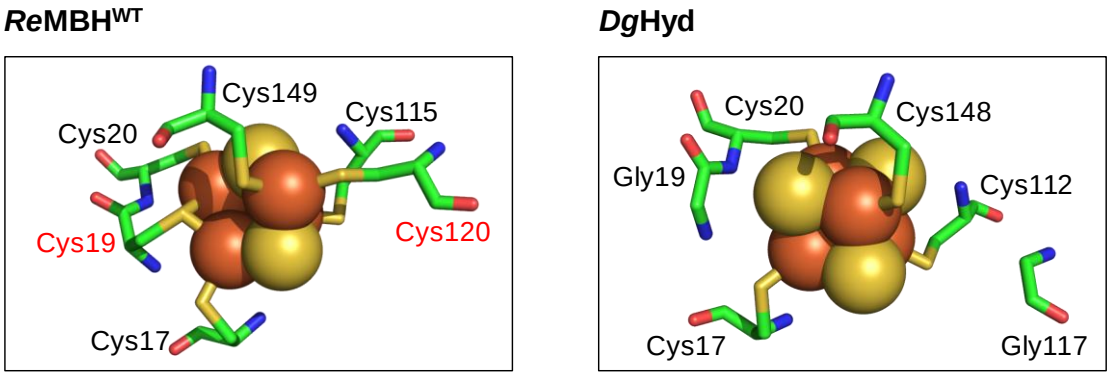


Figure 3.4. A comparison of the proximal FeS cluster region of *Re*MBH^{WT} and the periplasmic [NiFe]-hydrogenase from *Desulfovibrio gigas* (*Dg*Hyd, PDB code: 1YQ9).[41,194] The residues in red correspond to the cysteines conserved only in the O_2-tolerant [NiFe]-hydrogenases.

These structures confirm that the two additional cysteine residues, present only in the O_2-tolerant [NiFe]-hydrogenases, are close to the coordination sphere of the proximal FeS cluster. Importantly, the structure of *Re*MBH^{WT} also suggests that the proximal cluster of this enzyme is a [4Fe3S] species, rather than the [4Fe4S]-cluster identified in O_2-sensitive [NiFe]-hydrogenases. In the reduced form, the missing inorganic sulfide is replaced by the sulfur atom of Cys19 which serves as a bridging ligand for two Fe atoms.[41] Another Fe atom is apparently distorted from the regular cubic structure by combined ligation by both Cys149 and Cys120, as also predicted from studies using X-ray absorption spectroscopy.[47]

3.1.5 The O_2 Tolerance of *Re*MBH^{WT}

As described in Section 3.1, the Knallgas bacterium *Re* lives under aerobic conditions and *in vivo* H_2 oxidation by *Re*MBH^{WT} is ultimately coupled to O_2 reduction. Therefore this

hydrogenase must be able to function in the presence of O_2 (that is, it must exhibit O_2 tolerance). This is in contrast to the 'standard' [NiFe]-hydrogenases, which are O_2-sensitive (as discussed in Chapter 1). Previous electrochemical studies compared the O_2 tolerance of *Re*MBH^{WT} with that of *Av*MBH (Figure 3.5).[114]

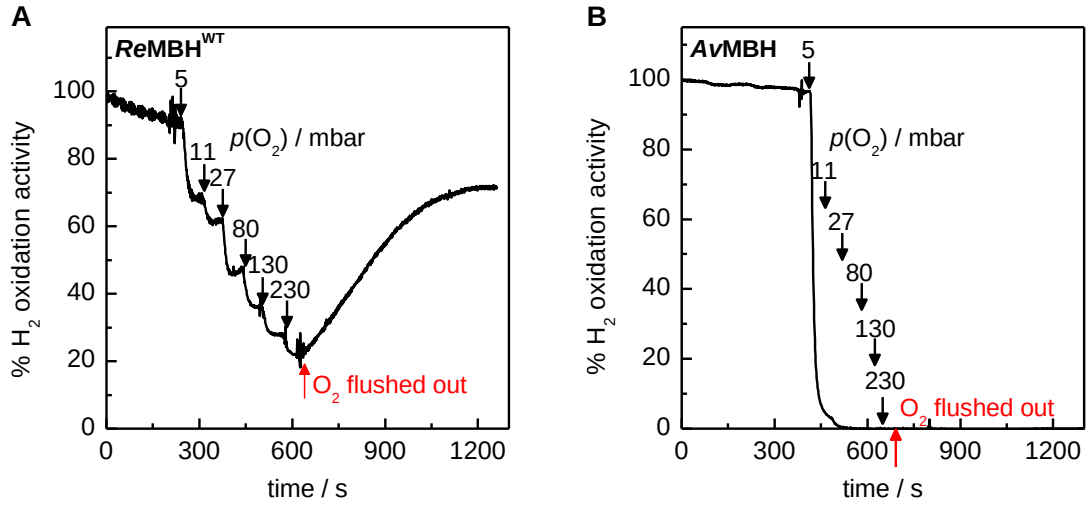


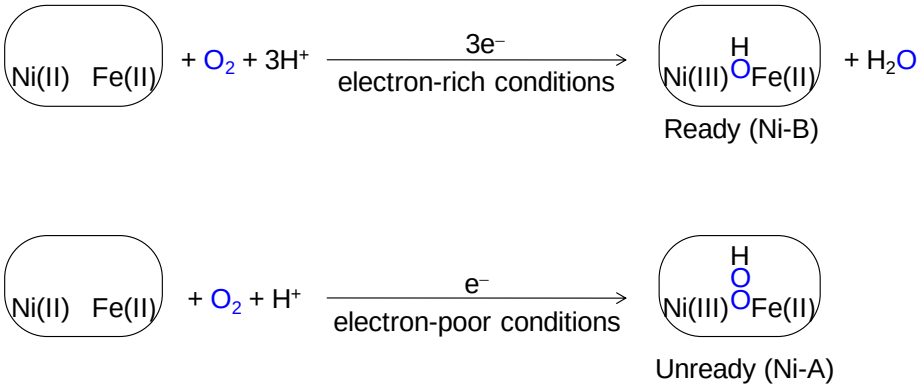
Figure 3.5. A comparison of the O_2 tolerance of (A) *Re*MBH^{WT} and (B) *Av*MBH, a 'standard' [NiFe]-hydrogenase. In each case, the electrode potential was held at +142 mV and the cell headspace flushed with H_2. At 240 s (A) and 400 s (B), the cell was sealed and the $p(O_2)$ increased stepwise to the values indicated. At 650 s (A) and 815 s (B), the cell headspace was again flushed with H_2 to remove the O_2. Other conditions: pH 5.6, 30 °C, electrode rotation rate 2000 rpm. Data taken from reference 114.

During a chronoamperometry experiment, the partial pressure of O_2 ($p(O_2)$) was increased in a stepwise fashion and the resulting decrease in H_2 oxidation current measured over time. For *Re*MBH^{WT}, greater than 20% of the original H_2 oxidation activity remained even following the final injection to give $p(O_2)$ = 230 mbar. In contrast, *Av*MBH lost all of its H_2 oxidation activity after the first injection alone (corresponding to $p(O_2)$ = 5 mbar). In addition, following removal of the O_2 by flushing the cell headspace with H_2, *Re*MBH^{WT} quickly recovered H_2 oxidation activity, whereas no recovery was detected for *Av*MBH in this experiment. The results outlined in this chapter probe the origins of this unusual O_2 tolerance using PFE. The nature of the inactive states formed in

the presence of O_2 and their ability to recover are likely to have a great impact on the ability of a [NiFe]-hydrogenase to retain activity under aerobic conditions.

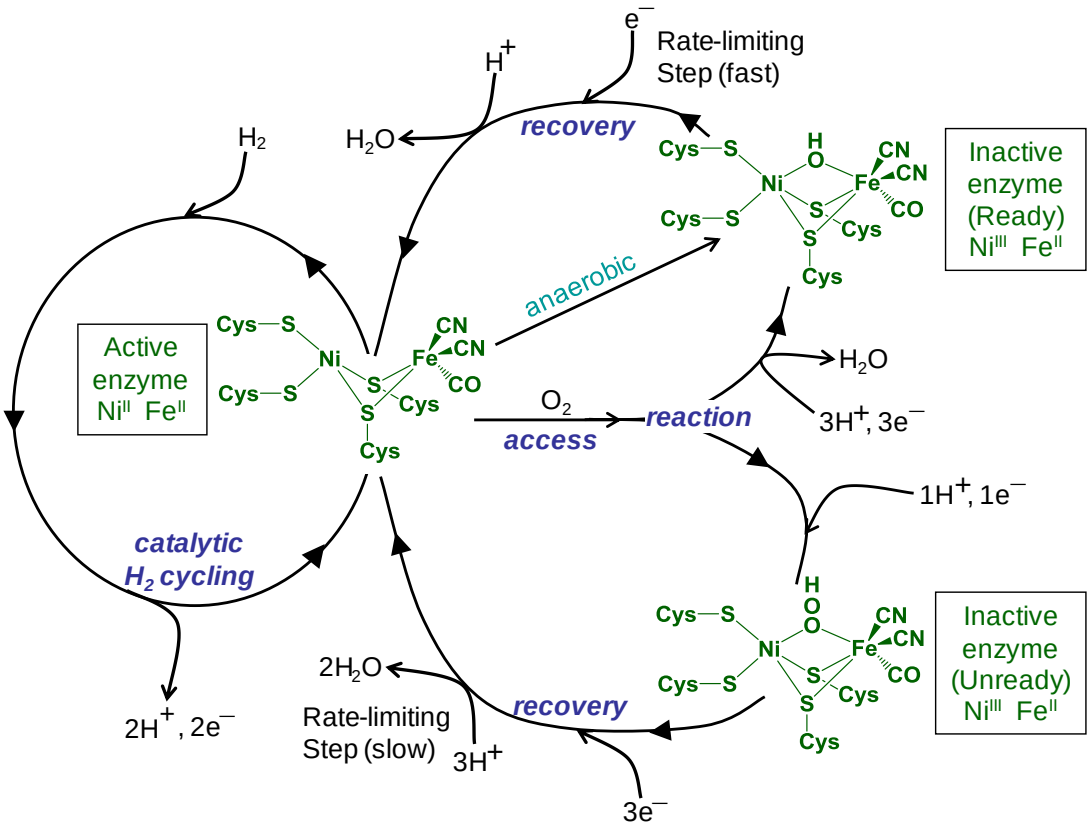
3.1.6 Summary of the Inactive States Formed

As described in Chapter 1, a 'standard' O_2-sensitive [NiFe]-hydrogenase reacts with O_2 to generate two inactive species: the Ready (Ni-B) state of the enzyme (containing a hydroxide bridging ligand)[60] forms during exposure to O_2 under electron-rich conditions, and the Unready (Ni-A) state (believed to contain a bridging peroxide)[194] is produced under electron-deficient conditions. Scheme 3.1 illustrates the chemical equations for the formation of these two states in the presence of O_2.[31]



Scheme 3.1. Representations of the chemical equations for formation of the Ready (Ni-B) and Unready (Ni-A) states in the presence of O_2. Figure adapted from references 31 and 195.

The Ready state is also formed at high potential under anaerobic conditions (Section 3.1.7.2). The Ready and Unready states are kinetically distinct, with the Ready state recovering rapidly and the Unready state recovering only very slowly.[66,194,195] The simplified cycles shown in Scheme 3.2 summarise the reactions of a 'standard' [NiFe]-hydrogenase with H_2 and O_2.[31,196]



Scheme 3.2. A representation of the reactions of a 'standard' [NiFe]-hydrogenase with H_2 and O_2. Active enzyme molecules catalyse H_2 oxidation and are aerobically inactivated to form either the Ready or Unready state, depending on the availability of protons and electrons. The Ready state is also produced via high potential anaerobic inactivation. Figure reproduced from reference 196.

It is important to note that Scheme 3.2 assumes that only the EPR-active Ni-B (Ready) and Ni-A (Unready) inactive states are formed by the enzyme. There is a possibility that other oxygenated inactive states (such as the 'dead' state in Chapter 1), that are not so clearly distinguished by spectroscopy, may be generated and may involve, for example, damage to an FeS cluster.[60,197] It is clear from Scheme 3.2 that in order for a [NiFe]-hydrogenase to retain catalytic H_2-cycling activity in the presence of O_2, the enzyme must remain in the left-hand cycle, by avoiding the generation of inactive states or recovering rapidly from any that are formed.

In order to predict whether a [NiFe]-hydrogenase will be O_2-tolerant, the inactivation cycles depicted on the right-hand side of Scheme 3.2 can be considered in three distinct stages: *Access*, *Reaction* and *Recovery*.[31,196] *Access* considers how quickly O_2 can reach the active site, and may be affected by the size of gas channels that allow transport of gases through the protein. *Reaction* involves the binding of O_2 at the active site, followed by its reduction to either a hydroxide or peroxide bridging ligand. *Recovery* considers both the kinetics and thermodynamics of reductive reactivation back to the active enzyme. The O_2 tolerance of a hydrogenase is also expected to depend on the enzyme's affinity for H_2 (represented by its Michaelis constant for H_2, $K_M(H_2)$) since there will be competition by O_2 for binding at the active site.

Experiments to probe the roles of *Access* and *Reaction* on the O_2 tolerance of *Re*MBH^{WT} were performed by Dr. James Cracknell.[196,198] Section 3.2 of this thesis focuses on the use of PFE to investigate both the kinetics (measured as rates) and thermodynamics (measured as potentials) of the *Reactivation* stages of the cycle.

3.1.7 Introduction to the Electrochemistry of *Re*MBH^{WT}

It has previously been shown that *Re*MBH^{WT} adsorbs onto pyrolytic graphite edge-plane (PGE) surfaces and can therefore be studied using Protein Film Electrochemistry.[97,114] This chapter uses PFE to investigate, firstly, the fundamental electrocatalytic behaviour of the enzyme and secondly the origins of its O_2 tolerance, including studies on a genetically modified variant of the enzyme.

3.1.7.1 Catalytic Bias

The catalytic bias of *Re*MBH^{WT} towards H_2 oxidation and production can be investigated by performing cyclic voltammetry on an enzyme-modified pyrolytic graphite edge-plane

rotating disk electrode (Figure 3.6). A voltammogram was first performed under 100% N_2 (red line). Under these conditions, negative current corresponding to catalytic H^+ reduction (H_2 production) is observed at potentials below approximately -250 mV. Since the electrode is rotating, H_2 produced at low potential is rapidly removed from the electrode surface, and therefore there is no positive current corresponding to H_2 oxidation when the potential is scanned to higher values. Thus at higher potentials, the voltammogram resembles that of the unmodified electrode (represented by the grey line in Figure 3.6).

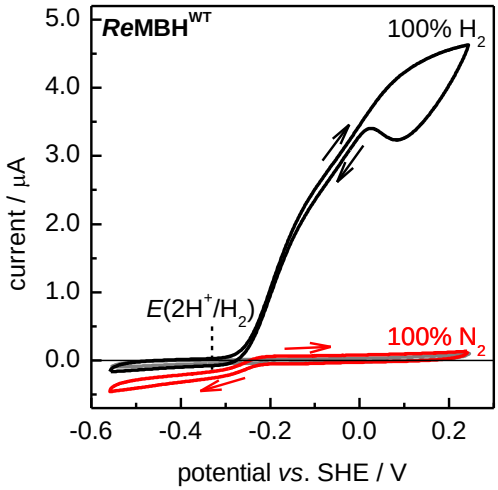


Figure 3.6. Cyclic voltammograms showing the catalytic bias of *Re*MBH^{WT} recorded at 20 mV s^{-1} under 100% N_2 (red line) and then 100% H_2 (black line). The response of a blank, unmodified electrode is overlaid in grey. Other conditions: pH 5.5, 30 °C, electrode rotation rate 2500 rpm.

The gas flowing through the cell was then changed to 100% H_2 and left for 5 min to allow re-equilibration. Under 100% H_2 (equivalent to 0.8 mM dissolved H_2,[199] represented by the black line in Figure 3.6), the electrode modified with *Re*MBH^{WT} shows positive current corresponding to catalytic H_2 oxidation at potentials above approximately -280 mV *vs.* SHE. At lower potentials no negative current is observed; no H^+ reduction is detected under 100% H_2 due to strong product inhibition by H_2, as characterised by the

low K_i^{app} (H_2) determined previously for this enzyme.[108] The onset of H_2 oxidation is around 50-80 mV more positive than $E(2H^+/H_2)$ calculated at 100% H_2 under these conditions[97,108] (represented by a dotted line in Figure 3.6). This overpotential, which corresponds to the enzyme requiring a higher driving force than expected for H_2 oxidation, is also observed for other O_2-tolerant [NiFe]-hydrogenases.[59,115]

Although some enzyme activity may have been lost between the scans due to film loss, the effect is relatively small over the time course of these experiments. Therefore, the data shown in Figure 3.6 can be used to gain an understanding of the bias of *Re*MBH^{WT} towards H_2 oxidation or production. As for other O_2-tolerant [NiFe]-hydrogenases,[115] *Re*MBH^{WT} is more biased towards H_2 oxidation than H_2 prodcution and, while *Re*MBH^{WT} is able to reduce protons under 100% N_2, the reaction is severely inhibited by H_2.[108] Since the voltammogram under 100% N_2 was recorded prior to that under 100% H_2, the small amount of film loss will lead to a slightly lower than expected H_2 oxidation current, and therefore the enzyme may be even more biased towards H_2 oxidation than is apparent in Figure 3.6.

A more detailed analysis of the cyclic voltammogram recorded under H_2 (black line) yields the observation that the catalytic wave is not an ideal sigmoid. Firstly, the current does not reach a plateau (limiting current) at high potential. As described in Chapter 2, this is believed to be due to a distribution of orientations of enzyme molecules adsorbed onto the surface, leading to a dispersion of interfacial electron transfer rates.[200] Secondly, on the reverse scan there is an increase in current just above 0 mV. This is due to recovery from the inactive Ni-B (Ready) state generated by high potential anaerobic inactivation,

and is discussed in detail in Section 3.1.7.2, where slower scan rates provide sufficient time for a greater extent of inactivation to be observed.

3.1.7.2 Anaerobic Inactivation

Figure 3.7A shows a cyclic voltammogram for *Re*MBH^{WT} under 100% H_2, recorded at a slow scan rate (1 mV s^{-1}).

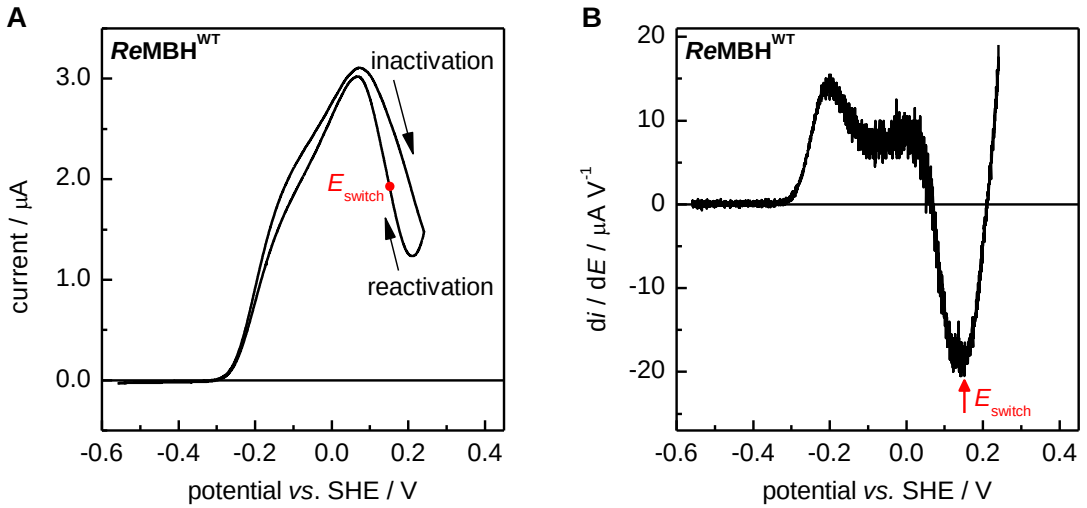


Figure 3.7. (A) Cyclic voltammogram of *Re*MBH^{WT} recorded at 1 mV s^{-1} under 100% H_2 at pH 5.5, 30 ºC, electrode rotation rate 4500 rpm. (B) Shows a plot of the first derivative of the current with respect to potential and the minimum in this curve (corresponding to the value E_{switch}) is labelled in red. (This value of E_{switch} is also indicated by the red dot on the reductive scan of the voltammogram in (A)).

At this scan rate, the catalytic H_2 oxidation current begins to drop off at high potentials due to anaerobic inactivation. As described previously, this corresponds to the trapping of a water molecule as a hydroxide ligand bridging the Ni and Fe atoms, forming the Ni-B (Ready) state.[201] In Figure 3.7A, this inactivation becomes visible as a decrease in H_2 oxidation current at potentials above ~+30 mV. This effect is much more pronounced than in Figure 3.6 since the slower scan rate allows more time for the hydrogenase to 'switch-off', thus increasing the extent of inactivation. On the return scan, sweeping

towards more negative potentials, the enzyme undergoes reductive reactivation, and the catalytic current recovers. Thus, the anaerobic inactivation is reversible.

The switch potential, E_{switch}, has been defined previously[201] as the minimum in the derivative plot of current with respect to potential, as shown in Figure 3.7B. Under these conditions, E_{switch} for *Re*MBH^{WT} was calculated to be ~+150 mV.

3.1.7.3 The Effect of Varying the H_2 Concentration

Cyclic voltammograms recorded under varying percentages of H_2 diluted in N_2 were performed on the same enzyme film and are shown in Figure 3.8A. Throughout these experiments a rotation rate of 4500 rpm was used to minimise mass transport limitation at low levels of substrate (H_2).

The Michaelis constant, $K_M(H_2)$, for *Re*MBH^{WT} was determined previously using an electrochemical method described in detail in Section 3.3.1.3.[109,202] The calculated value was low (6.1 μM at -108 mV, pH 5.5, 30 ºC)[202] and therefore the enzyme shows a high affinity for its substrate, H_2. From Figure 3.8A it is clear that, even under 0.01% H_2 (brown line, corresponding to a solution H_2 concentration of just 80 nM),[199] some H_2 oxidation current can be observed. In the H_2 oxidation region of the voltammograms, the currents recorded under 100% H_2 (black line) and 10% H_2 (blue line) largely overlay in the region -250 to -50 mV. However, the amount of anaerobic inactivation increases with decreasing H_2 partial pressure, seen as a more pronounced attenuation in current at high potential as the H_2 level is decreased. This strongly suggests that H_2 protects the hydrogenase against anaerobic inactivation, as demonstrated previously for *Av*MBH.[203]

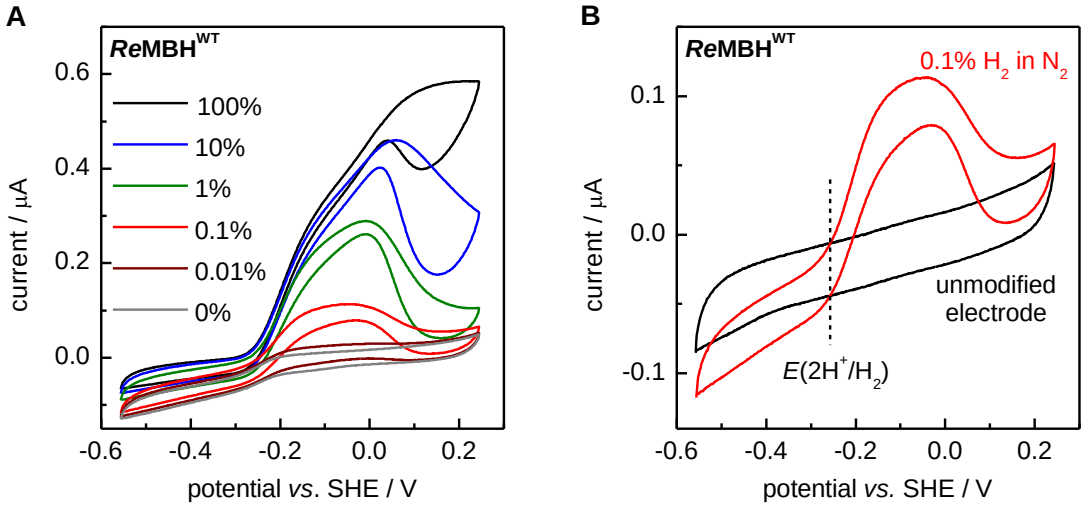


Figure 3.8. (A) Cyclic voltammograms of *Re*MBH^{WT} recorded at 10 mV s^{-1} under varying percentages of H_2 diluted in N_2. The percentages of H_2 given correspond to the following concentrations of dissolved H_2: 100% = 0.8 mM H_2; 10% = 80 µM H_2, 1% = 8 µM; 0.1% = 0.8 µM H_2; 0.01% = 80 nM H_2.[199] A voltammogram recorded under 0% H_2 (100% N_2) is shown for comparison (grey line). (B) Shows an enlargement of the 0.1% H_2 voltammogram in (A) (red line), overlaid on the response of an unmodified electrode (black line). Also labelled is the calculated value of $E(2H^+/H_2)$ under these conditions (dashed line). Other conditions: pH 5.5, 30 °C, electrode rotation rate 4500 rpm.

The amount of negative H_2 production current increases as the H_2 concentration decreases, as expected due to decreasing H_2 product inhibition. The cyclic voltammograms recorded under 1% H_2 or lower show both H_2 oxidation and H_2 production. These cyclic voltammograms each cross the zero current axis as the enzyme changes its direction of catalysis. The value of $E(2H^+/H_2)$ can be calculated at each concentration of H_2 according to the Nernst equation, and under these conditions it shifts by +30 mV per 10-fold decrease in H_2. Figure 3.8B shows an enlargement of the voltammogram recorded under 0.1% H_2 (red line, corresponding to 0.8 µM dissolved H_2).[199] Th dashed line highlights the point of zero current, which is in this case consistent with the calculated value of $E(2H^+/H_2)$ under these conditions. Since the potential of the onset of activity for the enzyme is constant between the varying H_2 concentrations, whereas the value of $E(2H^+/H_2)$ varies, it is clear that, whereas under 100% H_2 *Re*MBH^{WT}

exhibits an overpotential for H_2 oxidation (Figure 3.6), under low levels of H_2 catalysis is reversible and cuts the zero current axis at a potential very close to $E(2H^+/H_2)$.[108]

3.2 Probing the Recovery of Inactive States

3.2.1 Rates of Recovery from Anaerobic Inactivation

Chronoamperometry experiments were designed to measure the rates of reactivation from the Ready state of *Re*MBH^{WT} formed via high potential anaerobic inactivation. An electrode modified with *Re*MBH^{WT} was held at -508 mV under a constant flow of H_2 for 120 s, to ensure that all enzyme molecules were in an active, H_2-cycling state. The electrode potential was then stepped to a high value (+442 mV) in order to anaerobically inactivate the enzyme. After 900 s, the potential was stepped to a lower value at which the rate of recovery was to be measured. The chronoamperometric trace obtained from an example experiment (in this case monitoring recovery at +192 mV) is shown in Figure 3.9. For each experiment, the reactivation section of the current *vs.* time trace fits well to a single exponential curve (red line in Figure 3.9) and therefore a single rate constant, *k*, can be determined in each case. The data points collected during the first 10 s following the step to the reactivation potential cannot be included in the fitting process because during this time high charging currents are observed as a result of the discharge of electrode capacitive current following the potential step (Chapter 2). The experiments were therefore performed at a relatively low temperature (10 °C) since the rate of recovery at 30 °C is so rapid that *Re*MBH^{WT} regains full activity within the 'dead time' caused by the capacitance.

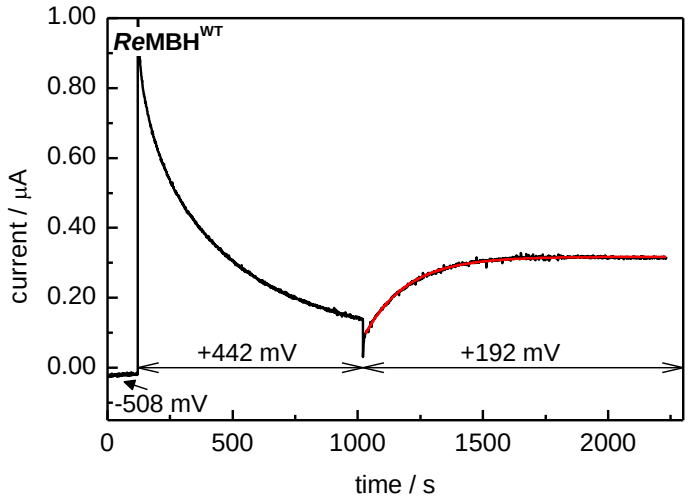


Figure 3.9. A typical experiment to measure the rate of reactivation of *Re*MBH^{WT} under 100% H_2 following anaerobic inactivation. In this example, reactivation was measured at +192 mV. The calculated single exponential fit to the reactivation section of the data is overlaid (red line). Other conditions: pH 5.5, 10 ºC, electrode rotation rate 2500 rpm.

Figure 3.10 shows the reactivation traces obtained from a series of experiments performed using the method outlined above in which the final reactivation potential was varied. In each case, the current has been normalised so that the maximum (limiting) current reached is equal to 1 and the time corrected so that the step to the reactivation potential is at t = 0 s. A single exponential fit is overlaid on each current *vs.* time trace, demonstrating that the reactivation can be regarded as a monophasic process that corresponds to the reactivation of a single species (the Ready state).

It is clear from Figure 3.10 that the rate of reactivation increases as the potential decreases. This is as expected because the driving force for the reductive reactivation process increases as the potential is lowered. The potential dependence of this recovery will be discussed in more detail in Section 3.2.2. It can be seen in Figure 3.10 that even at 10 ºC the rate of reactivation is very rapid at potentials below +40 mV. Under these conditions, the reaction is complete within 30 s and therefore, accounting for the loss of

the first 10 s of data in the capacitive 'dead time' of the experiment, there is likely to be considerable scatter in the calculated rate constants at low potentials.

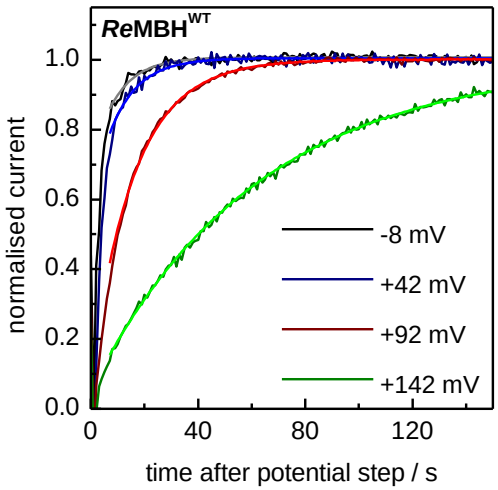


Figure 3.10. Reactivation of the anaerobically-generated Ready state of *Re*MBH^{WT} at various potentials. In each case, the current has been normalised so that the maximum (limiting) current reached is equal to 1 and the time corrected so that the step to the reactivation potential is at time = 0 s. For each current *vs.* time trace, a single exponential fit is overlaid. The rate constants for reactivation obtained from these fits are as follows: 0.10 s^{-1} at -8 mV, 0.09 s^{-1} at +42 mV, 0.06 s^{-1} at +92 mV and 0.02 s^{-1} at +142 mV. Other conditions: pH 5.5, 10 ºC, electrode rotation rate 2500 rpm.

3.2.2 Rates of Recovery from Aerobic Inactivation

Experiments similar to those described in Section 3.2.1 were used to determine the rates of recovery following aerobic inactivation. Figure 3.11 shows an example experiment, in which the reactivation was monitored at +192 mV. As before, the electrode was initially held at -508 mV under 100% H_2 for 120 s. The potential was then stepped to +92 mV; at this potential anaerobic inactivation of *Re*MBH^{WT} is negligible, but reaction of the enzyme with O_2 does occur. The gas flowing through the cell was then changed from 100% H_2 to a mixture of 80% H_2 and 20% O_2, resulting in a decrease in current due to aerobic inactivation of the enzyme (green line in Figure 3.11). After 900 s, by which time the current had reached a plateau level, the electrode potential was stepped to +442 mV

and the gas flowing through the cell changed back to 100% H_2. At +442 mV, the enzyme does not reactivate, thus allowing a clear time window for gas exchange. After 900 s (to ensure that all the O_2 was removed from the cell solution), the electrode potential was stepped to a lower value at which the rate of recovery was to be measured.

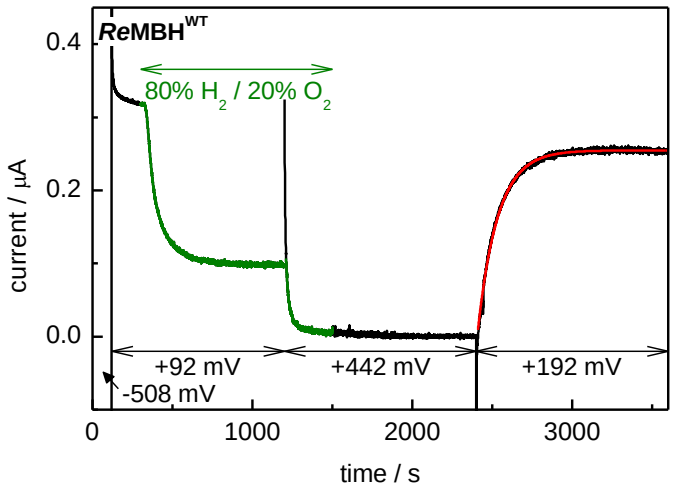


Figure 3.11. A typical experiment to measure the rate of reactivation of *Re*MBH^{WT} under 100% H_2 following aerobic inactivation. In this example, reactivation was measured at +192 mV. The green region corresponds to the gas flowing through the cell headspace being changed from 100% H_2 to a mixture of 80% H_2 and 20% O_2. The calculated single exponential fit to the reactivation section of the data is overlaid (red line). Other conditions: pH 5.5, 10 °C, electrode rotation rate 2500 rpm.

This experiment was repeated over a range of reactivation potentials and in each case the rate of reactivation fits well to a single exponential (as exemplified by the red line in Figure 3.11). This suggests that even after exposure to O_2, the recovery is from a single inactivated species, thus implying that *Re*MBH^{WT} forms only the Ni-B (Ready) state. It should be noted that although formation of the Ni-A (Unready) state is in general favoured by exposure to O_2 at higher potentials than the +92 mV used in these experiments,[195] PFE studies by Dr. James Cracknell have confirmed that, even following exposure to 100% O_2 at +442 mV, formation of only the Ready state of *Re*MBH^{WT} can be detected by this technique.[198] These results are consistent with those obtained in

spectroscopic studies on *Re*MBH^{WT}, which also show no evidence for the Ni-A (Unready) state.[193]

Figure 3.12 compiles the rates of reactivation for *Re*MBH^{WT} following both anaerobic and aerobic inactivation (represented as white and black circles respectively), plotted as a function of reactivation potential.

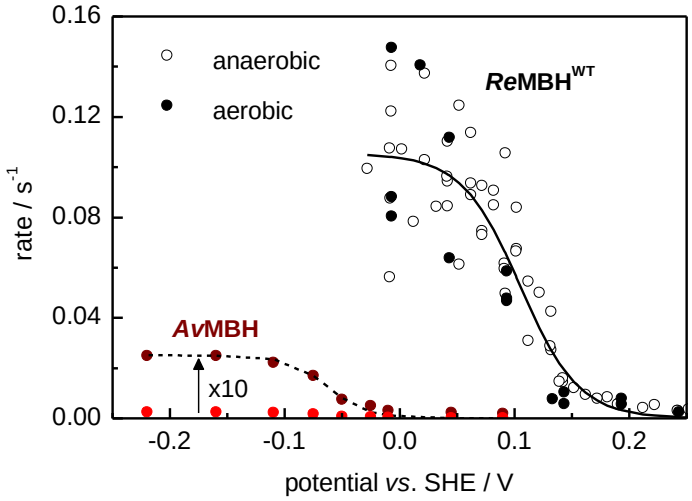


Figure 3.12. Rates of reactivation for *Re*MBH^{WT} following anaerobic (white circles) and aerobic (black circles) inactivation as a function of potential, with a sigmoidal fit to the data overlaid (solid line). Data for the reactivation for *Av*MBH from the Unready state (red circles, pH 6, 45° C, taken from reference 195) are also shown, and have been multiplied by 10 for clarity (burgundy circles). A sigmoidal fit to this data is also shown (dashed line). Other conditions: pH 5.5, 10° C, electrode rotation rate 2500 rpm.

As predicted in Section 3.2.1, there is a relatively large amount of scatter in the calculated rates in the low potential region due to a large proportion of the reactivation occurring within the disregarded first 10 s following the potential step. The rates of recovery are similar following both anaerobic and aerobic inactivation of *Re*MBH^{WT}, and the potential dependence shows a sigmoidal profile. This sigmoidal shape arises because the rate initially increases with increasing driving force (*decreasing* potential) until it becomes

limited by a chemical process rather than electron transfer. At potentials below 0 mV the rate is independent of potential; it reaches a limiting rate of approximately 0.1 s^{-1}.

The data in Figure 3.12 can be fitted to a sigmoid given by Equation 3.1, where $E_{1/2}$ is the reduction potential of the centre(s) responsible, E is the electrode potential, n is the apparent number of electrons transferred, F is Faraday's constant, R is the gas constant, T is the absolute temperature and A,B, and C are complex constants.[195]

$$k = \frac{A \exp\left(\frac{nF(E_{1/2}-E)}{RT}\right)}{B + C \exp\left(\frac{nF(E_{1/2}-E)}{RT}\right)} \qquad [3.1]$$

The derivation of this equation and the definitions of the complex constants are provided in Appendix A3. Fitting the data to this sigmoid enables the number of electrons involved in the reactivation process, n, to be calculated.[195] The best fit to the data for *Re*MBH^{WT} yields n = 0.96 (overlaid in Figure 3.12, solid black line), which is consistent with the single electron transfer that would be required to reactivate the Ready state (Scheme 3.2).

Also overlaid in Figure 3.12 are the rates of recovery at 45 °C from the Unready state of the O_2-sensitive *Av*MBH (data taken from reference 195). The Unready state is produced in large amounts by O_2 inactivation of *Av*MBH and previous studies have shown that the Ready and Unready states reactivate at similar potentials in *Av*MBH.[66] It is clear from Figure 3.12 that reactivation of *Re*MBH^{WT} following aerobic inactivation is much faster than for *Av*MBH. The rate is approximately 40 times larger for *Re*MBH^{WT} than for *Av*MBH despite the fact that the data for *Av*MBH were collected at a much higher temperature. The data in Figure 3.12 also show that *Re*MBH^{WT} recovers at a higher potential than *Av*MBH, requiring a lower driving force for reductive reactivation.

3.2.3 The Potential of Reactivation

The differences between the potentials of reactivation from O_2 exposure for *Re*MBH^{WT} and *Av*MBH can be more clearly compared using voltammetry, as determined previously by Vincent *et al.*[97] Figure 3.13 shows data obtained using the same method,[97] except that in this case a scan rate of 0.1 mV s^{-1} was used for both enzymes, and the voltammograms were recorded under 100% H_2 at pH 5.5 and 10 ºC, to allow direct comparison with the *Re*MBH^{WT} data in Figure 3.12. After initially being held at -558 mV under 100% N_2, the electrode potential was stepped to +392 mV and an aliquot of O_2-saturated buffer simultaneously injected into the cell solution, causing the enzyme to inactivate aerobically. After 300 s, the gas flowing through the cell headspace was changed to 100% H_2, and then after a further 900 s (after which all the O_2 was removed and the cell solution was fully equilibrated to 100% H_2) the potential was swept back to -558 mV, allowing the recovery process to be monitored.

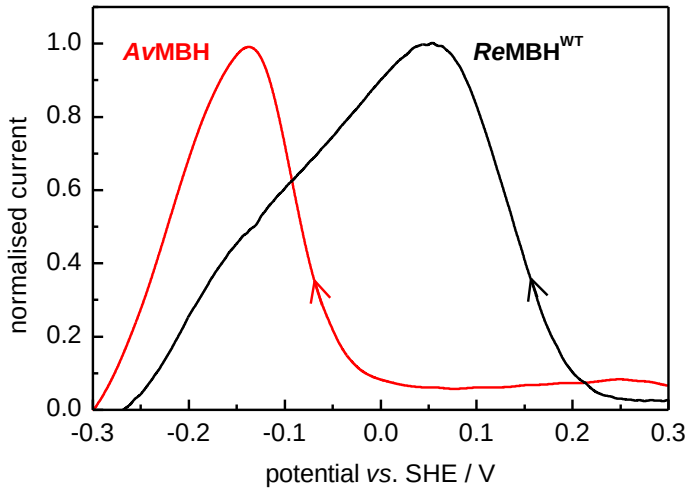


Figure 3.13. Voltammograms of *Re*MBH^{WT} (black line) and *Av*MBH (red line) recorded at 0.1 mV s^{-1} under 100% H_2 showing recovery following aerobic inactivation at +392 mV under N_2. Other conditions: pH 5.5, 10° C, electrode rotation rate 2500 rpm.

The voltammograms presented in Figure 3.13 show the same characteristics as those obtained by Vincent *et al.*: *Re*MBH^{WT} recovers at a potential ~200 mV higher than that

required for reductive reactivation of *Av*MBH.[97] The potentials of reactivation obtained from the voltammograms in Figure 3.13 (characterised by E_{switch}) are similar to the midpoint potentials of the sigmoids in Figure 3.12. It is important to note that these potentials of reactivation, measured during steady-state H_2 oxidation, are not equivalent to the spectroscopically determined midpoint potentials for the one electron reduction of Ni-B to a Ni-SI_r state.[204] As discussed in Chapter 1, despite containing Ni(II) rather than Ni(III), the Ni-SI_r states contain either a bridging water molecule or HO^- that must be released in order to regenerate active enzyme.

3.2.4 Implications of Reactivation Behaviour for O_2 Tolerance

Experiments performed by Dr. James Cracknell have shown that the O_2 tolerance of *Re*MBH^{WT}, as characterised by an O_2 tolerance factor, $K_I^{O2,app}$, depends strongly on electrode potential and temperature but is unaffected by pH in the region 4.5–6.5.[196,198] The greatest O_2 tolerance is observed at low potentials and high temperatures. These trends correlate well with the trends observed for reactivation in this thesis, but not for the trends in H_2 affinity ($K_M(H_2)$) or O_2 attack determined by Cracknell.[196,198] The value of $K_M(H_2)$ increases with increasing electrode potential and increasing temperature. Thus, while an increase in affinity for H_2 at low potential should protect the enzyme against O_2, this parameter cannot be used to explain the increase in O_2 tolerance observed at high temperature. The rates of reaction of *Re*MBH^{WT} with O_2 are not altered by changing the potential or pH but increase strongly with increasing temperature. Therefore, if the rate of O_2 attack (which includes its *access* to the active site) were the controlling factor then the hydrogenase should be less O_2-tolerant at higher temperatures, which is not the case.[196,198]

The reactivation studies presented in this chapter demonstrate that the rate of recovery from the O_2-inactivated state increases with decreasing electrode potential. The rate also increases with increasing temperature (the rate at 30 ºC is too fast to accurately measure). These trends correlate with the O_2 tolerance increasing with decreasing potentials and at high temperatures. Thus, these studies suggest that the dominant factor in determining the O_2 tolerance of *Re*MBH^{WT} is its ability to recover from the inactive state.

Furthermore, the results discussed in this chapter support the spectroscopic evidence[193] that, in contrast with standard O_2-sensitive [NiFe]-hydrogenases, *Re*MBH^{WT} generates only the Ready (Ni-B) state upon reaction with O_2. The reactivation process is monophasic, fitting to a single exponential, showing that only one inactive state is being recovered. This is in contrast with the recovery of *Av*MBH, which is biphasic due to reactivation of a mixture of both the Ready and Unready states.[66] In addition, the rates of recovery of *Re*MBH^{WT} following anaerobic and aerobic inactivation cannot be distinguished. This strongly suggests that the same state is formed regardless of whether the active site is oxidised by O_2 or anaerobically at high potential. The value of *n* (the number of electrons involved in the reductive reactivation of inactive Ni(III) to an active Ni(II) state) is 0.96, which implies that a single electron transfer is involved. This is consistent with reactivation of the Ready state (recovery from the Unready state would require three electrons, according to Scheme 3.2). The rate of reactivation from O_2 inactivation is much faster for *Re*MBH^{WT} than for *Av*MBH (*i.e.* *Re*MBH^{WT} has the kinetic advantage). Furthermore, the potential of reactivation of *Re*MBH^{WT} is more than 200 mV more positive than for the O_2-sensitive *Av*MBH[97] and its reactivation is therefore thermodynamically more favourable.

In conclusion, the potential and temperature dependencies of the O_2 tolerance of *Re*MBH^{WT} are consistent with the rate of recovery being the most important factor in determining whether or not a [NiFe]-hydrogenase will be O_2 tolerant.[196] These studies suggest a kinetic and thermodynamic model for O_2 tolerance in which a) O_2 tolerance depends upon O_2 attack generating only the rapidly-reactivating Ready state (rather than the slowly-reactivating Unready state) and b) rapid reductive reactivation of this Ready state occurs at a reasonably high potential (to ensure that reactivation is spontaneous under most conditions). This ability to fully reduce O_2 means that *Re*MBH^{WT} can be viewed as acting not only in H_2 cycling, but also as a very slow oxidase[31], catalysing the four-electron reduction of O_2 to water with a rate constant in the order of 10^{-1}-10^{-2} s^{-1}. *In vivo*, the ready supply of electrons available to *Re*MBH^{WT} due to its location embedded in the cytoplasmic membrane may protect the enzyme against O_2 inactivation.

The remaining experiments in this chapter investigate a possible way in which *Re*MBH^{WT} may avoid formation of the Unready State. Generation of the Ready state requires a greater immediate availability of electrons (and protons) than are required for formation of the Unready state (Scheme 3.1). Therefore, an ability of *Re*MBH^{WT} to provide the active site with a more reliable source of electrons than in O_2-sensitive [NiFe]-hydrogenases such as *Av*MBH could explain its generation of only the Ready state in the presence of O_2. The following sections describe PFE experiments performed on a variant of *Re*MBH that has undergone mutagenesis to remove a possible additional redox centre.

3.3 Role of Modified Proximal Cluster in O_2 Tolerance

To investigate the possible role of a modified proximal cluster in conferring O_2 tolerance, the two additional cysteines in *Re*MBH^{WT} were changed by site-directed mutagenesis

(performed by Tobias Goris at Humboldt Universität, Berlin) to the glycine residues found in the 'standard' O_2-sensitive hydrogenases. As the cysteines at positions 19 and 120 (*Re*MBH numbering, see red residues in Figure 3.4) were changed to glycines, the variant can be referred to as *Re*MBH$^{C19G/C120G}$.

Preliminary experiments confirmed that the *Re*MBH$^{C19G/C120G}$ variant hydrogenase is electrocatalytically active when adsorbed onto a PGE electrode, and thus can be studied using PFE. The remaining experiments in this chapter use PFE to compare the electrocatalytic behaviour of this variant, in particular its response to O_2, with that of the wild-type MBH.

3.3.1 Electrochemical Characterisation of *Re*MBH$^{C19G/C120G}$

3.3.1.1 Catalytic Bias

Figure 3.14 compares the catalytic bias of *Re*MBH^{WT} (Figure 3.14A) and *Re*MBH$^{C19G/C120G}$ (Figure 3.14B). The data for the wild-type enzyme are reproduced from Figure 3.6 and the cyclic voltammograms performed on the variant were recorded under identical conditions to those described previously for *Re*MBH^{WT} (Section 3.1.7.1). It can be seen that, as for the wild-type enzyme, the variant exhibits very little H_2 production activity, even under 100% N_2.

However, the voltammograms recorded under 100% H_2 for each enzyme illustrate that, even at this relatively rapid scan rate of 20 mV s^{-1}, the *Re*MBH$^{C19G/C120G}$ variant undergoes a much greater extent of high potential anaerobic inactivation than the wild-type. In Figure 3.14A, little inactivation is observed during the oxidative scan, whereas in Figure 3.14B a considerable amount of H_2 oxidation activity is lost at potentials higher than ~+50 mV, as indicated by the arrow.

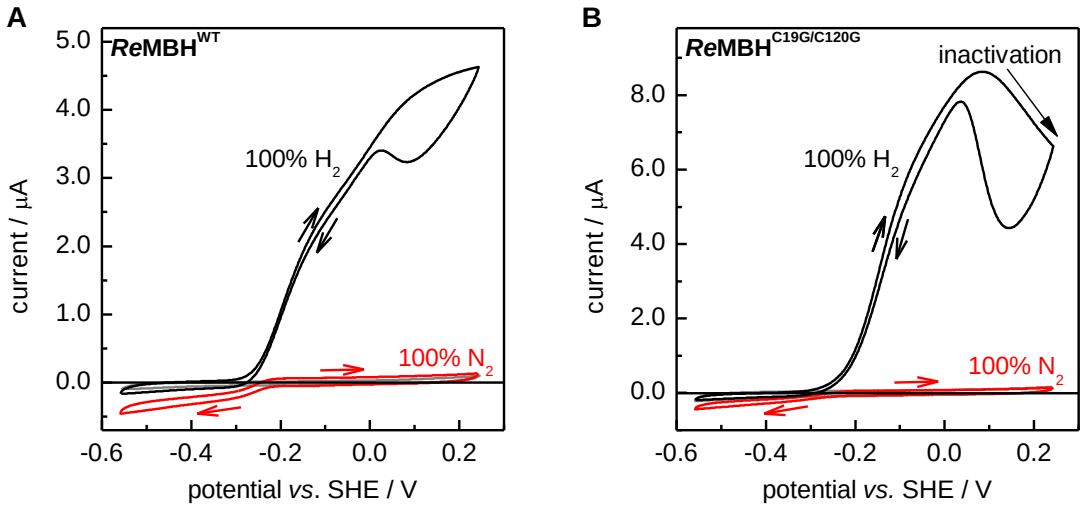


Figure 3.14. Cyclic voltammograms showing the catalytic bias of (A) *Re*MBH^{WT} and (B) *Re*MBH$^{C19G/C120G}$, recorded at 20 mV s^{-1} under 100% H_2 (black line) and N_2 (red line). The response of a blank, unmodified electrode is overlaid in grey. Other conditions: pH 5.5, 30 °C, electrode rotation rate 2500 rpm. The wild-type data is reproduced from Figure 3.6 to allow direct comparison.

3.3.1.2 Potential of Anaerobic Inactivation

As described for the wild-type enzyme in Section 3.1.7.2, anaerobic inactivation is more clearly observed during cyclic voltammograms recorded at a slower scan rate. Figure 3.15 compares cyclic voltammograms recorded under 100% H_2 at 1 mV s^{-1} for *Re*MBH^{WT} (Figure 3.15A, reproduced from Figure 3.7A) and *Re*MBH$^{C19G/C120G}$ (Figure 3.15C). As noted in the previous section, anaerobic inactivation occurs to a greater extent for the variant enzyme than for the wild-type.

Figures 3.15B and D show the plots of the first derivative of the current *vs.* potential that were used to calculate E_{switch} for *Re*MBH^{WT} and *Re*MBH$^{C19G/C120G}$ respectively (Figure 3.15B is reproduced from Figure 3.7). The value of E_{switch} for the variant lies at ~+150 mV and is therefore indistinguishable from that measured for the wild-type enzyme in Section 3.1.7.2. This indicates that, despite the greater extent of inactivation for the variant, the potential at which reactivation occurs is unaffected by the mutation.

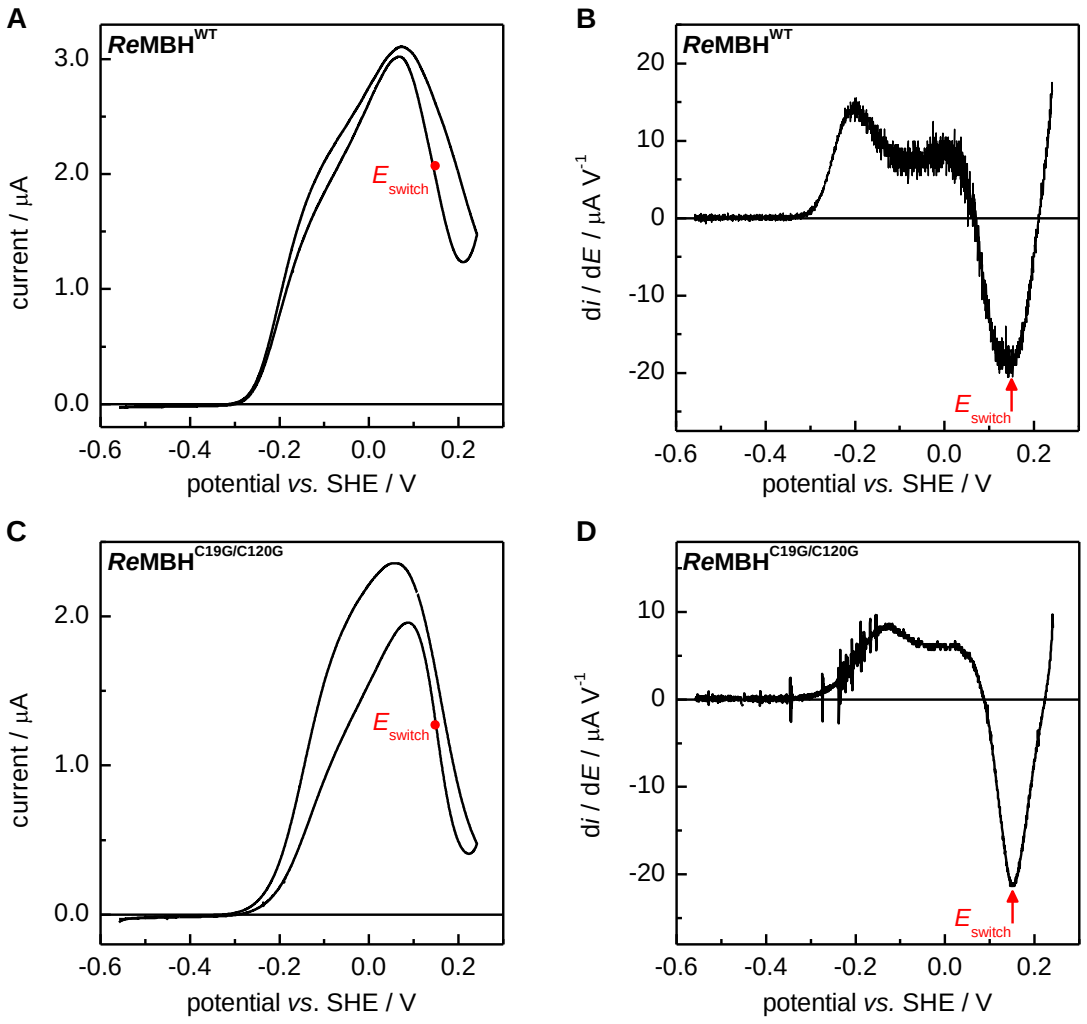


Figure 3.15. Cyclic voltammograms for (A) *Re*MBH^{WT} and (C) *Re*MBH$^{C19G/C120G}$ recorded at 1 mV s^{-1} under 100% H_2 at pH 5.5, 30 °C and electrode rotation rate 3500 rpm. (B) and (D) show the plots of the first derivative of the current with respect to potential for the wild-type and variant respectively and the minima in these curves (corresponding to the values of E_{switch}) are labelled in red. (The values of E_{switch} are also indicated by the red dots on the reductive scans of the voltammograms in (A) and (C)). The data in (A) and (B) are reproduced from Figure 3.6 to allow direct comparison.

3.3.1.3 Comparison of the $K_M(H_2)$ for *Re*MBH^{WT} and *Re*MBH$^{C19G/C120G}$

In Section 3.1.7.3, a correlation was drawn between the extent of anaerobic inactivation and the amount of H_2 available to the hydrogenase; the lower the H_2 concentration, the greater the extent of inactivation. Therefore, it may also be predicted that the affinity of a hydrogenase for H_2 (defined by its $K_M(H_2)$) may impact on the extent of anaerobic inactivation observed for that enzyme.

An electrochemical method[109,202] was used to determine the value of $K_M(H_2)$ for *Re*MBH$^{C19G/C120G}$. In this procedure the enzyme is held at a constant electrode potential, initially under 100% H_2, and the H_2 is then removed from the electrochemical cell over time by a constant flow of 100% N_2. This method assumes that the H_2 oxidation activity of the enzyme depends on substrate concentration according to the Michaelis-Menten equation (Equation 3.2)[171] and that the rate at which H_2 is flushed from the electrochemical cell can be modelled as an exponential decay (Equation 3.3)[109]:

$$v = \frac{v_{max}\,[S]}{K_M + [S]} \qquad [3.2]$$

$$[H_2]_t = [H_2]_0\, e^{-t/\tau} \qquad [3.3]$$

In these equations, v represents the rate of reaction, v_{max} is the maximum rate, [S] is the substrate (H_2) concentration, K_M is the Michaelis constant, $[H_2]_t$ is the H_2 concentration at a time = t, $[H_2]_0$ is the initial H_2 concentration and τ is the time constant. The derivation of Equation 3.2 is given in Appendix A4.

Since the limiting current at saturating substrate (H_2) concentration, i_{max}, is equivalent to v_{max}, the current *vs.* time trace obtained as the H_2 is removed from the electrochemical cell is expected to be sigmoidal, according to the following equation[109]:

$$i_t = \frac{i_{max}}{1 + \frac{K_M(H_2)}{[H_2]_0} e^{t/\tau}} \qquad [3.4]$$

In Equation 3.4, i_t refers to the H_2 oxidation current measured at time = t and all other quantities are as defined above. The derivation of this equation is also given in Appendix A4.

Figure 3.16 shows example current *vs.* time traces obtained during experiments to determine the $K_M(H_2)$ for *Re*MBH^{WT} (A) and *Re*MBH$^{C19G/C120G}$ (B). In each experiment, the electrode potential was held at a constant value of -108 mV and the H_2 oxidation current was initially monitored under 100% H_2. Then, at time designated t = 0 s, the gas flowing through the cell headspace was changed to 100% N_2.

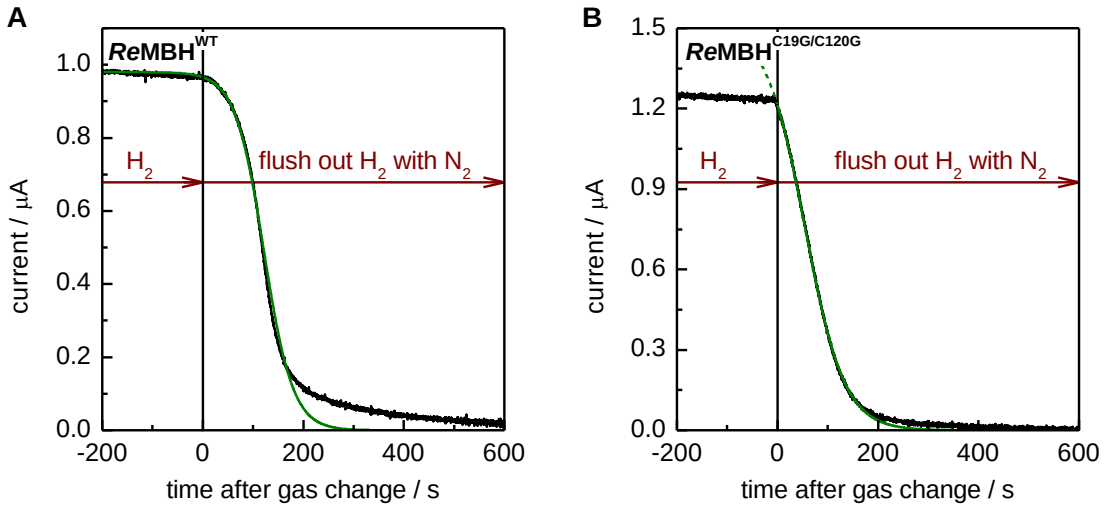


Figure 3.16. Chronoamperometry experiments used to determine the values of $K_M(H_2)$ for (A) *Re*MBH^{WT} and (B) *Re*MBH$^{C19G/C120G}$. In each case, the H_2 oxidation current was initially monitored under 100% H_2 at -108 mV. At time designated t = 0 s, the gas flowing through the cell headspace was changed to 100% N_2 to flush the H_2 out of the system. The values of $K_M(H_2)$ were obtained by fitting the current *vs.* time traces to the sigmoid given by Equation 3.4. Other conditions: pH 5.5, 30 ºC, electrode rotation rate 4500 rpm.

Control experiments[198,202] have confirmed that flushing the cell with N_2 leads to an exponential decay in the concentration of H_2 over time, according to Equation 3.3. From Figure 3.16 it is clear that *Re*MBH^{WT} and *Re*MBH$^{C19G/C120G}$ respond very differently to the changing H_2 concentration. For the wild-type enzyme, there is initially no change in H_2 oxidation current upon changing the gas flow to N_2, and the response is sigmoidal as expected from Equation 3.4. However, the H_2 oxidation current for the *Re*MBH$^{C19G/C120G}$ variant rapidly decreases immediately after the change in gas, showing that the activity of

the variant is sensitive to the H_2 concentration even at levels close to 100% H_2. This indicates that the variant has a higher $K_M(H_2)$ than the wild-type.

Overlaid in Figure 3.16 are the sigmoidal fits used to calculate the values of $K_M(H_2)$. The value obtained for *Re*MBH^{WT} was consistent with the published value of 6.1 μM (-108 mV, pH 5.5, 30 °C).[202] However, since the activity of *Re*MBH$^{C19G/C120G}$ was still dependent on the H_2 concentration even at 100% H_2 (corresponding to ~760 μM dissolved H_2) the data collected for this enzyme were more difficult to analyse accurately. Since an enzyme is usually considered to be substrate-saturated at substrate concentrations more than 10 x K_M,[202] this suggests that the $K_M(H_2)$ for the *Re*MBH$^{C19G/C120G}$ variant should be greater than 76 μM. To obtain an approximate value for $K_M(H_2)$ for *Re*MBH$^{C19G/C120G}$, the data were extrapolated to fit a sigmoid (overlaid in Figure 3.16) given by Equation 3.4. The estimated value of $K_M(H_2)$ determined in this way was ~160 μM.

These results clearly show that that $K_M(H_2)$ for *Re*MBH$^{C19G/C120G}$ is much higher than for *Re*MBH^{WT}, suggesting that the variant has a lower affinity for H_2. This is consistent with the greater extent of anaerobic inactivation observed for the variant, since an enzyme molecule less able to bind H_2 will be more likely to undergo anaerobic inactivation, during which a water molecule binds to the active site to form the HO^- bridge present in the Ready state.

The extent of anaerobic inactivation will depend on the relative rates of inactivation and reactivation. Therefore, experiments were performed to compare the kinetics of these processes for the wild-type and variant enzyme.

3.3.1.4 Rates of Anaerobic Inactivation and Reactivation

The rate of high potential anaerobic inactivation of *Re*MBH$^{C19G/C120G}$ was measured by a method previously used to determine the rates for *Av*MBH and *Re*MBH^{WT}.[198,203] An enzyme-modified electrode was initially held at -558 mV for 300 s under 100% H_2 to ensure that all the enzyme molecules were in an active state. The potential was then stepped to a high value, significantly above E_{switch}, to initiate anaerobic inactivation. The resulting decrease in current was recorded for 900 s. The potential was then stepped back to -558 mV for 300 s to reactivate the enzyme before the potential was again increased to a high value. Figure 3.17A shows an experiment performed using this method, in which data were collect for anaerobic inactivation at four different potentials. The black sections of the current *vs.* time trace correspond to the periods of time during which the enzyme was activated at -558 mV, and the coloured regions show the decreases in current caused by anaerobic inactivation at the potentials indicated in the figure.

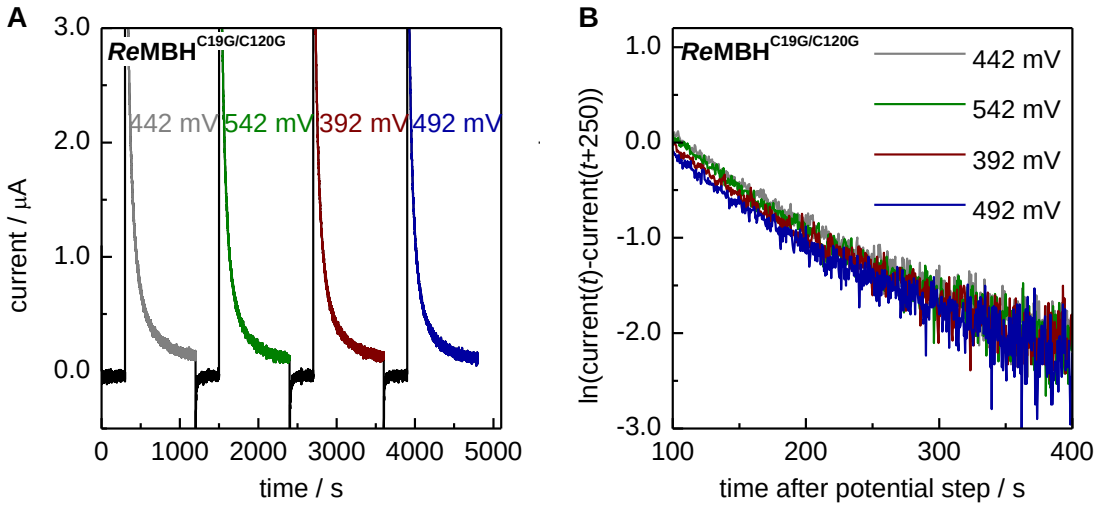


Figure 3.17. (A) A chronoamperometry experiment used to determine the rate of anaerobic inactivation of *Re*MBH$^{C19G/C120G}$ at various potentials. The black sections of the current *vs.* time trace correspond to the periods of time during which the enzyme was activated at -558 mV, and the coloured regions show the decreases in current caused by anaerobic inactivation at the potentials indicated in the figure. (B) Shows the data transformed using a Guggenheim analysis.[205,206] Conditions: 100% H_2, pH 5.5, 30 °C, electrode rotation rate 4500 rpm.

In Figure 3.17B, the anaerobic inactivation data from Panel A have been transformed using a Guggenheim analysis.[205,206] As previously determined for *Re*MBH^{WT}, the Guggenheim traces for *Re*MBH$^{C19G/C120G}$ are parallel to one another, indicating that the rate (calculated from the negative of the gradient) is independent of potential. To calculate accurate rates of inactivation, the coloured current *vs.* time traces in Figure 3.17A were fitted to single exponential curves. This yielded a value of 0.006 s^{-1} at every potential, thus confirming that the rate of anaerobic inactivation does not depend on potential over this range. This rate of anaerobic inactivation obtained for *Re*MBH$^{C19G/C120G}$ is double the value determined previously for *Re*MBH^{WT} under the same conditions (0.003 s^{-1}).[198] A rate of 0.006 s^{-1} was also obtained for *Re*MBH$^{C19G/C120G}$ in a set of experiments designed to correct the data for film loss of the enzyme from the electrode surface during the course of the experiment (data not shown).

Attempts were also made to determine the rates of reductive recovery for *Re*MBH$^{C19G/C120G}$ following anaerobic inactivation, using the method outlined in Section 3.2.1. The rates determined for recovery at potentials between +100 and +200 mV were in general slightly higher than those for the wild-type enzyme, but lie within the scatter of the data in Figure 3.12. At low potentials, below -50 mV, accurate rates of reactivation could not be determined for the *Re*MBH$^{C19G/C120G}$ variant since, even at 10 ºC, the rate of recovery was so fast that most of the data were lost during the capacitive 'dead-time', as was also observed for the wild-type enzyme. Additional problems arose in the analysis of the data for the variant enzyme since the sample of ReMBH$^{C19G/C120G}$ used in these experiments was unstable on the electrode surface, which further hindered accurate exponential fits to the data.

3.3.1.5 The Effect of Short-term Exposure to O_2

Experiments were performed to assess the effect of the removal of the two additional cysteine residues from the surroundings of the proximal FeS cluster on the ability of *Re*MBH to catalyse H_2 oxidation in the presence of O_2. Firstly, the ability of the enzyme to recover from transient, short-term exposure to O_2 was monitored using cyclic voltammetry. Figures 3.18A and B compare the immediate responses of *Re*MBH^{WT} and *Re*MBH$^{C19G/C120G}$ following transient exposure to O_2. The cyclic voltammograms were recorded at 1 mV s^{-1} under 100% H_2. In each case, at 0 mV on the forward scan, 300 μL of O_2-saturated buffer was injected to the 2 mL solution already in the cell to give a final concentration of dissolved O_2 ~142 μM.[199] The addition of O_2 resulted in only a small attenuation in current for both enzymes, indicating that *Re*MBH^{WT} and *Re*MBH$^{C19G/C120G}$ respond similarly to short-term exposure to O_2.

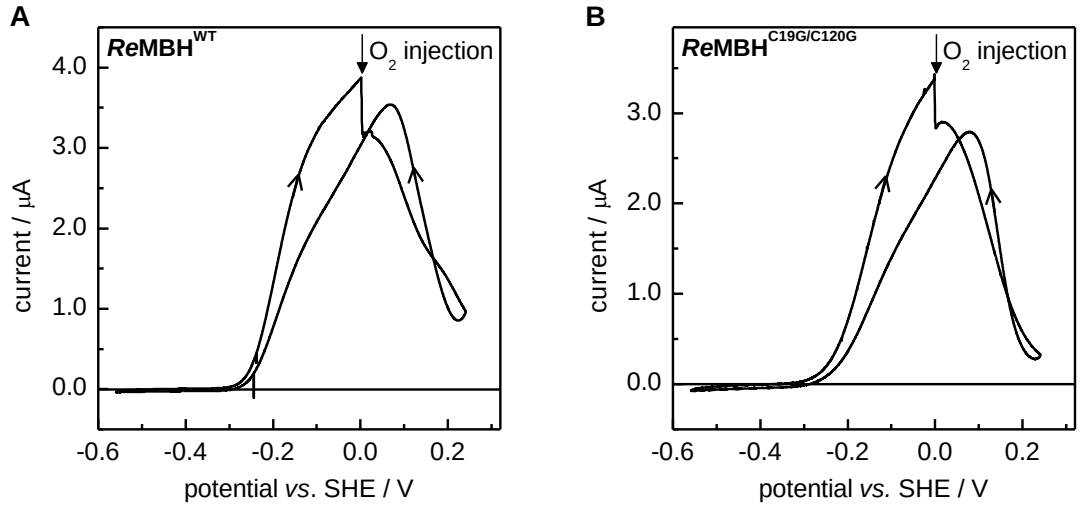


Figure 3.18. Cyclic voltammograms recorded at 1 mV s^{-1} for (A) *Re*MBH^{WT} and (B) *Re*MBH$^{C19G/C120G}$ under 100% H_2. At 0 mV on the oxidative sweep, O_2-saturated buffer was injected (indicated by a solid arrow, final concentration ~142 μM) and then rapidly removed by flushing with H_2. Other conditions: 30 °C, pH 5.5, electrode rotation rate 3500 rpm.

Following the O_2 injection at 0 mV, the O_2 was flushed out of the cell by the flow of H_2 during the remainder of the forward scan. As the O_2 was removed from the cell, the

enzymes each recovered some H_2 oxidation activity before undergoing anaerobic inactivation at high potential. All the O_2 was removed from the cell prior to commencing the return scan (starting at +242 mV). On this scan towards low potential, both enzymes recovered considerable activity and the switch potentials are indistinguishable from those determined under fully anaerobic conditions.

These data suggest that the *Re*MBH$^{C19G/C120G}$ variant is able to cope with short-term exposure to O_2. However, in order to be classed as truly O_2-tolerant an enzyme must be able to function even during long-term exposure to O_2.

3.3.1.6 The Effect of Long-term Exposure to O_2

To further probe the O_2 tolerance of *Re*MBH$^{C19G/C120G}$ compared to that of *Re*MBH^{WT}, chronoamperometry experiments (Figures 3.19A and B) were performed to test the ability of the variant to sustain H_2 oxidation activity during prolonged exposure to O_2.

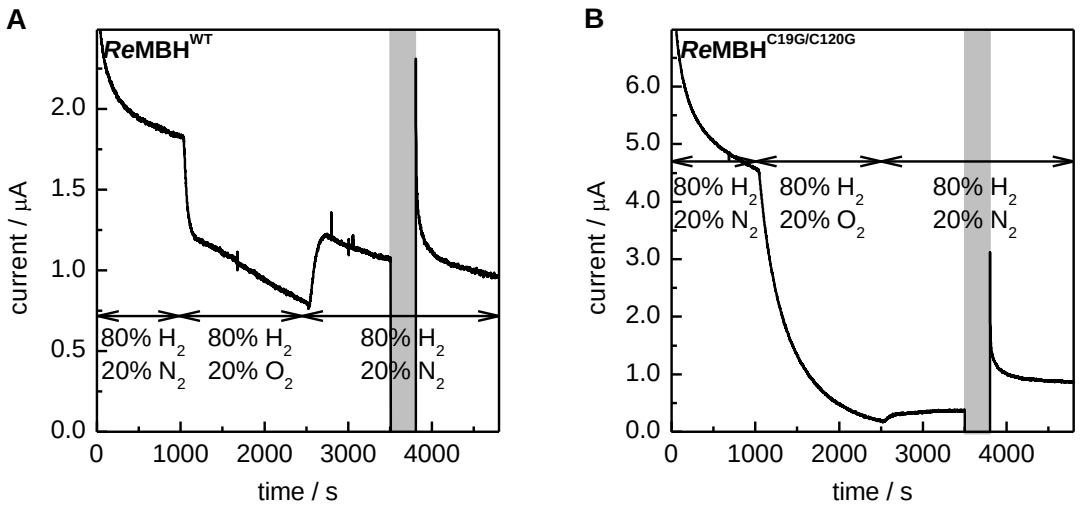


Figure 3.19. A comparison of the responses of (A) *Re*MBH^{WT} and (B) *Re*MBH$^{C19G/C120G}$ to long-term exposure to O_2. The measurements were made under a constant H_2 concentration of 80% at -8 mV. After 1000 s, the remaining 20% gas fraction was changed from N_2 to O_2, then after an additional 1500 s it was restored to 20% N_2. Finally, a step down to -558 mV was performed (grey box), followed by an increase of the potential back to –8 mV.

In each case, the enzyme was initially held at an electrode potential of -8 mV for 1000 s under a gas flow of 80% H_2 in N_2. At this potential, both O_2 reduction at exposed regions of bare graphite (favoured at lower potentials) and anaerobic inactivation (favoured at higher potentials) are minimised. Therefore, the decrease in current observed during the initial time period can be attributed to film loss from the electrode surface. At 1000 s, the N_2 was replaced by O_2 to give a gas mixture of 80% H_2 and 20% O_2. For both wild-type and the variant enzyme, this led to a decrease in H_2 oxidation current as the enzyme became inhibited by O_2. Then, after 1500 s, the O_2 was removed by flushing with the original gas composition of 80% H_2 and 20% N_2. After a further 1000 s, the potential was stepped down to -558 mV (indicated by the grey boxes in Figure 3.19) for 300 s before the potential was returned to -8 mV.

For *Re*MBH^{WT} (Figure 3.19A), exposure to O_2 leads to a rapid decrease in H_2 oxidation current to ~70% of the original level. This current then remains relatively stable, excluding the slow decrease in current caused by film loss. Removal of O_2 leads to a significant recovery of the initial activity and the step to low potential results in little further increase in current. This is consistent with the previous observations that, for *Re*MBH^{WT}, even long-term exposure to O_2 does not generate an inactive state, such as Unready (Ni-A), that requires prolonged incubation at low potentials for reactivation.[193,196]

In contrast, *Re*MBH$^{C19G/C120G}$ (Figure 3.19B) shows very different behaviour under these conditions; exposure to 20% O_2 leads to almost complete loss of H_2 oxidation current over 1500 s. Only a small amount of H_2 oxidation current is recovered as the O_2 is flushed out by 80% H_2 in N_2. However, holding the enzyme at -558 mV for 300 s results in

recovery of a significant amount of additional activity. A further step to low potential does not produce a further increase in H_2 oxidation current, although a small increase may be obscured by film loss of the enzyme from the electrode surface. The final recovered H_2 oxidation current is considerably smaller than the original level, even accounting for film loss. Therefore, it appears that a major fraction of O_2-inactivated enzyme does not recover under these conditions.

These data show that long-term exposure to O_2 has a much greater affect on H_2 oxidation by *Re*MBH$^{C19G/C120G}$ than by *Re*MBH^{WT}. Although the variant enzyme is able to recover and continue H_2 oxidation following transient exposure to O_2, it is unable to sustain H_2 oxidation activity during long-term exposure to O_2. This is in contrast to the O_2-tolerant wild-type enzyme, which can maintain catalytic activity even in the presence of 20% O_2.

3.3.1.7 The Extent of Inhibition by CO

Previous electrochemical studies into the carbon monoxide (CO) inhibition of H_2 oxidation by *Re*MBH^{WT} suggested that the activity of the enzyme is completely unaffected by CO.[114] This greatly contrasts the case of O_2-sensitive [NiFe]-hydrogenases, for which CO is a potent competitive inhibitor of H_2 oxidation.[39,109,114,116] However, the published data for *Re*MBH^{WT} were obtained from a chronoamperometry experiment in which the gas flowing through the cell headspace was changed from 10% H_2 in N_2 to 13% H_2 in CO. Any weak inhibition of H_2 oxidation by CO may therefore have been obscured by a small increase in activity owing to the slightly higher concentration of H_2.

The cyclic voltammograms in Figures 3.20A and B compare the activity of *Re*MBH^{WT} in the presence and absence of CO. The voltammograms shown in Figure 3.20A were recorded on the same film of enzyme under 10% H_2 in N_2 and 10% H_2 in CO

(corresponding to 90% CO). By comparing these two voltammograms it can be seen that, in agreement with the previous work, H_2 oxidation by *Re*MBH^{WT} is largely unaffected by the presence of even 90% CO. The largest attenuation in current is observable in the potential region -150 to +20 mV, whereas at +142 mV, the potential at which the previously reported experiment[114] was performed, very little inhibition is observable in Figure 3.20A.

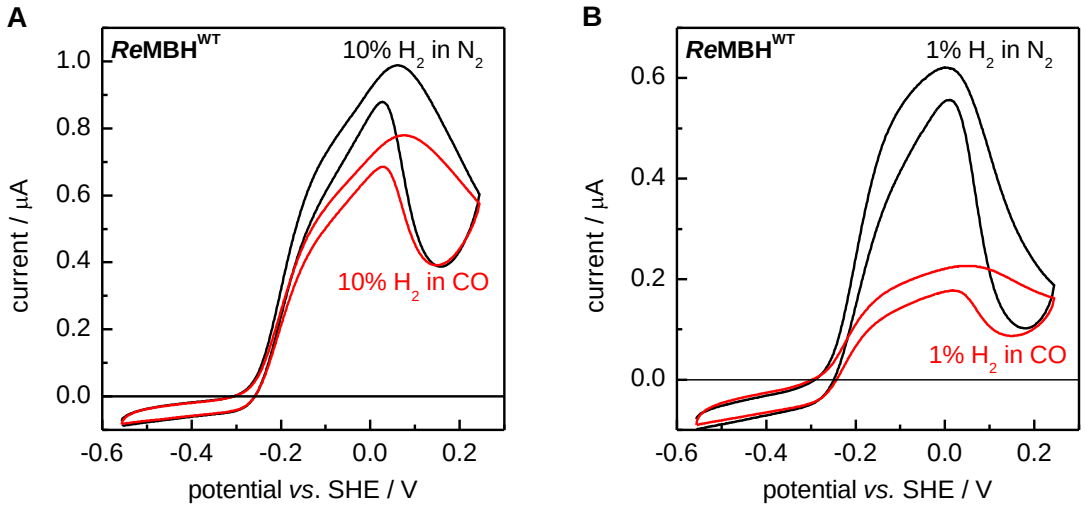


Figure 3.20. Cyclic voltammograms showing CO inhibition of H_2 oxidation by *Re*MBH^{WT}. The voltammograms were recorded at 10 mV s^{-1} under (A) 10% H_2 in N_2 (black line) and 10% H_2 in CO (red line) and (B) 1% H_2 in N_2 (black line) and 1% H_2 in CO (red line) at pH 5.5, 30 °C, electrode rotation rate 3500 rpm.

The cyclic voltammograms in Figure 3.20B were recorded under just 1% H_2 in N_2 or CO (corresponding to 99% N_2 or CO). The inhibition occurs to a much greater extent under these conditions, and at -50 mV only one third of the H_2 oxidation is retained in CO compared to N_2. This inhibition is reversible, and taking into consideration any decrease in current with time caused by film loss, activity is completely restored on changing the gas mixture from H_2 in CO back to H_2 in N_2.

Carbon monoxide is a well-known competitive inhibitor of O_2-sensitive [NiFe]-hydrogenases and structural and spectroscopic studies performed on the 'standard' [NiFe]-hydrogenase from *Desulfovibrio vulgaris* Miyazaki F (*Dv*) have shown that CO binds to the Ni atom of the bimetallic active site.[39] Studies have also shown that CO can replace H_2 in the reactivation of inactive hydrogenase.[66,195] In Figures 3.20A and B, the shapes of the cyclic voltammograms recorded in the presence of CO differ from those obtained in its absence. The differences between them can be considered in three regions.

At potentials below -200 mV, the current *vs.* potential traces overlay because the driving force is so low that the current is limited by electron transfer rather than the reactions occurring at the active site. In the central region, at potentials between -150 and +20 mV, the ratio of the current under N_2 to that obtained under CO is constant (the current under CO is ~76% of that obtained under N_2 at 10% H_2 and this decreases to just ~33% at 1% H_2). At high potentials (greater than +200 mV), the voltammograms reach similar currents regardless of whether or not they are recorded in the presence of CO. Since the currents at lower potentials are attenuated in the presence of CO relative to those obtained in its absence, this effectively represents a smaller extent of anaerobic inactivation of active enzyme in the presence of CO. This suggests that CO, as discussed for H_2 in Section 3.1.7.3, can protect the enzyme against anaerobic inactivation

These results demonstrate that carbon monoxide can act as a competitive inhibitor of H_2 oxidation by *Re*MBH^{WT}, although its binding is very weak. This insensitivity towards CO is a property shared by other O_2-tolerant [NiFe]-hydrogenases.[115,117] Suggestions have been made that the link between CO insensitivity and O_2 tolerance may result from a gas channel affect; an enzyme may be unaffected by both molecules if it has sufficiently

narrow access to the active site.[33,49,76,207-209] Experiments were therefore performed to test whether the *Re*MBH$^{C19G/C120G}$ variant, which is sensitive towards long-term exposure to O_2, is inhibited by CO to a greater extent than the O_2-tolerant wild-type enzyme.

The CO sensitivity of the variant was compared to that of wild-type using chronoamperometry, and the results are shown in Figure 3.21. In each case, the enzyme-modified electrode was held at a constant potential of -58 mV under 10% H_2 in N_2 for 600 s, to monitor the slow decrease in current due to film loss. The gas flowing through the cell headspace was then changed to 10% H_2 in CO, and a small attenuation in current is observed for both *Re*MBH^{WT} and *Re*MBH$^{C19G/C120G}$. Upon removal of the CO, the H_2 oxidation current recovers in each case, confirming that CO is a reversible inhibitor of both the variant and wild-type enzyme. Despite the much greater O_2 sensitivity of *Re*MBH$^{C19G/C120G}$ compared to the wild-type, the variant shows tolerance towards CO very similar to that exhibited by the wild-type enzyme.

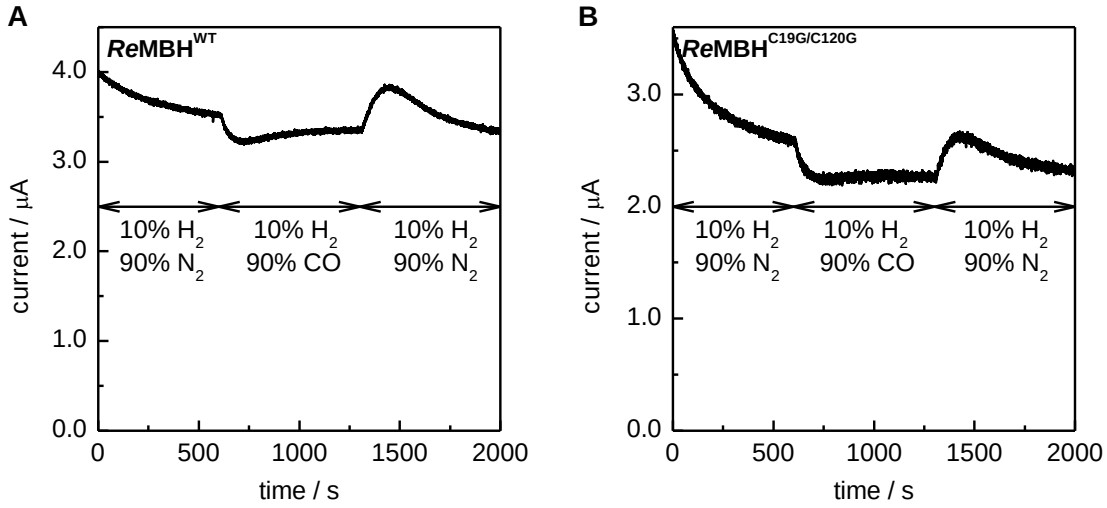


Figure 3.21. Chronoamperometry experiments comparing CO inhibition of H_2 oxidation by (A) *Re*MBH^{WT} and (B) *Re*MBH$^{C19G/C120G}$. In each case, the gas flow was changed from 10% H_2 in N_2 to 10% H_2 in CO and back again, as indicated by the arrows in the figure. Other conditions: -58 mV, pH 5.5, 30 ˚C, electrode rotation rate 2500 rpm.

The current *vs.* time traces in Figure 3.21 have slightly more complex shapes than might be expected. They do not show steady decreases in current following introduction of CO, and the current obtained immediately after its removal is higher than would be expected based on the size of the initial currents. Carbon monoxide is known to replace H_2 as an activator of inactive states of hydrogenases[66,195] and Section 3.1.7.3 discussed protection against inactivation by high levels of H_2. Given the rapid rates of reactivation discussed in this chapter, any enzyme in the Ni-B (Ready) state should activate during the initial 600 s under 10% H_2 in N_2. Therefore, the observed shape of the traces in Figure 3.21 may be explained by CO reactivating any inactive states, other than Ni-B, that are present in the sample. Such states may include S-oxygenates involving either bridging or terminal thiolates.[197] The enzyme samples were not activated prior to the experiments and therefore any states that are not reactivated under 10% H_2 in N_2 may be activated under 10% H_2 in CO (which effectively resembles '100%' H_2). Therefore, as the carrier gas is changed from N_2 to CO, the current initially decreases due to competitive inhibition, but then increases slightly as more enzyme is activated to a catalytically active state. Therefore, upon removal of the CO the immediate current is higher than that recorded before the introduction of CO since more enzyme molecules are available in an active state for H_2 oxidation. Similar experiments involving a second step to 90% CO before returning to 90% N_2 may confirm whether the unexpected shape of the current *vs*. time trace is in fact due to such a reactivation process.

The fact that the *Re*MBH$^{C19G/C120G}$ variant shows CO tolerance similar to that of *Re*MBH^{WT} suggests that the removal of the two cysteine residues close to the proximal FeS cluster does not alter the size of the gas channel (*i.e.* the ability of a small molecule such as CO or O_2 to access the active site). It is therefore likely that the differences in O_2

sensitivity between the wild-type and variant are due to the differences imposed on the proximal FeS cluster itself, as will be discussed in detail below.

3.4 Discussion

The results outlined in this chapter strongly suggest that O_2 tolerance may be conferred in *Re*MBH^{WT} as a result of its ability to avoid formation of the Unready (Ni-A) inactive state by ensuring a reliable supply of the three electrons required for generation of the Ready (Ni-B) state. Section 3.2.4 discussed the strong correlation between the rates of reactivation from O_2-inactivation and the degree of O_2 tolerance exhibited by the enzyme. In collaboration with Dr. James Cracknell, a kinetic and thermodynamic description of O_2 tolerance has been characterised: the ability to generate only a rapidly-reactivating state that recovers at high potential is essential for O_2-tolerance.[196]

The electrochemical studies performed on the *Re*MBH$^{C19G/C120G}$ variant demonstrate that the removal of the two additional cysteine residues, present only in O_2-tolerant [NiFe]-hydrogenases, results in an enzyme that is now O_2-sensitive. Although *Re*MBH$^{C19G/C120G}$ can recover from transient exposure to O_2 (Figure 3.18), the variant is unable to sustain H_2 oxidation during prolonged exposure to O_2, and requires a low potential for reactivation from the O_2-inactivated state (Figure 3.19).

The observations made using PFE are consistent with biochemical growth measurements performed by Tobias Goris at the Humboldt Universität, Berlin.[210] The cells were grown in minimal medium under conditions of 80% H_2 and 10% CO_2 with either 2% or 10% O_2, made up to 100% with N_2. Growth is independent of O_2 concentration over this range for the strain containing the O_2-tolerant wild-type hydrogenase, reflecting the ability of *Re*MBH^{WT} to sustain H_2 oxidation under aerobic conditions. However, the doubling time

increases from 15 hr at 2% O_2 to 155 hr at 10% O_2 for the *Re*MBH$^{C19G/C120G}$ variant strain and an *Re*MBH^{C19G} strain, in which only cysteine residue 19 is mutated to a glycine, shows only very slow growth, even under just 2% O_2. These results are summarised in Figure 3.22.[210]

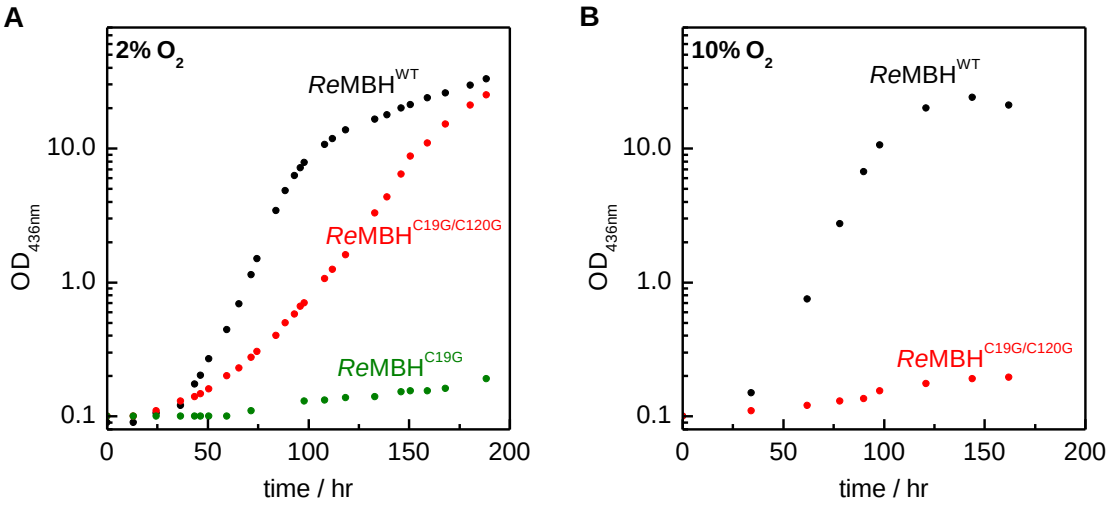


Figure 3.22. Growth curves monitoring the lithoautotrophic growth of cells containing *Re*MBH^{WT} (black), *Re*MBH$^{C19G/C120G}$ (red) and *Re*MBH^{C19G} (green) in the presence of (A) 2% O_2 and (B) 10% O_2. The cells were grown in minimal medium under conditions of 80% H_2 and 10% CO_2 with either 2% or 10% O_2, made up to 100% with N_2. This data was recorded by Tobias Goris and is taken from reference [211].

Tobias Goris also attempted to grow a variant strain with only the cysteine at position 120 exchanged for glycine (*Re*MBH^{C120G}), but this variant proved unable to grow on H_2 in the presence of O_2. Only small traces of the hydrogenase subunits were identified during immunoblot analysis of this variant, but a band corresponding to a cytoplasmic precursor form of HoxK was observed. This suggests that the FeS clusters may not assemble correctly in this variant, which would prevent translocation through the membrane.[210]

Section 3.1.4 introduced EPR studies performed on the O_2-tolerant membrane-bound [NiFe]-hydrogenases *Re*MBH^{WT}, *Ec*Hyd1 and *Aa*Hase1, which all suggest the presence of an additional paramagnetic centre at high potential located at or close to the proximal

[4Fe4S]-cluster.[115,193,212] The work performed on *Aa*Hase1, which also included ^{57}Fe Mössbauer studies, identifies the paramagnetic centre (seen as 'wings' in the high potential spectra) as the proximal cluster (assumed to be a [4Fe4S] species) in a 3+ oxidation state, thus suggesting that this FeS cluster can undergo two redox transitions, 2+/1+ and 3+/2+.[212] A situation in which a [4Fe4S]-cluster can perform two sequential redox transitions is highly unusual, and the authors propose that the two additional cysteines, conserved only in O_2-tolerant hydrogenases, may alter the geometry and redox properties of the FeS cluster in order to lower the potential of the 3+/2+ transition.[212]

The crystal structure of *Re*MBH^{WT} (Figure 3.4) supports the theory that the proximal cluster of O_2-tolerant [NiFe]-hydrogenases has a modified geometry. In this enzyme, the proximal cluster appears to be a [4Fe3S]-species with the residue Cys19 replacing one of the inorganic sulfate ligands. In addition, the high potential EPR spectrum for the *Re*MBH$^{C19G/C120G}$ variant (recorded by Miguel Saggu at the Technische Universität, Berlin)[210] does not show the splitting ('wings') seen in wild-type samples, suggesting that the ability to undergo the additional high potential transition has been removed by replacement of the two cysteine residues. A positive potential for a transition suggests a more stable reduced state. Therefore, an FeS cluster with a high potential is more able to stabilise electrons, thus rendering them more available for transfer back to the active site upon O_2 attack.

Generation of only the rapidly-reactivating Ready (Ni-B) state requires fast and reliable delivery of three electrons to the active site, to avoid formation of reactive oxygen species, such as peroxide (as found in the Ni-A, Unready state). These three electrons could in theory be released one from each of the three FeS clusters (proximal, medial and

distal), but this requires that all three clusters are in their reduced state at the time of O_2 attack. (*In vitro*, these electrons originate from the electrode, whereas *in vivo* they may be present if O_2 attacks just after H_2 oxidation or they may originate from the quinone/quinol pool (Figure 3.1)). If the modified proximal cluster in *Re*MBH^{WT} is able to provide an additional electron, this will increase the probability that three electrons will always be available to reduce O_2 at the active site, thus ensuring that only the Ready state is formed, even during prolonged exposure to O_2. Conversely, if the proximal cluster in the *Re*MBH$^{C19G/C120G}$ variant is no longer able to furnish this additional electron, the probability of three electrons being available will decrease. This may explain the observation that the variant can cope with short-term, but not long-term exposure to O_2, since over a long period of time a lower probability of three electrons being available for complete O_2 reduction may lead to an accumulation of Unready inactive state(s). Since no Ni-A has been detected even for the *Re*MBH$^{C19G/C120G}$ variant, these states likely include oxidatively-damaged EPR silent species.[210]

In conclusion, the work outlined in this chapter emphasises the importance for O_2 tolerance of generating only an O_2-inactivated state that recovers rapidly and at high potential. In *Re*MBH^{WT} the redox potentials of the FeS cluster relay (-180 mV to +160 mV)[213] lie within the potential range of the haem cofactors in the cytochrome *b* (+10 mV and +166 mV) and the quinone/quinol pool (+90 mV) in the membrane that it connects to.[188] Therefore, in wild-type *Re*, H_2 oxidation by the MBH can be sustained even under aerobic conditions since electrons removed from the quinone/quinol pool to fully reduce O_2 to generate the Ready state of the enzyme are replenished by H_2 oxidation by active hydrogenase molecules. The PFE experiments discussed in this chapter show that removal of two cysteine residues, Cys19 and Cys120, renders *Re*MBH O_2-sensitive.

This is likely due to modifications of the proximal cluster that prevent it from providing an additional electron upon O_2 attack, as required to ensure generation of only the rapidly reactivating Ready state, as produced by the wild-type. The variant enzyme forms inactive states that recover significantly only at low potential and thus formation of these inactive states would act as a dead end *in vivo*, since the biological conditions are not sufficiently reducing.[211]

Chapter 4 Characteristics of an Enzymatic H_2/O_2 Fuel Cell Using an O_2-Tolerant Hydrogenase as the Anode Catalyst

Abstract

It has been proposed that O_2-tolerant hydrogenases may prove useful in biotechnological applications, such as fuel cells. This chapter evaluates the power characteristics of an enzymatic fuel cell employing an O_2-tolerant [NiFe]-hydrogenase from *Escherichia coli* as the anodic biocatalyst for H_2 oxidation and bilirubin oxidase as the cathodic biocatalyst for O_2 reduction. The following three limiting operating conditions were investigated: a) the anode and cathode separated by a Nafion proton exchange membrane, with 100% H_2 and 100% O_2 provided to the separate compartments; b) a membraneless mixed-feed cell with a fuel-rich (96% H_2) H_2/O_2 mixture, and c) a membraneless mixed-feed cell with a fuel-weak (4% H_2) H_2/air mixture. The H_2-poor fuel cell produces power only if a high resistance is applied to maintain a high output voltage; a low resistance collapses the power (like a circuit breaker) due to inactivation of even an O_2-tolerant [NiFe]-hydrogenase when subjected to O_2 at high potential. Recovery of this H_2-poor fuel cell is not achieved simply by reapplying a high resistance, but rather by briefly connecting a second anode containing active hydrogenase, which releases electrons from H_2 oxidation to provide a 'jump start'. The second anode remains active despite experiencing the same O_2 environment as the first because it is not electrochemically connected to an oxidising source (the cathode). This work therefore demonstrates that, under 4% H_2, the presence of 20% O_2 alone is not sufficient to cause inactivation of an O_2-tolerant [NiFe]-hydrogenase, since simultaneous connection to an oxidising potential is also required. This work aids the understanding of suitable operating conditions for hydrogenases in fuel cells and highlights obstacles that must be overcome for their successful application. The biological relevance of this work is also discussed.

This chapter is reproduced in part from: Wait, A. F.; Parkin, A.; Morley, G. M.; dos Santos, L.; Armstrong F. A. *J. Phys. Chem. C*, **2010**, *114*, 12003–12009 (http://pubs.acs.org/doi/abs/10.1021/jp102616m).

4.1 Introduction

4.1.1 An Introduction to Enzymatic Fuel Cells

A fuel cell is a device that combines oxidation of a fuel (at the anode) with reduction of an oxidant (at the cathode), converting the chemical energy into electrical energy. The electrons released by oxidation at the anode are transported to the cathode via an external circuit, thus generating electrical current.[214] This concept was first demonstrated in the late 1830s, through independent studies by Grove and Schoenbein.[12,13] They showed that the combination of two platinum wires, one for oxidising H_2 and the other for reducing O_2, resulted in both the production of water and an electrical current between the two wires. Figure 4.1 shows a schematic representation of a simple fuel cell.

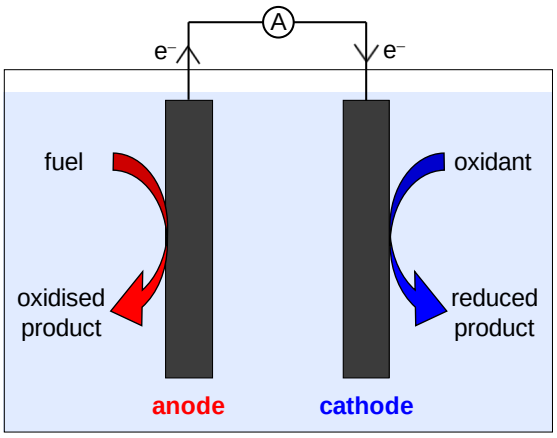


Figure 4.1. Schematic representation of a fuel cell converting chemical energy to electrical energy.

Currently, precious metal catalysts, such as platinum, are widely used in fuel cells.[215] However, in order to allow the widespread use of fuel cells and other related technologies, it is desirable to develop electrocatalysts that are inexpensive, while exhibiting high catalytic turnover. Enzymes at first glance represent an attractive solution. Their active sites contain only common metals or organic cofactors, and their high efficiency and substrate selectivity may be useful in niche low-power applications such as

self-powered sensors.[150,216] Enzymatic fuel cells, in which the oxidation and/or reduction reactions are catalysed by isolated and purified enzymes, often operate under ambient conditions, close to neutral pH.[214] The strong specificity of enzymes also means that these fuel cells can operate on a mixed fuel-oxidant feed, thus removing the need for a proton exchange membrane (Section 4.5.1). In addition, enzymes enable the use of a wide range of fuels, since any substrate that is oxidised by an enzyme may in principle be used as a fuel.[216]

However, there are several disadvantages to using enzymes as electrocatalysts. The large size of these molecules means that they impose a large footprint on the electrode surface and therefore, although their activity per active site is often very large,[217,218] the activity per volume is low. In addition, the active site is often buried within the bulky protein environment and therefore mediators are usually required to transfer electrons from the electrode to the active site, unless the enzyme contains an electron transfer relay, such as the chain of FeS clusters present in hydrogenases. Electron transfer is a major challenge, particularly in enzyme fuel cells utilising sugars as fuel, and efforts have been made to overcome this problem.[219,220] Furthermore, enzymatic fuel cells suffer from long-term instability, which may be caused by denaturation or inactivation of the enzyme or, in cases where the enzyme is immobilised onto the electrodes, desorption from the electrode surface.[221]

Due to its possible future role as an energy carrier, there has been much interest in developing fuel cells that use H_2 as the fuel. Combination of H_2 and O_2 to form water is highly exothermic (ΔG = -237.2 kJ mol^{-1} at 25 ºC)[166] and therefore H_2/O_2 fuel cells could provide an efficient means of converting chemical energy into electricity.[9] The following

section introduces the H_2/O_2 fuel cell in more detail and introduces the use of enzymes as the catalysts in such a system.

4.1.2 Enzyme Biocatalysts for H_2/O_2 Fuel Cells

Fuel cells operating with H_2 as the fuel and O_2 as the oxidant provide a clean method of converting chemical energy into electricity, with water as the only by-product. They also operate with high thermodynamic efficiencies (45-60% efficiency compared to around 15% for internal combustion engines), but currently most H_2 is produced from the energy-intensive steam reformation of fossil fuels, which are non-renewable.[9] However, the generation of H_2 from sunlight represents an attractive method for producing H_2 from a renewable energy source and there has been much interest in recent years in the use of solar energy to convert water into H_2 and O_2 (termed artificial photosynthesis).[18,23-25] In one example, an enzyme fuel cell was even used to combine the generation of electricity with H_2 production; an [FeFe]-hydrogenase adsorbed onto a carbon felt electrode acted as the cathode, while the dye-sensitised TiO_2 photo-anode drove the oxidation of a biofuel substrate via oxidation of NADH.[145] More recently, Chader *et al.* used biohydrogen produced by hydrogenases present in green microalgae to fuel a small proton exchange membrane fuel cell.[222] The possibility of generating H_2 from solar energy means that H_2/O_2 fuel cells could present an appealing route to clean and renewable electricity generation.

Hydrogen fuel cells are available in various forms. Low-temperature (80–100 °C) H_2/O_2 fuel cells use platinum as both the H_2 oxidation and O_2 reduction catalysts, with individual H_2 and O_2 gas feeds and a proton exchange membrane (allowing selective proton transport) to separate the two reactions.[215,223] However, platinum is poisoned by

even trace amounts of CO[154] or sulfide[224] that may be present in H_2 produced by steam reformation, and thus these fuel cells require high purity gases. In contrast, as mentioned in the previous chapter, certain [NiFe]-hydrogenases are highly tolerant to CO,[114,115,117] and studies have also shown that some are tolerant to sulfide.[31] There is also strong evidence[217,218] to suggest that the catalytic centres of hydrogenases are comparable with Pt in terms of activity. Therefore, these enzymes provide an interesting alternative to platinum in H_2/O_2 fuel cells.

However, there have been very few descriptions of the actual incorporation of hydrogenases into a fuel cell, despite the concept having been patented.[225] In 2001, Tsujimura *et al.*[226] reported a H_2/O_2 biofuel cell that used methyl viologen-mediated H_2 oxidation catalysed by whole cells of the bacterium *Desulfovibrio vulgaris* at the anode. The cathode catalysed O_2 reduction with ABTS-mediated bilirubin oxidase (where ABTS is 2,2'-azinobis(3-ethylbenzothiazoline-6-sulfonic acid)). The isolated O_2-tolerant [NiFe]-hydrogenase *Re*MBH studied in the previous chapter was first used in a H_2/O_2 fuel cell in 2005, in combination with a laccase as the O_2 reduction catalyst.[114] Furthermore, the membrane-bound hydrogenase from the closely related *Ralstonia metallidurans* CH34 was demonstrated to generate electricity in a membraneless fuel cell in a mixture of just 3% H_2 in still air.[113]

The initial studies on the incorporation of O_2-tolerant hydrogenases into a fuel cell led to suggestions that these enzymes may be ideal candidates for the replacement of Pt in H_2/O_2 fuel cells. However, the work outlined in this chapter reveals that, even for an O_2-tolerant hydrogenase, the characteristic electrochemical behaviour of the enzyme (most

notably its reaction with O_2 at oxidising potentials) means that, realistically, incorporation of these enzymes into a H_2/O_2 fuel cell is more complicated than may at first be expected.

4.1.3 Characteristics of an Ideal Fuel Cell

The individual electrocatalytic behaviours of the anodic and cathodic catalysts of a fuel cell can be studied using cyclic voltammetry. Figure 4.2 shows a representation of the individual sigmoidal-shaped voltammograms expected for 'ideal' electrocatalysts, working as anodic and cathodic catalysts with equal current magnitudes.

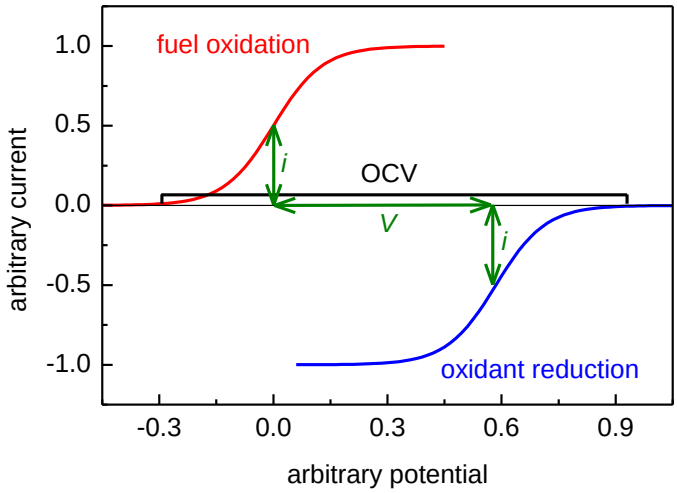


Figure 4.2. The electrochemical characteristics of ideal anodic and cathodic electrocatalysts. The values of the current (*i*) and cell voltage (*V*) corresponding to a particular power (*P* = *iV*) are shown by the green arrows and the open circuit voltage (OCV) is labelled in black.

The sigmoidal nature of the voltammograms is described in detail in Chapter 2; the current magnitude increases with overpotential as the concentration of the required redox species increases until the rate is no longer limited by electron transfer and the current plateaus. Oxidation of the fuel (red line) generates a positive current that increases with increasing potential (driving force) until it reaches a limiting value that reflects the maximum turnover rate of the enzyme. Likewise, reduction of the oxidant (blue line) produces a sigmoidal wave with a negative current that increases in magnitude as the

potential becomes more negative. Importantly, the oxidation process occurs at lower potential than the reduction; the difference in potential between the two processes should be maximised in order to yield a fuel cell with the highest possible cell voltage.[214]

The open circuit voltage (OCV) of a fuel cell is the maximum potential measured when no current flows (*i.e.* the approximate difference between the onset potentials of the two catalysts). In an ideal case, this corresponds to the difference between the thermodynamic potentials of the fuel/oxidised product and the oxidant/reduced product redox couples under the conditions of the fuel cell. The performance of a fuel cell is characterised by its power output. The power ($P = iV$) for a fuel cell based on the electrodes in Figure 4.2 (and ideally having negligible internal resistance) depends on equalising the current outputs (i) at each electrode as a function of voltage (V) (green arrows). A simple power curve can be generated by using a variable resistor to set the resistance (load, R) between the anode and cathode and recording the potential difference between them. For the ideal catalysts in Figure 4.2, this would produce a bell-shaped power *vs.* resistance curve (calculated by $P = V^2/R$, Figure 4.3A), displaying the maximum achievable power and the resistance at which this is obtained.

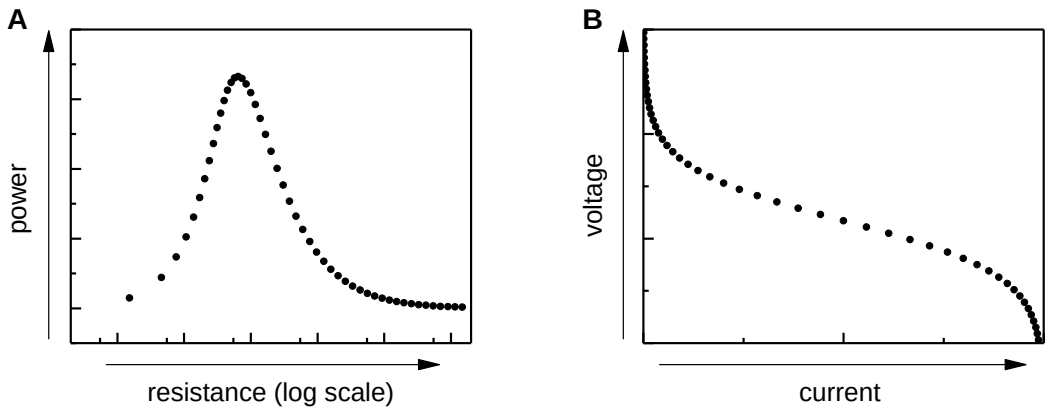


Figure 4.3. Representative power *vs.* resistance (A) and voltage (potential difference) *vs.* current (B) plots for the ideal catalysts shown in Figure 4.2.

Figure 4.3B shows a plot of cell voltage against current ($i = V/R$) for the ideal catalysts represented in Figure 4.2. This graph has a sigmoidal shape; at high voltage (close to the open circuit voltage) little current flows, whereas a maximum current is reached when the cell voltage is equal to zero (short circuit conditions).

4.2 Experimental Design

4.2.1 The Fuel Cell

A fuel cell was designed to incorporate reference and counter electrodes alongside the anode and cathode, in order to enable *in situ* voltammetry of the individual electrodes within a fuel cell configuration. Figures 4.4A and B show representations of the fuel cell, which comprises two halves that can be assembled with or without the inclusion of a proton exchange membrane (PEM). For membrane fuel cells, a reference electrode is required in each side of the cell, but for membrane-free experiments, only one reference electrode is necessary.

For membraneless mixed-feed fuel cells, only certain, non-explosive combinations of H_2/O_2 or H_2/air can be used. The flammability ranges of H_2 are 4-76% in air and 4-96% in pure O_2.[227] Therefore, the membraneless fuel cells described in this chapter were investigated under two limiting conditions: 96% H_2 in O_2 (hydrogen-rich) and 4% H_2 in air (hydrogen-poor).

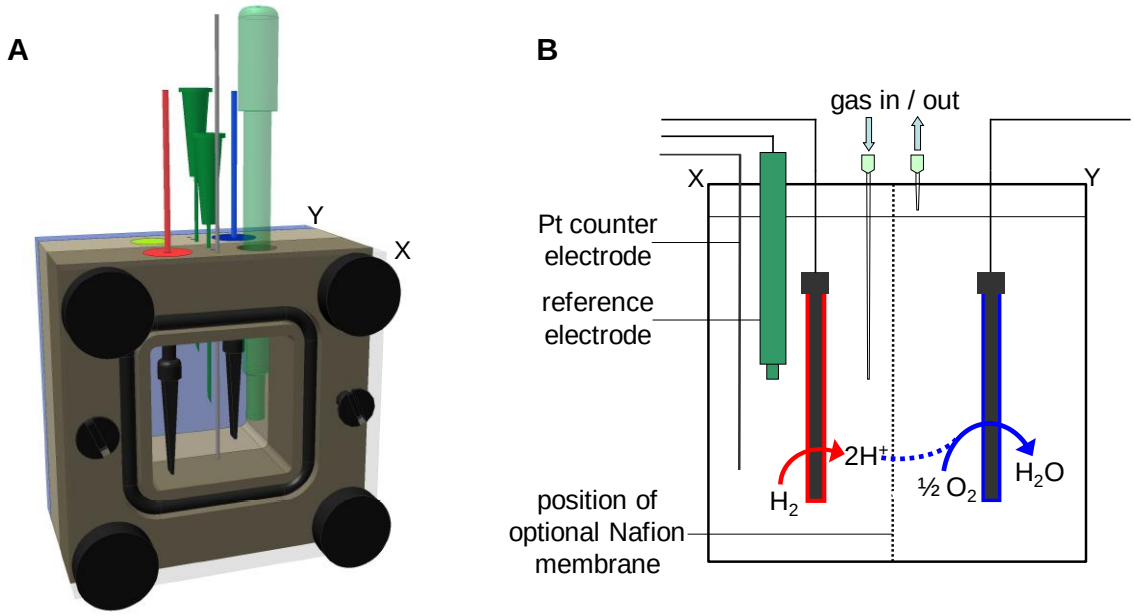


Figure 4.4. A schematic diagram showing the fuel cell used for 1.25 cm^2 geometric surface area graphite edge-plane strip electrodes. The cell can be operated either for voltammetry or for observing fuel cell characteristics. (A) Shows the fuel cell set-up without a membrane and (B) is a schematic representation of a cross section of the fuel cell (points X and Y are marked on both diagrams to illustrate the cross section that has been drawn.) The anodic biocatalyst is represented by the red line, while the blue corresponds to the cathodic biocatalyst. It is important to note that when a Nafion PEM is included in the set-up, an additional reference electrode and counter electrode must be included in the cathode compartment, along with an additional inlet and outlet needle to allow for separate gas flows on either side of the membrane. The computer-aided design used to produce (A) was performed by Andrew Green.

4.2.2 The Anodic Biocatalyst

Hydrogenases have been suggested since the 1970s[228] as catalysts for the H_2 anode reaction ($H_2 \rightarrow 2H^+ + 2e^-$) but, as discussed in Section 4.1.2, there have to date been few examples of their incorporation into a fuel cell. A major problem for applying hydrogenases in fuel cells is their inactivation by O_2 and therefore most fuel cell studies have focussed on the use of O_2-tolerant hydrogenases, such as *Re*MBH.[114]

It was recently established[115] that *Escherichia coli* Hydrogenase 1 (*Ec*Hyd1), which is membrane-bound *in vivo*, combines the ability to sustain H_2 oxidation activity in the

presence of O_2 with high activity and stability on an electrode. The sequences of *Ec*Hyd1 and *Re*MBH are similar; the large subunits of these enzymes share 58% sequence identity, while the small subunits show 70% identity (see Appendix A5 for sequence alignments). The MBH from *E. coli* shows similar O_2 tolerance to *Re*MBH,[115] and due to the ease of growing *E. coli*, isolation and purification of *Ec*Hyd1 is much easier than for *Re*MBH. Therefore, *Ec*Hyd1 may be an ideal anodic biocatalyst for a H_2/O_2 fuel cell, and studying how its catalytic properties affect the fuel cell power output will provide a much clearer picture of future prospects and directions for hydrogenase-based devices.

4.2.3 The Cathodic Biocatalyst

For the cathode, 'blue copper' oxidases are well established examples of O_2-reduction catalysts ($O_2 + 4H^+ + 4e^- \rightarrow 2H_2O$)[229-232] and enzymes such as laccases and bilirubin oxidases reduce O_2 at a lower overpotential than required at platinum.[229,233,234] Advantages of bilirubin oxidase also include its ability to operate at near-neutral pH[229] and the fact that this enzyme can show significant tolerance towards chloride ions.[235,236] *In vivo*, bilirubin oxidase catalyses the oxidation of the tetrapyrrole bilirubin with concomitant reduction of the electron acceptor, O_2, and its sequence shows strong similarities with laccases. Figure 4.5 shows the structure of the bilirubin oxidase from *Myrothecium verrucaria* (*Mv*), a fungus that is a plant pathogen.[237]

This enzyme contains four redox-active Cu atoms assigned according to their spectroscopic signatures: the Type 1 'blue' Cu is located close to the protein surface and has been shown to be involved in an electron transfer pathway to the trinuclear centre that comprises one Type 2 Cu and a Type 3 Cu pair.[238] The Type 1 Cu atom is located 1.2-1.3 nm away from the trinuclear cluster and is linked to the Type 3 Cu atoms via a

highly conserved His-Cys-His sequence, which may allow fast electron transfer.[239] It is proposed that the Type 1 Cu accepts electrons from the organic substrate and then transfers them (one at a time) to the trinuclear centre, where they are used in the reduction of O_2 to H_2O.[240-242]

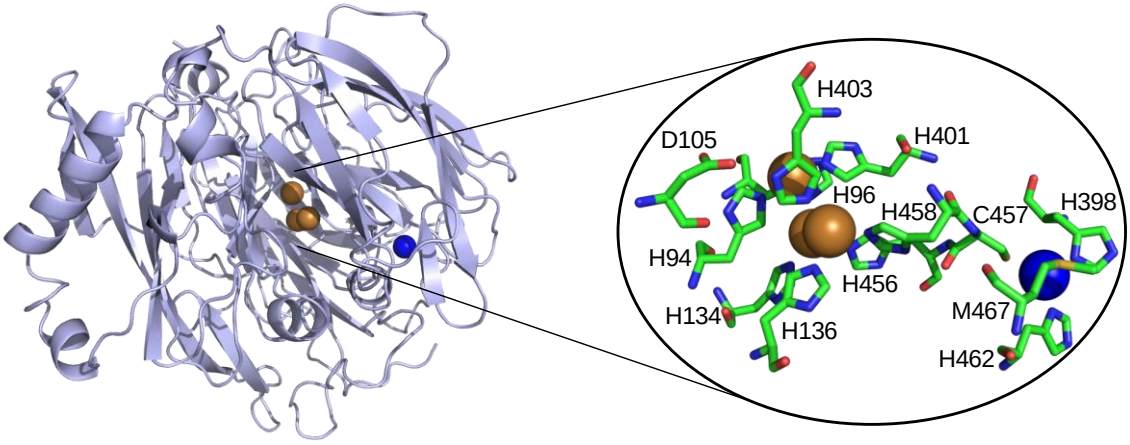


Figure 4.5. The structure of bilirubin oxidase from *Myrothecium verrucaria*, constructed using PyMOL (Protein Data Bank code: 2XLL).[237] The insert shows the four Cu atoms and surrounding amino acid residues that are highly conserved among 'blue Cu' oxidases. The Type 1 Cu atom is represented by a blue sphere, and the Cu atoms in the trinuclear centre are shown in gold.

Myrothecium verrucaria bilirubin oxidase (*Mv*BO) can be attached to a pyrolytic graphite edge-plane (PGE) electrode surface via a diazonium coupling method (described in Chapter 7).[234,243] The aromatic compound 6-amino-2-napththoic acid is believed to bind the enzyme onto the electrode surface by interacting with the organic substrate binding pocket close to the Type 1 Cu atom.[243] This modification yields a relatively stable and active cathodic catalyst that can be used in fuel cell investigations.

4.3 Electrochemical Characterisation of the Catalysts

4.3.1 Enzyme Activity under Varying Substrate Concentrations

In a membraneless H_2/O_2 fuel cell, a mixed-feed of H_2 in either O_2 or air is flushed into the fuel cell compartment. Therefore, it is necessary to investigate the catalytic properties of *Ec*Hyd1 and *Mv*BO under varying H_2/O_2 concentrations. Figure 4.6 shows cyclic voltammograms recorded for each enzyme on a PGE rotating disk electrode (0.03 cm^2 geometric surface area) in a sealed electrochemical cell.

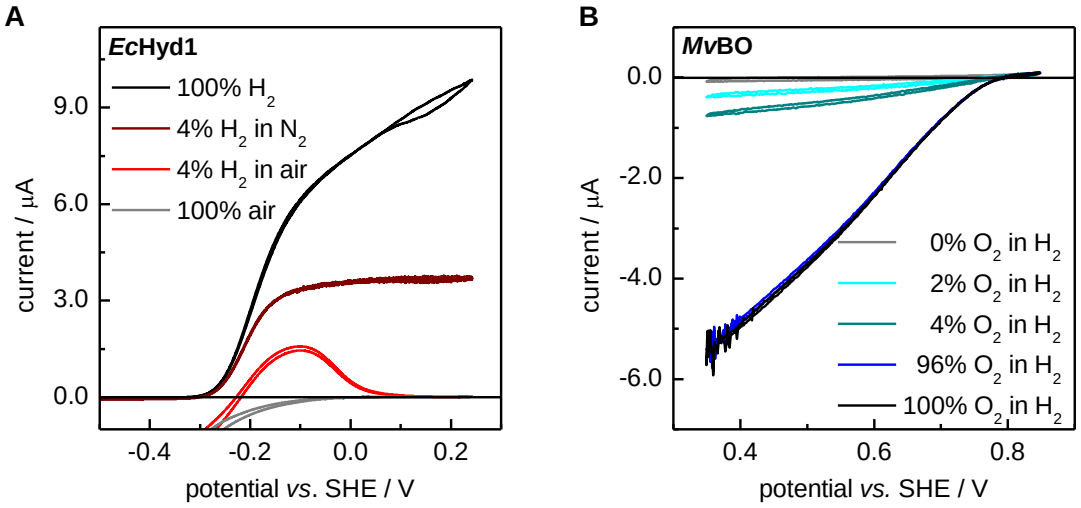


Figure 4.6. Cyclic voltammograms demonstrating the effect of varying substrate concentration on the activity of (A) *Ec*Hyd1 and (B) *Mv*BO. The voltammograms in (A) were performed at 1 mV s^{-1}, electrode rotation rate 4500 rpm and those in (B) at 10 mV s^{-1}, electrode rotation rate 2500 rpm. Other conditions: pH 6, 25 °C.

Figure 4.6A shows cyclic voltammograms of a single film of *Ec*Hyd1 performed at 1 mV s^{-1} under 100% H_2 (black), 4% H_2 in N_2 (dark red) and 4% H_2 in air (red). The black voltammogram, recorded under 100% H_2, confirms that H_2 oxidation by this enzyme under 100% H_2 requires a small overpotential,[115] as discussed for *Re*MBH in the previous chapter. This voltammogram also shows a residual increase in current at high potential rather than a plateau due to dispersion in the orientation of enzyme molecules on

the electrode surface, as discussed previously.[244] There is also evidence of a small amount of high potential anaerobic inactivation to form the Ni-B (Ready) state; a small increase in current is observed at ~+100 mV on the return scan, corresponding to reactivation of this inactive state.

The dark red voltammogram reveals that considerable H_2 oxidation activity by *Ec*Hyd1 is observable even under 4% H_2 in N_2, due to the high affinity of this enzyme for H_2 (the Michaelis constant for H_2 ($K_M(H_2)$) of *Ec*Hyd1 has been previously determined as 9 μM at -175 mV, pH 6, 30 °C).[115] However, the plateau in the current at potentials above ~-50 mV suggests that mass transport to the electrode surface may be limiting the observed current. Importantly, *Ec*Hyd1 is O_2 tolerant and sustains significant H_2 oxidation activity even under 4% H_2 in air (as seen in the red scan). However, the shape of the voltammogram changes greatly in the presence of air, with the potential window for H_2 oxidation significantly reduced. Aerobic inactivation of the *Ec*Hyd1 to form predominantly the Ni-B (Ready) state occurs at potentials above ~-100 mV, observed as a decrease in current. As the potential is swept above 0 mV, the current tends towards zero. However, on the reverse scan towards low potential the catalytic current retraces the forward scan, demonstrating that the hydrogenase can be reductively reactivated. In addition, the potential at which the voltammogram crosses the axis (*i.e.* the onset of positive current) is shifted to higher potentials under 4% H_2 in air compared to 4% H_2 in N_2. This is due to the direct reduction of O_2 at exposed regions of bare graphite, resulting in a negative current at potentials below ~-100 mV that opposes the positive current produced by enzymatic H_2 oxidation. A cyclic voltammogram for the *Ec*Hyd1-modified electrode performed under 100% air (grey line) is overlaid for comparison; only negative current corresponding to O_2 reduction at the graphite is observable, since no H_2 is present.

The high selectivity of an enzyme for its substrate is demonstrated by the cyclic voltammograms of *Mv*BO performed under varying concentrations of O_2 in H_2 (Figure 4.6B). The maximum current obtained under 96% O_2 in 4% H_2 (blue trace) is almost indistinguishable from that obtained under 100% O_2 (black). However, the affinity of *Mv*BO for its substrate is much weaker than the affinity of the hydrogenase for H_2; the $K_M(O_2)$ for *Mv*BO is 0.7 mM at pH 5, +342 mV.[234] Therefore, the O_2 reduction activity of *Mv*BO is much more sensitive to the substrate concentration, as demonstrated by the much lower current observed under 4% O_2 in H_2 (turquoise trace) compared to that recorded in the presence of 100% O_2.

4.3.2 The Effect of pH on Catalytic Activity

In the fuel cell shown in Figure 4.4, the anodic and cathodic catalysts (*Ec*Hyd1 and *Mv*BO respectively) reside in the same electrolyte solution. Therefore, it is necessary to determine an optimal pH at which both enzymes show significant catalytic activity. Figure 4.7 shows cyclic voltammograms of *Ec*Hyd1 and *Mv*BO[234] recorded over the pH range 5-8, with each enzyme in the presence of 100% substrate. The data for *Mv*BO were recorded by Dr. Luciano dos Santos and are taken from reference [234].

The onset potential of activity for the cyclic voltammograms of each enzyme shifts to more negative potential as the pH increases, in accordance with the Nernst equation. The catalytic activity of *Ec*Hyd1 is similar across the pH range, whereas for *Mv*BO there is a definite pH optimum in the region pH 5-6 (Figure 4.7B).[234] In addition, the O_2 tolerance of *Ec*Hyd1 is expected to increase with decreasing pH; three protons and three electrons are required to generate the Ni-B (Ready) state upon reaction with O_2 (Section 3.1.6)

whereas the Ni-A (Unready) state, which recovers only very slowly, requires just one proton and one electron.[201,245]

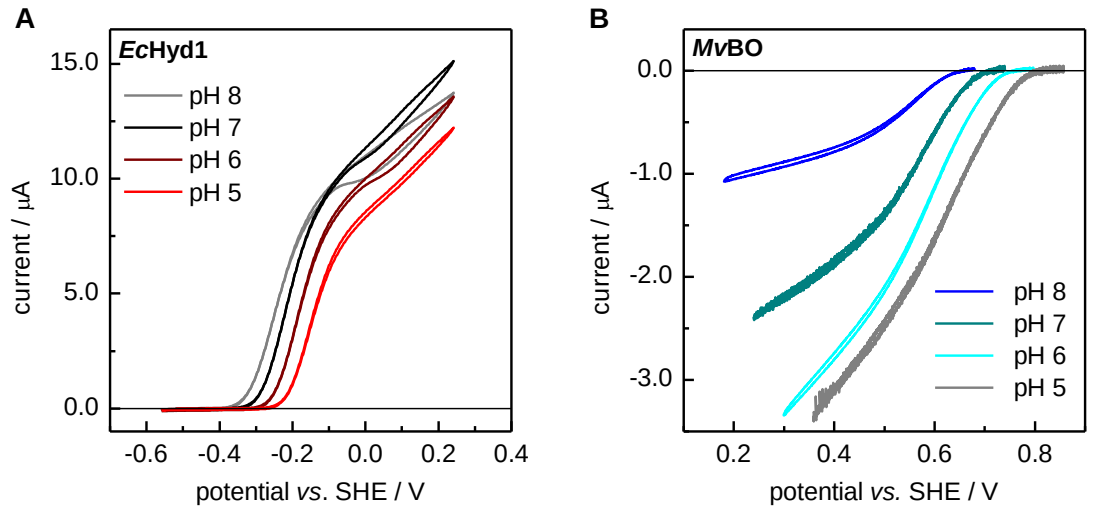


Figure 4.7. Cyclic voltammograms demonstrating the effect of pH on the catalytic activity of (A) *Ec*Hyd1 and (B) *Mv*BO on PGE rotating disk electrodes. In (A) the voltammograms were performed at 10 mV s^{-1} under 100% H_2 in a mixed buffer system.‡ Other conditions: 25 °C, electrode rotation rate 2500 rpm. The data in (B) are taken from reference 234 and were collected at 5 mV s^{-1} under 100% O_2 in 0.1 M phosphate buffer. Other conditions: 0 °C, electrode rotation rate 2500 rpm.

As discussed in Chapter 3, for a hydrogenase to sustain H_2 oxidation in the presence of O_2 it must form only the Ni-B (Ready) state, which recovers very rapidly upon lowering the potential (Figure 4.6A, red scan).[196] Thus, to maximise the ability of *Ec*Hyd1 to perform in a H_2/O_2 fuel cell, a low pH is preferable. Since pH 5 is also close to the pH optimum for *Mv*BO, this value was chosen for use in the fuel cells discussed in this chapter.

‡ The mixed buffer system (used to study the behaviour of *Ec*Hyd1 over a wide pH range) consisted of 15 mM in each of sodium acetate (Fisher), MES (2-[*N'*-morpholino]-ethane sulfonic acid, Melford), HEPES (*N'*-[2-hydroxyethyl]piperazine-*N'*-2-ethane sulfonic acid, Fisher), TAPS (*N'*-tris[hydroxymethyl]methyl-3-amino propane sulfonic acid, Sigma), and CHES (2-[*N'*-cyclohexylamino]ethane sulfonic acid, Sigma), with 0.1 M NaCl as the supporting electrolyte. Titration to the desired pH was achieved using NaOH and HCl.

4.3.3 Temperature Dependence of Enzyme Activity

The rate of a catalytic reaction may be strongly influenced by temperature and therefore it is necessary to consider the temperature dependencies for H_2 oxidation by *Ec*Hyd1 and O_2 reduction by *Mv*BO. Figures 4.8A and B show cyclic voltammograms performed at various temperatures for *Ec*Hyd1 and *Mv*BO respectively. The H_2 oxidation activity of *Ec*Hyd1 is strongly dependent on temperature, and the current is around four times larger at 45 ºC than at 25 ºC (Figure 4.8A). The change in activity of *Mv*BO with temperature is much smaller, suggesting a smaller enthalpy of activation for this enzyme. For *Mv*BO, the current increases as the temperature is raised up to 35 ºC but this increase does not continue as the temperature is taken to 45 ºC. This is believed to be due to a combination of desorption of the enzyme from the electrode surface and denaturation.[234]

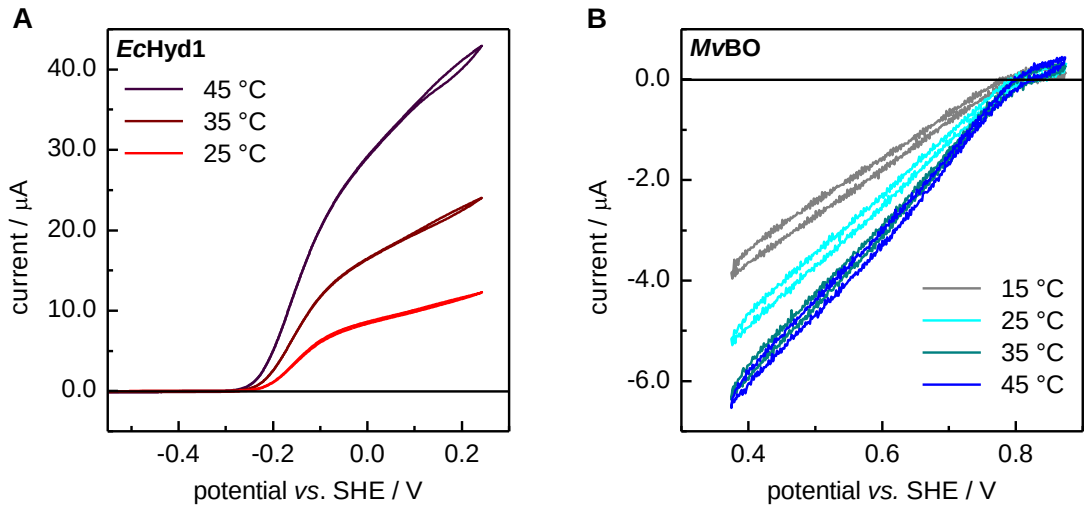


Figure 4.8. Cyclic voltammograms showing the temperature dependence of the catalytic activity of (A) *Ec*Hyd1 and (B) *Mv*BO under 100% H_2 and 100% O_2 respectively. In each case, the voltammograms were performed at 10 mV s^{-1}. Other conditions: pH 5, electrode rotation rate 2500 rpm.

A fuel cell requires both high catalytic activity of the enzymes and good stability on the electrode surface. Therefore, a compromise must be made between the increased activity observed at higher temperatures and the loss of stability under these conditions. At room

temperature (25 ºC) both enzymes show a significant degree of activity, as well as reasonable stability on the electrode surface. Additionally, minimal or no energy input is required to maintain a fuel cell at this temperature. Therefore, the fuel cell studies described in this chapter were performed at 25 ºC.

4.3.4 Cell Voltage Available from *Ec*Hyd1/*Mv*BO Electrodes

Cyclic voltammograms performed using *Ec*Hyd1 and *Mv*BO adsorbed onto separate PGE rotating disk electrodes are shown in Figure 4.9.

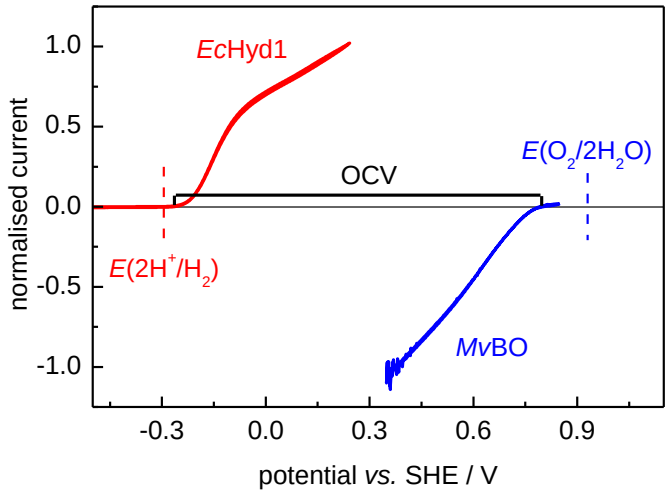


Figure 4.9. Cyclic voltammograms for *Ec*Hyd1 and *Mv*BO adsorbed on PGE electrodes (0.03 cm^2), performed under 100% H_2 and 100% O_2 respectively. The open circuit voltage (OCV) is labelled and the dashed lines correspond to the reduction potentials of the $2H^+/H_2$ (red) and $O_2/2H_2O$ (blue) couples under these conditions. Other conditions: pH 5, 25 °C, 10 mV s^{-1}, electrode rotation rate 2500 rpm.

In order to obtain a 'best case scenario', each enzyme was monitored under a gas atmosphere containing 100% of its gaseous substrate (100% H_2 for *Ec*Hyd1 and 100% O_2 for *Mv*BO) and the electrode was rotated at 2500 rpm to ensure a constant and adequate supply of substrate to and removal of product from the electrode surface. The voltammograms confirm that both enzymes exhibit significant activity in the same buffer

solution at pH 5, and thus verify the feasibility of incorporating these enzymes into a single compartment fuel cell with one electrolyte.

From the standard electrode potentials of the $2H^+/H_2$ and $O_2/2H_2O$ redox couples (Figure 4.9), a H_2/O_2 fuel cell operating reversibly at 25 °C and 1 bar pressure of each gas should have an OCV of 1.23 V, where the water product is assumed to be in the liquid phase.[246] However, this value is not achieved in practice, principally due to the sluggish electrode kinetics of four-electron O_2 reduction (noting, nonetheless, that the overpotential for O_2 reduction is smaller for 'blue' Cu oxidases than it is at Pt[233,247]). Additionally, as described for O_2-tolerant hydrogenases in the previous chapter, *Ec*Hyd1 shows only negligible H_2 production activity, and displays a small overpotential for H_2 oxidation. The potential at which *Ec*Hyd1 commences H_2 oxidation is more or less constant between the limits of 100% H_2 and 4% H_2.[115] This constant onset potential across varying H_2 levels was also observed for *Re*MBH (Section 3.1.7.3) and so far appears to be a property of O_2-tolerant [NiFe]-hydrogenases.[97,115]

Figure 4.9 illustrates that, at pH 5 and 25 ºC, and with each enzyme under a gas atmosphere containing 100% substrate, the pairing of *Ec*Hyd1 and *Mv*BO could, in principle, produce a fuel cell with an OCV slightly greater than 1.0 V.

4.4 *Ec*Hyd1/*Mv*BO Membrane Fuel Cell

4.4.1 An Introduction to Proton Exchange Membranes

In fuel cells that use Pt as both the anodic and cathodic catalyst, a proton exchange membrane (PEM) is essential to separate the electrode compartments, due to the poor selectivity of Pt for H_2 *vs.* O_2.[215] A PEM is an ionomer that allows transport of protons

from the anode side to the cathode compartment, but does not allow transport of anions or electrons. The most commonly used PEM is Nafion, and its structure is described in Chapter 7. The main challenges preventing the widespread use of PEM fuel cells are the high cost and limited lifetime of the membrane itself.[223]

4.4.2 Characteristics of an *Ec*Hyd1/*Mv*BO PEM Fuel Cell

The fuel cell shown in Figure 4.4 was assembled with a membrane (Nafion 115, DuPont) to separate the anode and cathode compartments. In this set-up, 100% H_2 was bubbled into the solution of the anode compartment and 100% O_2 was bubbled into the cathode compartment.

Figure 4.10A shows cyclic voltammograms recorded for the individual enzyme-modified fuel cell strip electrodes within this fuel cell configuration. These electrodes are stationary and the current density is smaller than would be obtained using a rotating disk electrode. The cyclic voltammogram of the hydrogenase shows a small drop in current above ~50 mV (leading to approximately 20% current loss), corresponding to inactivation of the enzyme by traces of O_2. This may arise due to O_2 leakage into the anode compartment across the PEM from the cathode compartment or directly from the laboratory environment (Section 4.4.3). The presence of O_2 can also be detected as the small negative current at low potential in the *Ec*Hyd1 voltammogram in Figure 4.10A, caused by direct O_2 reduction at the bare graphite (by contrast, no such negative current is observable in the red trace of Figure 4.9, which was recorded under completely anaerobic conditions). The inactivation of the hydrogenase is reversed upon reduction (the current recovers during the return scan), as seen in Figure 4.6.

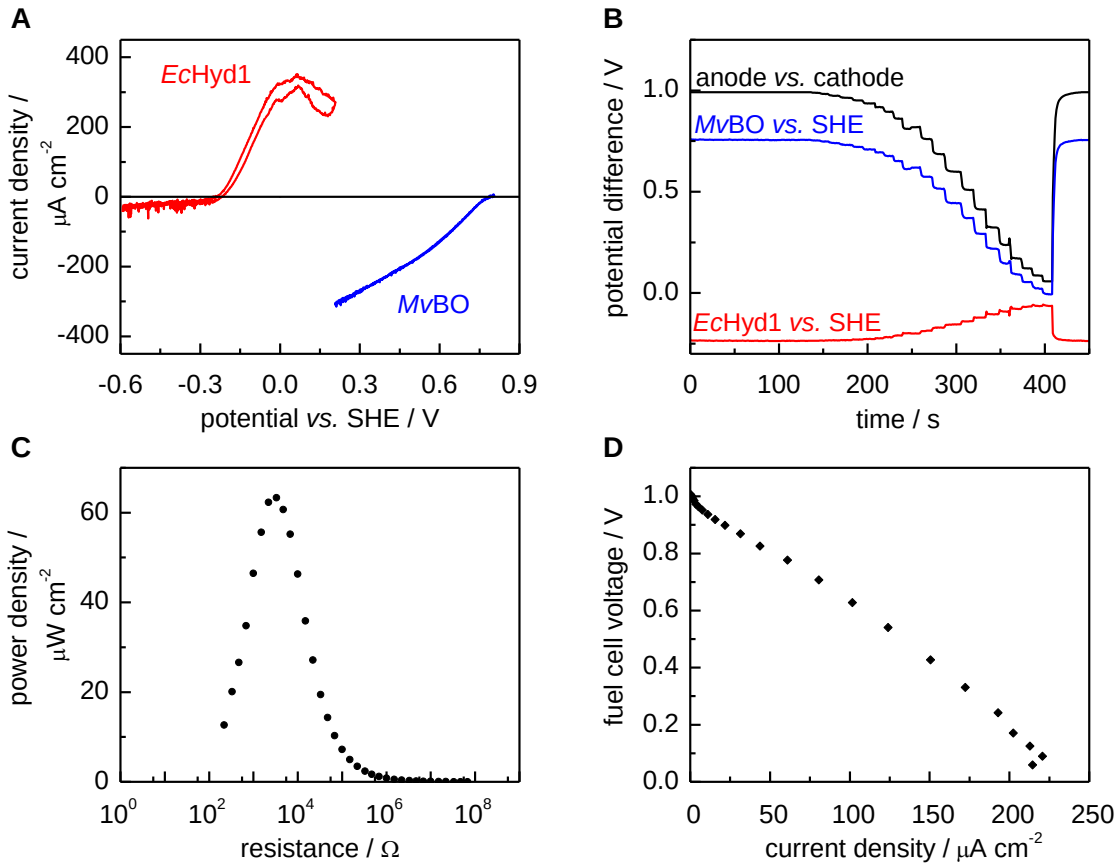


Figure 4.10. A PEM *Ec*Hyd1/*Mv*BO H_2/O_2 fuel cell operating at 25 °C, pH 5 using stationary electrodes of geometric surface area 1.25 cm^2. (A) Shows cyclic voltammograms for *Ec*Hyd1 (red) and *Mv*BO (blue) recorded in the fuel cell at 10 mV s^{-1}. (B) Shows the time dependent changes in potential difference for the fuel cell (black) and the individual electrodes with respect to the reference electrode (anode *vs.* reference shown in red, cathode *vs.* reference shown in blue, quoted *vs.* SHE) over the course of the power curve being recorded. Each step is the potential response to changing resistance, and each resistance was held until the potential stabilised. The resistance was decreased until the fuel cell voltage approached zero.[§] Finally, the resistance was returned to 9.9 x 10^7 Ω to restore open circuit conditions. (C) Shows the power density of the fuel cell as a function of resistance and (D) shows a plot of fuel cell voltage against current density (calculated from the fuel cell voltage and resistance).

[§] The following sequence of resistance (Ω) steps was applied: 9.9 x 10^7, 6.8 x 10^7, 4.7 x 10^7, 3.3 x 10^7, 2.2 x 10^7, 1.5 x 10^7, 1.0 x 10^7, 6.8 x 10^6, 4.7 x 10^6, 3.3 x 10^6, 2.2 x 10^6, 1.5 x 10^6, 1.0 x 10^6, 6.8 x 10^5, 4.7 x 10^5, 3.3 x 10^5, 2.2 x 10^5, 1.5 x 10^5, 1.0 x 10^5, 6.8 x 10^4, 4.7 x 10^4, 3.3 x 10^4, 2.2 x 10^4, 1.5 x 10^4, 1.0 x 10^4, 6.8 x 10^3, 4.7 x 10^3, 3.3 x 10^3, 2.2 x 10^3, 1.5 x 10^3, 1.0 x 10^3, 6.8 x 10^2, 4.7 x 10^2, 3.3 x 10^2, 2.2 x 10^2.

For this PEM fuel cell, the OCV (the potential difference between the anode and cathode recorded at a resistance of 9.9 x 10^7 Ω) was 990 mV. In order to obtain a power curve, the resistance was decreased in a stepwise fashion and the cell voltage recorded at each value. Once the cell voltage had approached zero, the resistance was returned to 9.9 x 10^7 Ω. The changes in potential difference between (i) the anode and cathode (the fuel cell voltage), (ii) the anode and a reference electrode and (iii) the cathode and a reference electrode over the time course of the power curve measurement are shown in Figure 4.10B. The fuel cell voltage (black line) decreases as the resistance decreases; the potential of the anode (red) increases with decreasing resistance, while the cathode potential (blue) decreases with decreasing resistance. Importantly, after recording the power curve and returning the resistance to 9.9 x 10^7 Ω, the original OCV of the fuel cell was restored, showing that the operations are reversible.

Figure 4.10C shows the power curve recorded during the measurements. A maximum power density of 63 μW cm^{-2} was drawn from this fuel cell at a resistance of 3.3 x 10^3 Ω (corresponding to a fuel cell voltage of 511 mV) and the power curve is almost symmetrical, with a shape similar to that expected for the ideal electrocatalysts shown in Figure 4.3A. Figure 4.10D shows a plot of the fuel cell voltage against current density, calculated from the values of the fuel cell voltage at each resisitance. A maximum current density of 227 μA cm^{-2} was achieved at a fuel cell voltage of 90 mV.

4.4.3 O_2 Crossover into the Anode Compartment

The voltammogram for *Ec*Hyd1 shown in Figure 4.10A exhibits a degree of inactivation at high potential, suggesting that trace levels of O_2 may be present in the anode compartment. To test whether this is due to the leakage of air from the laboratory

environment or O_2-crossover from the cathode compartment, cyclic voltammograms of *Ec*Hyd1 were recorded with 100% H_2 bubbling into the anode compartment, with and without O_2 bubbling into the cathode compartment. The results are shown in Figure 4.11.

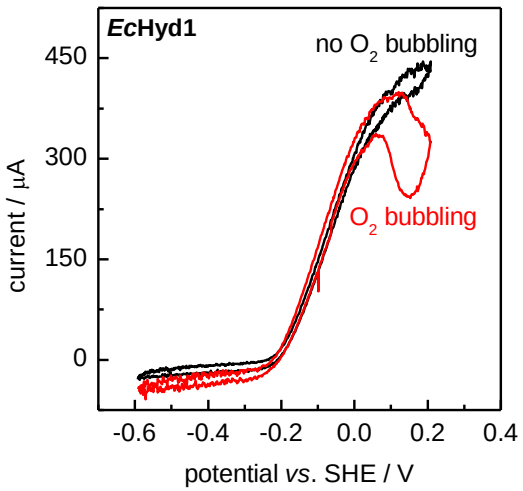


Figure 4.11. Inactivation of *Ec*Hyd1 due to O_2 crossover through the Nafion PEM of a fuel cell. The black line shows a cyclic voltammogram recorded for an *Ec*Hyd1 anode (geometric surface area 1.25 cm^2) in a membrane fuel cell with 100% H_2 bubbling into the anode compartment and no O_2 bubbling in the cathode compartment. The red scan was recorded under the same conditions except that O_2 was bubbled into the cathode compartment of the fuel cell. Other conditions: pH 5, 25 °C, 10 mV s^{-1}.

These results demonstrate that O_2 does appear to crossover into the anode compartment and confirm that the H_2 oxidation current is attenuated only at high potential. By contrast with the rigorous conditions ensured when experiments are carried out in an anaerobic glovebox, under these more realistic fuel cell conditions small amounts of O_2 are continuously crossing the PEM. This will eventually affect the performance of the fuel cell, due to the prolonged inactivation of the hydrogenase.

4.5 Membraneless *Ec*Hyd1/*Mv*BO Fuel Cells

4.5.1 An Introduction to Membraneless Fuel Cells

As mentioned in Section 4.4.1, the major obstacle to the use of PEMs in fuel cells is that they are both expensive, and have limited lifetimes. Another drawback is that, as seen in the previous section, even using a membrane some degree of O_2 crossover may occur. In order to miniaturise fuel cells for use in portable microdevices or implantable devices, it is preferable to simplify the spatial design by not having a membrane. This can be achieved using enzymes as the fuel cell catalysts due to their high selectivity towards their substrates, which eliminates the need for a membrane.[113,235]

Previous attempts to create H_2/O_2 fuel cells operating on a pre-mixed fuel and oxidant supply have included studies using a porous anode-electrolyte-cathode arrangement in which a partially selective cathode, such as Ag or Au, depletes O_2 from the mix before it reaches the H_2-oxidising Pt or Pd anode.[248] In 1990, Dyer described a mixed-feed H_2/O_2 fuel cell based on membrane-coated thin-film Pt, but the precise mechanism of gas discrimination was not clear.[249] It has been suggested that the Pt cathode may have been oxidised to platinum oxide, which is more selective than Pt for the reduction of O_2 in the presence of H_2.[248,250] More recently, a membraneless all-enzyme H_2/air fuel cell using the O_2-tolerant *Ralstonia metallidurans* MBH and a laccase was shown to power a wrist-watch for 24 hours.[19,113]

Additionally, there have been examples of enzyme-based membraneless fuel cells operating with different fuels. In 1999, Katz *et al.*[251] reported a non-compartmentalised glucose oxidase fuel cell, comprising a glucose oxidase anode (catalysing the oxidation of glucose to gluconic acid) and a cytochrome *c*/cytochrome oxidase layered cathode at

which the reduction of O_2 to water took place. Several more investigations[27,48,49] have focused on glucose/oxygen fuel cells and the possibility of using such enzyme fuel cells as implantable devices was demonstrated in a study by Mano *et al.*, in which a glucose oxidase/bilirubin oxidase fuel cell was implanted into, and drew power from, a grape.[235] Other examples of 'blue copper' oxidases in membraneless fuel cells include the combination of laccase from *Trametes versicolor* with a D-fructose dehydrogenase in a single compartment biofuel cell[252] and the use of osmium redox polymers to wire cellobiose dehydrogenase to a graphite anode and laccase to the cathode in a membrane-free fuel cell.[253]

As introduced in Section 4.2.1, an added difficulty associated with H_2/O_2 membraneless fuel cells is that only certain compositions of these two substrates are non-explosive. The following sections investigate the behaviour of *Ec*Hyd1/*Mv*BO fuel cells operating in the high H_2 limit (96% H_2/4% O_2, denoted the H_2-rich fuel cell) and the low H_2 limit (4% H_2 in air, referred to as the H_2-poor fuel cell).

4.5.2 Hydrogen-rich *Ec*Hyd1/*Mv*BO Membraneless Fuel Cell

4.5.2.1 Characteristics of a Hydrogen-rich Membraneless Fuel Cell

To generate a 'hydrogen-rich' membraneless fuel cell, the fuel cell was constructed without the PEM and a mixture of 96% H_2/4% O_2 was supplied into the single compartment containing both the *Ec*Hyd1 anode and *Mv*BO cathode. Cyclic voltammograms were recorded for both the *Ec*Hyd1 and *Mv*BO inside the fuel cell (Figure 4.12A).

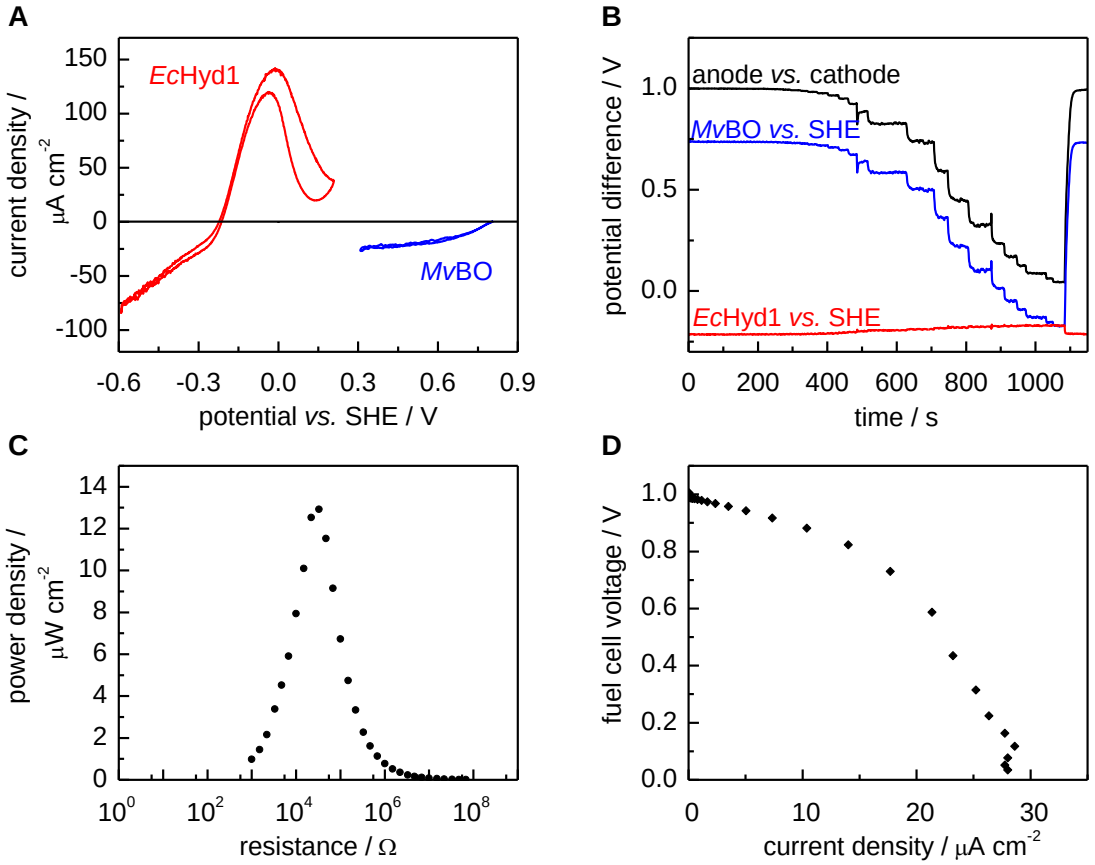


Figure 4.12. An *Ec*Hyd1/ *Mv*BO H_2/O_2 fuel cell operating under 96% H_2/4% O_2 at 25 °C, pH 5 using stationary electrodes (geometric surface area 1.25 cm^2). (A) Shows cyclic voltammograms for the *Ec*Hyd1 (red) and *Mv*BO (blue) recorded in the fuel cell at 10 mV s^{-1}. (B) Shows the time dependent changes in potential difference for the fuel cell (black) and the individual electrodes with respect to the reference electrode (anode *vs.* reference shown in red, cathode *vs.* reference shown in blue, quoted *vs.* SHE) over the course of the power curve being recorded. Each step is the potential difference response to changing resistance, and each resistance was held until the potential stabilised. The resistance was decreased until the fuel cell voltage approached zero. Finally, the resistance was returned to 9.9 x 10^7 Ω to restore open circuit conditions. (C) Shows the power density of the fuel cell as a function of resistance and (D) shows a plot of the fuel cell voltage against current density (calculated from the fuel cell voltage and resistance).**

Under these H_2-rich conditions, the positive current produced by H_2 oxidation by *Ec*Hyd1 is much larger in magnitude than the O_2 reduction current generated by *Mv*BO. This is as expected, since the hydrogenase is in the presence of 96% substrate, compared to only 4%

** The following sequence of resistance (Ω) steps was applied: 9.9 x 10^7, 6.8 x 10^7, 4.7 x 10^7, 3.3 x 10^7, 2.2 x 10^7, 1.5 x 10^7, 1.0 x 10^7, 6.8 x 10^6, 4.7 x 10^6, 3.3 x 10^6, 2.2 x 10^6, 1.5 x 10^6, 1.0 x 10^6, 6.8 x 10^5, 4.7 x 10^5, 3.3 x 10^5, 2.2 x 10^5, 1.5 x 10^5, 1.0 x 10^5, 6.8 x 10^4, 4.7 x 10^4, 3.3 x 10^4, 2.2 x 10^4, 1.5 x 10^4, 1.0 x 10^4, 6.8 x 10^3, 4.7 x 10^3, 3.3 x 10^3, 2.2 x 10^3, 1.5 x 10^3, 1.0 x 10^3.

O_2 for the bilirubin oxidase, which is further enhanced by the fact that *Mv*BO has a much lower affinity for its substrate, as discussed in Section 4.3.1. Furthermore, at such low concentrations of O_2, mass transport of substrate to the stationary electrode may limit the rate of catalytic O_2 reduction activity. It is therefore anticipated that, at such low O_2 concentrations, the activity of *Mv*BO will be limiting in a fuel cell (since the dimensions of the anode and cathode electrodes are the same).

The cyclic voltammogram of *Ec*Hyd1 in Figure 4.12A shows significant direct, non-enzymatic reduction of O_2 at exposed bare graphite (observed as negative current). There is much more aerobic inactivation of *Ec*Hyd1 than observed when O_2 transfer to the anode is limited by a membrane; the attenuation in current due to inactivation is potential dependent and only about 25% of the maximum H_2 oxidation current remains when the voltage is swept up to 240 mV.

The OCV of this fuel cell was 950 mV, which is lower than obtained for the PEM fuel cell. This is largely due to the negative current arising from O_2 reduction at the bare graphite of the anode opposing the positive H_2 oxidation current and thus shifting the onset of positive current to higher potential. The reduction of the O_2 concentration also lowers the OCV since as the O_2 concentration decreases, the onset of O_2 reduction shifts to lower potential, according to the Nernst equation (as seen in Figure 4.6B).

Figure 4.12B shows the changes in potential difference between (i) the anode and cathode (the fuel cell voltage), (ii) the anode and a reference electrode and (iii) the cathode and a reference electrode over the time course of the power curve measurement. In this case, it is clear that the fuel cell voltage mainly reflects the changing potential of the *Mv*BO, while the potential of *Ec*Hyd1 varies very little. As the resistance is decreased, a small

shift of the *Ec*Hyd1 to more positive potential leads to a large increase in H_2 oxidation current which must be balanced by the same magnitude of O_2 reduction current. Since the *Mv*BO is much less active under these H_2-rich conditions, the potential of the *Mv*BO must therefore decrease to a much larger extent (*i.e.* leading to a greater driving force) in order to equal the magnitude of the H_2 oxidation current. Thus, over the course of the power curve, the potential of the *Mv*BO decreases much more than that of the *Ec*Hyd1 increases. Importantly, as with the membrane fuel cell, full power was regained upon restoring a high resistance ($9.9 \times 10^7\ \Omega$).

The power curve has a symmetrical bell-shape (as seen for the PEM fuel cell), maximising at 12.9 μW cm^{-2} at $3.3 \times 10^4\ \Omega$ (730 mV, Figure 4.12C). From Figure 4.12D it can be seen that the maximum current density for this fuel cell was 28 μA cm^{-2}, obtained at cell voltages below 163 mV. This corresponds to the maximum current of the *Mv*BO (Figure 4.12A) and provides further confirmation that the *Mv*BO limits the performance of the fuel cell under these conditions.

4.5.2.2 The Effect of Adding a Second *Mv*BO Electrode

For a fuel cell in which the *Mv*BO is limiting, it is expected that increasing the amount of current produced by the cathode should increase the overall power of the fuel cell. A membraneless fuel cell was constructed with a mixed feed of 96% H_2/4% O_2, as in the previous section. However, in this instance, two *Mv*BO electrodes were included rather than one. Figure 4.13A shows the cyclic voltammograms recorded for the electrodes in the fuel cell. The red voltammogram was recorded using a single *Ec*Hyd1 electrode as in Figure 4.12A, but in this case the voltammogram is displayed in terms of absolute current rather than current density. In the blue voltammogram, one *Mv*BO electrode was

connected to give a PGE geometric surface area of 1.25 cm^2, whereas in the green voltammogram the two *Mv*BO electrodes were connected together, analogous to one large electrode with twice the surface area (2.5 cm^2). It is clear from Figure 4.13A that combining the two *Mv*BO electrodes approximately doubles the O_2 reduction current.

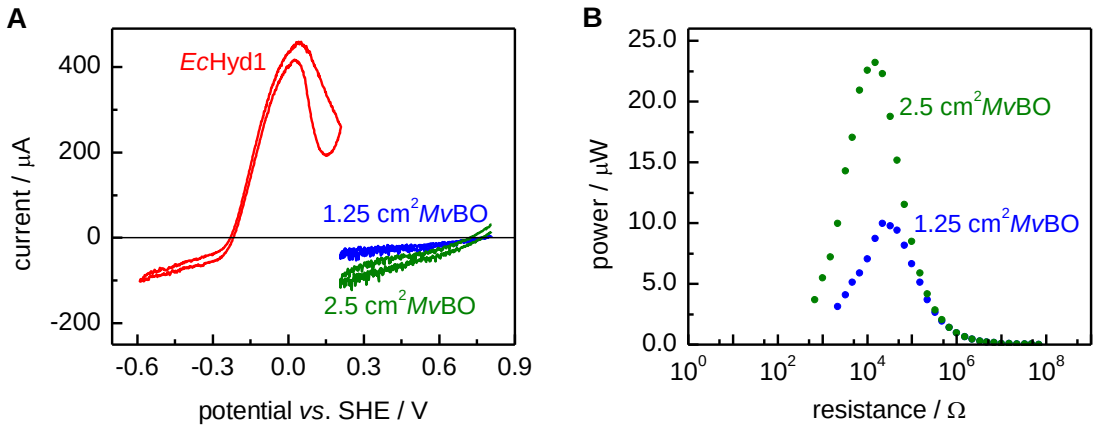


Figure 4.13. (A) Cyclic voltammograms recorded at 10 mV s^{-1} for a 1.25 cm^2 geometric surface area PGE electrode modified with *Ec*Hyd1 (red) and for either one *Mv*BO electrode (1.25 cm^2, blue) or two *Mv*BO electrodes connected together to make an electrode with twice the surface area (2.5 cm^2, green). (B) A plot showing power *vs.* resistance for a fuel cell comprised of the *Ec*Hyd1 and *Mv*BO electrodes in (A). The data were obtained using the *Ec*Hyd1 electrode combined with either one *Mv*BO electrode (blue) or both *Mv*BO electrodes (green). Other conditions: 96% H_2/4% O_2, 25 °C, pH 5.

A power curve was recorded by varying the resistance between the anode and cathode (where the cathode can be either one or two *Mv*BO electrodes connected together) as in the previous section. The plots of power *vs.* resistance are shown in Figure 4.13B (the blue points were obtained with one *Mv*BO connected and the green points with two *Mv*BO electrodes connected to the anode). It should be noted that in this case the power is given as an absolute value rather than a power density. It is clear from the data that the power of the fuel cell is indeed limited by the bilirubin oxidase, and doubling the geometric surface area of the *Mv*BO electrode leads to approximately twice the maximum power.

Figure 4.14 shows a transform of the data in Figure 4.13B to show the fuel cell voltage plotted against current.

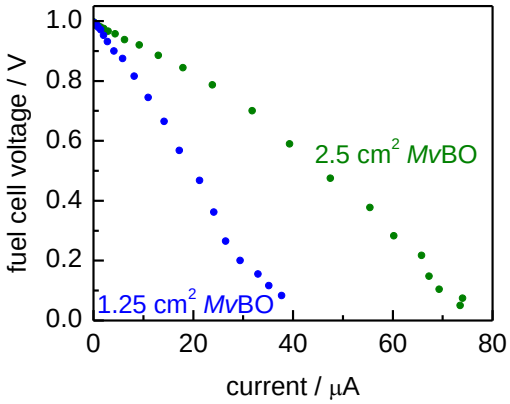


Figure 4.14. A transform of the data in Figure 4.13B to show the fuel cell voltage against current.

Again, it can be seen that adding the second *Mv*BO electrode has the effect of doubling the maximum current attained, which directly impacts the power output of the fuel cell. Since under H_2-rich conditions an *Ec*Hyd1 electrode with the same surface area as an *Mv*BO electrode consistently produces a current with much greater magnitude, the maximum current of a fuel cell containing an equally sized anode and cathode will always be limited by the *Mv*BO under these conditions.

4.5.2.3 The Effect of CO on Fuel Cell Performance

The Pt catalysts used in PEM fuel cells are poisoned by carbon monoxide (CO), which is present in H_2 produced via steam reformation. The CO binds strongly to the Pt surface, blocking the surface active sites and thus reducing H_2 oxidation activity.[254] In contrast, O_2-tolerant [NiFe]-hydrogenases including *Re*MBH,[114] *Ec*Hyd1[115] and *Aa*Hase1[255] show little or no inhibition by CO and can continue H_2 oxidation in its presence (as demonstrated for *Re*MBH in the previous chapter). This tolerance was further

demonstrated by the ability of a fuel cell combining *Re*MBH and *Trametes versicolor* laccase to generate power in the presence of CO.[114]

An experiment was performed to confirm that the presence of CO does not affect power generation by an *Ec*Hyd1/*Mv*BO fuel cell, and the data are displayed in Figure 4.15. A resistance corresponding to 60% power was set between the anode and cathode of a fuel cell operating under 96% H_2/4% O_2. The potential difference between (i) the anode and cathode (the fuel cell voltage), (ii) the anode and a reference electrode and (iii) the cathode and a reference electrode were monitored over time. After 310 s, CO was introduced to the system, creating a gas mixture that contained 95% H_2, 4% O_2 and 1% CO (grey box in Figure 4.15). The fuel cell was operated with the CO-containing gas mixture for 420 s, before the original 96% H_2/4% O_2 composition was restored.

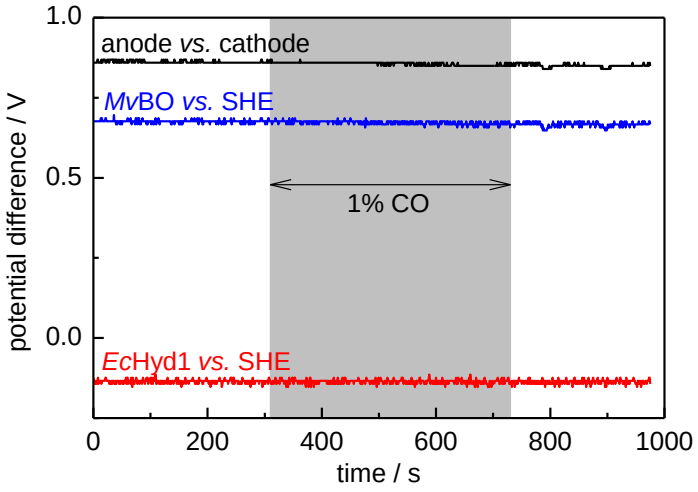


Figure 4.15. The effect of CO on the performance of an *Ec*Hyd1/*Mv*BO fuel cell operating under 96% H_2/4% O_2 at 60% power (the resistance set between the anode and cathode was 6 x 10^4 Ω in this case). The voltage of the fuel cell (black) and the individual electrodes with respect to the reference electrode (anode *vs.* reference shown in red, cathode *vs.* reference shown in blue, quoted *vs.* SHE) were monitored over the course of the experiment. Between 310 s and 730 s (grey box) the gas mixture was changed to 95% H_2/4% O_2/1% CO.

Figure 4.15 shows that no decrease in fuel cell voltage (or change in the potential of either electrode) was detected during exposure to CO, thus confirming that under these conditions the fuel cell is unaffected by this level of CO. It should be noted that the H_2 concentration decreased from 96% to 95% to allow for inclusion of the 1% CO but that this did not affect the H_2 oxidation activity of the *Ec*Hyd1 since these levels of H_2 are so far in excess of its $K_M(H_2)$, as discussed in Section 4.3.1.

4.5.3 Hydrogen-poor *Ec*Hyd1/*Mv*BO Membraneless Fuel Cell

4.5.3.1 Introduction to Low H_2 Fuel Cells

The second non-explosive limit for H_2 and O_2 exists at low H_2 concentrations ($\leq$ 4% H_2 in air).[227] This extreme opens the possibility of providing a fuel cell with a fuel-weak gas mixture, *i.e.* 4% H_2 diluted in air. Power generation from such a mixture is desirable due to the minimal use of H_2 in naturally present atmospheric air. A fuel cell using *Ralstonia metallidurans* MBH as the anode catalyst was shown previously to be capable of generating power from even just 1% H_2 in air[113] and the cyclic voltammogram for *Ec*Hyd1 shown in Figure 4.6A confirms that this hydrogenase can also catalyse H_2 oxidation under low levels of H_2 in air. Therefore, experiments were performed to test the performance of an *Ec*Hyd1/*Mv*BO fuel cell operating on a hydrogen-poor mixed gas feed, as described in the following section.

4.5.3.2 Characteristics of a Hydrogen-Poor Membraneless Fuel Cell

For the 'hydrogen-poor' membraneless fuel cell, 4% H_2 was diluted in air. The cyclic voltammograms recorded for the *Ec*Hyd1 and *Mv*BO electrodes in the fuel cell are shown in Figure 4.16A.

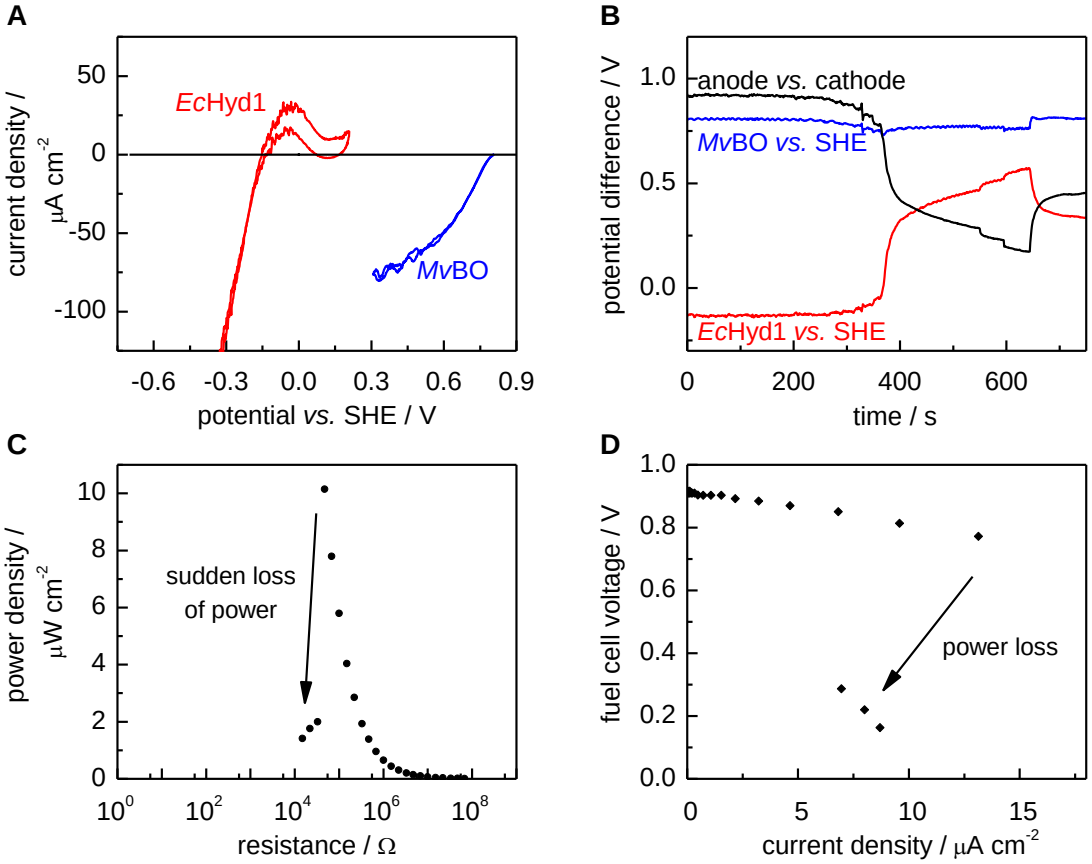


Figure 4.16. An *Ec*Hyd1/*Mv*BO H_2/O_2 fuel cell operating under 4% H_2/ 96% air at 25 °C using stationary electrodes (geometric surface area 1.25 cm^2). (A) Shows cyclic voltammograms for the *Ec*Hyd1 (red) and *Mv*BO (blue) recorded in the fuel cell at 10 mV s^{-1}. (B) Shows the time dependent changes in potential difference for the fuel cell (black) and the individual electrodes with respect to the reference electrode (anode *vs.* reference shown in red, cathode *vs.* reference shown in blue, quoted *vs.* SHE) over the course of the power curve being recorded. Each step is the potential difference response to changing resistance, and each resistance was held until the potential stabilised. The resistance was decreased until the fuel cell voltage collapsed.[††] Finally, the resistance was returned to 9.9 x 10^7 Ω to restore open circuit conditions. (C) Shows the power density of the fuel cell as a function of resistance and (D) shows a plot of the fuel cell voltage against current density (calculated from the fuel cell voltage and resistance).

It is clear that, under these conditions, the *Ec*Hyd1 H_2 oxidation current is significantly smaller than the *Mv*BO O_2 reduction current. Mass transport of H_2 to the stationary anode is likely to limit the rate of H_2 oxidation under these low H_2 conditions, and the

[††] The following sequence of resistance (Ω) steps was applied: 9.9 x 10^7, 6.8 x 10^7, 4.7 x 10^7, 3.3 x 10^7, 2.2 x 10^7, 1.5 x 10^7, 1.0 x 10^7, 6.8 x 10^6, 4.7 x 10^6, 3.3 x 10^6, 2.2 x 10^6, 1.5 x 10^6, 1.0 x 10^6, 6.8 x 10^5, 4.7 x 10^5, 3.3 x 10^5, 2.2 x 10^5, 1.5 x 10^5, 1.0 x 10^5, 6.8 x 10^4, 4.7 x 10^4, 3.3 x 10^4, 2.2 x 10^4, 1.5 x 10^4.

hydrogenase now undergoes complete aerobic inactivation upon scanning above 0 mV, although reductive reactivation occurs on the return scan.

The OCV for this fuel cell was much smaller than that obtained for the H_2-rich and PEM fuel cells; the value was just 930 mV. The lowered OCV is largely due to greatly increased O_2 reduction occurring directly at the bare surface of the graphite anode, which opposes the H_2 oxidation current, thus moving the point at which the anode current passes through zero to more positive potentials.

Figure 4.16B shows that, as the resistance between the anode and cathode is decreased during the power curve measurements, the potential of the *Ec*Hyd1 anode increases to a much greater extent than the potential of the *Mv*BO cathode decreases. Therefore, under low H_2 conditions the fuel cell output is controlled by the hydrogenase anode, and the fuel cell voltage drop is largely the result of the anode potential increasing rather than the cathode potential decreasing. Importantly, the anode potential does not return to its initial value when the open circuit resistance (9.9×10^7 Ω) is re-applied and thus the original OCV of this fuel cell cannot be recovered simply by increasing the resistance. This contrasts with the PEM and H_2-rich fuel cells described above, for which the power curve measurements are reversible.

From Figure 4.16C, it can be seen that a maximum power of 10.1 μW cm^{-2} was obtained for this fuel cell at 4.7×10^4 Ω (772 mV). However, instead of the symmetrical bell-shaped curves observed in previous sections, the H_2-poor fuel cell generates a power curve in which the power density drops sharply to zero at low resistances. Similarly, the voltage *vs.* current density plot shown in Figure 4.16D shows that this loss of power corresponds to a drop in both the fuel cell voltage and the current density below a certain

resistance. This can be explained in terms of the potential *vs.* time traces in Figure 4.16B: at 3.3 x 10^4 Ω (corresponding to time = 360 s) the potential of the *Ec*Hyd1 anode approaches 0 mV, favouring aerobic inactivation. This 'catastrophic power loss' will be discussed in detail in Section 4.6. The irreversible nature of this power loss is due to the fact that the conditions now overwhelmingly favour the aerobic inactivation of *Ec*Hyd1.[115] The observation that recovery of power does not occur simply upon re-applying a large resistance shows that, in the presence of excess O_2, the Ni-B (Ready) state is not reactivated by the low level of H_2 available without a supply of electrons.[201]

4.5.3.3 Recovery of Fuel Cell Performance using a Second Anode

Since reactivation of the *Ec*Hyd1 Ni-B (Ready) state under 4% H_2/96% air does not occur without a supply of electrons, attempts were made to recover the fuel cell activity by connecting the inactivated anode to an external electron source. The electrons were provided by a second anode containing *active Ec*Hyd1 and located in the same cell. These experiments were performed in an all-glass sealed electrochemical cell using stationary PGE disk electrodes (0.03 cm^2). Two *Ec*Hyd1 electrodes and one *Mv*BO electrode were combined in the working compartment of the cell and connected via steel rods that were attached to the top of each electrode and passed out of the cell via the sealing rubber septum.

In each case, a power curve of similar shape to that shown in Figure 4.16C was recorded as before, using one of the *Ec*Hyd1-modified electrodes as the anode (henceforth referred to as anode 1) and the *Mv*BO electrode as the cathode. After full power loss had occurred, the system was returned to 9.9 x 10^7 Ω and an OCV of only 200-300 mV was recovered. Anode 2, the second *Ec*Hyd1-modified electrode, which had been present in the fuel cell

but not previously connected to the circuit (and therefore not exposed to oxidising potentials), was then connected to anode 1 across a resistance of 1 x 10^6 Ω. The results of these experiments are shown in Figures 4.17A and B.

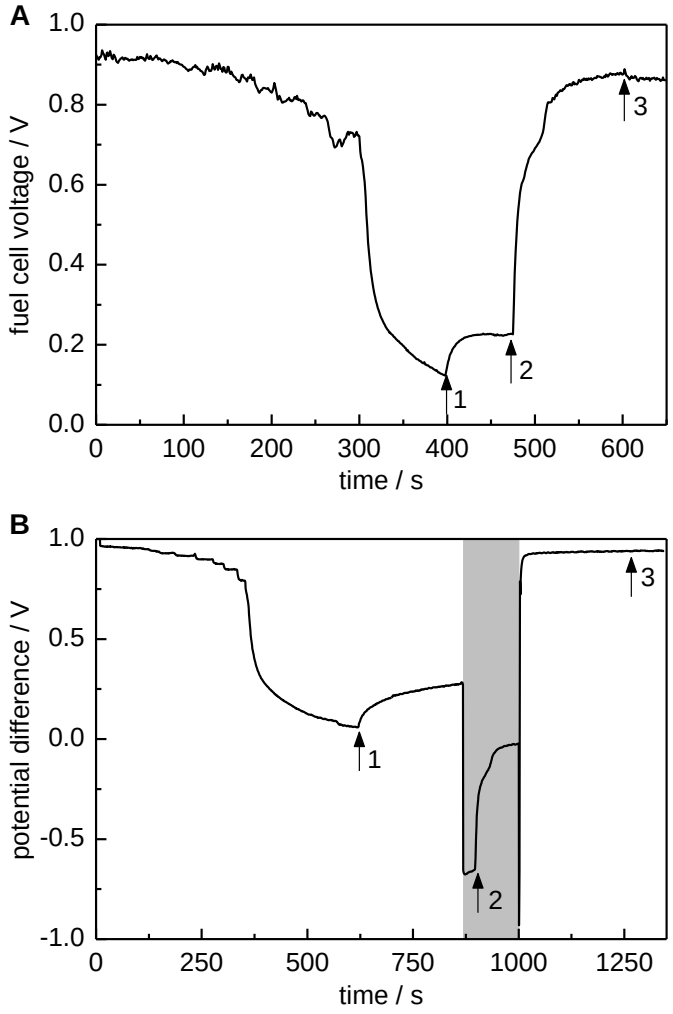


Figure 4.17. Two separate experiments showing the recovery of the fuel cell voltage achieved by reactivation of the inactive hydrogenase anode 1 by connection to an active second anode. (A) Shows the recovery as a function of fuel cell voltage and (B) shows the decrease in voltage between the two anodes (shaded region) leading to recovery of anode 1 and thus the fuel cell voltage. In the non-shaded region, the voltage difference is the fuel cell voltage (the potential difference between anode 1 and the cathode). In each case, a power curve was recorded by decreasing the resistance in a stepwise fashion until the cell voltage collapsed. The resistance was then returned to 9.9 x 10^7 Ω (arrows 1). The arrows numbered 2 correspond to connection of anode 2 to anode 1 across a resistance of 1 x 10^6 Ω, and arrows 3 show the point at which anode 2 was disconnected. A mixed feed of 4% H_2/96% air and stationary 0.03 cm^2 PGE electrodes were used, at 25 °C, pH 5.

Figure 4.17A shows the anode 1/cathode fuel cell voltage returning to its original OCV, following reactivation of the hydrogenase on anode 1 by connection to anode 2. The gradual decrease in cell voltage during the first 300 s in Figure 4.17A is a result of the stepwise lowering of the resistance applied between anode 1 and the cathode during the measurement of the power curve. Between 300 and 400 s, the cell voltage collapses as the potential of the hydrogenase increases to a point at which aerobic inactivation occurs. Arrow 1 represents the point at which a resistance of 9.9×10^7 Ω was restored, resulting in an OCV of only ~200 mV. Arrow 2 corresponds to connection of the inactivated anode 1 to the active anode 2; following this, the OCV rapidly recovers to close to its original value. Following disconnection of anode 2 (represented by arrow 3), the fuel cell retains its high OCV, confirming that the recovery is due to reactivation of the hydrogenase at anode 1.

Figure 4.17B records, alternatively, the reactivation in terms of the anode 1/anode 2 potential difference, which drops to zero during reactivation. As in the previous experiment, it can be seen that the cell voltage collapses following a stepwise decrease in resistance. Returning to 9.9×10^7 Ω (indicated by arrow 1) does not restore the original OCV. During the time represented by the grey box in Figure 4.17B, the potential difference was monitored between anode 1 and anode 2 rather than between anode 1 and the cathode. Following connection of anode 2 (represented by arrow 2), it can be seen that the potential difference between the two electrodes quickly falls to zero, corresponding to the electrons produced by H_2 oxidation at anode 2 reactivating the *Ec*Hyd1 molecules at anode 1.

The reactivation of anode 1 commences immediately and is rapid (the process is complete well within 80 s). Following this reactivation, the fuel cell voltage (measured between anode 1 and the cathode) returns to the original OCV and disconnection of anode 2 (indicated by the arrows numbered 3) has no effect on the fuel cell voltage. In each case, anode 2 remained fully active prior to connection to anode 1 because it was not connected to the cathode and therefore not subjected to an oxidising electrode potential.

4.6 Discussion

The results presented in this chapter evaluate the performance of *Ec*Hyd1/*Mv*BO fuel cells under different operating conditions. The maximum power output is achieved in a fuel cell using a PEM to separate the anode and cathode (Figure 4.10), although O_2 crossover may eventually affect the activity of even an O_2-tolerant hydrogenase (Figure 4.11). The work outlined also characterises the performance of the *Ec*Hyd1/*Mv*BO fuel cell operating without a membrane. In a H_2-rich membraneless fuel cell operating on a mixed-feed of 96% H_2/4% O_2, with anode and cathode of equal size, the catalytic activity of *Mv*BO is limiting and therefore changes in the fuel cell voltage reflect changes in the *Mv*BO electrode potential (Figure 4.12B). The *Ec*Hyd1 electrode potential remains almost constant and thus the hydrogenase does not experience a sufficiently positive potential to undergo aerobic inactivation, even when a low resistance is applied. In contrast, under H_2-poor aerobic conditions (4% H_2 in air) the power output is limited by the catalytic activity of *Ec*Hyd1 (Figure 4.16) and 'catastrophic power loss' occurs below a certain resistance due to O_2 inactivation of the hydrogenase anode, which increases as the anode potential rises.[19,113,216]

Figure 4.18 illustrates the changes in the potentials experienced by the *Ec*Hyd1 and *Mv*BO electrodes as the resistance between them is decreased for H_2-rich (Figure 4.18A) and H_2-poor (Figure 4.18B) membraneless fuel cells.

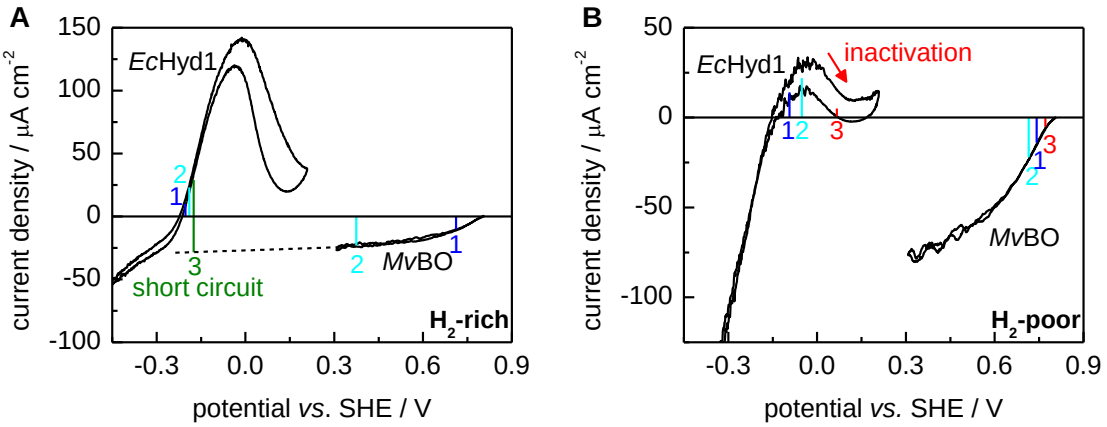


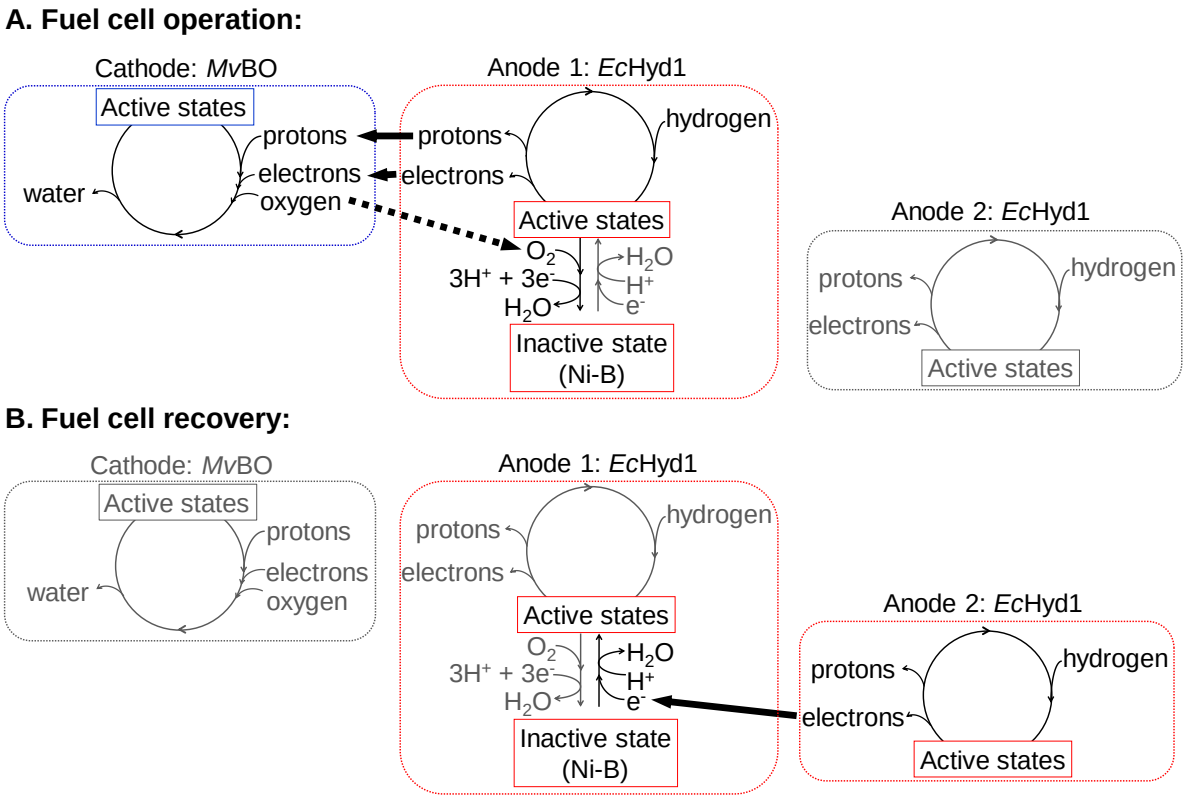
Figure 4.18. Representations of the cyclic voltammograms recorded in the 96% H_2/4% O_2 (A) and 4% H_2/96% air (B) fuel cells for *Ec*Hyd1 and *Mv*BO (data taken from Figure 4.12A and Figure 4.16A respectively). The numbered lines correspond to decreasing resistances (1 > 2 > 3). The *Mv*BO voltammogram in (A) has been extrapolated to show the approximate current flowing at short circuit (green). In (B) line 3 is dynamic because at this resistance the current and fuel cell voltage are both decreasing (indicated by the inactivation arrow), as described in the text.

The points 1, 2 and 3 correspond to the potentials of the individual electrodes obtained as the resistance between them is decreased from 1 to 3. In Figure 4.18A, the current increases with decreasing resistance (and fuel cell voltage), leading to a bell-shaped power curve (Figure 4.12C). The maximum current flows when the potentials of the two electrodes are equal (the short circuit situation, labelled in green). The situation is very different in the H_2-poor case, where the catalytic activity of *Ec*Hyd1 is limiting (Figure 4.18B). Initially, the current flow increases and the fuel cell voltage decreases as the resistance is decreased (points 1 and 2). However, between points 2 and 3, the hydrogenase is forced to a high positive potential at which aerobic inactivation is favoured. This leads to a decrease in H_2 oxidation current at the *Ec*Hyd1 anode that shifts

the bilirubin oxidase potential to a higher value (lower driving force) to balance the lower current. However, since $V = iR$ and the resistance is held at a constant value, a decrease in current should also decrease the fuel cell voltage. This leads to a further increase in the potential of the hydrogenase electrode, causing yet more inactivation and thus a greater loss of current. Therefore, under these conditions, the fuel cell enters into a cycle involving loss of both current and fuel cell voltage, resulting in a catastrophic loss of power (since $P = iV$).

Given the sudden loss of power at low resistances for a H_2-poor fuel cell, the anode can effectively be regarded as a circuit breaker. An important point to note is that the Ni-B (Ready) state of *Ec*Hyd1 is formed much more rapidly by reaction with O_2 than by anaerobic electrochemical oxidation.[115] The inactivation is therefore the result of O_2 reacting directly with *Ec*Hyd1 rather than the indirect action of O_2 drawing electrons away from the hydrogenase through its reduction at the *Mv*BO cathode or exposed regions of bare graphite at the anode. Furthermore, under the H_2-poor conditions, the *Ec*Hyd1/*Mv*BO fuel cell OCV does not recover simply upon reapplying the initial high resistance; instead, electrons must be provided to activate the O_2-inhibited hydrogenase and recover the fuel cell power. In cyclic voltammetry experiments, these electrons are provided instrumentally, but a fuel cell is a self-powered system and therefore requires an external electron source. The work in this chapter shows that reactivation can be achieved using a second active hydrogenase anode that has not been connected to the electrical circuit and thus has not been inactivated. The second active anode 'jump starts' the first, inactivated anode, analogous to recharging the flat battery of one car with the live battery of another. The reactions involved in these processes are represented in Scheme 4.1.[256] Anode 2 is able to provide electrons to anode 1 because it has sat *passively* under the

low H_2/high air conditions of the fuel cell and has not been subjected to an oxidising electrode potential (provided by the cathode to inactivate anode 1).



Scheme 4.1. (A) The reactions occurring at each electrode in the H_2-poor fuel cell and (B) the anode recovery cycle for the fuel cell system. Scheme reproduced from reference 256.

Technologically, H_2 oxidation catalysts that are both selective for H_2 and tolerant towards O_2 make possible the design of mixed-feed H_2/O_2 fuel cells. However, the work in this chapter demonstrates that the reactions of even O_2-tolerant [NiFe]-hydrogenases with O_2 limit the maximum power output of enzyme-based hydrogen fuel cells, even when a Nafion PEM is included. Catastrophic power loss occurs if the hydrogenase electrode reaches a potential above which aerobic inactivation occurs, and therefore in order to ensure long-term stability of a fuel cell, the bilirubin oxidase electrode should be current limiting (Figure 4.18A) or the hydrogenase must be very stable on the electrode. For example, power was drawn for 30 hours from a H_2-rich fuel cell operating under

96% H_2/4% O_2 at a resistance corresponding to 60% of the maximum original power. The explanation for this observation is that the bilirubin oxidase current is so limiting in the H_2-rich case that, even allowing for film loss of the hydrogenase from the electrode surface over time, the potential of the anode does not reach a sufficiently high value to cause inactivation.

In biology, coupled pairs of different enzymes on a membrane behave analogously to fuel cells.[2] In *Escherichia coli*, the oxidation of fuels (such as succinate, formate, lactate and H_2), catalysed by enzymes facing the periplasmic side of the cytoplasmic membrane, is coupled to reduction of a wide range of electron acceptors (including fumarate, nitrate, nitrite and O_2) via the quinol pool in the membrane.[190] In this bacterium, H_2 is generally not used as a fuel under aerobic conditions. However, it has been suggested that *Ec*Hyd1 may be involved in the coupling of H_2 and O_2 (the Knallgas reaction) as a mechanism for decreasing the local partial pressure of O_2 to enable anaerobic respiration under conditions where the oxygen concentration is too low to allow aerobic metabolism.[257] Certain strictly aerobic bacteria, such as the Knallgas bacterium *Re*, are able to use H_2 as a fuel under oxic conditions and couple its oxidation directly to O_2 reduction via the quinol pool, as described in Section 3.1.2. The current flowing between the H_2 oxidation anode and the O_2 reduction cathode in the fuel cell can therefore be likened to the coupling of H_2 oxidation to O_2 reduction via the quinol pool. During H_2 oxidation under aerobic conditions, hydrogenase molecules are continually being inactivated by O_2. However, analogous to the use of a second anode to reactivate hydrogenase molecules in a fuel cell, an electron source is available to a membrane-bound hydrogenase through the reduced quinol pool that other hydrogenases, still in the active state, continue to replenish with electrons.

In summary, the work outlined in this chapter was performed with the aims of resolving and rationalising the power characteristics of an all-enzyme H_2/O_2 fuel cell containing an O_2-tolerant hydrogenase as the anodic catalyst, with and without a membrane. Further developments of similar Pt-free H_2/O_2 devices will require increased power outputs and stabilities of the enzymes on the electrodes. The surface stability of the enzymes may be improved by the development of robust chemical modifications for enzyme attachment or by utilizing 3D electrodes.[255,258-262] The functional stability of the enzymes may be realised through the discovery of hydrogenases with even greater O_2 tolerance, genetic modification of hydrogenase systems known to date or, most significantly, the synthesis of hydrogenase-inspired catalysts.[162]

Chapter 5 Aldehydes as Reversible Inhibitors of H_2 Production by [FeFe]-Hydrogenases

Abstract

In contrast to the previous chapters, which focused on H_2 oxidation, the work outlined in this chapter focuses on H_2 production by [FeFe]-hydrogenases. This work shows that H_2 production by these enzymes is strongly inhibited by formaldehyde (methanal) in a rapid and reversible reaction. Three [FeFe]-hydrogenases, with a conserved active site but otherwise structurally distinct, each show this inhibition, although the rates and extents of inhibition vary. By contrast, inhibition of a [NiFe]-hydrogenase is very weak. Formaldehyde inhibition of the [FeFe]-hydrogenases was confirmed by conventional solution assays, but studies into the extent of reversibility were only made possible by PFE, as this technique allows removal of the dissolved inhibitor by buffer exchange. Formaldehyde causes a rapid loss of H_2 production activity, which is restored following solution exchange. The inhibition is strongly dependent on the direction of catalysis: inhibition of H_2 oxidation is much weaker than that of H_2 production. Formaldehyde also protects an [FeFe]-hydrogenase against CO inhibition. These results strongly suggest that formaldehyde binds at, or close to, the active site of [FeFe]-hydrogenases at a location unique to this class of enzyme. Possible targets for binding include highly conserved lysine and cysteine residues close to the active site, the bridgehead N atom of the dithiolate ligand, or the reduced Fe_d that binds protons during catalysis.

Some of the results originally presented in this chapter cannot currently be made freely available as they are to be published at a later date in academic journals.

This chapter is reproduced in part from: Wait, A. F.; Brandmayr, C.; Stripp, S. T.; Cavazza, C.; Fontecilla-Camps, J. C.; Happe, T.; Armstrong, F. A., *J. Am. Chem. Soc.* **2011,** *133* (5), 1282-1285 (http://pubs.acs.org/doi/abs/10.1021/ja110103p).

5.1 Introduction

5.1.1 Introduction to the [FeFe]-Hydrogenases

5.1.1.1 The Hydrogenases Studied

This chapter discusses inhibition of three different [FeFe]-hydrogenases: *Desulfovibrio desulfuricans* HydAB (*Dd*HydAB), *Clostridium acetobutylicum* HydA (*Ca*HydA) and *Chlamydomonas reinhardtii* HydA1 (*Cr*HydA1). These hydrogenases share the same active site (known as the 'H-cluster', see Chapter 1) but vary significantly in overall protein structure (Figure 5.1).

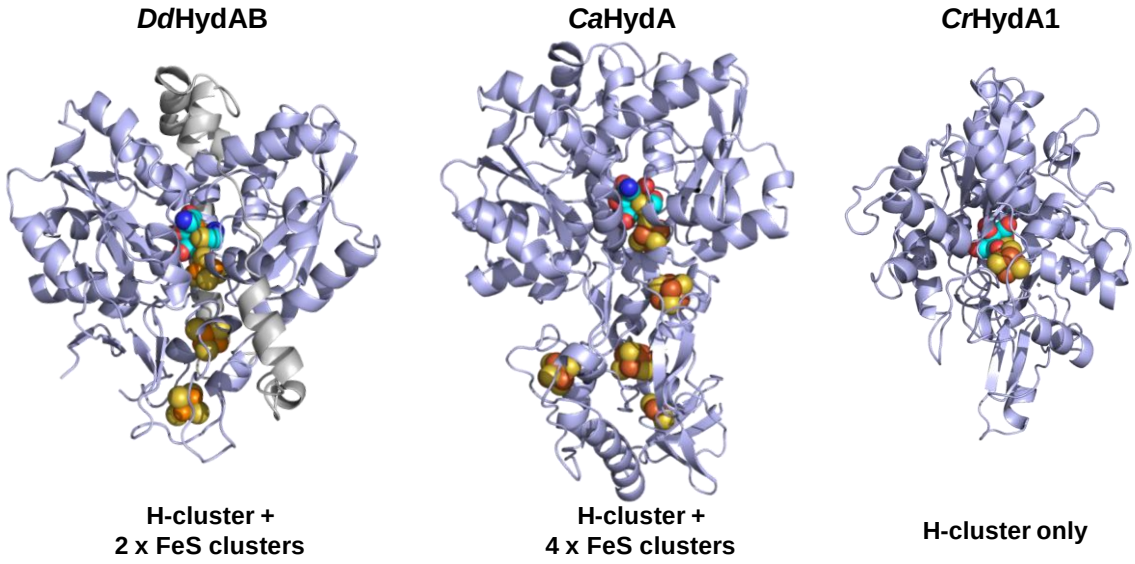


Figure 5.1. A comparison of the overall protein structures of the three [FeFe]-hydrogenases studied in this work. The structure of *Dd*HydAB was resolved by X-ray crystallography[37] (Protein Data Bank code 1HFE), the structure for *Ca*HydA was obtained by homology modelling using Modweb software,[263] and the model structure of *Cr*HydA1 was generated by Sven T. Stripp via Swiss Prot. The latter two models are both based on the structure of *Clostridium pasteurianum* hydrogenase-1 (Protein Data Bank code 3C8Y).

Desulfovibrio desulfuricans (*Dd*) is a sulfate-reducing bacterium that couples H_2 oxidation to the reduction of sulfate (SO_4^{2-}). These bacteria generally live under anoxic conditions, although even these 'strict anaerobes' can be found at the interfaces between

oxic and anoxic environments.[264] The [FeFe]-hydrogenase from *Dd* (*Dd*HydAB) is a soluble periplasmic hydrogenase that, in contrast to many other [FeFe]-hydrogenases, appears to catalyse H_2 uptake (oxidation) *in vivo*.[265] The electrons released from H_2 are believed to be transferred to cytochrome c_3 and then passed to a high molecular mass cytochrome, before being transported through the membrane via a transmembrane redox complex to the cytoplasm, where they are used to reduce sulfate. The protons can be used to generate ATP via an ATPase.[265] As mentioned in Chapter 1, the structure of *Dd*HydAB is heterodimeric, with two subunits of size 42 kDa and 11 kDa. The large subunit contains, in addition to the [4Fe4S]-cluster located in the H-cluster, two further [4Fe4S]-clusters that link the buried active site to the protein surface, and the small subunit resembles a belt that surrounds the large subunit (Figure 5.1).[37]

Clostridium acetobutylicum is a strictly anaerobic bacterium that carries out biphasic fermentation: acetic (ethanoic) acid and butyric (butanoic) acid are formed during the exponential growth phase, whereas the organism switches to production of acetone and butanol shortly before commencing the stationary phase.[266] The pathways involved in the production of the acids do not allow for removal of excess NADH generated during glycolysis. Therefore, the organism uses a hydrogenase to remove both excess protons and electrons via H_2 production.[267] The [FeFe]-hydrogenase *Ca*HydA is monomeric (64.3 kDa)[268] and shares 71% sequence identity with the crystallographically characterised *Clostridium pasteuranium* hydrogenase-1 (*Cp*I).[269] The active site (H-cluster) is located in the H-domain, whereas the F-domain contains FeS clusters to relay electrons between the H-cluster and the protein surface. Based on analogy with *Cp*I, *Ca*HydA contains, in addition to the [4Fe4S]-cluster present in the H-cluster, three [4Fe4S]-clusters and one [2Fe2S]-cluster (Figure 5.1).[40]

Chlamydomonas reinhardtii (*Cr*) is an example of a soil-dwelling eukaryotic green alga that can perform light-dependent H_2 production under anoxic conditions using an [FeFe]-hydrogenase (*Cr*HydA1).[270] The hydrogenase is localised in the chloroplast[271] and is coupled to the photosynthetic electron transfer chain. Light energy is used to oxidise water molecules to release electrons, which are transported from photosystem I to the hydrogenase via the ferredoxin PetF.[272,273] This enzyme is one of the smallest hydrogenases known and is monomeric, with size 47.5 kDa.[274] In contrast to the two bacterial [FeFe]-hydrogenases described above, the algal hydrogenase CrHydA1 contains only the H-cluster, with no additional FeS cluster relay.[80,81]

The work in this chapter compares the formaldehyde inhibition of these [FeFe]-hydrogenases with that of an O_2-sensitive [NiFe]-hydrogenase, *Escherichia coli* Hydrogenase 2 (*Ec*Hyd2). As described for *Ec*Hyd1 in the previous chapter, *Ec*Hyd2 is a membrane-bound periplasmic enzyme, believed to be involved in H_2 uptake (oxidation).[275,276] *In vivo*, *Ec*Hyd2 reduces quinones via a periplasmic ferredoxin and an integral membrane protein (possibly a *b*-type cytochrome).[115,277,278]

5.1.1.2 Bidirectional Catalysis

Figure 5.2 shows a typical cyclic voltammogram for *Ca*HydA performed under 100% H_2 at pH 6, recorded at 10 mV s^{-1}. This [FeFe]-hydrogenase is bidirectional, catalysing both H_2 oxidation (observed as positive current) and H_2 production (recorded as negative current). The cyclic voltammogram cuts through the zero current axis at a potential equal to the value of $E(2H^+/H_2)$ under these conditions (represented by the red dashed line in Figure 5.2). Since the voltammogram cuts cleanly through the axis, with no point of inflection, the enzyme does not require an overpotential for H_2 oxidation or production.

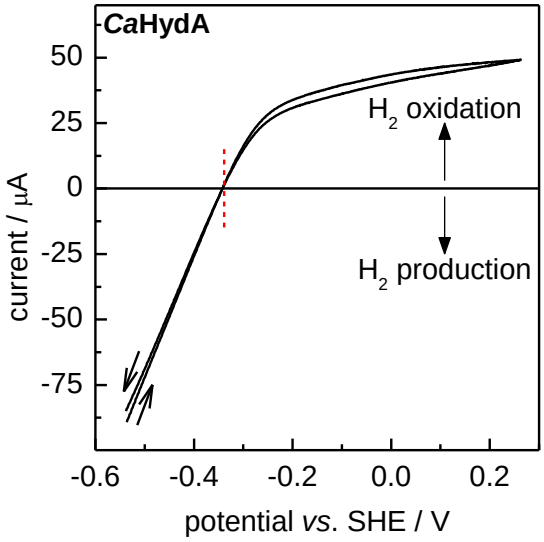


Figure 5.2. Cyclic voltammogram for *Ca*HydA recorded at 10 mV s^{-1} under 100% H_2. The current *vs.* potential trace cuts the axis at the thermodynamic potential of the $2H^+/H_2$ couple ($E(2H^+/H_2)$, shown by the red dashed line) calculated for these conditions. Hydrogen oxidation results in positive current at potentials more positive than $E(2H^+/H_2)$, whereas H_2 production (H^+ reduction) generates negative current at more negative potentials. The direction of the scan is illustrated by the arrows. Other conditions: pH 6, 10 ºC, electrode rotation rate 2500 rpm.

The magnitude of the H_2 oxidation current under these conditions is smaller than that due to H_2 production, indicating that the catalytic bias of *Ca*HydA favours H_2 production, as noted previously.[279] Considerable H_2 production currents are achieved even under 100% H_2, which is consistent with previous studies[101] that obtained a relatively high inhibition constant for product inhibition of H_2 production, corresponding to only weak inhibition. The plateau in the H_2 oxidation current at potentials above ~-200 mV suggests that as the potential is increased the rate of catalysis becomes limited by a chemical step rather than electron transfer.[279] The chemical step may involve processes such as association of the H_2 molecule with the active site or the breaking of a bond. As the potential increases, the rate of electron transfer increases (Section 2.3.4) until it reaches a point at which the electron transfer is much faster than the chemical step, which then becomes rate determining.

5.1.1.3 Anaerobic Inactivation to Form the H_{ox}^{inact} State

Figures 5.3A and B show cyclic voltammograms for *Dd*HydAB and *Cr*HydA1 respectively, recorded under the same conditions as the voltammogram for *Ca*HydA (Figure 5.2).

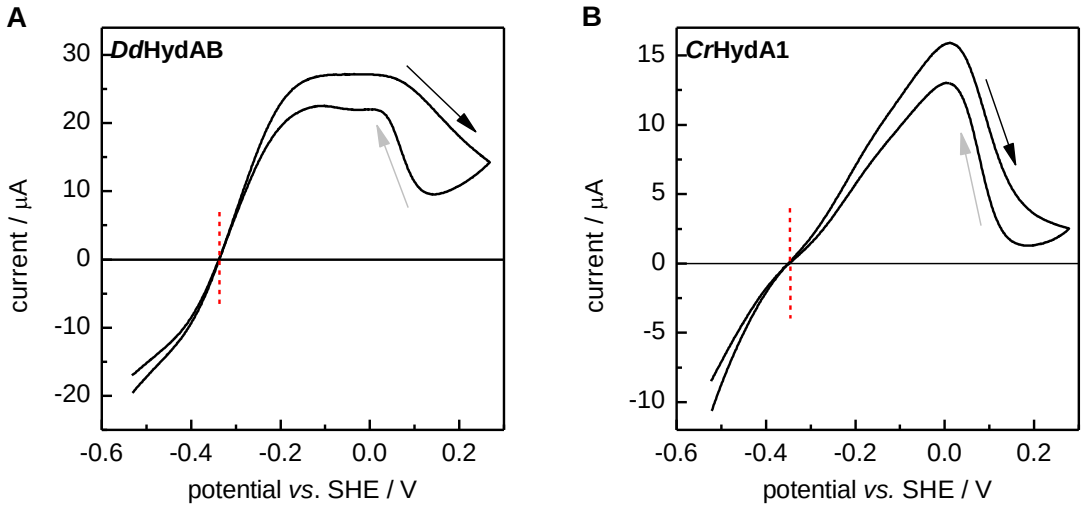


Figure 5.3. Cyclic voltammograms for (A) *Dd*HydAB and (B) *Cr*HydA1 recorded at 10 mV s^{-1} under 100% H_2. In each case, the current *vs.* potential trace cuts the axis at the thermodynamic potential of the $2H^+/H_2$ couple ($E(2H^+/H_2)$, shown by the red dashed lines) calculated under these conditions. Hydrogen oxidation results in positive current at potentials more positive than $E(2H^+/H_2)$ whereas H_2 production (H^+ reduction) generates negative current at more negative potentials. The processes of anaerobic inactivation and reactivation are indicated by the black and grey arrows respectively. Other conditions: pH 6, 10 ºC, electrode rotation rate 2500 rpm.

These [FeFe]-hydrogenases also show bidirectional catalysis and both voltammograms cut the zero current axis at the thermodynamic potential of the $2H^+/H_2$ couple under these conditions (red dashed lines in Figure 5.3). For *Dd*HydAB (Figure 5.3A), the voltammogram cuts sharply through the axis indicating that, as for *Ca*HydA, this enzyme does not require an overpotential for catalysis.[98] However, the voltammogram in Figure 5.3B demonstrates that *Cr*HydA1 does require a slight overpotential for both H_2 oxidation and production, seen as a point of inflection at the thermodynamic potential.[111] Since this overpotential is not observed for *Dd*HydAB or *Ca*HydA, which both contain FeS cluster

relay chains, this suggests that the extra driving force required by *Cr*HydA1 may be due to the distance required for electron tunnelling between the electrode and the active site,[279] which will depend on the orientation of the enzyme on the electrode surface.

For *Cr*HydA1, the rate of H_2 oxidation approximately equals that of H_2 production at a given driving force (equal to the difference between the applied potential and $E(2H^+/H_2)$). This is also observed for *Dd*HydAB, although this enzyme has previously been noted as slightly biased towards H_2 oxidation.[279] The relatively high H_2 oxidation current is as expected due to the proposed role of *Dd*HydAB *in vivo* as a H_2 uptake hydrogenase,[265] although the high H_2 production activity is also unsurprising since the H-cluster of this enzyme is almost identical to the two other [FeFe]-hydrogenases, which are involved in H_2 production *in vivo*.[98]

An important feature of the voltammograms in Figure 5.3 is the attenuation in current observed above 0 mV (highlighted by the black arrows in Figure 5.3). This is due to high potential anaerobic inactivation to form the H_{ox}^{inact} state, in which the 2Fe moiety in the H-cluster is oxidised to Fe(II)Fe(II) and an oxygenic species (H_2O or HO^-) occupies the vacant coordination site at the distal Fe.[40,85] At the scan rates used in Figure 5.3, the inactivation is largely reversible and reductive reactivation occurs on the return scan towards low potential (seen as a recovery in H_2 oxidation activity, indicated by the grey arrows in Figure 5.3). The inactivation process is very slow for *Ca*HydA[101] and therefore little (if any) attenuation in current is observable in Figure 5.2.

A further feature of the voltammogram for *Dd*HydAB is that, in the H_2 oxidation region, the current *vs.* potential trace shows two maxima: one at high potential, close to the potential of inactivation, and another at a more negative potential. The origins of this

shape are unknown, but may include inhomogeneity (of orientation of the enzyme molecules on the electrode or within the enzyme itself)[244] or the presence of trace levels of inhibitors (such as CO) that bind preferentially to one redox state of the enzyme.[98]

5.1.1.4 Sensitivity of [FeFe]-Hydrogenases Towards CO and O_2

In contrast to the O_2-tolerant [NiFe]-hydrogenases discussed in the previous chapters, [FeFe]-hydrogenases are highly sensitive to both CO and O_2.[31,101] Studies have shown that CO binding is strongest during H_2 oxidation, and this inhibitor is believed to target the H_{ox} state of the [FeFe]-hydrogenases,[95,118,119] binding to the distal Fe atom (Fe_d) of the H-cluster.[280-282] Experiments have also shown that CO inhibition of H_2 oxidation is mostly reversible, whereas during H_2 production CO-binding is largely irreversible.[101] The rates of CO inhibition decrease in the order *Dd*HydAB > *Cr*HydA1 > *Ca*HydA, which has been explained in terms of the notion of a gas 'filter' that is most successful in preventing access of CO in *Ca*HydA and least in *Dd*HydAB.[101] However, the rates of recovery from CO are similar for all three [FeFe]-hydrogenases.[101]

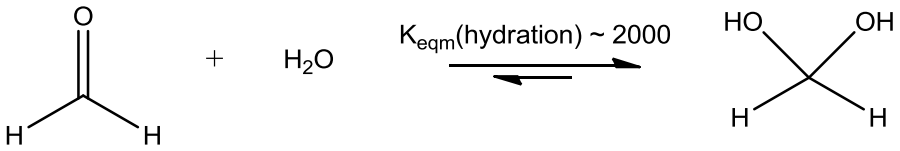
A major challenge for the potential use of [FeFe]-hydrogenases in biotechnological applications (such as the fuel cell described in the previous chapter, or large-scale biological H_2 production) is that these enzymes are generally irreversibly damaged by O_2. As discussed in Chapter 1, previous work has shown that this is likely due to oxidative damage to the [4Fe4S]-cluster located in the active site.[111] The O_2 molecule is believed to first bind to the distal Fe of the 2Fe moiety, generating a species that subsequently attacks the [4Fe4S]-cluster. The rates of O_2-inhibition of H_2 oxidation by the [FeFe]-hydrogenases follow the same trend as observed for CO inhibition

(*Dd*HydAB > *Cr*HydA1 > *Ca*HydA)[101] and it has been proposed that O_2 attacks the H_{ox} state of the enzyme, based on analogy with CO inhibition.[111]

5.1.2 Formaldehyde as an Inhibitor

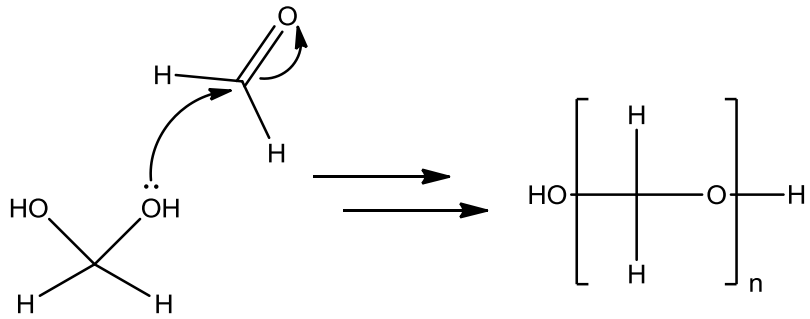
5.1.2.1 Common Reactions of Formaldehyde

Formaldehyde (methanal) is the simplest in a series of organic molecules known as aldehydes (with general formula RCHO). This aldehyde has the molecular formula CH_2O (R = H), and is therefore a small molecule (molecular mass 30 Da) that is gaseous at room temperature (boiling point ~19 ºC).[283] Aldehydes are highly electrophilic, and formaldehyde is particularly reactive due to its sterically unhindered C=O bond. Formaldehyde dissolves in water up to a maximum of 37% w/v, known as formalin solution, and undergoes hydration (attack by nucleophilic H_2O) to form a diol (hydrate). This reaction is shown in Scheme 5.1, and has an equilibrium constant, K_{eqm}(hydration), of ~ 2000 at 25°C.[284,285] Therefore, the equilibrium lies strongly in favour of the hydrate rather than the aldehyde.



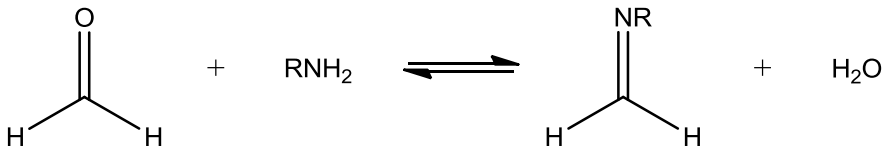
Scheme 5.1. The reaction of formaldehyde with water to give the hydrate.[284,285]

The hydrate formed by this reaction can lead to polymerisation, via nucleophilic attack by the OH group of the hydrate on the carbonyl group of a non-hydrated aldehyde molecule, as shown in Scheme 5.2.[283]



Scheme 5.2. The reaction leading to polymerisation of formaldehyde. The polymer is known as paraformaldehyde when n averages 8, and polyoxymethylene when n > 100.[283]

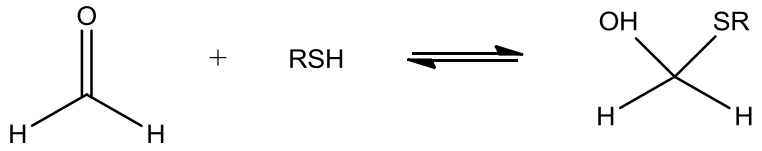
Formalin solution is widely used as a fixative in biology, since it chemically modifies proteins in an irreversible manner. Although the overall process is irreversible, the first stages are rapid and reversible, most commonly involving the reaction of the aldehyde with the nucleophilic N atom of an amine to form a Schiff-base adduct (Scheme 5.3).



Scheme 5.3. The reaction of formaldehyde with a primary amine to form a Schiff base.

Formaldehyde can be used to methylate lysine (-NH_2) residues in this way, by reducing the Schiff base with borohydride.[286,287] Alternatively, methylene crosslinks can be formed by attack of a protonated Schiff base by an XH group, where XH is most often a nucleophilic sidechain of another amino acid.[287]

Formaldehyde may also form an adduct with a nucleophilic S atom (such as that present in a cysteine residue, -SH) in a rapid and reversible reaction that forms a thioacetal (Scheme 5.4).[287]



Scheme 5.4. The reaction of formaldehyde with a thiol group to form a thioacetal.

Given its usual role as a biocide, formaldehyde at first glance seems an unlikely reversible inhibitor of enzyme catalysis. However, previous work (discussed in detail in the next section) has suggested that aldehydes may, in fact, act as inhibitors of hydrogenases, possibly even reversibly.

5.1.2.2 Previous Studies of Aldehyde Inhibition of Hydrogenases

It was first noted in the 1980s that aldehydes may inhibit hydrogenases. Studies by Slatyer *et al.* found that the hydrogenase from *Anabaena cylindrica* is inhibited by acetaldehyde (ethanal, CH_3CHO) and concluded that the inhibition is irreversible, since washing the cells with fresh medium did not recover hydrogenase activity.[288] In contrast, solution assays and EPR studies by Rao *et al.* concluded that neither acetaldehyde nor glutaraldehyde affect the active site of hydrogenases from *Clostridium pasteurianum* and *Desulfovibrio desulfuricans*.[289]

More recently, preliminary electrochemical studies in Prof. Fraser Armstrong's group showed that formaldehyde can act as an inhibitor of H_2 production by *Ca*HydA and *Cr*HydA1 [FeFe]-hydrogenases.[279,290] This work also suggested that the inhibition is reversible, although the reversibility could not be measured quantitatively due to a lack of a suitable experimental set-up.

The work described in this chapter exploits a new experimental design to perform detailed studies on formaldehyde inhibition and its reversibility.

5.1.2.3 Target Sites for Formaldehyde in [FeFe]-Hydrogenases

Aside from exposed cysteine, lysine or histidine residues on the protein surface, several possible target sites for formaldehyde binding exist in [FeFe]-hydrogenases. Figure 5.4 shows a representation of the H-cluster of *Dd*HydAB including nucleophilic amino acid residues within 5 Å of the active site that are conserved in the three [FeFe]-hydrogenases studied in this chapter.[85,291]

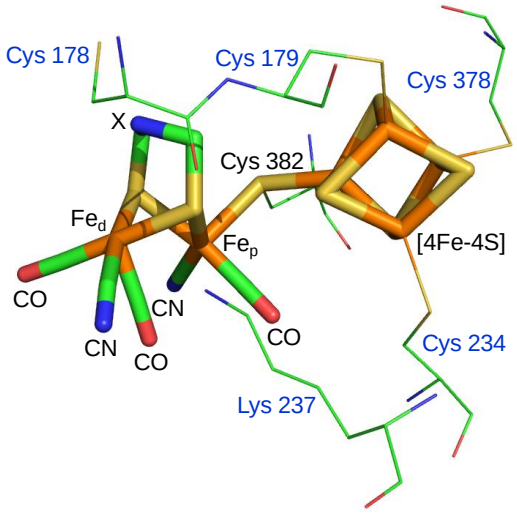


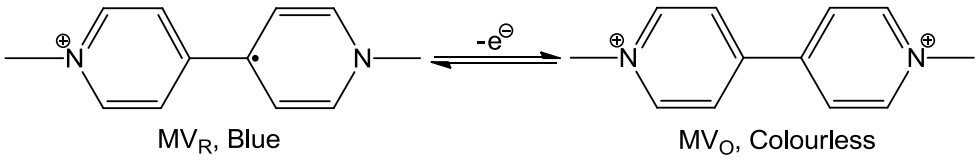
Figure 5.4. The H-cluster of *Dd*HydAB in the reduced H_{red} state highlighting the bridgehead atom, X (assigned as an N atom) and conserved nucleophilic residues within 5 Å of the active site that are possible targets for formaldehyde.[85]

As discussed in Chapter 1, in this thesis the bridgehead atom is assumed to be an N atom.[86] As shown in Figure 5.4, the active site region of [FeFe]-hydrogenases contains a highly conserved lysine (Lys237 in *Dd*HydAB) close to the distal Fe atom, Fe_d, and a conserved cysteine residue close to the bridgehead N atom (Cys178 in *Dd*HydAB).[85] The bridgehead N atom and the amine and thiol sidechains of the conserved amino acids are nucleophilic centres that could act as formaldehyde target sites (Section 5.1.2.1). There is also evidence, from crystal structures and modelling studies, to suggest that these sites may be directly involved in proton transfer, as discussed in Chapter 1.[60] In addition, there

is also the possibility that in reduced states of the enzyme the Fe_d itself may react with formaldehyde, since this atom is involved in the binding and redox conversion of H^+.[63,92,103,104]

5.2 Detection of Inhibition using an Assay

In order to confirm that the formaldehyde inhibition of [FeFe]-hydrogenases observed in the preliminary PFE experiments was not merely an artefact of this technique, solution assays were performed to establish that formaldehyde is also an inhibitor of H_2 production by a third [FeFe]-hydrogenase, *Dd*HydAB. Electrochemically reduced methyl viologen (MV_R) was used as the electron donor in these experiments. The electrochemical reduction was necessary because oxidation of the reducing agent dithionite produces bisulfite,[292] which reacts to form an adduct with the aldehyde.[289] In each assay, catalytic H_2 production by *Dd*HydAB was measured over time by monitoring the decrease in absorbance at 604 nm as the reduced methyl viologen (MV_R, blue) was oxidised to form a colourless compound (MV_O, see Scheme 5.5).



Scheme 5.5. Representation of the oxidation of methyl viologen, with the concomitant change in colour from blue to colourless.

The assays (Figure 5.5) were performed in an anaerobic glovebox, in a cuvette open to the N_2 atmosphere. The cuvette was filled with 1 mL solution of 200 μM MV_R dissolved in 50 mM phosphate buffer containing 100 mM NaCl. In the blue and black traces in Figure 5.5, 2 μL *Dd*HydAB solution (9 μM) was injected at 40 s (red arrow) and in the grey and blue traces 5 μL formaldehyde solution (13.4 M, as purchased) was injected at 65 s (black

arrow). This gave approximate final concentrations of 18 nM enzyme and 67 mM formaldehyde (corresponding to ~30 μM non-hydrated aldehyde). The black trace follows H_2 production by *Dd*HydAB as a decrease in colour (corresponding to oxidation of MV_R) over time. In the blue trace, the activity of the enzyme sharply decreases upon addition of formaldehyde (seen as a decrease in magnitude of the gradient after 65 s). No enzyme is present in the grey control trace and consequently there is little change in the absorbance at 604 nm over time.

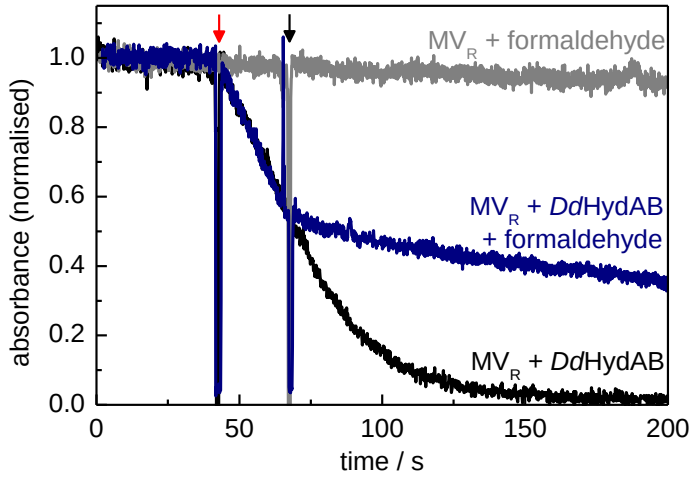


Figure 5.5. Solution assay demonstrating formaldehyde inhibition of H_2 production by *Dd*HydAB at pH 6, 20 °C. The black trace shows the activity of *Dd*HydAB (added at 40 s, red arrow) in the absence of formaldehyde, the blue shows the response of the enzyme activity to addition of formaldehyde (final concentration of 67 mM, added at 65 s (black arrow)), and the grey trace shows a control experiment run in the absence of hydrogenase. The absorbance at 604 nm (using a halogen lamp as light source) was measured over time and normalised so that absorbance of the initial solution of MV_R in buffer is equal to 1.

These results confirm that H_2 production by *Dd*HydAB is inhibited by formaldehyde. However, in these assays the enzyme is in solution with the formaldehyde and therefore the formaldehyde cannot easily be removed in order to test the reversibility of the inhibition. In PFE, the enzyme is immobilised onto the electrode surface and therefore the solution can be exchanged with minimal disturbance to the enzyme film. Therefore, the

remaining experiments in this chapter use this technique to study the formaldehyde inhibition of hydrogenases, including the extent of reversibility.

5.3 Studies using Protein Film Electrochemistry

5.3.1 Experimental Design

It is difficult to demonstrate the action of formaldehyde as a reversible enzyme inhibitor because the aldehyde must be removed in order to check for recovery of activity. Protein Film Electrochemistry (PFE) solves this problem: since the enzyme is immobilised onto the electrode surface as an electroactive film, the solution can be exchanged, thus allowing both introduction and removal of inhibitor. A set-up was designed to enable exchange of the solution in the electrochemical cell without the loss of electrical contact during the rinse. This arrangement (described in Chapter 7) comprises a pair of 50 mL syringes, attached to the electrochemical cell via tubing. One syringe is loaded with fresh buffer solution; the other empty. Thus, fresh solution can be introduced into the electrochemical cell at the same rate as undesired solution is removed. Despite pre-equilibration of the solution to the experimental temperature (Chapter 7), slight fluctuations in current often occur due to small temperature changes upon rinsing.

5.3.2 Inhibition of H_2 Production

Figure 5.6 shows chronoamperometry experiments comparing formaldehyde inhibition of H_2 production for the three [FeFe]-hydrogenases and *Ec*Hyd2 [NiFe]-hydrogenase.

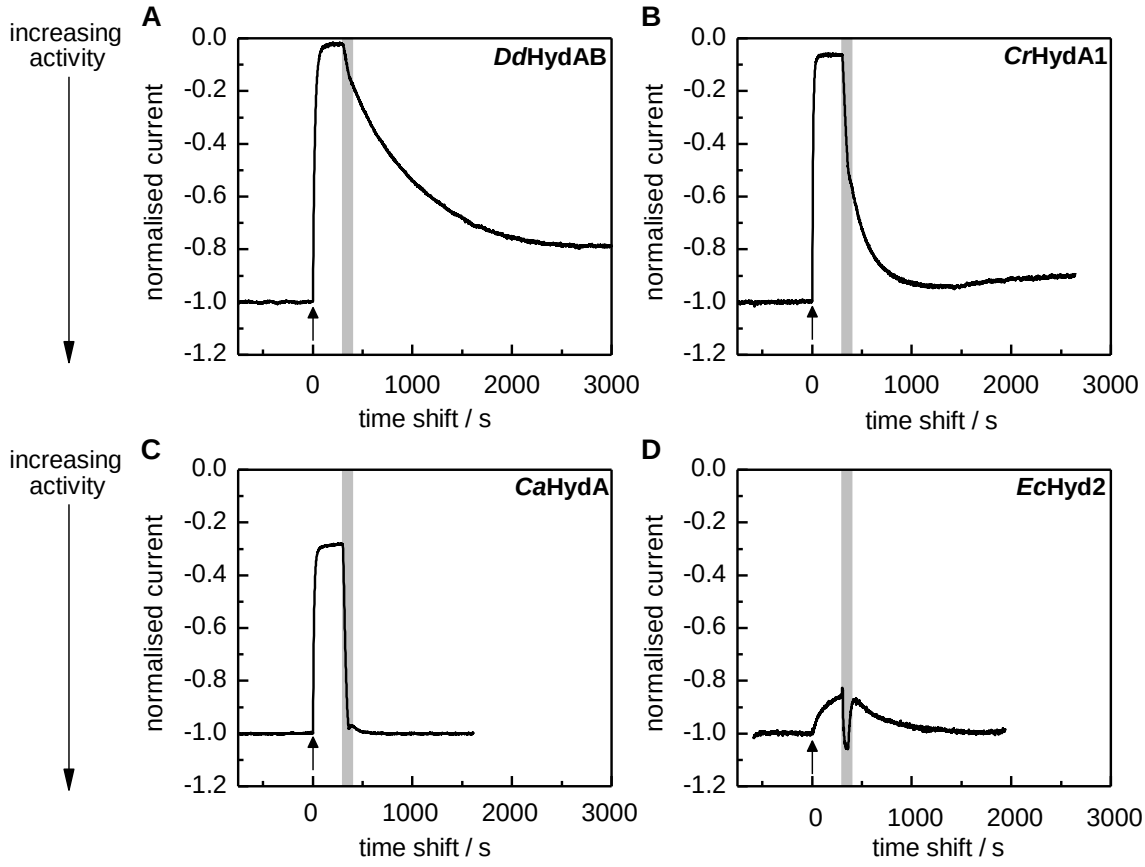


Figure 5.6. Inhibition of H_2 production by formaldehyde for various hydrogenases: (A) *Dd*HydAB [FeFe]-, (B) *Cr*HydA1 [FeFe]-, (C) *Ca*HydA [FeFe]-, and (D) *Ec*Hyd2 [NiFe]-hydrogenases. In each case, the electrode potential was held at -558 mV and formaldehyde injected at time = 0 s (indicated by the arrows) to give a final concentration of 4.5 mM. After 300 s, the cell was rinsed with 50 mL of fresh buffer solution pre-equilibrated to the temperature and gas composition already experienced by the enzyme (rinsing took ~100 s, represented by the grey bars). The data in (A), (B) and (C) were recorded under 100% H_2 and the data in (D) under 100% N_2, as discussed in the text. Other conditions: pH 6, 10 ºC, electrode rotation rate 2500 rpm.

In each case, the electrode potential was held at -558 mV, and H_2 production activity (corresponding to negative current) monitored over time. At time t = 0 s, 1 mL of 13.4 mM formaldehyde (in buffer of identical composition to that already present in the electrochemical cell) was injected into the cell solution (2 mL), to give a final concentration of 4.5 mM (corresponding to ~ 2.2 μM non-hydrated aldehyde). It should be noted that, to ease comparison, the time was shifted so that the injection occurs at t = 0 s in each case (hence the x-axes of Figure 5.6 are labelled 'time shift'). After 300 s,

the cell was rinsed with 50 mL of buffer solution, pre-equilibrated to the same temperature and gas composition as the buffer in the electrochemical cell, using the two syringes. As mentioned in Section 5.3.1, small dips in current (observed particularly clearly during the rinsing stage of Figure 5.6D) are due to small temperature changes upon rinsing.

In order to aid comparison, the data in Figure 5.6 have been normalised by fitting the slow 'baseline' decrease in current magnitude over time prior to the formaldehyde injection (film loss) to a single exponential process.[196,293] This exponential decrease in current was extrapolated over the time course of the experiment and for each data point the raw data were divided by the exponential to obtain a normalised current (this normalisation procedure is explained in detail in Appendix A2). To retain the convention that reduction processes generate negative currents, the resulting normalised currents were multiplied by (-1).

Figure 5.6 shows that, for all three [FeFe]-hydrogenases, injection of formaldehyde causes a rapid loss of activity that is recovered when the formaldehyde is removed. Under these conditions, inhibition of H_2 production by 4.5 mM formaldehyde is virtually complete for *Dd*HydAB, >90% complete for *Cr*HydA1 and 70-80% complete for *Ca*HydA. In contrast, inhibition of *Ec*Hyd2 [NiFe]-hydrogenase is much slower and occurs to a much lesser extent (~15% after 300 s). Preliminary experiments performed by Caterina Brandmayr show that other [NiFe]-hydrogenases show similarly weak inhibition.[290] It should be noted that inhibition of H_2 production by *Ec*Hyd2 was investigated under 100% N_2 rather than 100% H_2 as for the [FeFe]-hydrogenases, since product inhibition of H_2 production is greater for [NiFe]-hydrogenases.[101,115] However, as

will be discussed in the following chapter, the rate and extent of formaldehyde inhibition of H_2 production by an [FeFe]-hydrogenase appears to be independent of H_2 concentration, and thus the results in Figure 5.6 can be compared despite the varying gas composition.

The results in Figure 5.6 show that formaldehyde inhibition of H_2 production by [FeFe]-hydrogenases is reversible. Following exchange of the buffer solution (over a time period of ~100s, illustrated by the grey boxes in Figure 5.6), H_2 production activity is restored. The rates of recovery appear to increase in the order *Dd*HydAB < CrHydA1 < CaHydA. Binding of formaldehyde to *Dd*HydAB is so tight that a small amount of enzyme is still inhibited by traces remaining after the first rinse. However, full activity can be regained by a second buffer exchange (Appendix A6).

Figure 5.7 compares formaldehyde inhibition of H_2 production by the three [FeFe]-hydrogenases and *Ec*Hyd2 [NiFe]-hydrogenase at a lower final concentration of 447 μM. Each current *vs.* time trace fits well to a single exponential process and these exponentials are overlaid on the experimental data. These data more clearly show that the extent of inhibition is greatest for *Dd*HydAB, followed closely by *Cr*HydA1, and that *Ca*HydA is the least strongly inhibited of the [FeFe]-hydrogenases, consistent with the preliminary data shown in Figure 5.6. Figure 5.7 also confirms that inhibition is much weaker for the [NiFe]-hydrogenase *Ec*Hyd2. First order rate constants for the inhibition of the [FeFe]-hydrogenases were calculated from the single exponential fits to the data. These rates generally increase in the order *Dd*HydAB < *Cr*HydA1 < *Ca*HydA; the rates, k_{obs}, were determined as 0.01 s^{-1}, 0.02 s^{-1} and 0.05 s^{-1} respectively. The rate of inhibition for

*Ec*Hyd2 cannot be accurately determined from this data due to such a small extent of inhibition.

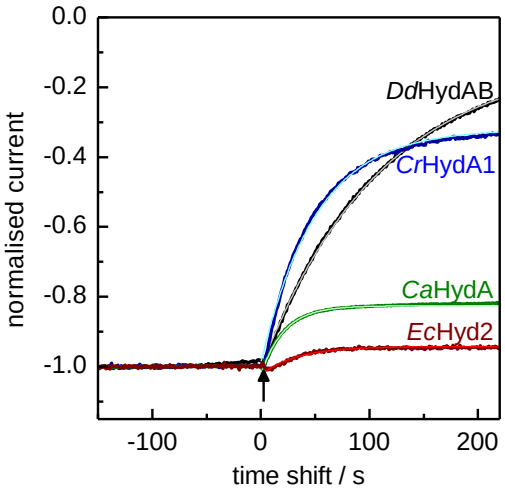


Figure 5.7. Experiments comparing formaldehyde inhibition of H_2 production by *Dd*HydAB [FeFe]-hydrogenase (black), *Cr*HydA1 [FeFe]-hydrogenase (blue), *Ca*HydA [FeFe]-hydrogenase (green) and *Ec*Hyd2 [NiFe]-hydrogenase (red). In each case, the enzyme was held at -556 mV and formaldehyde injected at time = 0 s to give a final concentration of 447 μM. For each current *vs.* time trace, the single exponential fit used to calculate the rate of inhibition, k_{obs}, is overlaid on the experimental data. The data for the [FeFe]-hydrogenases were recorded under 100% H_2 and the data for *Ec*Hyd2 under 100% N_2. Other conditions: pH 6, 10 °C, electrode rotation rate 2500 rpm.

The current for *Ca*HydA clearly plateaus at this low level of formaldehyde, rather than tending towards zero. The magnitude of the limiting current is much greater than for the higher concentration of formaldehyde used in Figure 5.6C. This is as expected, since the reversibility of the inhibition demonstrated in Figure 5.6 means that, for a given concentration of formaldehyde, an equilibrium will be reached. The concentration dependence of this limiting current is discussed in more detail in the following chapter.

5.3.3 Inhibition of H_2 Oxidation

Analogous experiments to those described in the previous section were performed to investigate formaldehyde inhibition of H_2 oxidation, and the normalised data are shown in

Figure 5.8. For each enzyme, the electrode potential was held at -58 mV under 100% H_2, and formaldehyde was injected at time designated t = 0 s (final concentration 4.5 mM).

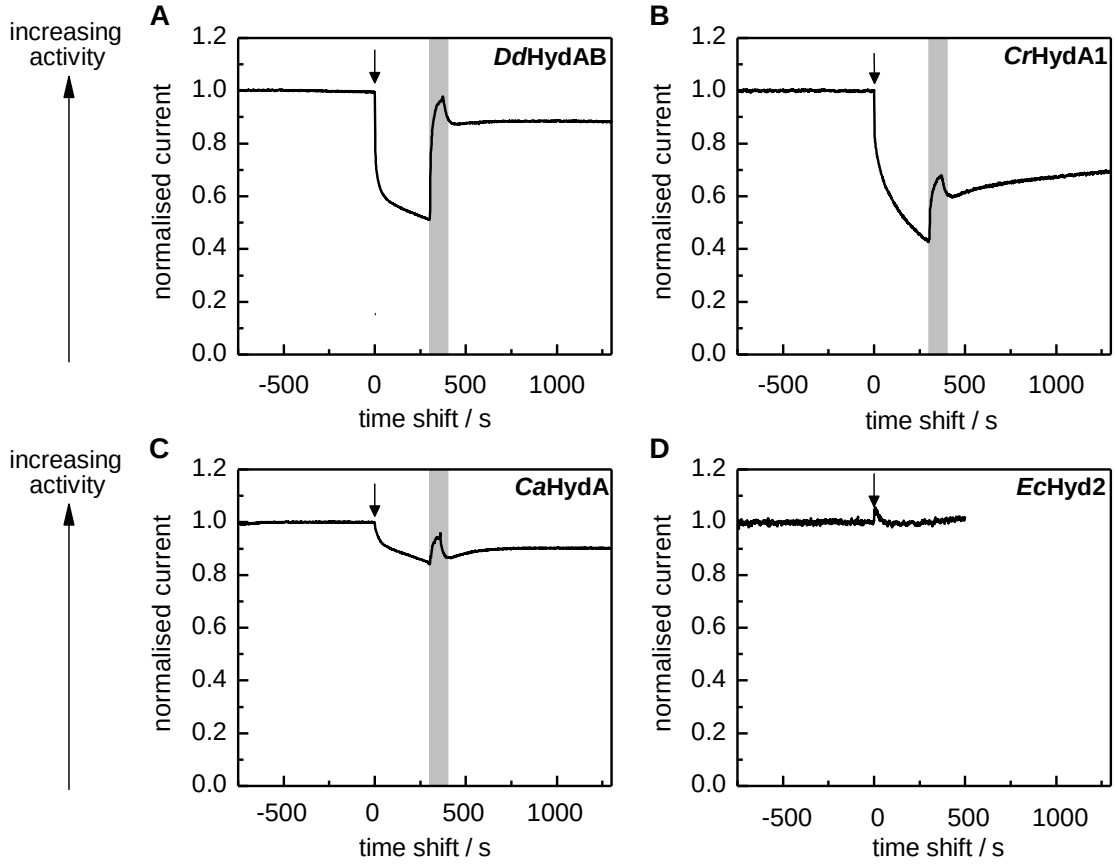


Figure 5.8. Inhibition of H_2 oxidation by formaldehyde for various hydrogenases: (A) *Dd*HydAB [FeFe]-, (B) *Cr*HydA1 [FeFe]-, (C) *Ca*HydA [FeFe]-, and (D) *Ec*Hyd2 [NiFe]-hydrogenases. In each case, the electrode potential was held at -58 mV and formaldehyde injected at time = 0 s (indicated by the arrows) to give a final concentration of 4.5 mM. After 300 s, the cell was rinsed with 50 mL of fresh buffer solution pre-saturated with 100% H_2 (rinsing took ~100 s, represented by the grey bars), except for in the case of *Ec*Hyd2 (D), in which no inhibition was detected at this formaldehyde concentration. Other conditions: 100% H_2, pH 6, 10 ºC, electrode rotation rate 2500 rpm.

From Figure 5.8 it is clear that formaldehyde inhibits H_2 oxidation by [FeFe]-hydrogenases, but the extent of inhibition is less than observed during H_2 production. During H_2 oxidation, a proportion of each [FeFe]-hydrogenase reacts rapidly with formaldehyde, seen as a fast phase of the current decrease, but this is then followed by a slow phase. Upon removal of formaldehyde, the current does not recover to the original

level, indicating that some enzyme molecules remain inactive. Thus, in contrast to inhibition of H_2 production, formaldehyde inhibition of H_2 oxidation is not fully reversible. The fraction of activity that is lost, after allowing for the initial increase in current due to a slight temperature increase during the rinse, appears to correlate with the extent of the slow phase during the inhibition process. No inhibition of H_2 oxidation by *Ec*Hyd2 [NiFe]-hydrogenase was detected under these conditions (Figure 5.8D).

5.3.4 The Effect of the Direction of Catalysis on Inhibition

The results originally presented in this section cannot currently be made freely available as they are to be published at a later date in an academic journal.

5.4 Formaldehyde Protection Against CO

As discussed in Section 5.1.1.4, [FeFe]-hydrogenases are highly sensitive to CO, and therefore an experiment was designed to determine whether formaldehyde protects against CO inhibition. This experiment exploited the fact that *Ca*HydA releases formaldehyde very rapidly (Figure 5.6C) but binds CO only relatively slowly.[101] If CO binds at or near the target site for formaldehyde, then removal of the formaldehyde in the presence of CO should reveal transient activity that decreases as the newly-exposed site binds CO.

An electrode modified with *Ca*HydA was held at -558 mV, initially under 100% N_2, in 2 mL cell solution. In the control experiment (Figure 5.9A), 1 mL of N_2-saturated buffer was injected into the electrochemical cell at 2500 s (indicated by the black arrow). Then, at 2550 s, 0.35 mL of CO-saturated buffer was injected (as shown by the red arrow). The gas flowing through the cell headspace was simultaneously changed to 10% CO in N_2.

The presence of CO leads to a slow decrease in H_2 production activity towards zero. At 3000 s, the cell was rinsed with 50 mL of buffer pre-saturated with 10% CO in N_2, resulting in little change in enzyme activity.

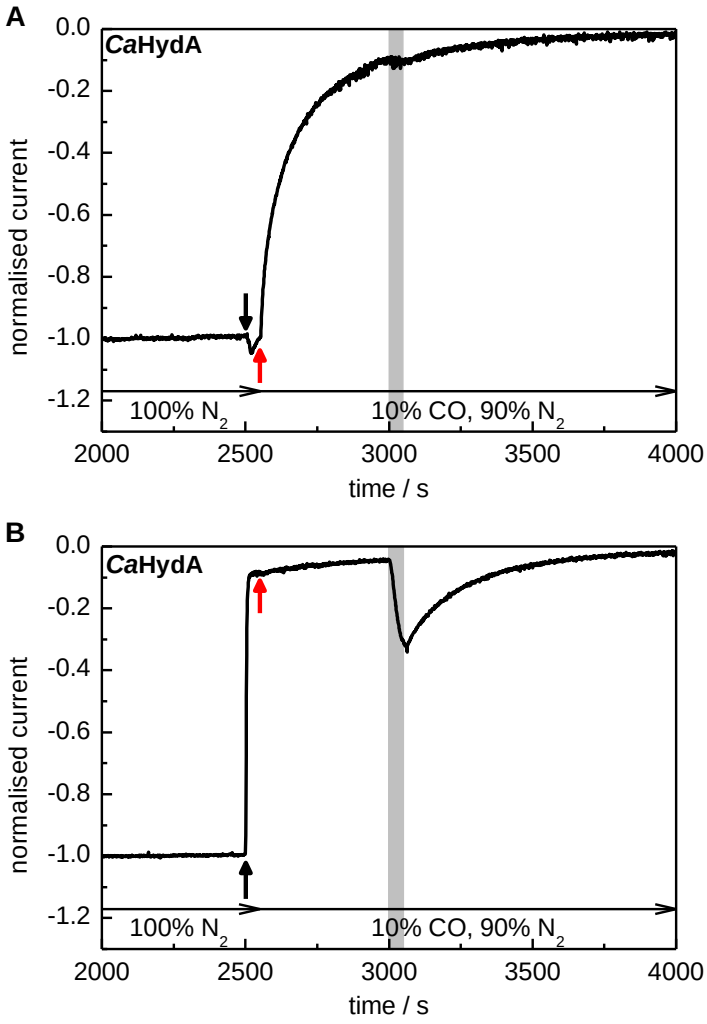


Figure 5.9. Chronoamperometry experiments performed at -558 mV to show that formaldehyde protects *Ca*HydA against CO. The black arrow corresponds to injection of 1 mL buffer (A) or 1 mL buffer containing 134 mM formaldehyde (B), each into 2 mL buffer solution already present inside the electrochemical cell. In both cases, the red arrow corresponds to injection of 0.35 mL CO-saturated buffer with a simultaneous change in the gas flowing through the cell headspace from 100% N_2 to 10% CO in N_2. In both experiments, the cell was rinsed with 50 mL buffer (pre-saturated with 10% CO in N_2) at 3000 s (represented by the grey bar). Other conditions: pH 6, 10 ºC, electrode rotation rate 2500 rpm.

Figure 5.9B shows data collected for *Ca*HydA under conditions identical to those in Figure 5.9A except that the buffer injected at 2500 s contained 134 mM formaldehyde. This concentration is 10-fold higher than used in the experiments shown in Figure 5.6, to ensure that as little activity as possible remained by the time CO was introduced. At 3000 s, the electrochemical cell was rinsed with 50 mL buffer saturated with 10% CO in N_2. Upon rinsing the cell with this solution, containing 10% CO but not formaldehyde, the H_2 production activity initially increases and then decreases.

The changes in enzyme activity following the exchange of cell solution in Figure 5.9B demonstrate that, immediately following release of formaldehyde (observed as an increase in H_2 production activity), the hydrogenase reacts with CO that has been present throughout, leading to a slow attenuation in activity. The control experiment in Figure 5.9A confirms that the increase in activity during the rinse (indicated by the grey box) is not an artefact of the experimental set-up. This experiment therefore provides strong evidence that formaldehyde protects the enzyme against CO binding.

5.5 Inhibition by Other Aldehydes

The results originally presented in this section cannot currently be made freely available as they are to be published at a later date in academic journals.

5.6 Discussion

The work outlined in this chapter demonstrates that formaldehyde is a potent inhibitor of H_2 production by [FeFe]-hydrogenases. This aldehyde reacts rapidly and reversibly with all three [FeFe]-hydrogenases studied, despite their differing structures and topologies away from the active site (Figure 5.1). The inhibition appears to be specific for [FeFe]-

hydrogenases, and this work shows that inhibition of *Ec*Hyd2 [NiFe]-hydrogenase is significantly weaker.

The degree of formaldehyde inhibition is strongly dependent on the direction of catalysis. During H_2 production, the inhibition can be represented as a single, rapid process that is fully reversible at low potential (~-556 mV). In contrast, inhibition of H_2 oxidation is best represented by the sum of two processes (one fast, one slow), and both the extent and reversibility of inhibition are lower than for H_2 production.

The strong dependence of the inhibition on the direction of catalysis (and/or the electrode potential) suggests strongly that formaldehyde binds at, or close to, the active site (the H-cluster). The electronic state of the H-cluster is greatly influenced by the electrode potential under steady-state catalytic conditions, whereas the applied potential will influence target sites further from the active site to a much lesser extent. The binding of formaldehyde at or near the active site is also supported by its protection against CO, which binds at the distal Fe atom.[280-282]

Assuming that formaldehyde binds at the active site, the affinities of the [FeFe]-hydrogenases for formaldehyde may be expected to follow the same trend as that determined previously for inhibition by CO (*Ca*HydA < *Cr*HydA1 < *Dd*HydAB).[101] For the [FeFe]-hydrogenases studied in this work, the extent of inhibition by formaldehyde increases in the order *Ca*HydA << *Cr*HydA1 ~ *Dd*HydAB (Figure 5.7) and is therefore consistent with the trend observed for CO. The calculated rates of formaldehyde inhibition increase in the order *Dd*HydAB < *Cr*HydA1 < *Ca*HydA, as do the rates of recovery. This contrasts the case of CO inhibition, for which the rate of inhibition is fastest for *Dd*HydAB, and the reactivation rates are similar for all three enzymes.[101]

The remainder of this discussion cannot currently be made freely available as it relates to results that are to be published at a later date in academic journals.

Chapter 6 The Reactions of [FeFe]-Hydrogenases with Aldehydes as a Probe for the Mechanism of H_2 Production

Abstract

The mechanistic studies outlined in this chapter investigate the pH, temperature, concentration and potential dependencies of aldehyde inhibition of [FeFe]-hydrogenases. However, most of the results originally presented in this chapter cannot currently be made freely available as they are to be published at a later date in academic journals.

6.1 Introduction

6.1.1 The Aims of the Studies Outlined in this Chapter

The work described in the previous chapter concluded that some aldehydes are reversible inhibitors of H_2 production by [FeFe]-hydrogenases. However, although several possible binding sites unique to the [FeFe]-hydrogenases were presented in Section 5.1.2.3, the exact target for aldehyde binding was not determined. This chapter therefore outlines more detailed studies on aldehyde inhibition of the [FeFe]-hydrogenases, which were performed in order to obtain more information on the site of aldehyde binding. The wider implications of these results for the overall understanding of the redox states of [FeFe]-hydrogenases and the mechanism of H_2 production by these enzymes are also discussed.

6.1.2 Summary of the Redox States of [FeFe]-Hydrogenases

Figure 6.1 summarises the different redox states accessible to the active site (H-cluster) of an [FeFe]-hydrogenase, as discussed in detail in Chapter 1. It is important to note that, in order to be studied, a state must persist for a reasonable amount of time. Therefore, states that exist only transiently cannot be well characterised and are therefore unlikely to be fully understood.

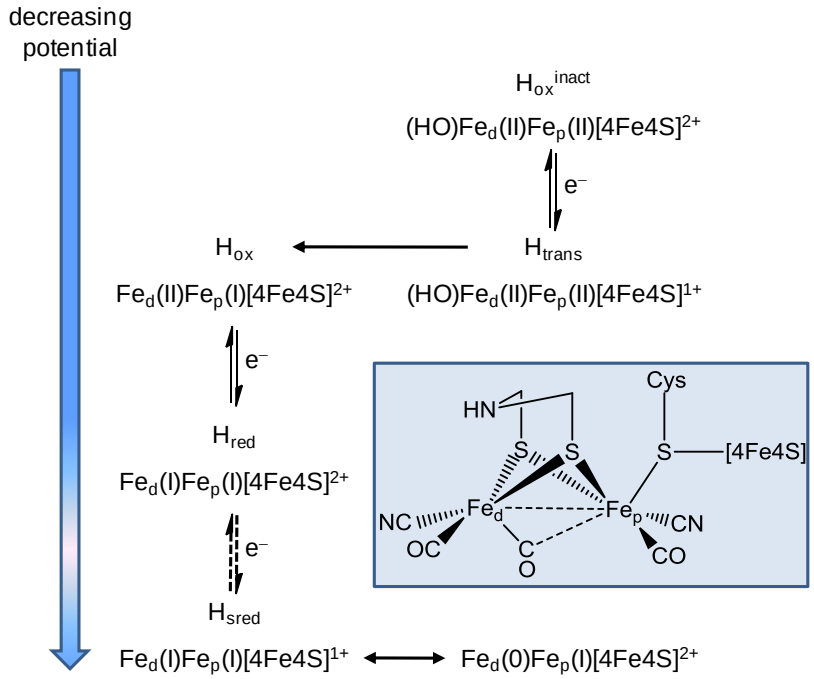


Figure 6.1. Schematic diagram showing the different redox states of an [FeFe]-hydrogenase, with the structure of the H-cluster shown in the inset, assuming the bridgehead atom to be a N atom. The dashed line between the Fe atoms of the H-cluster indicate that metal-metal bonding may occur in some or all redox states. Similarly, the dashed bond between the proximal Fe (Fe_p) and a CO ligand represents the movement of this ligand between a bridging and terminal position (terminally bound to Fe_d) depending on the identity and redox state of the hydrogenase.[19,45,69,87]

For each state in Figure 6.1, the oxidation states of the proximal (Fe_p) and distal (Fe_d) atoms and the H-cluster [4Fe4S]-cluster are given. The (HO) in the H_{ox}^{inact} and H_{trans} states corresponds to a HO^- or H_2O ligand bound to the Fe_d, as discussed in Chapter 1. The H_{ox}, H_{red}, H_{trans} and H_{ox}^{inact} states have been characterised using a combination of EPR, FTIR, Mössbauer and crystallography.[45,69] The 'super-reduced' H_{sred} state has been detected using spectroelectrochemistry but is poorly characterised to date.[87,93,100] This state should be EPR-active, but spectra are yet to be obtained. At the low potentials required to generate H_{sred}, the enzyme is efficient at catalysing H_2 production and thus it is difficult to trap the enzyme in this redox state.

6.1.3 Proposed Mechanisms for [FeFe]-Hydrogenases

As discussed in Chapter 1, most studies suggest that only two redox states of the [FeFe]-hydrogenases, H_{ox} and H_{red}, can be stable intermediates in the catalytic cycle.[45,69,93,94] The majority of the proposed mechanisms also do not consider a role for the [4Fe4S] moiety of the H-cluster; either this cluster remains as $[4Fe4S]^{2+}$ throughout the cycle, or the computational studies were performed on a model lacking this FeS cluster for simplification. The two redox states, H_{ox} and H_{red}, differ by only one electron, and therefore it has been suggested that the FeS cluster relay plays a role in providing or removing sufficient electrons in order to catalyse the two-electron processes of H_2 production or oxidation.[69] However, some [FeFe]-hydrogenases, such as *Cr*HydA1, catalyse H_2-cycling despite the lack of an FeS cluster relay in addition to the H-cluster.[294] The mechanism of H_2-cycling by [FeFe]-hydrogenases is therefore not yet fully understood. Recent studies suggest that a role for the H_{sred} state (or a redox state at the same oxidation level) cannot be ruled out from the catalytic cycle.[87,104,105]

6.2 Detailed Studies of Aldehyde Inhibition

The results originally presented in this section cannot currently be made freely available as they are to be published at a later date in academic journals.

6.3 Potential Dependence of Formaldehyde Inhibition

The results originally presented in this section cannot currently be made freely available as they are to be published at a later date in an academic journal.

6.4 Studies using Density Functional Theory (DFT)

These studies, performed by Tobias Krämer, cannot currently be made freely available as they are to be published at a later date in an academic journal.

6.5 Attempts to Ascertain if Alcohol is Produced

The results originally presented in this section cannot currently be made freely available as they are to be published at a later date in an academic journal.

6.6 Discussion

The discussion originally presented here cannot currently be made freely available as it relates to results that are to be published at a later date in academic journals.

Chapter 7 Materials and Methods

7.1 Working Electrodes

In the experiments performed throughout this thesis, enzyme molecules were adsorbed onto pyrolytic graphite edge-plane (PGE) electrodes, in which the graphite is aligned so that the plane perpendicular to the basal (aromatic) layers is exposed. Abrasion of the edge-plane surface creates a rough surface with polar -COOH and –COH functional groups, as well as hydrophobic regions. It has been suggested that the range of functionalities increases the probability of effective enzyme adsorption.[164,178]

Rotating disk electrodes (RDEs, Figure 7.1A) were used in conjunction with a rotator (EG&G or EcoChemie) or connected via banana plugs inserted into the screw threads for use as stationary electrodes.

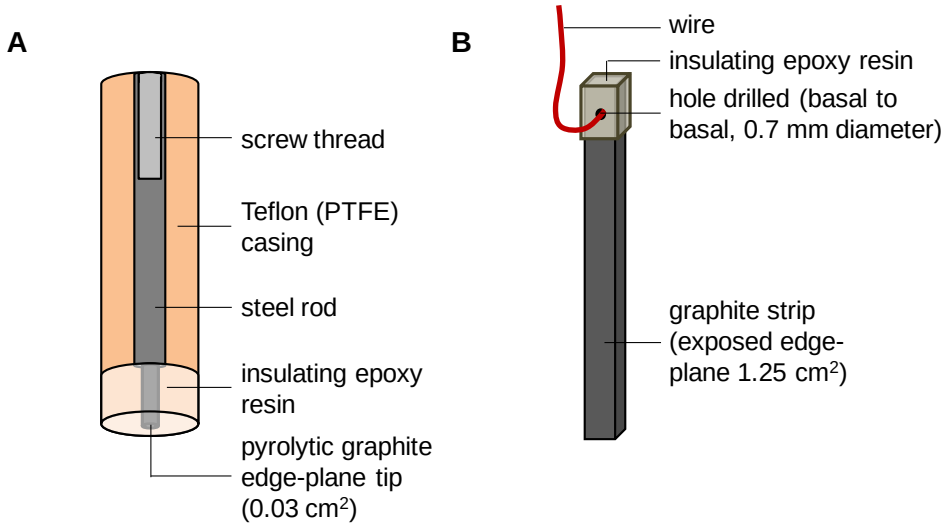


Figure 7.1. Schematic diagrams showing the construction of (A) rotating disk electrodes (geometric edge-plane surface area 0.03 cm^2) and (B) large strip electrodes (geometric exposed edge-plane surface area 1.25 cm^2).

To construct an RDE, a cylindrical piece of graphite (Momentive Performance, USA) was glued onto a steel rod, which was housed inside a Teflon (PTFE) casing, using conductive silver-loaded epoxy resin (RS electronics). The graphite was then surrounded by

insulating epoxy resin (Robnor Resins), leaving an exposed circular surface of edge-plane graphite with a geometric surface area of 0.03 cm^2.

For fuel cell experiments, larger 'strip' electrodes (Figure 7.1B) were used. Each strip electrode was constructed from a piece of graphite (Momentive Performance, USA) with dimensions 2 cm^2 x 0.3 cm^2 x 0.3 cm^2. A hole with a diameter of 0.7 mm was drilled from basal plane to basal plane close to one end of the graphite. A wire (stripped of insulation at one end) was fed through this hole and an electrical connection was achieved by using a small amount of silver-loaded epoxy resin. This connection was then insulated using epoxy resin, leaving a total edge-plane geometric surface area of approximately 1.25 cm^2.

7.2 Electrochemical Cell

A sealed glass electrochemical cell (Figure 7.2, constructed by Terri Adams) with a three-electrode configuration was used for PFE experiments throughout this project. The PGE working electrode was combined with a Pt wire counter electrode.

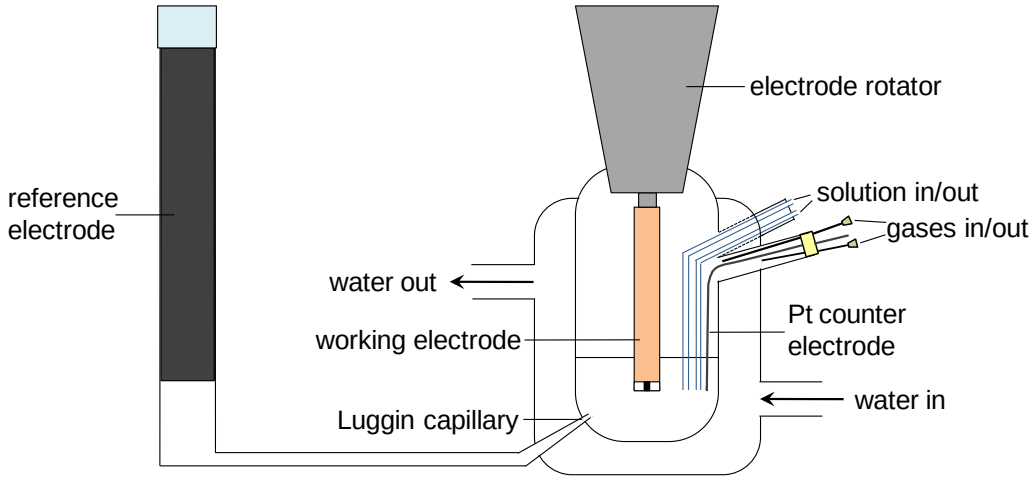


Figure 7.2. A schematic diagram showing the all-glass, sealed electrochemical cell.

The reference arm contained aqueous 0.1 M NaCl, and the saturated calomel electrode (SCE) used as the reference electrode was separated from the working electrode compartment via a Luggin capillary. A water circulator was used to maintain the temperature of the working compartment throughout the experiments, by pumping water through the cell jacket. In contrast, the reference electrode remained at ambient temperature, which was monitored frequently. The reference potential was corrected with respect to the standard hydrogen electrode (SHE) using the following formulae[166]:

$$E_{SHE} = E_{SCE} + E_{corr} \qquad [7.1]$$

$$E_{corr} = 0.2412 - 6.61\text{x}10^{-4}\,(T\text{-}25) - 1.75\text{x}10^{-6}\,(T\text{-}25)^2 - 9.0\text{x}10^{-10}\,(T\text{-}25)^3 \qquad [7.2]$$

where T is the temperature in degrees Celsius.

The internal environment of the electrochemical cell was sealed by the snug fit of the Teflon shaft of the electrode rotator into the ground glass joint of the electrochemical cell, or by use of an all-glass head clamped tightly into place. Protein Film Electrochemistry experiments were performed in a glove box (M. Braun or Vacuum Atmospheres) under an anaerobic N_2 atmosphere (< 2 ppm O_2). In some experiments, the rotator was replaced by a glass head sealed by a rubber septum to allow multiple stationary electrodes to be included to create a mini fuel cell (Chapter 4).

The all-glass cell included two inlets: one was sealed with a septum and the other was used to feed two tubes into the cell solution, and sealed using Nescofilm (Alfresa Pharma, Japan). Gases were flushed through the cell headspace via inlet and outlet needles through the side-arm sealed by a septum (Section 7.3). The tubes were used to exchange the buffer solution in the electrochemical cell (Section 7.13).

7.3 Gas Control

Throughout this project, gases flowed into the glove box and through the headspace of the electrochemical cell via a closed loop system, with the outlet line vented outdoors (this is particularly important when using toxic gases such as CO). Water bubblers were used to prevent the back-flow of air into the glove box or electrochemical cell. Since tiny samples (typically less than a picomole) of enzyme are addressed in PFE experiments, even trace impurities in the gas supply may affect the activity of the enzymes.[19] Therefore, high purity gases were used and the gas inlet line included an O_2-scrubbing catalyst (Varian Gas Clean Oxygen Filter, output < 50 ppb O_2) wherever possible. Hydrogen (Premier Grade), Protec10 (10% H_2 in N_2), 1% H_2 in N_2, and O_2 were purchased from Air Products; CO (Research Grade) and N_2 (Oxygen-free) were obtained from BOC. Specific mixtures of these gases were created using mass flow controllers (Sierra Instruments).

7.4 Electrochemical Apparatus

The electrochemical analysers (Autolab PGSTAT 10 or 128N, both EcoChemie), controlled by GPES or NOVA 1.5 software programs (EcoChemie), were used to set the potential and measure current. An electrochemical detection module (ECD) was also used to increase sensitivity for low current measurements.

7.5 Buffer Solutions

All buffer solutions were prepared using purified water (Millipore, 18 MΩ cm) and were titrated to the required pH, monitored using a pH meter (Accumet 950, Fisher Scientific). Experiments were performed in sodium phosphate buffer, (50 mM, created using Analytical Grade NaH_2PO_4 and Na_2HPO_4, both from Fisher Scientific) containing NaCl (100 mM, Analytical Grade from Fisher Scientific) as supporting electrolyte. However,

for experiments using bilirubin oxidase, 100 mM sodium phosphate buffer was used (with no NaCl) because there is electrochemical evidence to suggest that this enzyme may be slightly inhibited by halide ions.[236] Deuterated buffer solutions were made in the same way, except that the NaH_2PO_4, Na_2HPO_4 and NaCl were dissolved in D_2O and the pH meter reading adjusted according to the relationship pD = pH + 0.4.[295]

7.6 Enzyme Preparation

7.6.1 *Ralstonia* Hydrogenases (*Re*MBH^{WT} and *Re*MBH$^{C19G/C120G}$)

The samples of *Re*MBH^{WT} and *Re*MBH$^{C19G/C120G}$ used in this thesis were prepared by Marcus Ludwig, Tobias Goris and Johannes Fritsch, in the group of Bärbel Friedrich and Oliver Lenz at the Humboldt Universität, Berlin. The mutagenesis was performed by Tobias Goris and the hydrogenases were purified as described in references 202 and 210.

7.6.2 *Escherichia coli* Hydrogenases (*Ec*Hyd1 and *Ec*Hyd2)

The *Ec*Hyd1 used in the fuel cell experiments in Chapter 4 was purified using a previously published protocol.[115] The sample of *Ec*Hyd2 used in Chapters 5 and 6 was kindly provided by Suzannah Hexter and was obtained using a similar procedure.[115]

7.6.3 Bilirubin oxidase from *Myrothecium verrucaria* (*Mv*BO)

The bilirubin oxidase was purchased from Amano Enzyme Inc. ("Amano-3", 2.55 units mg^{-1}) and purified from the crude powder by chromatography using a DEAE-Sepharose CL-6B weak anionic exchange column (GE Healthcare) followed by a linear reverse salt gradient HiTrap Phenyl HP hydrophobic column (GE Healthcare).

7.6.4 The [FeFe]-Hydrogenase *Dd*HydAB

The *Dd*HydAB samples used in Chapters 5 and 6 were prepared by Christine Cavazza under the supervision of Juan Fontecilla-Camps at the CNRS Grenoble, France, using a previously published protocol.[88]

7.6.5 The [FeFe]-Hydrogenases *Ca*HydA and *Cr*HydA1

Samples of the bacterial [FeFe]-hydrogenase *Ca*HydA and the algal hydrogenase *Ca*HydA1 were prepared by Sven Stripp and Camilla Lambertz under the supervision of Thomas Happe at the Ruhr University, Germany, using previously published protocols.[268]

7.7 Preparation of Hydrogenase Films

For experiments using *Re*MBH^{WT} or *Re*MBH$^{C19G/C120G}$, the PGE electrode was polished using an aqueous slurry of 1 μm α-alumina (Buehler) on cotton wool. The electrode was then sonicated for 10 s and rinsed with purified water (Millipore: 18 MΩ cm). For *Ec*Hyd1, *Ec*Hyd2, *Ca*HydA, *Dd*HydAB and *Cr*HydA1, the electrode was abraded using sandpaper (P400 Tufbak Durite) and wiped with cotton wool. For RDEs, a film of hydrogenase was then obtained by spotting 1-1.5 μL of enzyme solution (concentration range 0.1 - 0.2 mg mL^{-1}) onto the electrode and then withdrawing any excess from the surface. Removal of excess protein from the surface ensured that no free enzyme was present in solution, as this may result in the exchange of protein between the electrode and solution, leading to complications in the interpretation of results. For fuel cell strip electrodes, 10 μL of *Ec*Hyd1 was applied, 5 μL to each edge-plane surface. The solutions of *Dd*HydAB contained the positively charged co-adsorbate polymyxin B sulfate (Duchefa Biochemie, 20 mg mL^{-1}), which aids adsorption onto PGE by acting as a non-

covalent 'cross-linker' between the negatively charged protein surface and acidic groups on the graphite.[296]

7.8 Activation of *Ec*Hyd1 and *Ec*Hyd2

Prior to use in cyclic voltammetry or fuel cell experiments, the *Ec* [NiFe]-hydrogenases required activation from the as-isolated states. This was achieved by performing successive cyclic voltammograms at 10 mV s^{-1} under 100% H_2, holding the potential at -558 mV for 5 min between each scan. The procedure was repeated until two consecutive scans overlaid, indicating that the enzyme was fully activated. For *Ec*Hyd1 this process took around 90 min; for *Ec*Hyd2 approximately 30 min.

7.9 Modification of Electrodes for *Mv*BO

Films of *Mv*BO were prepared on the PGE electrodes using a previously published diazonium coupling method to attach 6-amino-2-naphthoic acid (6A2NA, 90%, Acros Organics) to the graphite surface (Figure 7.3).[234,243]

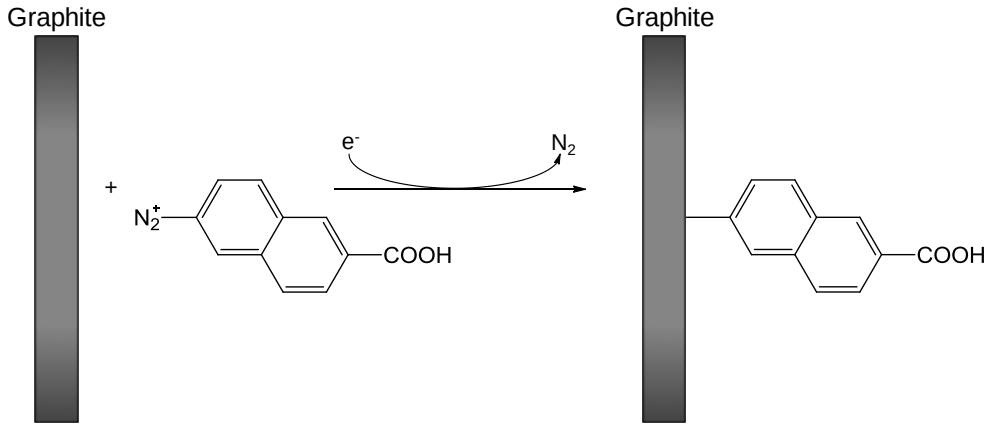
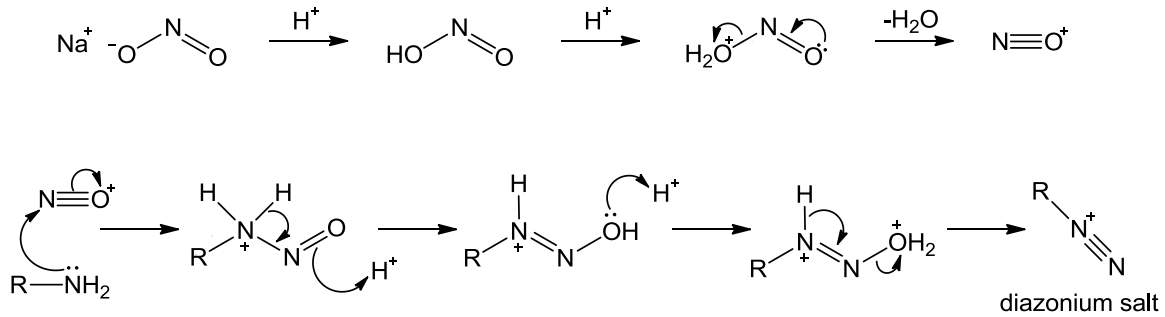


Figure 7.3. A representation of the coupling of the diazonium salt of 6-amino-2-naphthoic acid to a pyrolytic graphite edge-plane surface.

A 4.2 mM solution of 6A2NA was first made in 1 M HCl diluted in a 50:50 mixture of ethanol and water. The diazonium salt of 6A2NA was then obtained by adding 88 μL of 7.6 mg mL^{-1} $NaNO_2$ to 1.912 mL of the 6A2NA solution and leaving the mixture on ice for 5 min (Scheme 7.1).



Scheme 7.1. The reaction of a primary amine with $NaNO_2$ and acid to generate a diazonium salt.[283]

For strip electrodes, the 2 mL of diazonium salt solution was then added to 5 mL of 0.1 M HCl (diluted in a 50:50 mixture of ethanol and water) in the working compartment of an electrochemical cell equilibrated to 0 ºC. For RDEs, 400 μL of the diazonium solution was added to 8 mL 0.1 M HCl in the electrochemical cell. The PGE electrode was abraded using sandpaper (P400 Tufbak Durite), sonicated and rinsed with purifed water before being immersed in the diazonium and acid solution. The diazonium salt was coupled to the electrode surface by performing two cyclic voltammograms (recorded at 50 mV s^{-1}) between +742 mV and -58 mV at 0 ºC, using a platinised Pt counter electrode. The PGE working electrode was rinsed with ethanol, then purified water and finally with pH 5 100 mM phosphate buffer solution, before the enzyme was spotted onto the surface (10 μL of 50 μM enzyme used for the strip electrodes; 1 μL for the RDEs.)

7.10 Proton Exchange Membrane

In this thesis, Nafion 115 (DuPont) was used as the proton exchange membrane (PEM) in fuel cell experiments. This PEM is a sulfonated tetrafluoroethylene copolymer that is known as an ionomer as a result of its ionic properties. The sulfonic acid groups on the sidechains are hydrophilic whereas the bulk of the polymer chain is hydrophobic; these hydrophilic regions cluster together forming highly hydrated regions. Within these regions, the protons on the sulfonic acid groups (SO_3H) can 'hop' between sites. Therefore, as long as the Nafion is well hydrated, it is a good transporter of protons but not anions or electrons. A general structure of Nafion is shown in Figure 7.4.[297]

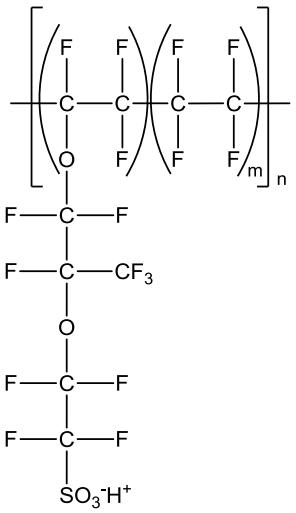


Figure 7.4. The general structure for a Nafion sulfonated tetrafluoroethylene copolymer.

The Nafion membrane was regenerated to full conductive form prior to use by immersion in boiling solutions of hydrogen peroxide, sulfuric acid and water in the following sequence: hydrogen peroxide (6%, 1 hr), deionised water (1 hr), sulfuric acid (0.5 M, 1 hr), deionised water (1 hr).

7.11 Fuel Cell Measurements

In fuel cell experiments, the resistance between the anode and cathode was set using an analogue variable resistor (Time Electronics Decade Resistance Model 8000) and the fuel cell voltage was monitored using a high impedance digital voltmeter (Keithley 195A, internal resistance ~1 GΩ). In more detailed experiments, a high impedance amplifier (made by Nenad Vranjes) was used, in conjunction with an analogue-to-digital converter (LabJack U12) and LJSimpleLog software, to monitor the potential between the anode and cathode (the fuel cell voltage) and between both the anode and a reference electrode and the cathode and a reference electrode over time.

The reference electrode used in fuel cell experiments was an Ag/AgCl electrode (3 M NaCl, BASi). The potentials were corrected with respect to SHE using the following formula[298]:

$$E_{SHE} = E_{Ag/AgCl} + 206 \text{ mV } (25\ ^{o}C) \qquad [7.3]$$

7.12 Solution Assay

Solution assays were performed in an anaerobic glovebox (Belle, O_2 < 3 ppm). The cuvette (open to the N_2 atmosphere of the glovebox) was filled with 1 mL solution of 200 μM electrochemically reduced methyl viologen (MV_R) in 50 mM phosphate buffer containing 100 mM NaCl. Hydrogenase was added to give a final concentration of 18 nM. The absorbance at 604 nm (using a halogen lamp as the light source) was measured over time using a spectrometer (Ocean Optics Inc.) and normalised in each case so that absorbance of the initial solution of MV_R in buffer was set to 1.

7.13 Buffer Exchange

The aldehyde inhibition studies presented in Chapters 5 and 6 relied upon the ability to remove aldehyde from the electrochemical cell in order to study the reversibility of the reactions. Removal of the aldehyde was achieved by rinsing the cell with 50 mL of fresh buffer solution. This buffer exchange was performed using two tubes passing into the cell solution through one of the cell side-arms (Figure 7.2). Each tube was connected to a 50 mL syringe, one empty and the other charged with fresh buffer, equilibrated to the same temperature and gas concentration as the buffer already in the electrochemical cell. This equilibration was achieved prior to loading the syringe, by flowing gas into the buffer solution whilst it was contained in a round bottomed flask sealed with a rubber septum and located in a water bath set to the desired temperature. The full syringe was used to pump buffer solution into the cell at the same rate as the solution leaving the cell was collected in the empty syringe (Figure 7.5).

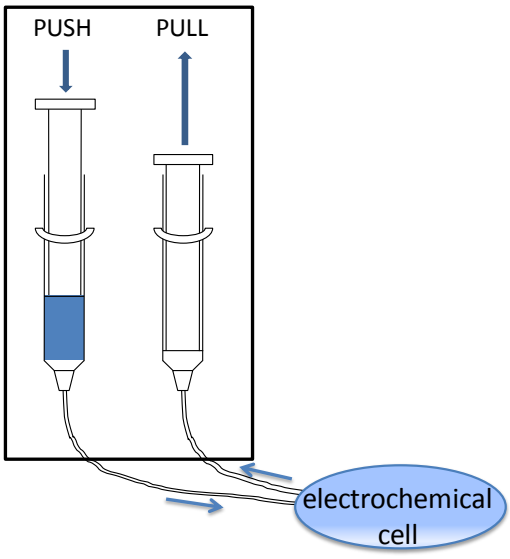


Figure 7.5. Representation of the pair of syringes used to rinse the electrochemical cell by exchanging the solution with fresh buffer. As fresh buffer was introduced into the electrochemical cell by pushing down on the left-hand syringe, buffer was simultaneously removed from the cell by pulling the right-hand syringe.

This two-syringe assembly therefore allowed rapid exchange of the cell solution without the loss of electrical contact, since the working electrode was not removed from the electrolyte solution.

7.14 Aldehydes

The structures and nomenclature for the aldehydes used in this work were given in Chapter 5. The aldehydes used were as follows: formaldehyde (ACS reagent, 37 wt % in H_2O, containing 10-15% methanol, Sigma-Aldrich); acetaldehyde (ACS reagent, ≥ 99.5%, Sigma-Aldrich); propionaldehyde (≥ 97%, Sigma-Aldrich); butyraldehyde (redistilled, ≥ 99.5%, Sigma-Aldrich); isobutyraldehyde (redistilled, ≥ 99.5%, Sigma-Aldrich) and isovaleraldehdye (97%, Sigma-Aldrich).

References

(1) *International Energy Outlook*, US Department of Energy, 2010.
(2) Das, D.; Veziroglu, T. N. *Int. J. Hydrogen Energ.* **2001**, *26*, 13.
(3) *The Mini Rough Guide to Energy and Our Planet*; Lockett, A.; Milton, M., Eds.; Rough Guides Ltd., 2008.
(4) *IPCC Fourth Assessment Report: Climate Change 2007*, IPCC 2007.
(5) *Committee on Climate Change Annual Report*, 2010.
(6) Lewis, N. S.; Nocera, D. G. *Proc. Natl. Acad. Sci. U. S. A.* **2006**, *103*, 15729.
(7) *The Hydrogen Economy:Opportunities, Costs, Barriers and R&D Needs*, National Research Council and National Academy of Engineering Report, 2004.
(8) *Hydrogen Posture Plan*, U.S. Department of Energy, 2006.
(9) Cammack, R.; Frey, M.; Robson, R. *Hydrogen As a Fuel: Learning From Nature*; Taylor and Francis: London, 2001.
(10) Sartbaeva, A.; Kuznetsov, V. L.; Wells, S. A.; Edwards, P. P. *Energ. Environ. Sci.* **2008**, *1*, 79.
(11) Greenwood, N. N.; Earnshaw, A. *Chemistry of the Elements*; Second ed.; Butterworth-Heinemann: Oxford, U.K., 1997.
(12) Grove, W. *Philosophical Magazine and Journal of Science* **1839**, *14*.
(13) Schoebein, C. F. *Philos. Mag.* **1839**, *43-45*.
(14) Cleghorn, S. J. C.; Ren, X.; Springer, T. E.; Wilson, M. S.; Zawodzinski, C.; Zawodzinski, T. A.; Gottesfeld, S. *Int. J. Hydrogen Energ.* **1997**, *22*, 1137.
(15) www.bbc.co.uk/news/business-11297952.
(16) Edwards, P. P.; Kuznetsov, V. L.; David, W. I. F.; Brandon, N. P. *Energ. Policy* **2008**, *36*, 4356.
(17) Sørensen, B. *Hydrogen and Fuel Cells*; Elsevier Academic Press: Burlington, USA, 2005.
(18) Hambourger, M.; Moore, G. F.; Kramer, D. M.; Gust, D.; Moore, A. L.; Moore, T. A. *Chem. Soc. Rev.* **2009**, *38*, 25.
(19) Vincent, K. A.; Parkin, A.; Armstrong, F. A. *Chem. Rev.* **2007**, *107*, 4366.
(20) *World Energy Assessment Report: Energy and the Challenge of Sustainability*, United Nations, 2003.
(21) Meral, M. E.; Dincer, F. *Renew. Sust. Energ. Rev.* **2011**, *15*, 2176.
(22) Gratzel, M. *Nature* **2001**, *414*, 338.
(23) Reisner, E. *Eur. J. Inorg. Chem.* **2011**, 1005.
(24) Kalyanasundaram, K.; Graetzel, M. *Curr. Opin. Biotechnol.* **2010**, *21*, 298.
(25) Gust, D.; Moore, T. A.; Moore, A. L. *Acc. Chem. Res.* **2009**, *42*, 1890.
(26) Lakadamyali, F.; Reisner, E. *Chem. Commun.* **2011**, *47*, 1695.
(27) Schuler, S.; Conrad, R. *Fems Microbiol. Ecol.* **1990**, *73*, 77.
(28) Madamwar, D.; Garg, N.; Shah, V. *World J. Microb. Biot.* **2000**, *16*, 757.
(29) Devos, P.; Stevens, P.; Deley, J. *Biotechnol. Lett.* **1983**, *5*, 69.
(30) Conrad, R. *Microbiol. Rev.* **1996**, *60*, 609.
(31) Armstrong, F. A.; Belsey, N. A.; Cracknell, J. A.; Goldet, G.; Parkin, A.; Reisner, E.; Vincent, K. A.; Wait, A. F. *Chem. Soc. Rev.* **2009**, *38*, 36.
(32) Vignais, P. M.; Colbeau, A. *Curr. Issues Mol. Biol.* **2004**, *6*, 159.
(33) Buhrke, T.; Lenz, O.; Krauss, N.; Friedrich, B. *J. Biol. Chem.* **2005**, *280*, 23791.
(34) Thauer, R. K.; Klein, A. R.; Hartmann, G. C. *Chem. Rev.* **1996**, *96*, 3031.
(35) Volbeda, A.; Charon, M. H.; Piras, C.; Hatchikian, E. C.; Frey, M.; Fontecillacamps, J. C. *Nature* **1995**, *373*, 580.

(36) Volbeda, A.; Garcia, E.; Piras, C.; deLacey, A. L.; Fernandez, V. M.; Hatchikian, E. C.; Frey, M.; FontecillaCamps, J. C. *J. Am. Chem. Soc.* **1996**, *118*, 12989.
(37) Nicolet, Y.; Piras, C.; Legrand, P.; Hatchikian, C. E.; Fontecilla-Camps, J. C. *Struct. Fold. Des.* **1999**, *7*, 13.
(38) Ogata, H.; Kellers, P.; Lubitz, W. *J. Mol. Biol.* **2010**, *402*, 428.
(39) Ogata, H.; Mizoguchi, Y.; Mizuno, N.; Miki, K.; Adachi, S.; Yasuoka, N.; Yagi, T.; Yamauchi, O.; Hirota, S.; Higuchi, Y. *J. Am. Chem. Soc.* **2002**, *124*, 11628.
(40) Peters, J. W.; Lanzilotta, W. N.; Lemon, B. J.; Seefeldt, L. C. *Science* **1998**, *282*, 1853.
(41) Fritsch, J.; Scheerer, P.; Frielingsdorf, S.; Kroschinsky, S.; Friedrich, B.; Lenz, O.; Spahn, C. M. *Nature* **2011**, *479*, 249.
(42) Bagley, K. A.; Duin, E. C.; Roseboom, W.; Albracht, S. P. J.; Woodruff, W. H. *Biochemistry* **1995**, *34*, 5527.
(43) Bagley, K. A.; Vangarderen, C. J.; Chen, M.; Duin, E. C.; Albracht, S. P. J.; Woodruff, W. H. *Biochemistry* **1994**, *33*, 9229.
(44) Happe, R. P.; Roseboom, W.; Pierik, A. J.; Albracht, S. P. J.; Bagley, K. A. *Nature* **1997**, *385*, 126.
(45) Lubitz, W.; Reijerse, E.; van Gastel, M. *Chem. Rev.* **2007**, *107*, 4331.
(46) Gessner, C.; Stein, M.; Albracht, S. P. J.; Lubitz, W. *J. Biol. Inorg. Chem.* **1999**, *4*, 379.
(47) Fritsch, J.; Loscher, S.; Sanganas, O.; Siebert, E.; Zebger, I.; Stein, M.; Ludwig, M.; De Lacey, A. L.; Dau, H.; Friedrich, B.; Lenz, O.; Haumann, M. *Biochemistry* **2011**, *50*, 5858.
(48) Scott, R. A. *Method. Enzymol.* **1985**, *117*, 414.
(49) Volbeda, A.; Montet, Y.; Vernede, X.; Hatchikian, E. C.; Fontecilla-Camps, J. C. *Int. J. Hydrogen Energ.* **2002**, *27*, 1449.
(50) Page, C. C.; Moser, C. C.; Chen, X. X.; Dutton, P. L. *Nature* **1999**, *402*, 47.
(51) Higuchi, Y.; Yagi, T.; Yasuoka, N. *Structure* **1997**, *5*, 1671.
(52) Bleijlevens, B.; van Broekhuizen, F. A.; De Lacey, A. L.; Roseboom, W.; Fernandez, V. M.; Albracht, S. P. J. *J. Biol. Inorg. Chem.* **2004**, *9*, 743.
(53) Langmuir, I. *Science* **1921**, *54*, 59.
(54) Pyykko, P. *J. Organomet. Chem.* **2006**, *691*, 4336.
(55) van der Zwaan, J. W.; Coremans, J.; Bouwens, E. C. M.; Albracht, S. P. J. *Biochim. Biophys. Acta* **1990**, *1041*, 101.
(56) Carepo, M.; Tierney, D. L.; Brondino, C. D.; Yang, T. C.; Pamplona, A.; Telser, J.; Moura, I.; Moura, J. J. G.; Hoffman, B. M. *J. Am. Chem. Soc.* **2002**, *124*, 281.
(57) Garcin, E.; Vernede, X.; Hatchikian, E. C.; Volbeda, A.; Frey, M.; Fontecilla-Camps, J. C. *Struct. Fold. Des.* **1999**, *7*, 557.
(58) Marques, M. C.; Coelho, R.; De Lacey, A. L.; Pereira, I. A. C.; Matias, P. M. *J. Mol. Biol.* **2010**, *396*, 893.
(59) Pandelia, M. E.; Fourmond, V.; Tron-Infossi, P.; Lojou, E.; Bertrand, P.; Leger, C.; Giudici-Orticoni, M. T.; Lubitz, W. *J. Am. Chem. Soc.* **2010**, *132*, 6991.
(60) Fontecilla-Camps, J. C.; Volbeda, A.; Cavazza, C.; Nicolet, Y. *Chem. Rev.* **2007**, *107*, 4273.
(61) Huyett, J. E.; Carepo, M.; Pamplona, A.; Franco, R.; Moura, I.; Moura, J. J. G.; Hoffman, B. M. *J. Am. Chem. Soc.* **1997**, *119*, 9291.
(62) Pierik, A. J.; Roseboom, W.; Happe, R. P.; Bagley, K. A.; Albracht, S. P. J. *J. Biol. Chem.* **1999**, *274*, 3331.

(63) Siegbahn, P. E. M.; Tye, J. W.; Hall, M. B. *Chem. Rev.* **2007**, *107*, 4414.
(64) Armstrong, F. A. *Curr. Opin. Chem. Biol.* **2004**, *8*, 133.
(65) Pandelia, M. E.; Ogata, H.; Lubitz, W. *ChemPhysChem* **2010**, *11*, 1127.
(66) Lamle, S. E.; Albracht, S. P. J.; Armstrong, F. A. *J. Am. Chem. Soc.* **2004**, *126*, 14899.
(67) Stein, M.; van Lenthe, E.; Baerends, E. J.; Lubitz, W. *J. Am. Chem. Soc.* **2001**, *123*, 5839.
(68) Pandelia, M. E.; Ogata, H.; Currell, L. J.; Flores, M.; Lubitz, W. *J. Biol. Inorg. Chem.* **2009**, *14*, 1227.
(69) De Lacey, A. L.; Fernandez, V. M.; Rousset, M.; Cammack, R. *Chem. Rev.* **2007**, *107*, 4304.
(70) Keith, J. M.; Hall, M. B. *Inorg. Chem.* **2010**, *49*, 6378.
(71) Teixeira, V. H.; Baptista, A. M.; Soares, C. M. *Biophys. J.* **2006**, *91*, 2035.
(72) Pardo, A.; De Lacey, A. L.; Fernandez, V. M.; Fan, H. J.; Fan, Y. B.; Hall, M. B. *J. Biol. Inorg. Chem.* **2006**, *11*, 286.
(73) Wu, H.; Hall, M. B. *C. R. Chim.* **2008**, *11*, 790.
(74) Stein, M.; Lubitz, W. *J. Inorg. Biochem.* **2004**, *98*, 862.
(75) Siegbahn, P. E. M. *Adv. Inorg. Chem.* **2004**, *56*, 101.
(76) Montet, Y.; Amara, P.; Volbeda, A.; Vernede, X.; Hatchikian, E. C.; Field, M. J.; Frey, M.; FontecillaCamps, J. C. *Nat. Struct. Biol.* **1997**, *4*, 523.
(77) Galvan, I. F.; Volbeda, A.; Fontecilla-Camps, J. C.; Field, M. J. *Proteins* **2008**, *73*, 195.
(78) Teixeira, V. H.; Soares, C. M.; Baptista, A. M. *Proteins* **2008**, *70*, 1010.
(79) Peters, J. W. *Curr. Opin. Struct. Biol.* **1999**, *9*, 670.
(80) Stripp, S.; Sanganas, O.; Happe, T.; Haumann, M. *Biochemistry* **2009**, *48*, 5042.
(81) Kamp, C.; Silakov, A.; Winkler, M.; Reijerse, E. J.; Lubitz, W.; Happe, T. *BBA-Bioenergetics* **2008**, *1777*, 410.
(82) Pierik, A. J.; Hulstein, M.; Hagen, W. R.; Albracht, S. P. J. *Eur. J. Biochem.* **1998**, *258*, 572.
(83) Nicolet, Y.; Lemon, B. J.; Fontecilla-Camps, J. C.; Peters, J. W. *Trends Biochem. Sci.* **2000**, *25*, 138.
(84) Pandey, A. S.; Harris, T. V.; Giles, L. J.; Peters, J. W.; Szilagyi, R. K. *J. Am. Chem. Soc.* **2008**, *130*, 4533.
(85) Nicolet, Y.; de Lacey, A. L.; Vernede, X.; Fernandez, V. M.; Hatchikian, E. C.; Fontecilla-Camps, J. C. *J. Am. Chem. Soc.* **2001**, *123*, 1596.
(86) Silakov, A.; Wenk, B.; Reijerse, E.; Lubitz, W. *Phys. Chem. Chem. Phys.* **2009**, *11*, 6592.
(87) Silakov, A.; Kamp, C.; Reijerse, E.; Happe, T.; Lubitz, W. *Biochemistry* **2009**, *48*, 7780.
(88) Hatchikian, E. C.; Forget, N.; Fernandez, V. M.; Williams, R.; Cammack, R. *Eur. J. Biochem.* **1992**, *209*, 357.
(89) van der Westen, H. M.; Mayhew, S. G.; Veeger, C. *FEBS Lett.* **1978**, *86*, 122.
(90) Pereira, A. S.; Tavares, P.; Moura, I.; Moura, J. J. G.; Huynh, B. H. *J. Am. Chem. Soc.* **2001**, *123*, 2771.
(91) Cao, Z. X.; Hall, M. B. *J. Am. Chem. Soc.* **2001**, *123*, 3734.
(92) Liu, Z. P.; Hu, P. *J. Am. Chem. Soc.* **2002**, *124*, 5175.
(93) Roseboom, W.; De Lacey, A. L.; Fernandez, V. M.; Hatchikian, E. C.; Albracht, S. P. J. *J. Biol. Inorg. Chem.* **2006**, *11*, 102.

(94) Patil, D. S.; Moura, J. J. G.; He, S. H.; Teixeira, M.; Prickril, B. C.; Dervartanian, D. V.; Peck, H. D.; Legall, J.; Huynh, B. H. *J. Biol. Chem.* **1988**, *263*, 18732.
(95) Silakov, A.; Reijerse, E. J.; Albracht, S. P. J.; Hatchikian, E. C.; Lubitz, W. *J. Am. Chem. Soc.* **2007**, *129*, 11447.
(96) van Dijk, C.; van Berkel-Arts, A.; Veeger, C. *FEBS Lett.* **1983**, *156*, 340.
(97) Vincent, K. A.; Parkin, A.; Lenz, O.; Albracht, S. P. J.; Fontecilla-Camps, J. C.; Cammack, R.; Friedrich, B.; Armstrong, F. A. *J. Am. Chem. Soc.* **2005**, *127*, 18179.
(98) Parkin, A.; Cavazza, C.; Fontecilla-Camps, J. C.; Armstrong, F. A. *J. Am. Chem. Soc.* **2006**, *128*, 16808.
(99) Albracht, S. P. J.; Roseboom, W.; Hatchikian, E. C. *J. Biol. Inorg. Chem.* **2006**, *11*, 88.
(100) Fernandez, V. M.; Munilla, R.; Ballesteros, A. *Arch. Biochem. Biophys.* **1982**, *215*, 129.
(101) Goldet, G.; Brandmayr, C.; Stripp, S. T.; Happe, T.; Cavazza, C.; Fontecilla-Camps, J. C.; Armstrong, F. A. *J. Am. Chem. Soc.* **2009**, *131*, 14979.
(102) Fontecilla-Camps, J. C.; Amara, P.; Cavazza, C.; Nicolet, Y.; Volbeda, A. *Nature* **2009**, *460*, 814.
(103) Fan, H. J.; Hall, M. B. *J. Am. Chem. Soc.* **2001**, *123*, 3828.
(104) Bruschi, M.; Greco, C.; Fantucci, P.; De Gioia, L. *Inorg. Chem.* **2008**, *47*, 6056.
(105) Hong, G.; Cornish, A. J.; Hegg, E. L.; Pachter, R. *BBA-Bioenergetics* **2011**, *1807*, 510.
(106) Cohen, J.; Kim, K.; King, P.; Seibert, M.; Schulten, K. *Structure* **2005**, *13*, 1321.
(107) Lautier, T.; Ezanno, P.; Baffert, C.; Fourmond, V.; Cournac, L.; Fontecilla-Camps, J. C.; Soucaille, P.; Bertrand, P.; Meynial-Salles, I.; Leger, C. *Faraday Discuss.* **2011**, *148*, 385.
(108) Goldet, G.; Wait, A. F.; Cracknell, J. A.; Vincent, K. A.; Ludwig, M.; Lenz, O.; Friedrich, B.; Armstrong, F. A. *J. Am. Chem. Soc.* **2008**, *130*, 11106.
(109) Léger, C.; Dementin, S.; Bertrand, P.; Rousset, M.; Guigliarelli, B. *J. Am. Chem. Soc.* **2004**, *126*, 12162.
(110) Cracknell, J. A.; Friedrich, B.; Armstrong, F. A. *Chem. Commun.* **2010**, *46*, 8463.
(111) Stripp, S. T.; Goldet, G.; Brandmayr, C.; Sanganas, O.; Vincent, K. A.; Haumann, M.; Armstrong, F. A.; Happe, T. *Proc. Natl. Acad. Sci. U. S. A.* **2009**, *106*, 17331.
(112) Adams, M. W. W. *Biochim. Biophys. Acta* **1990**, *1020*, 115.
(113) Vincent, K. A.; Cracknell, J. A.; Clark, J. R.; Ludwig, M.; Lenz, O.; Friedrich, B.; Armstrong, F. A. *Chem. Commun.* **2006**, 5033.
(114) Vincent, K. A.; Cracknell, J. A.; Lenz, O.; Zebger, I.; Friedrich, B.; Armstrong, F. A. *Proc. Natl. Acad. Sci. U. S. A.* **2005**, *102*, 16951.
(115) Lukey, M. J.; Parkin, A.; Roessler, M. M.; Murphy, B. J.; Harmer, J.; Palmer, T.; Sargent, F.; Armstrong, F. A. *J. Biol. Chem.* **2010**, *285*, 3928.
(116) Hallahan, D. L.; Fernandez, V. M.; Hatchikian, E. C.; Hall, D. O. *Biochimie* **1986**, *68*, 49.
(117) Pandelia, M. E.; Infossi, P.; Giudici-Orticoni, M. T.; Lubitz, W. *Biochemistry* **2010**, *49*, 8873.
(118) Baffert, C.; Bertini, L.; Lautier, T.; Greco, C.; Sybirna, K.; Ezanno, P.; Etienne, E.; Soucaille, P.; Bertrand, P.; Bottin, H.; Meynial-Salles, I.; De Gioia, L.; Leger, C. *J. Am. Chem. Soc.* **2011**, *133*, 2096.
(119) Lemon, B. J.; Peters, J. W. *Biochemistry* **1999**, *38*, 12969.
(120) Lee, S. B.; Wilson, J. B.; Wilson, P. W. *J. Biol. Chem.* **1942**, *144*, 273.

(121) Hyndman, L. A.; Burris, R. H.; Wilson, P. W. *J. Bacteriol.* **1953**, *65*, 522.
(122) Seefeldt, L. C.; Arp, D. J. *J. Bacteriol.* **1989**, *171*, 3298.
(123) Hexter, S.; Armstrong, F. A., *unpublished results*, University of Oxford.
(124) Higuchi, Y.; Ogata, H.; Miki, K.; Yasuoka, N.; Yagi, T. *Struct. Fold. Des.* **1999**, *7*, 549.
(125) Higuchi, Y.; Yagi, T. *Biochem. Biophys. Res. Co.* **1999**, *255*, 295.
(126) Vincent, K. A.; Belsey, N. A.; Lubitz, W.; Armstrong, F. A. *J. Am. Chem. Soc.* **2006**, *128*, 7448.
(127) Ogata, H.; Hirota, S.; Nakahara, A.; Komori, H.; Shibata, N.; Kato, T.; Kano, K.; Higuchi, Y. *Structure* **2005**, *13*, 1635.
(128) Belsey, N. A., *unpublished results*, University of Oxford, 2009.
(129) Krebs, J. F. *AIP Conf. Proc.*, **2003**; Vol. 671, p 101.
(130) Krasna, A. I.; Rittenberg, D. *Proc. Natl. Acad. Sci. U. S. A.* **1954**, *40*, 225.
(131) Hyman, M. R.; Arp, D. J. *Biochem. J.* **1988**, *254*, 469.
(132) Hyman, M. R.; Arp, D. J. *Biochim. Biophys. Acta* **1991**, *1076*, 165.
(133) Smith, L. A.; Hill, S.; Yates, M. G. *Nature* **1976**, *262*, 209.
(134) Tibelius, K. H.; Knowles, R. *J. Bacteriol.* **1984**, *160*, 103.
(135) Hyman, M. R.; Arp, D. J. *Biochemistry* **1987**, *26*, 6447.
(136) Hyman, M. R.; Seefeldt, L. C.; Arp, D. J. *Biochim. Biophys. Acta* **1988**, *957*, 91.
(137) He, S. H.; Woo, S. B.; Dervartanian, D. V.; Legall, J.; Peck, H. D. *Biochem. Biophys. Res. Co.* **1989**, *161*, 127.
(138) Ghirardi, M. L.; Dubini, A.; Yu, J. P.; Maness, P. C. *Chem. Soc. Rev.* **2009**, *38*, 3505.
(139) Mertens, R.; Liese, A. *Curr. Opin. Biotechnol.* **2004**, *15*, 343.
(140) Homann, P. H. *Photosynth. Res.* **2003**, *76*, 93.
(141) Schutz, K.; Happe, T.; Troshina, O.; Lindblad, P.; Leitao, E.; Oliveira, P.; Tamagnini, P. *Planta* **2004**, *218*, 350.
(142) Ihara, M.; Nishihara, H.; Yoon, K. S.; Lenz, O.; Friedrich, B.; Nakamoto, H.; Kojima, K.; Honma, D.; Kamachi, T.; Okura, I. *Photochem. Photobiol.* **2006**, *82*, 676.
(143) Joo, H.; Bae, S.; Kim, C.; Kim, S.; Yoon, J. *Sol. Energ. Mat. Sol. C.* **2009**, *93*, 1555.
(144) Hambourger, M.; Kodis, G.; Vaughn, M. D.; Moore, G. F.; Gust, D.; Moore, A. L.; Moore, T. A. *Dalton T.* **2009**, 9979.
(145) Hambourger, M.; Gervaldo, M.; Svedruzic, D.; King, P. W.; Gust, D.; Ghirardi, M.; Moore, A. L.; Moore, T. A. *J. Am. Chem. Soc.* **2008**, *130*, 2015.
(146) Reisner, E.; Powell, D. J.; Cavazza, C.; Fontecilla-Camps, J. C.; Armstrong, F. A. *J. Am. Chem. Soc.* **2009**, *131*, 18457.
(147) Nedoluzhko, A. I.; Shumilin, I. A.; Nikandrov, V. V. *J. Phys. Chem.* **1996**, *100*, 17544.
(148) Cuendet, P.; Rao, K. K.; Gratzel, M.; Hall, D. O. *Biochimie* **1986**, *68*, 217.
(149) Nikandrov, V. V.; Shlyk, M. A.; Zorin, N. A.; Gogotov, I. N.; Krasnovsky, A. A. *FEBS Lett.* **1988**, *234*, 111.
(150) Barton, S. C.; Gallaway, J.; Atanassov, P. *Chemical Reviews* **2004**, *104*, 4867.
(151) Lojou, E.; Bianco, P. *Electroanal.* **2004**, *16*, 1093.
(152) Qian, D. J.; Nakamura, C.; Wenk, S. O.; Ishikawa, H.; Zorin, N.; Miyake, J. *Biosens. Bioelectron.* **2002**, *17*, 789.
(153) Vincent, K. A.; Li, X.; Blanford, C. F.; Belsey, N. A.; Weiner, J. H.; Armstrong, F. A. *Nat. Chem. Biol.* **2007**, *3*, 760.

(154) Igarashi, H.; Fujino, T.; Watanabe, M. *J. Electroanal. Chem.* **1995**, *391*, 119.
(155) Lazarus, O.; Woolerton, T. W.; Parkin, A.; Lukey, M. J.; Reisner, E.; Seravalli, J.; Pierce, E.; Ragsdale, S. W.; Sargent, F.; Armstrong, F. A. *J. Am. Chem. Soc.* **2009**, *131*, 14154.
(156) Mertens, R.; Greiner, L.; van den Ban, E. C. D.; Haaker, H.; Liese, A. *J. Mol. Catal. B-Enzym.* **2003**, *24-5*, 39.
(157) Canaguier, S.; Artero, V.; Fontecave, M. *Dalton T.* **2008**, 315.
(158) Liu, X. M.; Ibrahim, S. K.; Tard, C.; Pickett, C. J. *Coordin. Chem. Rev.* **2005**, *249*, 1641.
(159) Krassen, H.; Ott, S.; Heberle, J. *Phys. Chem. Chem. Phys.* **2011**, *13*, 47.
(160) Lubitz, W.; Reijerse, E. J.; Messinger, J. *Energ. Environ. Sci.* **2008**, *1*, 15.
(161) Barton, B. E.; Olsen, M. T.; Rauchfuss, T. B. *J. Am. Chem. Soc.* **2008**, *130*, 16834.
(162) Helm, M. L.; Stewart, M. P.; Bullock, R. M.; DuBois, M. R.; DuBois, D. L. *Science* **2011**, *333*, 863.
(163) Armstrong, F. A.; Heering, H. A.; Hirst, J. *Chem. Soc. Rev.* **1997**, *26*, 169.
(164) Léger, C.; Elliott, S. J.; Hoke, K. R.; Jeuken, L. J. C.; Jones, A. K.; Armstrong, F. A. *Biochemistry* **2003**, *42*, 8653.
(165) Fisher, A. C. *Electrode Dynamics*; Oxford University Press: New York, USA, 1996.
(166) Bard, A. J.; Faulkner, L. R. *Electrochemical Methods: Fundamentals and Applications*; Second ed.; Wiley and Sons: USA, 2001.
(167) Compton, R. G.; Banks, C. E. *Understanding Voltammetry*; World Scientific Publishing Co. Pte. Ltd., 2007.
(168) Atkins, P. W. *Physical Chemistry*; 6th ed.; Oxford University Press, 1998.
(169) Compton, R. G.; Sanders, G. H. W. *Electrode Potentials*; Oxford University Press: New York, USA, 1998.
(170) Wright, M. R. *An Introduction to Chemical Kinetics*; John Wiley and Sons Ltd., 2004.
(171) Purich, D. L.; Allison, R. D. *Handbook of Biochemical Kinetics*; Academic Press, 2000.
(172) Heering, H. A.; Hirst, J.; Armstrong, F. A. *J. Phys. Chem. B* **1998**, *102*, 6889.
(173) Armstrong, F. A. *Curr. Opin. Chem. Biol.* **2005**, *9*, 110.
(174) Duff, J. L. C.; Breton, J. L. J.; Butt, J. N.; Armstrong, F. A.; Thomson, A. J. *J. Am. Chem. Soc.* **1996**, *118*, 8593.
(175) Pershad, H. R.; Duff, J. L. C.; Heering, H. A.; Duin, E. C.; Albracht, S. P. J.; Armstrong, F. A. *Biochemistry* **1999**, *38*, 8992.
(176) Parkin, A.; Goldet, G.; Cavazza, C.; Fontecilla-Camps, J. C.; Armstrong, F. A. *J. Am. Chem. Soc.* **2008**, *130*, 13410.
(177) Léger, C.; Jones, A. K.; Albracht, S. P. J.; Armstrong, F. A. *J. Phys. Chem. B* **2002**, *106*, 13058.
(178) Hirst, J.; Armstrong, F. A. *Anal. Chem.* **1998**, *70*, 5062.
(179) Burgdorf, T.; Lenz, O.; Buhrke, T.; van der Linden, E.; Jones, A. K.; Albracht, S. P. J.; Friedrich, B. *J. Mol. Microb. Biotech.* **2005**, *10*, 181.
(180) Casalot, L.; Rousset, M. *Trends Microbiol.* **2001**, *9*, 228.
(181) Lenz, O.; Ludwig, M.; Schubert, T.; Burstel, I.; Ganskow, S.; Goris, T.; Schwarze, A.; Friedrich, B. *ChemPhysChem* **2010**, *11*, 1107.
(182) Schwartz, E.; Voigt, B.; Zuhlke, D.; Pohlmann, A.; Lenz, O.; Albrecht, D.; Schwarze, A.; Kohlmann, Y.; Krause, C.; Hecker, M.; Friedrich, B. *Proteomics* **2009**, *9*, 5132.

(183) Lauterbach, L.; Liu, J. A.; Horch, M.; Hummel, P.; Schwarze, A.; Haumann, M.; Vincent, K. A.; Lenz, O.; Zebger, I. *Eur. J. Inorg. Chem.* **2011**, 1067.
(184) Happe, R. P.; Roseboom, W.; Egert, G.; Friedrich, C. G.; Massanz, C.; Friedrich, B.; Albracht, S. P. J. *FEBS Lett.* **2000**, *466*, 259.
(185) Bernhard, M.; Buhrke, T.; Bleijlevens, B.; De Lacey, A. L.; Fernandez, V. M.; Albracht, S. P. J.; Friedrich, B. *J. Biol. Chem.* **2001**, *276*, 15592.
(186) Schneider, K.; Schlegel, H. G. *Biochim. Biophys. Acta* **1976**, *452*, 66.
(187) Lenz, O.; Friedrich, B. *Proc. Natl. Acad. Sci. U. S. A.* **1998**, *95*, 12474.
(188) Bernhard, M.; Benelli, B.; Hochkoeppler, A.; Zannoni, D.; Friedrich, B. *Eur. J. Biochem.* **1997**, *248*, 179.
(189) Schink, B.; Schlegel, H. G. *Biochim. Biophys. Acta* **1979**, *567*, 315.
(190) *Fuel Cell Catalysis: A Surface Science Approach*; Koper, M. T. M., Ed.; John Wiley and Sons: New Jersey, 2009.
(191) Nicholls, D. G.; Ferguson, S. J. *Bioenergetics 3*; Elsevier: London, 2002.
(192) Bernhard, M.; Schwartz, E.; Rietdorf, J.; Friedrich, B. *J. Bacteriol.* **1996**, *178*, 4522.
(193) Saggu, M.; Zebger, I.; Ludwig, M.; Lenz, O.; Friedrich, B.; Hildebrandt, P.; Lendzian, F. *J. Biol. Chem.* **2009**, *284*, 16264.
(194) Volbeda, A.; Martin, L.; Cavazza, C.; Matho, M.; Faber, B. W.; Roseboom, W.; Albracht, S. P. J.; Garcin, E.; Rousset, M.; Fontecilla-Camps, J. C. *J. Biol. Inorg. Chem.* **2005**, *10*, 239.
(195) Lamle, S. E.; Albracht, S. P. J.; Armstrong, F. A. *J. Am. Chem. Soc.* **2005**, *127*, 6595.
(196) Cracknell, J. A.; Wait, A. F.; Lenz, O.; Friedrich, B.; Armstrong, F. A. *Proc. Natl. Acad. Sci. U. S. A.* **2009**, *106*, 20681.
(197) Darensbourg, M. Y.; Weigand, W. *Eur. J. Inorg. Chem.* **2011**, 994.
(198) Cracknell, J. A., *DPhil Thesis*, University of Oxford 2009.
(199) Sander, R. 1999., www.mpch-mainz.mpg.de/~sander/res/henry.html., 1999
(200) Léger, C.; Jones, A. K.; Roseboom, W.; Albracht, S. P. J.; Armstrong, F. A. *Biochemistry* **2002**, *41*, 15736.
(201) Jones, A. K.; Lamle, S. E.; Pershad, H. R.; Vincent, K. A.; Albracht, S. P. J.; Armstrong, F. A. *J. Am. Chem. Soc.* **2003**, *125*, 8505.
(202) Ludwig, M.; Cracknell, J. A.; Vincent, K. A.; Armstrong, F. A.; Lenz, O. *J. Biol. Chem.* **2009**, *284*, 465.
(203) Jones, A. K.; Lamle, S. E.; Pershad, H. R.; Vincent, K. A.; Albracht, S. P. J.; Armstrong, F. A. *J. Am. Chem. Soc.* **2003**, *125*, 8505.
(204) Fourmond, V.; Infossi, P.; Giudici-Orticoni, M. T.; Bertrand, P.; Leger, C. *J. Am. Chem. Soc.* **2010**, *132*, 4848.
(205) Guggenheim, E. A. *Philos. Mag.* **1926**, *2*, 538.
(206) Nieberga.Pj; Sugita, E. T. *J. Pharm. Sci.* **1968**, *57*, 1805.
(207) Duche, O.; Elsen, S.; Cournac, L.; Colbeau, A. *FEBS Journal* **2005**, *272*, 3899.
(208) Leroux, F.; Dementin, S.; Burlatt, B.; Cournac, L.; Volbeda, A.; Champ, S.; Martin, L.; Guigliarelli, B.; Bertrand, P.; Fontecilla-Camps, J.; Rousset, M.; Leger, C. *Proc. Natl. Acad. Sci. U. S. A.* **2008**, *105*, 11188.
(209) Dementin, S.; Leroux, F.; Cournac, L.; de Lacey, A. L.; Volbeda, A.; Leger, C.; Burlat, B.; Martinez, N.; Champ, S.; Martin, L.; Sanganas, O.; Haumann, M.; Fernandez, V. M.; Guigliarelli, B.; Fontecilla-Camps, J. C.; Rousset, M. *J. Am. Chem. Soc.* **2009**, *131*, 10156.

(210) Goris, T.; Wait, A. F.; Saggu, M.; Fritsch, J.; Heidary, N.; Stein, M.; Zebger, I.; Lendzian, F.; Armstrong, F. A.; Friedrich, B.; Lenz, O. *Nat. Chem. Biol.* **2011**, *7*, 310.
(211) Goris, T.; Wait, A. F.; Saggu, M.; Fritsch, J.; Heidary, N.; Stein, M.; Zebger, I.; Lendzian, F.; Armstrong, F. A.; Friedrich, B.; Lenz, O. *Nat. Chem. Biol.* **2011**, *7*, 310.
(212) Pandelia, M. E.; Nitschke, W.; Infossi, P.; Giudici-Orticoni, M. T.; Bill, E.; Lubitz, W. *Proc. Natl. Acad. Sci. U. S. A.* **2011**, *108*, 6097.
(213) Schneider, K.; Patil, D. S.; Cammack, R. *Biochim. Biophys. Acta* **1983**, *748*, 353.
(214) Bullen, R. A.; Arnot, T. C.; Lakeman, J. B.; Walsh, F. C. *Biosens. Bioelectron.* **2006**, *21*, 2015.
(215) Larminie, J.; Dicks, A. *Fuel Cell Systems Explained*; Second ed.; Wiley and Sons: Chichester, U.K., 2003.
(216) Cracknell, J. A.; Vincent, K. A.; Armstrong, F. A. *Chem. Rev.* **2008**, *108*, 2439.
(217) Jones, A. K.; Sillery, E.; Albracht, S. P. J.; Armstrong, F. A. *Chem. Commun.* **2002**, 866.
(218) Karyakin, A. A.; Morozov, S. V.; Karyakina, E. E.; Zorin, N. A.; Perelygin, V. V.; Cosnier, S. *Biochem. Soc. T.* **2005**, *33*, 73.
(219) Chen, T.; Barton, S. C.; Binyamin, G.; Gao, Z. Q.; Zhang, Y. C.; Kim, H. H.; Heller, A. *J. Am. Chem. Soc.* **2001**, *123*, 8630.
(220) Willner, I.; Yan, Y.-M.; Willner, B.; Tel-Vered, R. *Fuel Cells* **2009**, *1*, 7.
(221) Cooney, M. J.; Svoboda, V.; Lau, C.; Martin, G.; Minteer, S. D. *Energ. Environ. Sci.* **2008**, *1*, 320.
(222) Chader, S.; Mahmah, B.; Chetehouna, K.; Amrouche, F.; Abdeladim, K. *Int. J. Hydrogen Energ.* **2011**, *36*, 4089.
(223) Borup, R.; Meyers, J.; Pivovar, B.; Kim, Y. S.; Mukundan, R.; Garland, N.; Myers, D.; Wilson, M.; Garzon, F.; Wood, D.; Zelenay, P.; More, K.; Stroh, K.; Zawodzinski, T.; Boncella, J.; McGrath, J. E.; Inaba, M.; Miyatake, K.; Hori, M.; Ota, K.; Ogumi, Z.; Miyata, S.; Nishikata, A.; Siroma, Z.; Uchimoto, Y.; Yasuda, K.; Kimijima, K.-i.; Iwashita, N. *Chem. Rev.* **2007**, *107*, 3904.
(224) Mohtadi, R.; Lee, W. K.; Cowan, S.; Van Zee, J. W.; Murthy, M. *Electrochem. Solid St.* **2003**, *6*, A272.
(225) Varfolomeev, S. D.; Karyakin, A. A.; Karyakina, E. E.; Vagin, M. Y.; Morozov, S. V., Patent, 2004.
(226) Tsujimura, S.; Fujita, M.; Tatsumi, H.; Kano, K.; Ikeda, T. *Phys. Chem. Chem. Phys.* **2001**, *3*, 1331.
(227) http://www.gexcon.com//handbook/GEXHBcontents.htm.
(228) Varfolomeev, S. D.; Yaropolov, A. I.; Berezin, I. V.; Tarasevich, M. R.; Bogdanovskaya, V. A. *Bioelectroch. Bioener.* **1977**, *4*, 314.
(229) Mano, N.; Fernandez, J. L.; Kim, Y.; Shin, W.; Bard, A. J.; Heller, A. *J. Am. Chem. Soc.* **2003**, *125*, 15290.
(230) Mano, N. *Chem. Commun.* **2008**, 2221.
(231) Tsujimura, S.; Kamitaka, Y.; Kano, K. *Fuel Cells* **2007**, *7*, 463.
(232) Murata, K.; Kajiya, K.; Nakamura, N.; Ohno, H. *Energ. Environ. Sci.* **2009**, *2*, 1280.
(233) Mano, N.; Soukharev, V.; Heller, A. *J. Phys. Chem. B* **2006**, *110*, 11180.
(234) dos Santos, L.; Climent, V.; Blanford, C. F.; Armstrong, F. A. *Phys Chem Chem Phys* **2010**, *12*, 13962.

(235) Mano, N.; Mao, F.; Heller, A. *J. Am. Chem. Soc.* **2003**, *125*, 6588.
(236) dos Santos, L., *PhD Thesis*, Universidade de São Paulo, 2010.
(237) Cracknell, J. A.; McNamara, T. P.; Lowe, E. D.; Blanford, C. F. *Dalton T.* **2011**, *40*, 6668.
(238) Solomon, E. I.; Sundaram, U. M.; Machonkin, T. E. *Chem. Rev.* **1996**, *96*, 2563.
(239) Quintanar, L.; Stoj, C.; Taylor, A. B.; Hart, P. J.; Kosman, D. J.; Solomon, E. I. *Accounts Chem. Res.* **2007**, *40*, 445.
(240) Solomon, E. I.; Augustine, A. J.; Yoon, J. *Dalton T.* **2008**, 3921.
(241) Cole, J. L.; Clark, P. A.; Solomon, E. I. *J. Am. Chem. Soc.* **1990**, *112*, 9534.
(242) Rulisek, L.; Solomon, E. I.; Ryde, U. *Inorg. Chem.* **2005**, *44*, 5612.
(243) Blanford, C. F.; Heath, R. S.; Armstrong, F. A. *Chem. Commun.* **2007**, *17*, 1710.
(244) Léger, C.; Jones, A. K.; Albracht, S. P. J.; Armstrong, F. A. *J. Phys. Chem. B* **2002**, *106*, 13058.
(245) Lamle, S. E.; Vincent, K. A.; Halliwell, L. M.; Albracht, S. P. J.; Armstrong, F. A. *Dalton T.* **2003**, 4152.
(246) Bard, A. J.; Faulkner, L. R. *Electrochemical Methods Fundamentals and Applications*; John Wiley and Sons, 1980.
(247) Solomon, E. I.; Augustine, A. J.; Yoon, J. *Dalton T.* **2008**, *30*, 3921.
(248) Priestnall, M. A.; Kotzeva, V. P.; Fish, D. J.; Nilsson, E. M. *J. Power Sources* **2002**, *106*, 21.
(249) Dyer, C. K. *Nature* **1990**, *343*, 547.
(250) Gottesfeld, S. *Nature* **1990**, *345*, 673.
(251) Katz, E.; Willner, I.; Kotlyar, A. B. *J. Electroanal. Chem.* **1999**, *479*, 64.
(252) Kamitaka, Y.; Tsujimura, S.; Setoyama, N.; Kajino, T.; Kenji Kano *Phys. Chem. Chem. Phys.* **2007**, *9*, 1793.
(253) Stoica, L.; Dimcheva, N.; Ackermann, Y.; Karnicka, K.; Guschin, D. A.; Kulesza, P. J.; Rogalski, J.; Haltrich, D.; Ludwig, R.; Gorton, L.; Schuhmann, W. *Fuel Cells* **2009**, *1*, 53.
(254) Cheng, X.; Shi, Z.; Glass, N.; Zhang, L.; Zhang, J. J.; Song, D. T.; Liu, Z. S.; Wang, H. J.; Shen, J. *J. Power Sources* **2007**, *165*, 739.
(255) Luo, X. J.; Brugna, M.; Tron-Infossi, P.; Giudici-Orticoni, M. T.; Lojou, E. *J. Biol. Inorg. Chem.* **2009**, *14*, 1275.
(256) Wait, A. F.; Parkin, A.; Morley, G. M.; dos Santos, L.; Armstrong, F. A. *J. Phys. Chem. C* **2010**, *114*, 12003.
(257) Laurinavichene, T. V.; Tsygankov, A. A. *FEMS Microbiol. Lett.* **2001**, *202*, 121.
(258) Kurkin, S.; George, S. J.; Thorneley, R. N. F.; Albracht, S. P. J. *Biochemistry* **2004**, *43*, 6820.
(259) Lojou, E.; Luo, X.; Brugna, M.; Candoni, N.; Dementin, S.; Giudici-Orticoni, M. T. *J. Biol. Inorg. Chem.* **2008**, *13*, 1157.
(260) Alonso-Lomillo, M. A.; Rudiger, O.; Maroto-Valiente, A.; Velez, M.; Rodriguez-Ramos, I.; Munoz, F. J.; Fernandez, V. M.; De Lacey, A. L. *Nano Lett.* **2007**, *7*, 1603.
(261) Rudiger, O.; Abad, J. M.; Hatchikian, E. C.; Fernandez, V. M.; De Lacey, A. L. *J. Am. Chem. Soc.* **2005**, *127*, 16008.
(262) Lojou, E. *Electrochim. Acta* **2011**.
(263) Pieper, U.; Webb, B. M.; Barkan, D. T.; Sampathkumar, M. M.; Sjolander, K.; Ferrin, T. E.; Burley, S. K.; Sali, A. *Nucleic Acids Res.* **2011**, *39*, 465.

(264) Fareleira, P.; Santos, B. S.; Antonio, C.; Moradas-Ferreira, P.; LeGall, J.; Xavier, A. V.; Santos, H. *Microbiology* **2003**, *149*, 1513.
(265) Pereira, I. A. C.; Romao, C. V.; Xavier, A. V.; LeGall, J.; Teixeira, M. *J. Biol. Inorg. Chem.* **1998**, *3*, 494.
(266) Jones, D. T.; Woods, D. R. *Microbiol. Rev.* **1986**, *50*, 484.
(267) Santangelo, J. D.; Durre, P.; Woods, D. R. *Microbiology* **1995**, *141*, 171.
(268) von Abendroth, G.; Stripp, S.; Silakov, A.; Croux, C.; Soucaille, P.; Girbal, L.; Happe, T. *Int. J. Hydrogen Energ.* **2008**, *33*, 6076.
(269) Gorwa, M. F.; Croux, C.; Soucaille, P. *J. Bacteriol.* **1996**, *178*, 2668.
(270) Grossman, A. R.; Catalanotti, C.; Yang, W. Q.; Dubini, A.; Magneschi, L.; Subramanian, V.; Posewitz, M. C.; Seibert, M. *New Phytol.* **2011**, *190*, 279.
(271) Happe, T.; Mosler, B.; Naber, J. D. *Eur. J. Biochem.* **1994**, *222*, 769.
(272) Melis, A.; Happe, T. *Plant Physiol.* **2001**, *127*, 740.
(273) Florin, L.; Tsokoglou, A.; Happe, T. *J. Biol. Chem.* **2001**, *276*, 6125.
(274) Happe, T.; Naber, J. D. *European Journal of Biochemistry* **1993**, *214*, 475.
(275) Sawers, R. G.; Boxer, D. H. *Eur. J. Biochem.* **1986**, *156*, 265.
(276) Ballantine, S. P.; Boxer, D. H. *Eur. J. Biochem.* **1986**, *156*, 277.
(277) Dubini, A.; Pye, R. L.; Jack, R. L.; Palmer, T.; Sargent, F. *Int. J. Hydrogen Energ.* **2002**, *27*, 1413.
(278) Menon, N. K.; Chatelus, C. Y.; Dervartanian, M.; Wendt, J. C.; Shanmugam, K. T.; Peck, H. D.; Przybyla, A. E. *J. Bacteriol.* **1994**, *176*, 4416.
(279) Goldet, G., *DPhil Thesis*, University of Oxford, 2009.
(280) Erbes, D. L.; King, D.; Gibbs, M. *Plant Physiol.* **1979**, *63*, 1138.
(281) Purec, L.; Krasna, A. I.; Rittenberg, D. *Biochemistry* **1962**, *1*, 270.
(282) Thauer, R. K.; Kaufer, B.; Zahringe.M; Jungerma.K *Eur. J. Biochem.* **1974**, *42*, 447.
(283) Clayden, J.; Greeves, N.; Warren, S.; Wothers, P. *Organic Chemistry*; Oxford University Press, 2001.
(284) Bell, R. P. In *Advances in Physical Organic Chemistry*; Gold, V., Ed.; Academic Press: 1966; Vol. Volume 4, p 1.
(285) Hilal, S. H.; Bornander, L. L.; Carreira, L. A. *Qsar Comb. Sci.* **2005**, *24*, 631.
(286) Means, G. E.; Feeney, R. E. *Biochemistry* **1968**, *7*, 2192.
(287) Means, G. E.; Feeney, R. E. *Anal. Biochem.* **1995**, *224*, 1.
(288) Slatyer, B.; Daday, A.; Smith, G. D. *Biochem. J.* **1983**, *212*, 755.
(289) Rao, K. K.; Hall, D. O. *Biochem. Soc. T.* **1985**, *13*, 631.
(290) Brandmayr, C. *Part II Thesis*, University of Oxford, 2009.
(291) Wait, A. F.; Brandmayr, C.; Stripp, S. T.; Cavazza, C.; Fontecilla-Camps, J. C.; Happe, T.; Armstrong, F. A. *J. Am. Chem. Soc.* **2011**, *133*, 1282.
(292) Van Dijk, C.; Mayhew, S. G.; Veeger, C. *Eur. J. Biochem.* **1981**, *114*, 201.
(293) Fourmond, V.; Lautier, T.; Baffert, C.; Leroux, F.; Liebgott, P. P.; Dementin, S.; Rousset, M.; Arnoux, P.; Pignol, D.; Meynial-Salles, I.; Soucaille, P.; Bertrand, P.; Leger, C. *Anal. Chem.* **2009**, *81*, 2962.
(294) Stripp, S. T.; Happe, T. *Dalton T.* **2009**, 9960.
(295) Glasoe, P. K.; Long, F. A. *J. Phys. Chem.* **1960**, *64*, 188.
(296) Armstrong, F. A.; Wilson, G. S. *Electrochim. Acta* **2000**, *45*, 2623.
(297) Mauritz, K. A.; Moore, R. B. *Chem. Rev.* **2004**, *104*, 4535.
(298) http://www.basinc.com/products/ec/faqele.html#Ref_Type.

Appendices

A1 Derivation of the Nernst Equation*

The following scheme represents a general reaction:

$$\nu_A A + \nu_B B \rightleftharpoons \nu_C C + \nu_D D$$

If the extent of reaction, ξ, increases by $d\xi$, then the amounts (in moles, n) of reactants and products change according to $dn_J = \nu_J d\xi$:

$$dn_A = \nu_A d\xi,\ dn_B = \nu_B d\xi,\ dn_C = \nu_C d\xi \text{ and } dn_D = \nu_D d\xi$$

where the stoichiometric number of species J, ν_J, is negative for the reactants and positive for the products.

The corresponding infinitesimal change in the Gibbs energy, dG, at constant pressure and temperature is given by:

$$dG = \left(\sum_J \nu_J \mu_J \right) d\xi$$

where μ_J is the chemical potential of species J. The reaction Gibbs energy, $\Delta_r G$, is therefore given by:

$$\Delta_r G = \left(\frac{\partial G}{\partial \xi} \right)_{p,T} = \nu_A \mu_A + \nu_B \mu_B + \nu_C \mu_C + \nu_D \mu_D$$

Then, since $\mu_J = \mu_J^\ominus + RT \ln a_J$ (where a_J is the activity of species J and R is the gas constant) and $\Delta G^\ominus = \nu_A \mu_A^\ominus + \nu_B \mu_B^\ominus + \nu_C \mu_C^\ominus + \nu_D \mu_D^\ominus$:

$$\Delta_r G = \Delta G^\ominus - RT \ln Q$$

* Atkins, P. W. (1998). Physical Chemistry, Oxford University Press

where Q is the reaction quotient, given by $\prod_J a_J^{\nu_J}$.

The maximum non-expansion work that can be performed as the reaction advances by $d\xi$ at constant temperature and pressure is given by $dw_e = \Delta_r G\, d\xi$. The total charge that must be transported from the anode to cathode in order for the reaction to proceed by this amount is given by $q = -nFd\xi$, where n is the number of electrons involved in the process and F is Faraday's constant. Therefore, the work done upon transport of this infinitesimal charge is given by the equation $dw_e = -nFE\, d\xi$, where E is the potential difference. Since $dw_e = \Delta_r G\, d\xi$, then $\Delta_r G = -nFE$ and $\Delta G^{\ominus} = -nFE^{o}$. Therefore:

$$E_{eq} = E^{\ominus} - \frac{RT}{nF} \ln Q$$

This is the Nernst equation.

An alternative derivation of this equation can be obtained by equating the electrochemical potentials of the reactants and products, where the electrochemical potential of species J, $\bar{u}_J$, is related to the chemical potential by $\bar{u}_J = \mu_J + zFE$ (where z is the charge on J).[†]

[†] Compton, R. G. and G. H. W. Sanders (1998). Electrode Potentials. New York, USA, Oxford University Press

A2 Normalising Data to Account for Film Loss

The electrocatalytic current of an enzyme slowly decreases over time due to a process known as 'film loss'. Possible explanations for this effect may include enzyme molecules dissociating from or re-orientating on the electrode surface, or denaturation of the enzyme on the electrode surface. In order to account for film loss, the slow decay in current can be fitted to a single exponential process by a least-squares regression analysis performed using the 'Solver' tool in Microsoft Excel. The exponential used to represent film loss is given by the following equation[‡]:

$$i_t = (i_0 - i_{lim}) \exp\left(\frac{t_0 - t}{\tau}\right) + i_{lim}$$

In this equation, i_t represents the current at a given time, t; i_0 is the current at $t = 0$ s (t_0); i_{lim} is the limiting current (at $t = \infty$) and τ is the time constant of the decay.

This exponential is extrapolated over the time course of the experiment and then, for each data point, the raw data were divided by the calculated exponential to obtain the normalised current, corrected for film loss.[§]

[‡] Ludwig, M., J. A. Cracknell, *et al*., *J. Biol. Chem.* **2009**, 284(1), 465-477.
§ Fourmond, V., T. Lautier, *et al*,. *Anal. Chem.* **2009**, 81(8): 2962-2968.

A3 Derivation of Equation 3.1

Investigations by Lamle *et al.*[**] described the reactivation of a [NiFe]-hydrogenase as proceeding via a rapid electrochemical pre-equilibrium, followed by a slow reversible step and finally a fast irreversible reaction with H_2 to produce the active state. Assuming that the reactivation of *Re*MBH follows a similar process, the overall reaction can be denoted as follows[**]:

$$O \underset{k_{-1}}{\overset{k_1}{\rightleftharpoons}} R \underset{k_{-2}}{\overset{k_2}{\rightleftharpoons}} P \xrightarrow{k_3} \text{active enzyme}$$

The simplifications $k_1 = k_1'[H^+]$ and $k_3 = k_3'[H_2]$ have been made, where k_1' and k_3' are second-order rate constants. The rate equation for this mechanism can be derived using steady-state kinetics. The simultaneous equations for the change in concentration of each intermediate over time can be written in matrix form[††]:

$$\begin{array}{c} \\ d[O]/dt \\ d[R]/dt \\ d[P]/dt \end{array} \begin{array}{c} \begin{array}{ccc} O & R & P \end{array} \\ \left| \begin{array}{ccc} -k_1 & k_{-1} & k_3 \\ k_1 & -(k_{-1}+k_2) & k_{-2} \\ 0 & k_2 & -(k_{-2}+k_3) \end{array} \right| \end{array} \begin{array}{l} \\ = 0 \\ = 0 \\ = 0 \end{array}$$

Solving these equations using the determinant method gives:

$$d[O]/dt = k_{-1}k_{-2} + k_3(k_{-1} + k_2)$$

$$d[R]/dt = k_1(k_{-2} + k_3)$$

$$d[P]/dt = k_1k_2$$

The rate is therefore given by the following equations:

[**] Lamle, S. E.; Albracht, S. P. J.; Armstrong, F. A. *J. Am. Chem. Soc.* **2005**, 127, 6595.
[††] Purich, D. L.; Allison, R. D. (2000). Handbook of Biochemical Kinetics, Academic Press.

$$\text{rate} = \frac{k_3[\text{P}]}{[\text{O}] + [\text{R}] + [\text{P}]}$$

$$\text{rate} = \frac{k_1 k_2 k_3}{k_{-1}k_{-2} + k_3 k_{-1} + k_2 k_3 + k_1 k_{-2} + k_1 k_3 + k_1 k_2}$$

Since $K_1 = k_1 / k_{-1}$:

$$\text{rate} = \frac{K_1 k_2 k_3}{K_1(k_{-2} + k_3 + k_2) + k_{-2} + k_3 + \left(\frac{k_2 k_3}{k_{-1}}\right)}$$

Then, because K_1 is an electrochemical equilibrium:

$$K_1 = \exp\left(\frac{nF(E_{1/2} - E)}{RT}\right)$$

Therefore:

$$\text{rate} = \frac{k_2 k_3 \exp\left(\frac{nF(E_{1/2} - E)}{RT}\right)}{k_{-2} + k_3 + \left(\frac{k_2 k_3}{k_{-1}}\right) + \exp\left(\frac{nF(E_{1/2} - E)}{RT}\right)(k_{-2} + k_3 + k_2)}$$

This is equivalent to Equation 3.1 (reproduced below) in which the complex constants in are defined as: $A = k_2 k_3$, $B = k_{-2} + k_3 + (k_2 k_3 / k_{-1})$ and $C = k_{-2} + k_3 + k_2$.

$$\text{rate} = \frac{A \exp\left(\frac{nF(E_{1/2} - E)}{\text{RT}}\right)}{B + C \exp\left(\frac{nF(E_{1/2} - E)}{RT}\right)}$$

A4 Derivation of Equations 3.2 and 3.4

It is assumed that the enzyme behaves according to Michaelis-Menten kinetics. In this model, the enzyme (E) binds reversibly to the substrate (S) to form a complex (ES), which then breaks down to the give the product (P) and free enzyme[‡‡]:

$$E + S \underset{k_{-1}}{\overset{k_1}{\rightleftharpoons}} ES \xrightarrow{k_{cat}} E + P$$

Applying the steady-state approximation to the enzyme-substrate complex, ES, yields the following equations:

$$d[ES] / dt = k_1[E][S] - (k_{-1} + k_{cat})[ES] = 0$$

$$[ES] = \frac{k_1[E][S]}{k_{-1} + k_{cat}} = \frac{[E][S]}{K_M}$$

The Michaelis constant, K_M, is therefore defined as $(k_{-1} + k_{cat}) / k_1$. The total amount of enzyme, $[E]_o$, must be equal to the sum of the concentrations of free enzyme ([E]) and enzyme-substrate complex ([ES]):

$$[E]_o = [E] + [ES]$$

Therefore:

$$[ES] = \frac{([E]_o - [ES])[S]}{K_M} = \frac{[E]_o[S]}{K_M + [S]}$$

The rate of the reaction (v, the rate of formation of P) is given by the following equation:

$$v = k_{cat}[ES]$$

[‡‡] Purich, D. L.; Allison, R. D. (2000) Handbook of Biochemical Kinetics; Academic Press

The maximum possible rate, v_{max}, will be achieved when all enzyme molecules are in the enzyme-substrate complex (*i.e.* when [ES] = $[E]_o$). Therefore:

$$v_{max} = k_{cat}\,[E]_o$$

Substituting the expressions for [ES] and v_{max} into the rate equation yields Equation 3.2:

$$v = \frac{v_{max}[S]}{K_M + [S]}$$

Assuming that the rate of reaction is proportional to the H_2 oxidation current, then the maximum rate, v_{max}, should be proportional to the maximum current detected, i_{max}. Equation 3.3 gave the dependence of the H_2 concentration on time:

$$[H_2]_t = [H_2]_0\, e^{-t/\tau}$$

Combining these equations yields the sigmoidal dependency of current on the value of $K_M(H_2)$ as determined by Equation 3.4[§§]:

$$i_t = \frac{i_{max}\left([H_2]_0 e^{-t/\tau}\right)}{K_M(H_2) + \left([H_2]_0 e^{-t/\tau}\right)} = \frac{i_{max}}{1 + \frac{K_M(H_2)}{[H_2]_0} e^{t/\tau}}$$

Therefore, fitting the sigmoidal current *vs.* time traces obtained as the H_2 concentration decreases enables determination of the value of $K_M(H_2)$ provided that $[H_2]_0$ and i_{max} are known and τ is constant over the duration of the experiment.

[§§] Léger, C.; Dementin, S.; Bertrand, P.; Rousset, M.; Guigliarelli, B. *J. Am. Chem. Soc.* **2004**, *126*, 12162

A5 Sequence Alignment for [NiFe]-Hydrogenases

A5.1 Small Subunit Alignment

```
ReMBH          METKPRTPVLWLHGLECTCCSESFIRSAHPLAKDVVLSMISLDYDDTLMAAAGHQAEAIL 60
EcHyd1         LENKPRIPVVWIHGLECTCCTESFIRSAHPLAKDVILSLISLDYDDTLMAAAGTQAEEVF 60
AaHase1        METKPRVPVLWIHGLECTCCSESFIRSATPLASDVVLSMISLEYDDTLSAAAGEAVEKHR 60
AvMBH          LEQARRPSVIWLSFQECTGCTESLTRAHAPTLEDLILDFISLDYHHTLQAASGEAAEAAR 60
DgHyd          LTAKKRPSVVYLHNAECTGCSESLLRTVDPYVDELILDVISMDYHETLMAGAGHAVEEAL 60
DfHyd          LTAKHRPSVVWLHNAECTGCTEAAIRTIKPYIDALILDTISLDYQETIMAAAGEAAEAAL 60
EcHyd2         VTNPQRPPVIWIGAQECTGCTESLLRATHPTVENLVLETISLEYHEVLSAAFGHQVEENK 60
               :    * .*:::   *** *:*:  *:  *  . ::*. **::*...: *. *  .*

ReMBH          EEIMTKYKGNYILAVEGNPP-LNQDGMSCIIGGRPFIEQLKYVAKDAKAIISWGSCASWG 119
EcHyd1         EDIITQYNGKYILAVEGNPP-LGEQGMFCISSGRPFIEKLKRAAAGASAIIAWGTCASWG 119
AaHase1        ERIIKEYWGNYILAVEGNPP-LGEDGMYCIIGGRPFVEILKESAEGAKAVIAWGSCASWG 119
AvMBH          LQAMDENRGQYLVIVDGSIPGPDANPGFSTVAGHSNYSILMETVEHAAAVIAVGTCAAFG 120
DgHyd          HEAIKG---DFVCVIEGGIP-MGDGGYWGKVGRRNMYDICAEVAPKAKAVIAIGTCATYG 116
DfHyd          HQALEGK-DGYYLVVEGGLP-TIDGGQWGMVAGHPMIETTKKAAAKAKGIICIGTCSAYG 118
EcHyd2         HNALEKYKGQYVLVVDGSIP-LKDNGIYCMVAGEPIVDHIRKAAEGAAAIIAIGSCSAWG 119
                  :      :   ::*. *           . .   .     .  * .:*. *:*:::*

ReMBH          CVQAAKPNPTQATPVHKVITD--KPIIKVPGCPPIAEVMTGVITYMLTFDRIPELDRQGR 177
EcHyd1         CVQAARPNPTQATPIDKVITD--KPIIKVPGCPPIPDVMSAIITYMVTFDRLPDVDRMGR 177
AaHase1        CVQAAKPNPTTAVPIDKVIKD--KPIIKVPGCPPIAEVMTGVIMYMVLFDRIPPLDSQGR 177
AvMBH          GLPQARPNPTGAMSVMDLVRD--KPVINVPGCPPIPMVITGVIAHYLVFGRLPELDGYGR 178
DgHyd          GVQAAKPNPTGTVGVNEALGKLGVKAINIAGCPPNPMNFVGTVVHLLTKG-MPELDKQGR 175
DfHyd          GVQKAKPNPSQAKGVSEALG---VKTINIPGCPPNPINFVGAVVHVLTKG-IPDLDENGR 174
EcHyd2         GVAAAGVNPTGAVSLQEVLPG--KTVINIPGCPPNPHNFLATVAHIITYGKPPKLDDKNR 177
                :  *  **: :  : . :       *::.**** .  : . : : :  .  * :*  .*

ReMBH          PKMFYSQRIHDKCYRRPHFDAGQFVEEWDDESARKGFCLYKMGCKGPTTYNACSTTRWNE 237
EcHyd1         PLMFYGQRIHDKCYRRAHFDAGEFVQSWDDDAARKGYCLYKMGCKGPTTYNACSSTRWND 237
AaHase1        PKMFYGNRIHDTCYRRSFFNAGQFVEQFDDEGAKKGWCLYKVGCRGPTTYNSCGNMRWYN 237
AvMBH          PLAFYGQSIHDRCYRRPFYDKGLFAESFDDEGAKQGWCLYRLGCKGPTTYNACATMKWND 238
DgHyd          PVMFFGETVHDNCPRLKHFEAGEFATSFGSPEAKKGYCLYELGCKGPDTYNNCPKQLFNQ 235
DfHyd          PKLFYGELVHDNCPRLPHFEASEFAPSFDSEEAKKGFCLYELGCKGPVTYNNCPKVLFNQ 234
EcHyd2         PTFAYGRLIHEHCERRPHFDAGRFAKEFGDEGHREGWCLYHLGCKGPETYGNCSTLQFCD 237
               *   :.. :*: * *  .:: . *. .:..   ::*:***.:**:** **. * .  : :

ReMBH          G-TSFPIQSGHGCIGCSED--GFWDKGS-FYDRLTGISQFGVEANADKIG----GTASVV 289
EcHyd1         G-VSFPIQSGHGCLGCAEN--GFWDRGS-FYSRVVDIPQMGTHSTADTVG----LTALGV 289
AaHase1        G-LSYPIQSGHGCIGCAEN--NFWDNGP-FYERIGGIPVPGIESKADKVG----AIAAAA 289
AvMBH          G-TSWPVEAGHPCLGCSEP--QFWDAGG-FYEPVSVPLTLG---PATLLG----AGAAGA 287
DgHyd          --VNWPVQAGHPCIACSEP--NFWDLYSPFYSA---------------------------- 264
DfHyd          --VNWPVQAGHPCLGCSEP--DFWDTMTPFYEQG--------------------------- 264
EcHyd2         VGGVWPVAIGHPCYGCNEEGIGFHKGIHQLANVENQTPRSQKPDVNAKEGGNVSAGAIGL 297
                   :*:  ** * .* *    * .    : .

ReMBH          VGAAVTAHAAASAIKRASKKNE-TSGSEH--------- 317
EcHyd1         VAAAVGVHAVASAVDQRRRHNQQPTETEHQPGNEDKQA 327
AaHase1        AAGGAIIHGIASKIRKSGEKEE---------------- 311
AvMBH          VVGGGLAALSRKKGRDAAATRQPVTVDELEQKL----- 320
DgHyd          ---------------------------------------
DfHyd          ---------------------------------------
EcHyd2         LGGVVGLVAGVSVMAVRELGRQQKKDNADSRGE----- 330
```

A5.2 Large Subunit Alignment

```
ReMBH           -MSAYATQGFNLDDRGRRIVVDPVTRIEGHMRCEVNVDANN-VIRNAVSTGTMWRGLEVI 58
EcHyd1          MSTQYETQGYTINNAGRRLVVDPITRIEGHMRCEVNINDQN-VITNAVSCGTMFRGLEII 59
AaHase1         ---------------MKRVVVDPVTRIEGHLRIEIMVDEETGQVKDALSAGTMWRGIELI 45
AvMBH           --------------MSERIVVDPITRIEGHLRIEAQMDGAT--IAQAYSSGTMVRGIETI 44
DgHyd           ---MSEMQ-------GNKIVVDPITRIEGHLRIEVEVEGGK--IKNAWSMSTLFRGLEMI 48
DfHyd           ---MAESKPTPQSTFTGPIVVDPITRIEGHLRIMVEVENGK--VKDAWSSSQLFRGLEII 55
EcHyd2          --------------MSQRITIDPVTRIEGHLRIDCEIENGV--VSKAWASGTMWRGMEEI 44
                              :.:**:******:*    ::     : .* : . : **:* *

ReMBH           LKGRDPRDAWAFVERICGVCTGCHALASVRAVENALDIRIPKNAHLIREIMAKTLQVHDH 118
EcHyd1          LQGRDPRDAWAFVERICGVCTGVHALASVYAIEDAIGIKVPDNANIIRNIMLATLWCHDH 119
AaHase1         VRNRDPRDVWAFTQRICGVCTSIHALASLRAVEDALEITIPKNANYIRNIMYGSLQVHDH 105
AvMBH           LKGRDPRDAWAFVQRICGVCTLVHGIASVRAVEDALRIELPLNAQLIRNLMIGAQYIHDH 104
DgHyd           LKGRDPRDAQHFTQRACGVCTYVHALASVRAVDNCVGVKIPENATLMRNLTMGAQYMHDH 108
DfHyd           LKGRDPRDAQHFTQRACGVCTYVHALASSRCVDDAVKVSIPANARMMRNLVMASQYLHDH 115
EcHyd2          VKNRDPRDAWMIVQRICGVCTTTHALSSVRAAESALNIDVPVNAQYIRNIILAAHTTHDH 104
                ::.*****.  :.:* *****  *.::*  . :..: : :* **  :*::   :   ***

ReMBH           AVHFYHLHALDWVDVMSALKADPKRTSELQ--------------------QLVSPAHPLS 158
EcHyd1          LVHFYQLAGMDWIDVLDALKADPRKTSELA--------------------QSLS-SWPKS 158
AaHase1         VVHFYHLHALDWVSPVEALKADPVATAALANKILEKYGVLNEFMPDFLGHRAYPKKFPKA 165
AvMBH           VMHFYHLHALDWVDVVSALSADPRATSELA--------------------QSIS-AWPKS 143
DgHyd           LVHFYHLHALDWVNVANALNADPAKAARLA--------------------NDLSPRK--T 146
DfHyd           LVHFYHLHALDWVDVTAALKADPNKAAKLA--------------------ASIAPARPGN 155
EcHyd2          IVHFYQLSALDWVDITSALQADPTKASEML--------------------KGVS-TWHLN 143
                 :***:* .:**:.   **.***  :: :                        .

ReMBH           SAGYFRDIQNRLKRFVESGQLGPFMNGYWG--SKAY-VLPPEANLMAVTHYLEALDLQKE 215
EcHyd1          SPGYFFDVQNRLKKFVEGGQLGIFRNGYWG--HPQY-KLPPEANLMGFAHYLEALDFQRE 215
AaHase1         TPGYFREFQKKIKKLVESGQLGIFAAHWWD--HPDYQMLPPEVHLIGIAHYLNMLDVQRE 223
AvMBH           SPGYFADTQKRIKTFVESGQLGIFANGYWG--HPAY-RLPPEANLMAVAHYLEALAWQRD 200
DgHyd           TTESLKAVQAKVKALVESGQLGIFTNAYFLGGHPAY-VLPAEVDLIATAHYLEALRVQVK 205
DfHyd           SAKALKAVQDKLKAFVESGQLGIFTNAYFLGGHKAY-YLPPEVDLIATAHYLEALHMQVK 214
EcHyd2          SPEEFTKVQNKIKDLVASGQLGIFANGYWG--HPAM-KLPPEVNLIAVAHYLQALECQRD 200
                :.  :   * ::* :* .**** *   ::         **.*..*:. :***: *  * .

ReMBH           WVKIHTIFGGKNPHPN-YLVGGVPCAINLDGIGAASAPVNMERLSFVKARIDEIIEFNKN 274
EcHyd1          IVKIHAVFGGKNPHPN-WIVGGMPCAINIDESGAVGA-VNMERLNLVQSIITRTADFINN 273
AaHase1         LFIPQVVFGGKNPHPH-YIVGGVNCSISMDD---MNAPVNAERLAVVEDAIYTQVESTDF 279
AvMBH           TAKFHAIFGGKNPHPN-FVVGGVPSPIDLDS----DSALNAKRLAEVRNLIQSMRTFVDQ 255
DgHyd           AARAMAIFGAKNPHTQFTVVGGCTNYDSLRP----------ERIAEFRKLYKEVREFIEQ 255
DfHyd           AASAMAILGGKNPHTQFTVVGGCSNYQGLTK----------DPLANYLALSKEVCQFVNE 264
EcHyd2          ANRVVALLGGKTPHIQNLAVGGVANPINLDG----LGVLNLERLMYIKSFIDKLSDFVEQ 256
                     .::*.*.** :   ***     .:           . :            .

ReMBH           VYVPDVLAIGTLYKQAG-WLYGGGLAATNVLDYGEYPNVA--------YNKSTDQLPGGA 325
EcHyd1          VMIPDALAIG-QFNKPW-SEIGTGLSDKCVLSYGAFPDIAND------FGEKSLLMPGGA 325
AaHase1         FYIPDILAIADIYLNQHNWFYGGGLSKKRVIGYGDYPDEPYTGIKNGDYHKKILWHSNGV 339
AvMBH           VYVPDTLAIAGFYKDWG--ERGEGLG--NFLCYGDLPTGAS-------LDPATFLFPRGA 304
DgHyd           VYITDLLAVAGFYKNWA----GIGKTS-NFLTCGEFPTD--------EYDLNSRYTPQGV 302
DfHyd           CYIPDLLAVAGFYKDWG----GIGGTS-NYLAFGEFATDDSS----PEKHLATSQFPSGV 315
EcHyd2          VYKVDTAVIAAFYPEWL----TRGKGAVNYLSVPEFPTDS---------KNGSFLFPGGY 303
                    *  .:.  : .        *      :     .                 . *

ReMBH           ILN-------GNWDEVFPVDPRDSQ----QVQEFVSHSWYKYAD-ESVGLHPWDGVTEPN 373
EcHyd1          VIN-------GDFNNVLPVDLVDPQ----QVQEFVDHAWYRYPN-DQVGRHPFDGITDPW 373
AaHase1         VEDFYKGVEKAKFYNLEGKDFTDPE----QIQEFVTHSWYKYPD-ETKGLHPWDGITEPN 394
AvMBH           ILD-------RDLSTIHEVDLEATG----EIQEFVNHSWYEYSVGNDRGLHPYEGQTNLE 353
DgHyd           IWG----------NDLSKVDDFNPD----LIEEHVKYSWYE-GA---DAHHPYKGVTKPK 344
DfHyd           ITG----------RDLGKVDNVDLG----AIYEDVKYSWYAPGG---DGKHPYDGVTDPK 358
EcHyd2          IEN-------ADLSSYRPITSHSDEYLIKGIQESAKHSWYKDEA----PQAPWEGTTIPA 352
                : .                          : * . ::**          *:.* *
```

```
ReMBH           YVLGANTKGTRTRIEQIDESAKYSWIKSPRWRGHAMEVGPLSRYILAYAHARSGNKYAER 433
EcHyd1          YNPGD-VKGSDTNIQQLNEQERYSWIKAPRWRGNAMEVGPLARTLIAYHKGDAAT----- 427
AaHase1         YTGPK--EGTKTHWKYLDENGKYSWIKAPRWRGKACEVGPLARYIIVYTKVKQGHIKPTW 452
AvMBH           YDRRG---GVAPPYKQLDVSDGYSWLKAPRWKGRSVEVGPLARVLMLYATGHDQAR---- 406
DgHyd           WTEFH-------------GEDRYSWMKAPRYKGEAFEVGPLASVLVAYAKKHEPTVK--- 388
DfHyd           YTKLD-------------DKDHYSWMKAPRYKGKAMEVGPLARTFIAYAKGQPDFKK--- 402
EcHyd2          YDGWS-------------DDGKYSWVKSPTFYGKTVEVGPLANMLVKLAAGRESTQN--- 396
                :                 .  ***:*:* : *.: *****:  ::

ReMBH           PKEQLEYSAQMINSAIPKALGLPETQYTLKQLLPSTIGRTLARALESQYCGEMMHSDWHD 493
EcHyd1          ----VESVDRMMS-----ALNLPLSG------IQSTLGRILCRAHEAQWAAGKLQYFFDK 472
AaHase1         VDELIVNQIDTVS----KILNLPPEK-----WLPTTVGRTIARALEAQMSAHTNLYWMKK 503
AvMBH           -----ELVDSTLS-----RLDLPVDA------LYSTLGRTAARALESKILVDAMQGWYDG 450
DgHyd           ------AVDLVLK-----TLGVGPEA------LFSTLGRTAARGIQCLTAAQEVEVWLDK 431
DfHyd           ------VVDMVLG-----KLSVPATA------LHSTLGRTAARGIETAIVCANMEKWIKE 445
EcHyd2          KLNEIVAIYQKLT-----GNTLEVAQ------LHSTLGRIIGRTVHCCELQDILQNQYSA 445
                          :         :          : :*:**   *  .

ReMBH           LVANIRAGDTATANVDKWDPATWPLQAKGVGTVAAPRGALGHWIRIKDGRIENYQCVVPT 553
EcHyd1          LMTNLKNGNLATASTEKWEPATWPTECRGVGFTEAPRGALGHWAAIRDGKIDLYQCVVPT 532
AaHase1         LYDNIKAGDTSVANMEKWDPSTWPKEAKGVGLTEAPRGALGHWVIIKDGKVANYQCVVPT 563
AvMBH           LIANVKSGDTKTFNETLWEPSSWPSRAQGVGIMEAPRGALGHWIVIEDGRIANYQAVVPS 510
DgHyd           LEANVKAGKDDLY-----TDWQYPTESQGVGFVNAPRGMLSHWIVQRGGKIENFQHVVPS 486
DfHyd           MADSG-AKDNTLC-----AKWEMPEESKGVGLADAPRGALSHWIRIKGKKIDNFQLVVPS 499
EcHyd2          LITNIGKGDHTTF-VKPNIPATG--EFKGVGFLEAPRGMLSHWMVIKDGIISNYQAVVPS 502
                :  .    .               . :***   **** *.**   ..  :  :* ***:

ReMBH           TWNGSPRDYKGQIGAFEASLMN-TPMVNPEQPVEILRTLHSFDPCLACSTHVMSAEGQEL 612
EcHyd1          TWNASPRDPKGQIGAYEAALMN-TKMAIPEQPLEILRTLHSFDPCLACSTHVLGDDGSEL 591
AaHase1         TWNGSPKDPKGQHGAFEESMID-TKVKVPEKPLEVLRGIHSFDPCLACSTHLYNEKGEEI 622
AvMBH           TWNAGPRDGRGQAGAYEAALQDNHQLVDVKQPIEILRTIHSFDPCIACAVHLADPESGES 570
DgHyd           TWNLGPRCAERKLSAVEQALIG-TPIADPKRPVEILRTVHSYDPCIACGVHVIDPESNQV 545
DfHyd           TWNLGPRGAQGDKSPVEEALIG-TPIADPKRPVEILRTVHAFDPCIACGVHVIEPETNEI 558
EcHyd2          TWNSGPRNFNDDVGPYEQSLVG-TPVADPNKPLEVVRTIHSFDPCMACAVHVVDADGNEV 561
                *** .*:  . . .. * :: .   :   ::*:*::* :*::***:**..*:   .  :

ReMBH           TTVKVR----- 618
EcHyd1          ISVQVR----- 597
AaHase1         ASVRVQGVVHV 633
AvMBH           FQVRVV----- 576
DgHyd           HKFRIL----- 551
DfHyd           LKFKVC----- 564
EcHyd2          VSVKVL----- 567
                  .::
```

A6 Reversibility of Formaldehyde Inhibition

The affinity of the [FeFe]-hydrogenases for formaldehyde is so high that even after the electrochemical cell has been rinsed with 50 mL fresh buffer solution, trace formaldehyde remaining may be sufficient to inhibit the enzyme. This is particularly the case for *Dd*HydAB. Figure A6 shows an experiment using this enzyme in which, following the first buffer exchange at 300 s most (but not all) H_2 production activity is recovered. However, a second rinse at 2000 s recovers the remaining enzyme activity, confirming that formaldehyde inhibition is fully reversible under these conditions.

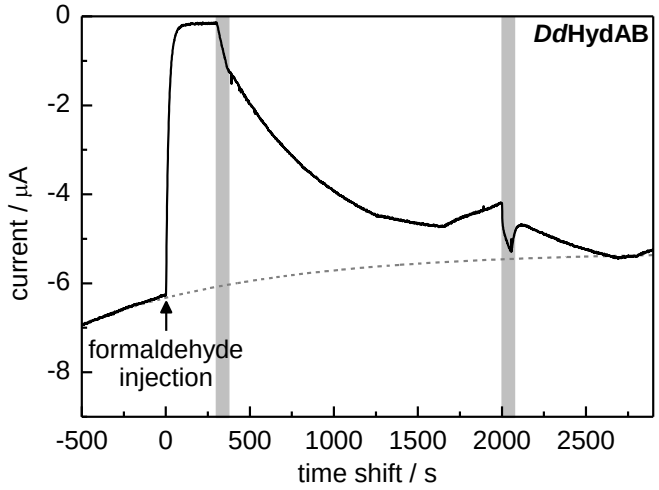


Figure A6. Confimation that formaldehyde inhibition of *Dd*HydAB can be fully reversed by rinsing the electrochemical cell with a second 50 mL of buffer solution. The electrode potential was held at -558 mV and formaldehyde injected at time = 0 s (indicated by the arrow) to give a final concentration of 4.5 mM. The cell was rinsed with 50 mL of fresh buffer solution at 300 s and then again at 2000 s (represented by the grey bars). The dotted line shows the exponential curve representing film loss (fitted to the current recorded prior to time = 0 s), extrapolated over the time course of the experiment. Other conditions: 100% H_2 pH 6, 10 °C, electrode rotation rate 2500 rpm.

.

A7 Straight *vs.* Branched-chain Aldehydes

The results originally presented in this section cannot currently be made freely available as they are to be published at a later date in academic journals.

A8 Determination of K_I

Competitive inhibition can be described by the following scheme, where E corresponds to free enzyme, S represents the substrate, ES is the enzyme-substrate complex, EI is the enzyme-inhibitor complex and P refers to product:

$$E + S \underset{k_{-1}}{\overset{k_1}{\rightleftharpoons}} ES \xrightarrow{k_{cat}} E + P$$

$$E + I \underset{k_{-2}}{\overset{k_2}{\rightleftharpoons}} EI$$

Applying the steady-state approximation to the enzyme-substrate complex, ES, gives the following equation:

$$[ES] = \frac{k_1[E][S]}{k_{-1} + k_{cat}} = \frac{[E][S]}{K_M}$$

The Michaelis constant, K_M, is defined as $(k_{-1} + k_{cat}) / k_1$, as introduced in Appendix A4. Rearrangement of this equation gives an expression for the concentration of free enzyme, [E]:

$$[E] = \frac{K_M[ES]}{[S]}$$

Applying the steady-state approximation to the enzyme-inhibitor complex, EI, and then substituting in the above expression for [E] yields:

$$[EI] = \frac{k_2}{k_{-2}}[E][I] = \frac{K_M[ES][I]}{K_I[S]}$$

The inhibitor constant, K_I, is defined as k_{-2}/k_2. The total amount of enzyme, $[E]_o$, must equal the sum of [E], [ES] and [EI]:

$$[E]_o = [E] + [ES] + [EI]$$

Substituting the above expressions for [E] and [EI] gives:

$$[E]_o = [ES]\left(\frac{K_M}{[S]} + 1 + \frac{K_M[I]}{K_I[S]}\right)$$

Rearranging to solve for [ES] yields the following expression:

$$[ES] = \frac{[E]_o[S]K_I}{K_M K_I + K_I[S] + K_M[I]}$$

As in Appendix A4, the rate of catalysis is given by:

$$v = k_{cat}[ES]$$

Therefore, substituting in the above expression for [ES], and remembering that $v_{max} = k_{cat}[E]_o$, gives the following expression for the rate:

$$v = \frac{v_{max}}{1 + \frac{K_M}{[S]}\left(1 + \frac{[I]}{K_I}\right)}$$

Since the current recorded in PFE experiments is proportional to the catalytic rate, this equation can be re-written as[***]:

$$i_t = \frac{i_{max}}{1 + \frac{K_M}{[S]}\left(1 + \frac{[I]}{K_I}\right)}$$

[***] Léger, C.; Dementin, S.; Bertrand, P.; Rousset, M.; Guigliarelli, B. *J. Am. Chem. Soc.* **2004**, *126*, 12162

Léger *et al.* defined the current recorded immediately before introduction of the inhibitor as $i_o = i_{max}/(1 + K_M/[S])$. Therefore, since

$$K_I^{app} = K_I \frac{[S]}{K_M}\left(1 + \frac{K_M}{[S]}\right)$$

then

$$i_t \approx \frac{i_o}{1 + \frac{[I]}{K_I^{app}}}$$

where i_t is the current at time t.

Modelling studies by Léger *et al.* have shown that, for H_2 production, the ratio of the current in the presence of inhibitor to the current in its absence simplifies to:

$$\frac{i_t}{i_o} = \frac{1}{1 + \frac{[I]}{K_I}}$$

Therefore, a plot of i_o/i_t against [I] yields a straight line with the gradient equal to $1/K_I$ and y-intercept equal to 1.

A9 The Arrhenius Equation

The Arrhenius equation[†††] describes the empirical observation that, for most reactions, the rate constant, *k*, increases as the temperature is raised:

$$k = A_{\mathrm{P}} \exp\left(\frac{-E_{\mathrm{a}}}{RT}\right)$$

The terms *R* and *T* correspond respectively to the gas constant and temperature in Kelvin. The activation energy, E_{a}, is the minimum kinetic energy required by reactants in order for a collision to lead to product formation. The exponential factor arises from a Boltzmann distribution of the fraction of collisions with sufficient energy to lead to reaction. The pre-exponential factor, A_{p}, corresponds to the rate of collisions, but does not take into consideration the energy of the reactants. Therefore, the product of A_{p} and the exponential factor represents the rate of successful collisions (*i.e.* the rate of reaction).

A natural logarithmic transform of the Arrhenius equation generates the following:

$$\ln k = \ln A_{\mathrm{p}} \; \square - \frac{E_{\mathrm{a}}}{RT}$$

Therefore, the activation energy, E_{a}, can be determined from the gradient of a plot of ln*k* against 1/*T*.

[†††] Atkins, P. W. (1998). Physical Chemistry, Oxford University Press

A10 The Eyring Equation

The Eyring equation is an expression for the rate constant of a reaction derived from Transition State Theory.[‡‡‡] This theory assumes that the reagents form an activated complex (transition state) before proceeding to generate the products. The activated complex, $C^{\ddagger}$, is assumed to be in equilibrium with the reagents, A and B, before forming the product(s), P:

$$A + B \overset{K^{\ddagger}}{\rightleftharpoons} C^{\ddagger} \longrightarrow P$$

The equilibrium constant for formation of the activated complex is represented by $K^{\ddagger}$. The rate constant, k, for the overall reaction to form product is given by:

$$k = \kappa \left(\frac{k_B T}{h}\right) K^{\ddagger}$$

The term κ is the transmission coefficient and accounts for the fact that the activated complex may not always lead to product formation; however, in the remainder of this derivation κ is assumed to equal unity, *i.e.* the transition state always proceeds to the product(s). The term k_B is the Boltzmann constant, T is the temperature in Kelvin and h is Planck's constant.

According to standard thermodynamics:

$$-RT\ln k = \Delta G^{\ddagger} = \Delta H^{\ddagger} - T\Delta S^{\ddagger}$$

[‡‡‡] Wright, M. R. (2004). An Introduction to Chemical Kinetics, John Wiley and Sons Ltd.

In this equation, $\Delta G^{\ddagger}$ is the free energy of activation, $\Delta H^{\ddagger}$ is the enthalpy of activation and $\Delta S^{\ddagger}$ is the entropy of activation for formation of the activated complex. The term R is the gas constant.

The equation for the rate constant can now be re-written as follows:

$$k = \left(\frac{k_B T}{h}\right) \exp\left(\frac{-\Delta H^{\ddagger}}{RT}\right) \exp\left(\frac{+\Delta S^{\ddagger}}{R}\right)$$

This is known as the Eyring equation. Rearrangment followed by a natural logarithmic transform generates the following equation:

$$\ln\left(\frac{k}{T}\right) = \frac{-\Delta H^{\ddagger}}{R}\frac{1}{T} + \ln\left(\frac{k_B}{h}\right) + \frac{\Delta S^{\ddagger}}{R}$$

Therefore, a plot of $\ln(k/T)$ *vs.* $1/T$ yields a straight line; $\Delta H^{\ddagger}$ can be determined from the gradient and $\Delta S^{\ddagger}$ can be calculated from the *y*-intercept.

A11 Calculated Structures of States

The structures originally presented in this section cannot currently be made freely available as they are to be published at a later date in an academic journal.

A12 Long-term NMR Experiment

The results originally presented in this section cannot currently be made freely available as they are to be published at a later date in an academic journal.

.

A13 The Effect of Methanol on *Dd*HydAB

The results originally presented in this section cannot currently be made freely available as they are to be published at a later date in an academic journal.